

CHEMIA

STUDIA UNIVERSITATIS BABEȘ-BOLYAI CHEMIA

1/2023

ISSN (print): 1224-7154;
ISSN (online): 2065-9520; ISSN-L: 2065-9520
©2023 STUDIA UBB CHEMIA
Published by Babeș-Bolyai University

EDITORIAL BOARD OF STUDIA UNIVERSITATIS BABEȘ-BOLYAI CHEMIA

ONORARY EDITOR:

IONEL HAIDUC – Member of the Romanian Academy

EDITOR-IN-CHIEF:

LUMINIȚA SILAGHI-DUMITRESCU

EXECUTIVE EDITOR:

CASTELIA CRISTEA

EDITORIAL BOARD:

PAUL ȘERBAN AGACHI, Babeș-Bolyai University, Cluj-Napoca, Romania

LIVAIN BREAU, UQAM University of Quebec, Montreal, Canada

HANS JOACHIM BREUNIG, Institute of Inorganic and Physical
Chemistry, University of Bremen, Bremen, Germany

JEAN ESCUDIE, HFA, Paul Sabatier University, Toulouse, France

ION GROSU, Babeș-Bolyai University, Cluj-Napoca, Romania

EVAMARIE HEY-HAWKINS, University of Leipzig, Leipzig, Germany

FLORIN DAN IRIMIE, Babeș-Bolyai University, Cluj-Napoca, Romania

FERENC KILAR, University of Pecs, Pecs, Hungary

BRUCE KING, University of Georgia, Athens, Georgia, USA

ANTONIO LAGUNA, Department of Inorganic Chemistry, ICMA,
University of Zaragoza, Zaragoza, Spain

JURGEN LIEBSCHER, Humboldt University, Berlin, Germany

KIERAN MOLLOY, University of Bath, Bath, UK

IONEL CĂȚĂLIN POPESCU, Babeș-Bolyai University, Cluj-Napoca,
Romania

CRISTIAN SILVESTRU, Babeș-Bolyai University, Cluj-Napoca, Romania

YEAR
MONTH
ISSUE

Volume 68 (LXVIII) 2023
MARCH
1

PUBLISHED ONLINE: 2023-03-27
PUBLISHED PRINT: 2023-04-30
ISSUE DOI: 10.24193/subbchem.2023.1

S T U D I A

UNIVERSITATIS BABEȘ–BOLYAI

CHEMIA

1

CONTENT/ SOMMAIRE/ INHALT/ CUPRINS

- Thi Thanh Hien NGO, Thi Hai Yen PHAM, Nguyen Thoai DANG, Thi Vuong Hoan NGUYEN, Thanh Huyen PHAM, Graziella Liana TURDEAN, Graphite Paste Electrode Modified with Zeolitic Imidazolate Framework (ZIF-67) for the Determination of Acetaminophen 7
- Mihaela-Cătălina HERGHELEGIU, Aude ERNAULT, Mihail Simion BELDEAN-GALEA, Maria-Virginia COMAN, HPLC-PDA *versus* GC-MS in the Analysis of Paracetamol and Non-steroidal Anti-inflammatory Drugs in Wastewater 19
- Monica OROIAN, Ana-Maria VLASE, Adriana MARCOVICI, Laurian VLASE, Kinetics of Dapagliflozin 10 mg Immediate Release Tablet in Healthy Caucasian Volunteers: Does Food Intake Affect Its Disposition in the Body? 37
- Ioan-Alexandru UDREA, Valentin ORDODI, Cristina PAUL, Cristian STĂNESE, Nicolae VASZILCSIN, Effects of Pulsed Electric Field on the Esterification Reactions 49

Syed Muhammad Saqib NADEEM, Rehana SAEED, The Study of Ionic Interactions of Potassium Iodide in the Vegetable Oil-N,N-dimethylformamide Solvent by Electrical Conductivity Measurements	59
Alhagie JADAMA, Seda YUKSEKDANACI, Demet ASTLEY, Ihsan YASA, Synthesis, Characterization and Biological Activity of Schiff and azo-Schiff Base Ligands	75
Réka BARABÁS, Oana CADAR, Liliana BIZO, Comparative Study of Two Commercial Stoneware Pastes for Plastic Shaping by Pottery Wheel.....	91
Daniel E. BOTHA, Paul S. AGACHI, Design and Construction of a Proof-of-concept Poultry Litter Pyrolysis Plant	105
Adrian PATRUT, Roxana T. PATRUT, Laszlo RAKOSY, Ileana Andreea RATIU, Pascal DANTHU, Jean-Michel LEONG POCK TSY, Karl F. VON REDEN, Radiocarbon Dating of the Historic Grand Baobab of Mahajanga, Madagascar.....	119
Nevena PRODANOVIĆ, Marijana KOSANIĆ, Aleksandar KOČOVIĆ, Jovica TOMOVIĆ, Emina MRKALIĆ, Miroslav SOVRLIĆ, Assessment of Biological Activity of Selected Species Mushrooms of the Order <i>Agaricales</i> and <i>Boletales</i>	131
Bunyamin YILDIRIM, Kamil EKICI, Mehmet Zeki KOCAK, Essential Oil Composition of Yarrow Species (<i>Achillea Millefolium</i> L. and <i>Achillea Wilhelmsii</i> L.): Antioxidant and Antibacterial Activities of Essential Oils.....	145
Hafize DILEK TEPE, Fatma DOYUK, Comparative Evaluation of Different Extraction Methods for Phytochemical Content and Elucidation of Microstructure from <i>Moringa Oleifera</i> Lam	159
Goran AMIN, Sandra KONSTANTINOVIC, Igor JORDANOV, Dragan DJORDJEVIC, Thermodynamics of Textile Cationic Dye Adsorption on Clinoptilolite.....	179
Giannin MOSOARCA, Cosmin VANCEA, Simona POPA, Sorina BORAN, Petru NEGREA, Maria Elena RADULESCU-GRAD, Studies Regarding Copper Ions Removal from Wastewaters Using Oak Wood Ash and the Effect of Exhausted Ash as Soil Amendment.....	193
Dejan PRVULOVIĆ, Danijela KOJIĆ, Protective Effects of Aluminosilicates on Lead-Acetate Toxicity in Broiler Chickens	211
Luiza-Andreea MÎRȚ, Dorin BOMBOȘ, Simona GHIMIȘ, Mihaela Mariana BOMBOȘ, Gabriel VASILIEVICI, Partial Desulfurization of Crumb Rubber in the Presence of Metallic Oxides.....	225

Madalina IVANOVICI, Adrian-Eugen CIOABLA, Gabriela-Alina DUMITREL, Ana-Maria PANA, Laurentiu-Valentin ORDODI, Experimental Lab-scale Biogas Production by Anaerobic Co-digestion of Agricultural Residues and Brewery Wastewater	239
Cecilia BACALI, Marioara MOLDOVAN, Stanca CUC, Corina Elena TISLER, Smaranda BUDURU, Water Sorption, Solubility and Monomer Release of a Fast Polymerized Heat-curing Resin Enhanced with Graphene Silver Nanoparticles.....	251
Ramona LEORDEAN, Alexandru OZUNU, Zoltán TÖRÖK, Preventive and Predictive Maintenance of Ammonium Nitrate Granulation Process Based on Preliminary Hazard Analysis Technique	265
Levi GABRIAN, Gavril-Ionel GIURGI, Lorant SZOLGA, Andreea Petronela CRIȘAN, Elena BOGDAN, Ramona GĂLĂTUȘ, Anamaria TEREÇ, Ion GROSU, Bulk and Bilayer Inverted Organic Solar Cells (OSCs) Exhibiting D-A and A-D-A Donors with 2,2'-Bi[3,2- <i>b</i>]thienothiophene Units and Pc ₆₁ BM or C ₇₀ Acceptors	275
Ana BALEA, Irina CIOTLĂUȘ, MARIA POJAR-FENEȘAN, Rahela CARPA, Comparative Chemical and Antimicrobial Characterization of Non-ozonated and Ozonated Vegetable Oils	285

Studia Universitatis Babes-Bolyai Chemia has been selected for coverage in Thomson Reuters products and custom information services. Beginning with V. 53 (1) 2008, this publication is indexed and abstracted in the following:

- Science Citation Index Expanded (also known as SciSearch®)
- Chemistry Citation Index®
- Journal Citation Reports/Science Edition

GRAPHITE PASTE ELECTRODE MODIFIED WITH ZEOLITIC IMIDAZOLATE FRAMEWORK (ZIF-67) FOR THE DETERMINATION OF ACETAMINOPHEN

Thi Thanh Hien NGO^{a*}, Thi Hai Yen PHAM^b, Nguyen Thoai DANG^a,
Thi Vuong Hoan NGUYEN^a, Thanh Huyen PHAM^c,
Graziella Liana TURDEAN^{d*}

ABSTRACT. A zeolitic imidazolate framework ZIF-67 was synthesized by an eco-friendly solvothermal method, using ethanol as solvent at room temperature. The morphology and structure of obtained ZIF-67 were characterized by X-ray diffraction, scanning electron microscopy (SEM), nitrogen adsorption/desorption isotherm, energy dispersive spectroscopy (EDS), and Fourier-transform infrared spectroscopy (FTIR). The ZIF-67 modified graphite paste electrode (ZIF-67-GPE) was prepared and used for the electrochemical detection of acetaminophen (AC). Cyclic voltammetry (CV) and square wave voltammetry (SWV) were employed to investigate the electrochemical behavior of AC at ZIF-67-GPE modified electrode. At the optimal working conditions, the limit of detection was 0.2 μM (S/N = 3) in the linear range of 2 - 10 μM AC. The good analytical parameters indicated its applicability for AC determination in real samples.

Keywords: *Zeolitic imidazolate framework, graphite paste modified electrode, acetaminophen*

^a Quy Nhon University, Faculty of Natural Sciences, 170 An Duong Vuong, Quy Nhon 55000, Vietnam

^b Institute of Chemistry, Vietnam Academy of Science Technology, 18 Hoang Quoc Viet, Cau Giay, Hanoi 100000, Vietnam

^c Ha Noi University of Science and Technology, School of Chemical Engineering, 1 Dai Co Viet, Ha Noi 100000, Vietnam

^d Babes-Bolyai University, Faculty of Chemistry and Chemical Engineering, Department of Chemical Engineering, Center of Electrochemistry and Non-conventional Materials, 11 Arany Janos, 400198 Cluj-Napoca, Romania

* Corresponding authors: graziella.turdean@ubbcluj.ro, ngothanhvien@qnu.edu.vn



INTRODUCTION

Zeolitic imidazolate frameworks (ZIFs) are a class of metal-organic frameworks (MOFs) that have gained widespread interest for their applications in catalysis [1-3], gas storage, chemical separation [4, 5], sensing [6,7], and drug delivery because of their porous structure, tunable pore size, and high surface area.

The cobalt-based metal-organic zeolitic imidazolate frameworks (ZIF-67) belonging to the zeolitic imidazolate frameworks (ZIFs) class of substances, consists of a transition metal ion (Co^{2+}) and organic ligands (2-methylimidazole). ZIF-67 is topologically isomorphic with zeolites, with a metal-imidazole metal angle of $\sim 145^\circ$, relatively similar to the Si-O-Si angle in zeolite [8-10]. The typical synthesis methods of ZIF-67 are solvothermal and hydrothermal methods which use large amounts of organic solvents, such as N,N-dimethyl formamide (DMF), N-methyl pyrrolidine, N,N-diethyl formamide, and methanol, etc. Nevertheless, these methods lead to disadvantages due to cost and environmental problems, because the used toxic organic solvents are found in the waste solutions. Therefore, the simple and environmentally friendly method is highly expected. In recent years, the synthesis of ZIF-67 by using either a friendly solvent, such as ethanol, or water, or a non-solvent synthesis route has been of interest [11, 12].

Acetaminophen (N-acetyl-p-aminophenol; paracetamol, AC) is a broadly recommended drug because it is used as a painkiller and antipyretic. However, in the case of an overdose, it would cause health problems to the liver or kidney. Therefore, AC detection has become an interesting research topic. Among the many techniques described in the literature for AC detection in the pharmaceutical formulation, the (i) optical methods (*i.e.*, UV/Vis spectrophotometric in the version of flow-injection, IR spectrophotometric (NIR or FTIR), spectrofluorimetric [1], (ii) electroanalytical methods (*i.e.*, titrimetry, amperometry, voltammetry, and immunoassays); (iii) chromatographic methods (*i.e.*, high-performance liquid chromatography (HPLC)), and (iv) capillary electrophoresis methods [2] are the most performant. In recent years, electrochemical techniques have been selected for AC determination due to their high sensitivity, simple technique, rapid response, and low expenses.

In this work, ZIF-67 was synthesized by an eco-friendly solvothermal method, using ethanol as solvent at room temperature and characterized by several techniques, such as X-ray diffraction (XRD), scanning electron microscopy (SEM), nitrogen adsorption/desorption isotherm, energy dispersive spectroscopy (EDS), Fourier-transform infrared spectroscopy (FTIR). The applicability of ZIF-67 material as a modifier for the development of a chemically modified electrode for AC electrochemical determination has been investigated by electrochemical methods (cyclic voltammetry, CV and square wave voltammetry, SWV) either in synthetic or in real sample solutions.

RESULTS AND DISCUSSION

Morpho-structural characterization of ZIF-67 material

The results obtained from different morpho-structural characterization techniques are described below.

Figure 1A shows the XRD pattern of the synthesized sample. Thus, the XRD pattern exhibited diffraction peaks at 2θ values of 7.4° , 10.4° , 12.7° , 14.8° , 16.5° , 18.0° , 22.1° , 24.5° , 25.5° , 26.7° , 29.5° , 30.6° , 31.6° and 32.5° , which correspond to (011), (002), (112), (022), (013), (222), (114), (233), (224), (134), (044), (334), (244) and (235) planes. These results are in good accordance with the already published pattern of ZIF-67 crystal [13].

The FT-IR spectrum of ZIF-67 is shown in Figure 1B. The peak observed at about 430 cm^{-1} was attributed to the stretching of the metal Co–N bond in 2-methylimidazolate [14–16]. The peak at about 997, 1140, and 1514 cm^{-1} are the stretching vibration of the C–N bond and C=N in 2-methylimidazolate, respectively [16, 17]. The stretching of the aromatic ring in 2-methylimidazolate and the C–H bond in the aliphatic hydrocarbon chain was revealed by the peaks at 2916 cm^{-1} and 3113 cm^{-1} [15–18].

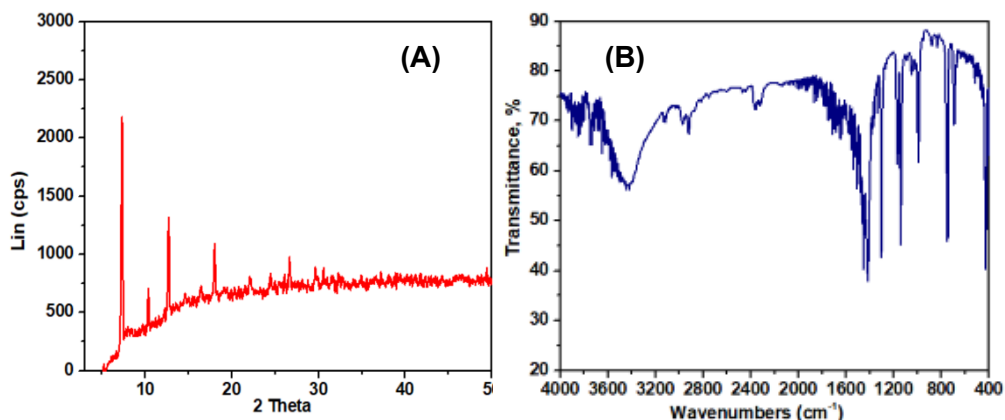


Figure 1. XRD pattern (A) and FTIR spectrum (B) of ZIF-67.

SEM images of the obtained ZIF-67 (Figure 2A) revealed the basic structure of the rhombohedral dodecahedron and smooth surfaces of ZIF-67 crystals with a particle size of about 500 - 1000 nm. Also, the results of the EDS analysis (Figure 2B) confirmed the presence of C, O, and Co elements on the surface of ZIF-67.

Figure 3 shows the nitrogen adsorption–desorption isotherm and the pore size distributions of ZIF-67 material. Thus, the N₂ adsorption-desorption isotherms (Figure 3A) used for the textural study of ZIF-67, displayed a typical reversible type I isotherm, according to the IUPAC classification, that is a characteristic of the microporous material because the adsorption of the sample ended at a low pressure ($P/P_0 = 0.01$) [19]. Also, the results showed the BET surface area of 1112 m²/g and the micropore size mainly distributed at around 1.1 nm.

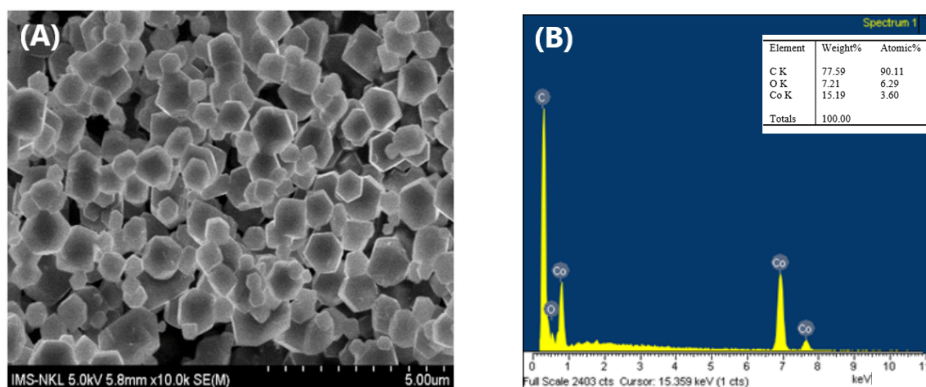


Figure 2. SEM images of ZIF-67 (A) and EDS spectra of ZIF-67 (B).

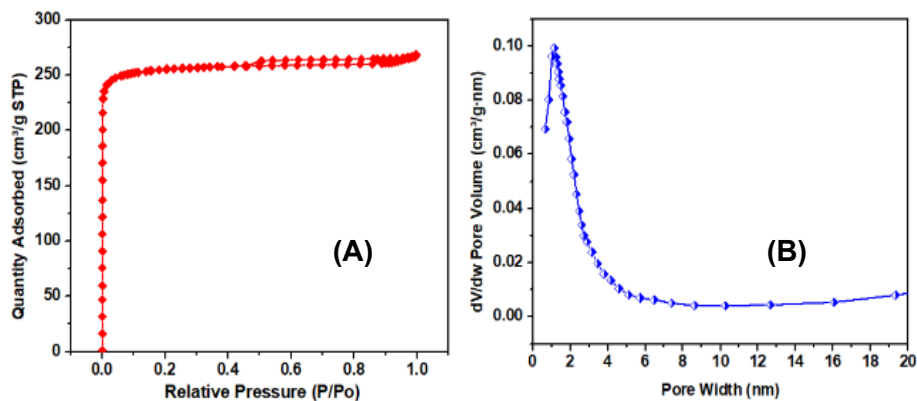


Figure 3. Nitrogen adsorption-desorption isotherms (A) and pore size distribution of ZIF-67 (B).

The morpho-structural characterization of the ZIF-67 material, by XRD, SEM-EDS, BET, and FTIR confirmed the successful synthesis of this microporous crystalline material.

Electrochemical behavior of ZIF-67-GPE modified electrode

Cyclic voltammograms were recorded to compare the electrochemical behavior of AC at unmodified GCE and ZIF67-GCE-modified electrodes (Figure 4).

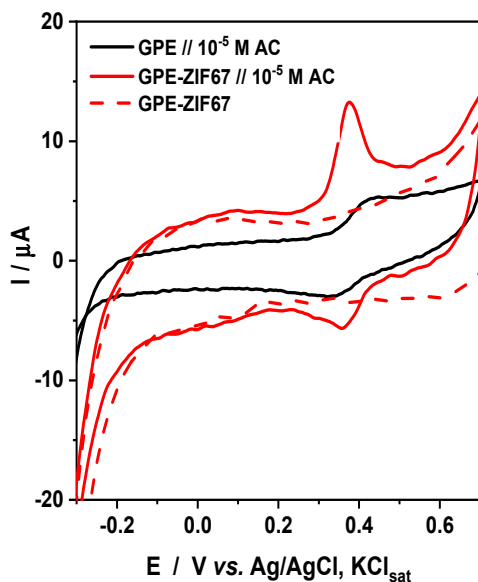


Figure 4. Cyclic voltammograms at GPE (black solid line) and ZIF-67-GPE (red solid line) modified electrode in the presence of 10^{-5} M AC and in the absence of AC (red dot line). Experimental conditions: electrolyte, 0.1 M phosphate buffer solution (PBS), pH = 7; scan rate, 50 mV s^{-1} ; starting potential, -0.25 V vs. Ag/AgCl, KCl_{sat} .

The oxidation and reduction peaks were attributed to the redox behaviour of the acetaminophen and are placed at the following values of anodic/cathodic potentials ($E_{\text{pa}}/E_{\text{pc}}$) of $+0.35 \text{ V}/+0.33 \text{ V}$ vs. Ag/AgCl, KCl_{sat} for ZIF-67-GPE and $+0.41 \text{ V}/+0.32 \text{ V}$ vs. Ag/AgCl, KCl_{sat} for GPE, respectively. Because the peak separation (calculated as $\Delta E = E_{\text{pa}} - E_{\text{pc}}$) is increasing from 0.02 V for ZIF-67-GPE modified electrode to 0.09 V in the case of GPE, it can be concluded that the presence of ZIF67 in the electrode matrix leads to a more reversible behaviour of the redox process. Also, the oxidation process is facilitated in the presence of ZIF-67 in the electrode matrix, because the anodic peak potential value is shifted towards a more negative potential value with 0.06 V . Moreover, the ratio of the peak current intensities ($I_{\text{pa}}/I_{\text{pc}}$) is 1 and 2.3 in the case of GPE and ZIF-67-GPE modified electrodes, respectively, the anodic redox process is visibly enhanced in the presence of ZIF-67.

Effect of pH

Square wave voltametry (SWV) was used to investigate the effect of pH on the AC oxidation at ZIF-67-GPE electrode (Figure 5A) in the range of 5.5 - 7.5.

As shown in figure 5B the oxidation peak current increased in the pH range of 5.5 - 6.5, reached a maximum at pH 6.5, and then decreased. Therefore, a pH value of 6.5 for the buffer solution was chosen for further experiments. The dependence of the oxidation peak potentials (E_{pa}) on pH in the same domain showed that the E_{pa} shifted linearly towards negative potential with the increase of the pH values.

This behavior indicated the involvement of protons in the redox reaction of AC.

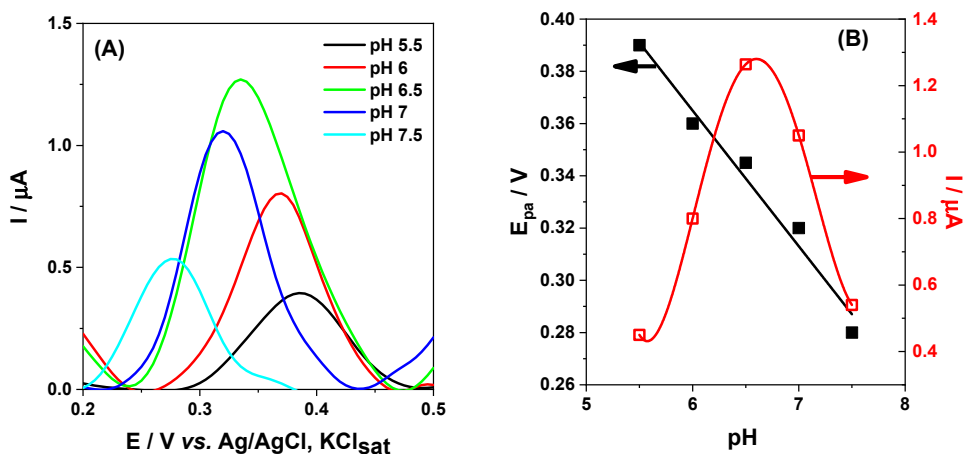
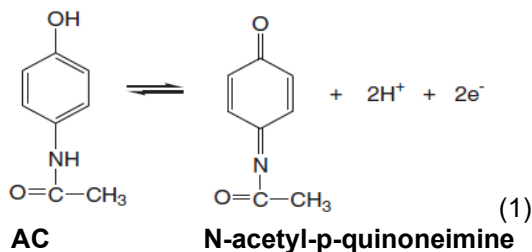


Figure 5. Square wave voltammograms at ZIF-67-GPE for 10^{-5} M AC in 0.1 M PBS at various pH value, see (A). Influence of pH on the formal potential E_o' and anodic peak current I_{pa} (B). Experimental conditions: electrolyte, 0.1 M phosphate buffer solution (PBS); starting potential -0.25 V vs. $Ag/AgCl, KCl_{sat}$; frequency, 20 Hz; step potential, 0.005 V; accumulation time, 150 s; deposition potential, 0 V.

The linear regression equation was expressed as follows: $E_{pa}/V = -0.052 \text{ pH} + 0.677$ ($R = 0.9884$, 5 points). The slope of 0.052 V/pH, close to the theoretical Nernstian value of 0.059 V/pH, corresponds to a ratio of protons and electrons involved in the oxidation reaction of 1:1. According with the obtained electrochemical parameters the AC oxidation mechanism is presented in the following reaction (1).

GRAPHITE PASTE ELECTRODE MODIFIED WITH ZEOLITIC IMIDAZOLATE FRAMEWORK (ZIF-67)
FOR THE DETERMINATION OF ACETAMINOPHEN



Analytical parameters of ZIF-67-GPE modified electrode

Square wave voltammograms recorded at the ZIF-67-GPE modified electrode in the presence of different concentrations of AC in the range of 10^{-6} M to 10^{-5} M (Figure 6A) lead to plotting the corresponding calibration curve (Figure 6B). The dependence I - AC concentration was linear in the range of concentrations 2 - 10 μM . The linear regression equation was $I_{\text{pa}}/\mu\text{A} = (-1.61 \pm 0.10) + (1.49 \pm 0.02) [\text{AC}]/\mu\text{M}$, ($R = 0.9996$, 9 points). The estimated detection limit of AC was 0.20 μM (for a signal/noise ratio of 3) at ZIF-67-GPE. This result was lower than those obtained at several electrodes reported in the literature, e.g., 1.1 μM at CPE-CNT-poly(3-aminophenol) [20]; 1.39 μM at PEDOT/SPE [21]; 6 μM at graphene oxide-GCE [21]; 1.45 μM at Pt/B(Al)SBA-15-GPE [23]; 1.4 μM at ZIF-67/GCE [24].

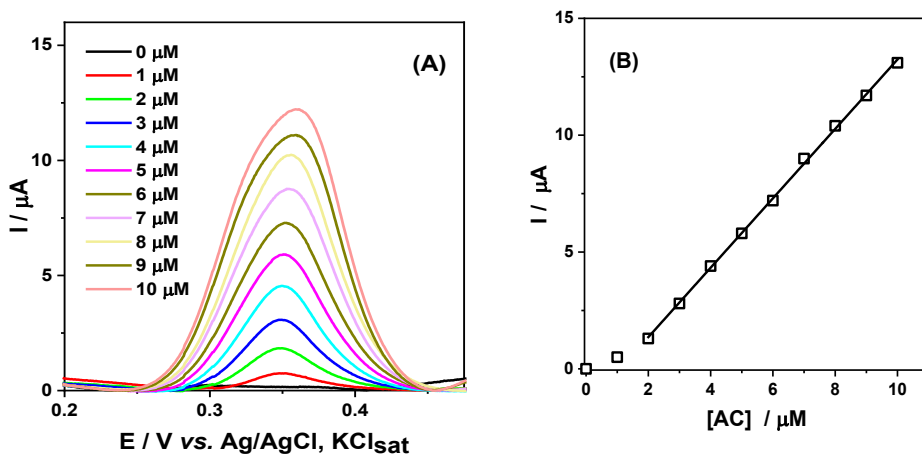


Figure 6. Square wave voltammograms recorded at ZIF-67-GPE increasing concentration of AC (A) and the corresponding calibration curve (B). Experimental conditions: electrolyte, 0.1 phosphate buffer solution (PBS), pH 6.5; starting potential -0.20 V vs. Ag/AgCl, KCl_{sat}; frequency, 20 Hz; step potential, 0.005 V; accumulation time, 150 s; deposition potential, 0 V.

Inteferences

In order to evaluate the interference effect of ascorbic acid (AA) on the detection of AC, 0.1 mM AA was added to a solution containing 5 μ M AC. The obtained square wave voltammograms (Figure 7) illustrate that the oxidation reaction of AA and AC are placed at completely different peak potentials, thus at the investigated electrode surface the AC oxidation was not affected by the presence of AA. Moreover, the oxidation peak potentials placed at 0.014 V vs. Ag/AgCl, KCl_{sat} and +0.33 V vs. Ag/AgCl, KCl_{sat} for AA and AC, respectively, shifted with 20 mV towards more positive values, when both AA and AC are present in solution.

Real sample analysis

The ZIF-67-GPE modified electrode was used to determine the acetaminophen content in the commercial pharmaceutical tablet, as Panadol Extra (from Sanofi VietNam), using the standard addition method. The results are summarized in Table 1.

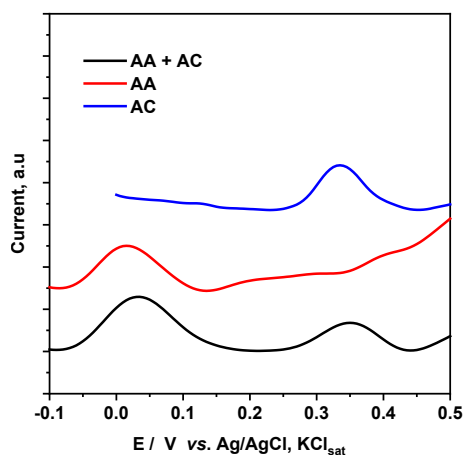


Figure 7. Square wave voltammograms recorded at ZIF-67-GPE modified electrode in the presence of 5 μ M AC and 0.1 mM AA. Experimental conditions: electrolyte, 0.1 phosphate buffer solution (PBS), pH 6.5; starting potential -0.1 V vs. Ag/AgCl, KCl_{sat}; frequency, 20 Hz; step potential, 0.005 V; accumulation time, 150 s; deposition potential, 0 V.

Table 1. Results of real sample analysis

Sample	Added/ μ M	Found/ μ M	Recovery%	RSD%
AC (500 mg/tablet)	4	3.96 \pm 0.04	99.0 \pm 1.09	1.1

From these results, it may be concluded that the ZIF-67-GPE electrode have good efficiency for the AC analysis in real sample. The mean value of the AC concentration obtained by the calibration curve corresponds well to the value declared by the producer. The recovery of AC were in the range of 98.01% - 100.09%, and the relative standard deviation was lower than 2%, indicating the applicability of ZIF-67-GPE modified electrode in real sample analysis.

CONCLUSIONS

The rhombic dodecahedron ZIF-67 crystals were synthesized by an eco-friendly solvothermal method, using ethanol as solvent at room temperature. The material was used for preparing a ZIF-67 graphite paste-modified electrode which was characterized for AC redox behavior, by cyclic voltammetry and square-wave voltammetry. The estimated electroanalytical and analytical parameters demonstrated good expected electrochemical behavior, adequate sensitivity, and low detection limit for AC detection. Thus, the Co metal-containing porous structure of ZIF-67 provided a promising platform for the detection of AC from the synthetic sample and commercial pharmaceutical.

EXPERIMENTAL SECTION

Chemicals

CH₃C₃H₂N₂H, Hmim), and acetaminophen (C₈H₉NO₂), graphite powder, and paraffin oil were received from Sigma - Aldrich. Cobalt nitrate hexahydrate (Co(NO₃)₂·6H₂O) were purchased from Macklin (China), absolute ethanol (C₂H₅OH), methanol (CH₃OH), KH₂PO₄, K₂HPO₄ were purchased from Guangdong - Guanghua Sci-Tech Co. Ltd (China). Acetaminophen tablet (Panadol, 500 mg AC, from Sanofi VietNam) was purchased from a local pharmacy.

Preparation of ZIF-67 material

1.455 g of Co(NO₃)₂·6H₂O was dissolved in 50 mL of ethanol and 1,64 g of 2-methylimidazole (Hmim) was dissolved in 50mL of ethanol. Mole ratio of Co²⁺: Hmim was 1 : 4. The Hmim solution was poured slowly into Co(NO₃)₂·6H₂O solution under stirring condition for 30 min at room temperature.

The obtained solution was kept at room temperature for 6 hours without stirring. The colloidal dispersion was observed, and the product was collected by centrifugation (4000 rpm, 30 min) and washed with ethanol three times, then dried at 80 °C, 12 hours.

Preparation of ZIF-67-GPE modified electrode

The ZIF-67-GPE modified electrode was prepared by thoroughly mixing 40 mg of graphite powder and 10 mg ZIF-67 powder with 15 μ l of paraffin oil. The obtained paste was put into the cavity of a Teflon holder. The obtained electrode surface was smoothed using paper. When necessary, a new electrode surface was obtained by removing 2 mm of the outer paste layer and adding freshly modified paste.

Electrochemical measurements

Electrochemical measurements (cyclic voltammetry and square wave voltammetry) were performed by a custom-made multifunctional potentiogalvanostat MPGS - HH10 manufactured in the Institute of Chemistry, Vietnam Academy of Science and Technology, Hanoi, Vietnam. A conventional three-electrodes cell equipped with a working electrode (ZIF-67-GPE modified electrode or GPE unmodified electrode, with a geometrical area of 0.07 cm²), a counter electrode (Pt wire), and a reference electrode (Ag/AgCl, KCl_{sat}) was used. The experimental conditions are presented in the capture of each figure.

ACKNOWLEDGMENTS

This research is conducted within the framework of Science and Technology Projects at institutional level of Quy Nhon University under the project code T2022.748.04

REFERENCES

1. J. Lee; O. K. Farha; J. Roberts; K. A. Scheidt; S. T. Nguyen; J. T. Hupp; *Chem. Soc. Rev.*, **2009**, *38*, 1450–1459.
2. F. Zhang; Y. Wei; X. Wu; H. Jiang; W. Wang; H. Li, *J. Am. Chem. Soc.*, **2014**, *136*, 13963–13966.
3. C. Dey; R. Banerjee; *Chem. Commun.*, **2013**, *49*, 6617–6619.
4. J. Qian; F. Sun; L. Qin; *Mater. Lett.*, **2012**, *82*, 220–223.

5. D.-Z. Shen; T.-T. Cai; X.-L. Zhu; X.-L. Ma; L.-Q. Kong; Q. Kang; *Chin. Chem. Lett.*, **2015**, *26*, 1022–1025.
6. D. Yu; L. Ge; B. Wu; L. Wu; H. Wang; T. Xu; *J. Mater. Chem. A*, **2015**, *3*, 16688–16694.
7. Y.-Y. Zheng; C.-X. Li; X.-T. Ding; Q. Yang; Y.-M. Qi; H.-M. Zhang; L.-T. Qu; *Chin. Chem. Lett.*, **2017**, *28*, 1473–1478.
8. D. Bradshaw; S. El-Hankari; L. Lupica-Spagnolo; *Chem. Soc. Rev.*, **2014**, *43*, 5431–5443.
9. A. Phan; C. J. Doonan; F. J. Uribe-Romo; C. B. Knobler; M. O'Keeffe; O. M. Yaghi; *Acc. Chem. Res.*, **2010**, *43*, 58–67.
10. B. Pattengale; S. Yang; J. Ludwig; Z. Huang; X. Zhang; J. Huang; *J. Am. Chem. Soc.*, **2016**, *138*, 8072–8075.
11. R. R. Kuruppathparambil; T. Jose; R. Babu; G. Y. Hwang; A. C. Kathalikkattil; D. W. Kim; D. W. Park; *Appl. Catal. B*, **2016**, *182*, 562–569.
12. Y. Xiao; A. N. Hong; D. Hu; Y. Wang; X. Bu; P. Feng; *Chem. Eur. J.*, **2019**, *25*, 1–9.
13. A. F. Gross; E. Sherman; J. J. Vajo; *Dalton Trans.*, **2012**, *41*, 5458–5460.
14. Z. Öztürk; M. Filez; B.M. Weckhuysen; *Chem. Eur. J.*, **2017**, *23*, 10915–10924.
15. S. Gadipelli; W. Travis; W. Zhou; Z. Guo; *Energy Environ. Sci.*, **2014**, *7*, 2232–2238.
16. T. Zhang; X. Zhang; X. Yan; L. Kong; G. Zhang; H. Liu; J. Qiu; K. L. Yeung; *Chem. Eng. J.*, **2013**, *228*, 398–404.
17. Z. Zhang; J. Zhang; J. Liu; Z. Xiong; X. Chen; *Water Air Soil Pollut.*, **2016**, *227*, 471–482.
18. M. J. C. Ordonez; K. J. Balkus; J. P. Ferraris; I. H. Musselman; *J. Membr. Sci.*, **2010**, *36*, 28–37.
19. S. Saeed; R. Bashir; S. U. Rehman; M. T. Nazir; Z. A. AL Othman; A. Muteb Aljuwayid; A. Abid; A. Adnan; *Front. Bioeng. Biotechnol.*, **2022**, *10*, 891549.
20. I. Noviandri; R. Rakhmana; *Int. J. Electrochem. Sci.*, **2012**, *7*, 4479–4487.
21. W. Y. Su; S. H. Cheng; *Electroanalysis*, **2010**, *22*, 707–714.
22. J. Song; J. Yang; J. Zeng; J. Tan; L. Zhang; *Sensors Actuators, B Chem.*, **2011**, *155*, 220–225.
23. T. T. H. Ngo, I. C. Fort, T. H. Pham, G. L. Turdean, *Electroanalysis*, **2021**, *33*, 323–335.
24. N. T. T. Tu; P. C. Sy; T. V. Thien; T. T. T. Toan; N. H. Phong; H. T. Long; D. Q. Khieu, *J. Mater. Sci.*, **2019**, *54*, 11654–11670.

HPLC-PDA VERSUS GC-MS IN THE ANALYSIS OF PARACETAMOL AND NON-STEROIDAL ANTI-INFLAMMATORY DRUGS IN WASTEWATER

Mihaela-Cătălina HERGHELEGIU^a, Aude ERNAULT^b,
Mihail Simion BELDEAN-GALEA^a, Maria-Virginia COMAN^{c,*}

ABSTRACT. The widespread use of paracetamol and non-steroidal anti-inflammatory drugs (NSAIDs) make them increasingly present in environmental factors, especially in water. The aim of this work was to develop an accurate, precise and sensitive analytical procedure for the simultaneous determination of Paracetamol and four NSAIDs (Ketoprofen, Naproxen, Diclofenac, and Ibuprofen). To this aim, the extraction (liquid-liquid extraction, LLE, and solid-phase extraction, SPE) as well as the chromatographic (high-performance liquid chromatography-photodiode array detector, HPLC-PDA, and gas chromatography-mass spectrometry in selected ion monitoring mode, GC-MS-SIM) techniques, in terms of the performances were compared. Different extraction solvents and types of cartridges at pH 3 of samples were tested for the extraction optimization. Low limits of detection and quantification at the $\mu\text{g/L}$ level were achieved. The developed HPLC-PDA and GC-MS-SIM methods were applied to the analysis of selected pharmaceuticals in different wastewater samples.

Keywords: *paracetamol and NSAIDs, solid-phase extraction, liquid-liquid extraction, GC-MS, HPLC-PDA*

^a Babeş-Bolyai University, Faculty of Environmental Science and Engineering, 30 Fântânele str., RO-400294, Cluj-Napoca, Romania

^b École Supérieure de Physique et de Chimie Industrielle de la Ville de Paris, Paris Sciences et Lettres Université, 10 Vauquelin Rue, 75231, Paris, France

^c Babeş-Bolyai University, "Raluca Ripan" Institute for Research in Chemistry, 30 Fântânele str., RO-400294, Cluj-Napoca, Romania

* Corresponding author: virginia.coman@ubbcluj.ro



INTRODUCTION

Pharmaceuticals are currently used for many valuable purposes of human and animal health and some of them are classified as “emerging” pollutants. These pharmaceuticals can enter the wastewater system through their excretion after ingestion, in unchanged and/or metabolized (glucuronide conjugates) form or through their incorrect disposal [1–4]. Due to their persistence and continuous input in the environment, pharmaceutical residues are frequently detected in water bodies [5–8] in the range of ng/L to µg/L, which may represent potential threats to living organisms and ecosystem viability [9].

The most commonly prescribed over-the-counter pharmaceuticals, available and popular, are paracetamol (PARA) and non-steroidal anti-inflammatory drugs (NSAIDs) [9, 10]. Paracetamol, also called acetaminophen, is a mild analgesic most widely used to treat fever and headache [11]. NSAIDs are antipyretics and non-narcotic analgesics used for mild to moderate pain, their use does not lead to euphoria and addiction [12]. The most studied NSAID on the Watch List of Substances for European Union-wide Monitoring is Diclofenac together with other NSAIDs (Naproxen, Ketoprofen, Ibuprofen), Paracetamol or hormones [13].

In analytical chemistry, sample preparation for analysis is a very important step with consequences in the identification, confirmation, and quantification of target analytes in various matrices. It involves sampling and extraction procedures [14, 15].

Liquid-liquid extraction (LLE) is one of the first and most well-known sample preparation techniques that use organic solvents to extract the target compounds from different matrices, based on the octanol-water partition coefficient [15]. A widely used extraction method is solid-phase extraction (SPE) which is based on the adsorption of target analytes on the solid-phase (cartridges filled with different adsorbents) that allows their transfer from the liquid sample to the adsorbent, a method that can be applied to analytes with a wide range of polarities [15, 16].

In general, the most popular and easy-to-use extraction procedure for Paracetamol and NSAIDs from different water samples is solid-phase extraction (SPE) [5, 6, 8–10, 17, 18]. Literature data also mention miniaturized extraction (microextraction) methods for Paracetamol and NSAIDs: dispersive liquid-liquid microextraction based on solidification of floating organic droplet [19], ultrasound-assisted emulsification microextraction (with the advantage of no water-miscible organic solvents as dispersers and accelerating the process of target components into the solvent) [7], headspace (migration of volatile target compounds onto the adsorbent material) [20], molecularly imprinted polymers (molecular recognition allowing highly selective retention mechanism) [21].

The continuous increase of high-precision analytical instrumentation in recent years, by high specificity and selectivity, made possible the qualitative and quantitative assessment of Paracetamol and NSAIDs in matrices of different complexity. Liquid chromatography (LC) is able to separate polar compounds from complex mixtures without derivatization [10, 11, 18, 21], while gas chromatography (GC) requires this step [17].

Liquid chromatography-mass spectrometry (LC-MS) technique associated with electrospray ionization has the disadvantage of suppression the analyte signal caused by the matrix effect, fact of which other detectors of higher sensitivity and resolution [11] and with lower matrix effect should be used (QTrap mass spectrometer [10], tandem-mass spectrometry (MS-MS) [11, 18, 21].

Gas chromatography-mass spectrometry (GC-MS) is a convenient, accessible, and versatile technique, commonly used in many laboratories, *versus* LC-MS. GC-MS is applicable to PARA and NSAID analysis, but involves a derivatization step with silylation, acylation or alkylation agents to convert polar compounds into volatile derivatives [9, 11, 20].

The aim of this work is to develop an accurate and sensitive analytical procedure for the simultaneous determination of PARA and four NSAIDs (Ketoprofen, Naproxen, Diclofenac and Ibuprofen) in different wastewater samples. The novelty of this work consists in a pertinent comparison regarding the performance of the most common extraction (LLE and SPE) and chromatographic (high-performance liquid chromatography-photodiode array detector HPLC-PDA and GC-MS) techniques used for the analysis these compounds and their applicability to various wastewater samples.

RESULTS AND DISCUSSION

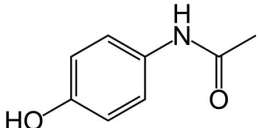
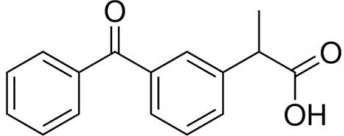
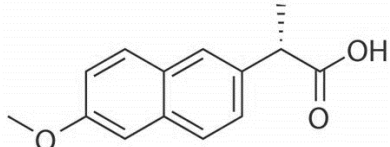
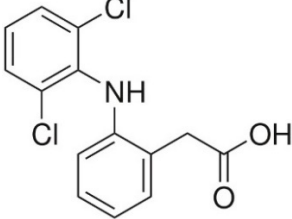
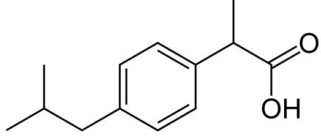
NSAIDs are carboxylic acid derivatives, whereas paracetamol is an N-acetyl-p-aminophenol. The molecular structure, molecular weight (MW), lipophilicity (LogP) and acidity (pKa) constants are presented in Table 1.

Analyzing the physicochemical properties of the compounds in Table 1, it can be seen that, while NSAIDs are weakly lipophilic (log P between 3.12 and 4.51) PARA is rather hydrophilic (log P = 0.91). More NSAIDs have pKa values between 4.15 and 4.91, while the pKa value of PARA is 9.38. These differences could lead to a different behavior of the studied compounds, especially when it is intended to isolate them from aqueous matrices. For these reasons, a study on the influence of pH on the extraction of these compounds from aqueous matrices is necessary.

According to our previously research [19], the pH value of 3 gives the maximum recovery for the studied NSAIDs because due to their pKa values between 4.15 and 4.91. Thus, a low pH value keeps these compounds in neutral form avoiding their dissociation.

Therefore, as a starting point, our experiments were done at pH 3, following which the study of the influence of pH to be done for the extraction method with the highest recovery yield.

Table 1. Molecular structure, molecular weight (MW), lipophilicity (LogP) and acidity (pKa) of the studied pharmaceuticals

Analyte (Abbreviation)	Chemical Structure	MW	LogP	pKa
Paracetamol (PARA)		151.16	0.91	9.38
Ketoprofen (KET)		254.28	3.12	4.45
Naproxen (NAP)		230.26	3.18	4.15
Diclofenac (DIC)		296.14	4.51	4.15
Ibuprofen (IBU)		206.28	3.97	4.91

Physicochemical properties (MW, LogP, pKa) from PubChem databases.
<https://pubchem.ncbi.nlm.nih.gov/> (Accessed November 2022).

Liquid-liquid extraction. According to the scientific literature [22, 23] the extraction of selected pharmaceuticals from liquid samples are performed using solvent of medium polarity (ethyl acetate, dichloromethane, chloroform) or mixtures of nonpolar to polar solvents such as hexane, acetonitrile, acetone, 1-butanol. For our purpose the efficiency of ethyl acetate and mixture of *n*-hexane:isopropanol (3:2, v/v) were considered. The recovery of each pharmaceutical at the selected pH 3 was calculated for each of the two extraction solvents, ethyl acetate and *n*-hexane:isopropanol (3:2, v/v) respectively, and the results are plotted in Figure 1.

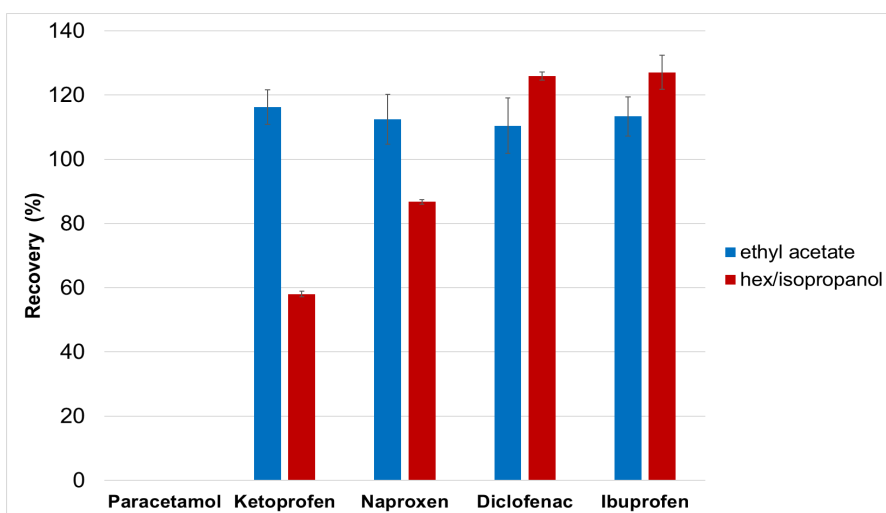


Figure 1. Recovery of studied pharmaceuticals using two extraction solvents

Naproxen, Ketoprofen, Diclofenac and Ibuprofen were detected in the extracts obtained with the both extraction solvents. The recovery over 100% for all the four anti-inflammatories was obtained in the case of ethyl acetate solvent. Paracetamol could not be quantified with either of the two extraction solvents due to the presence of different impurities that co-eluted with it.

These impurities come from the extraction solvent and even if they are present at the trace level, through concentration they reach concentration levels that disturb the analysis. Moreover, the poor retention of PARA in the analysis conditions makes its elution very close to the hold-up volume of the column, which leads to the overlap of the solvent peak and the impurities associated with PARA (see Results and Discussion section, Figure 4).

Since Paracetamol could not be analysed simultaneously with the four NSAIDs, the LLE method was not considered suitable for our aim.

Solid-phase extraction. The three types of SPE cartridges (C18-U, C18-E, Strata X) were tested at pH 3. The best extraction of the studied pharmaceuticals from distilled water samples was obtained on Strata X cartridges that are capable of adsorbing a large group of analytes. Recoveries for all pharmaceuticals were from 41.57 to 89.94% (Figure 2). Therefore, Strata X cartridges were chosen for SPE of the target pharmaceuticals in the wastewater samples.

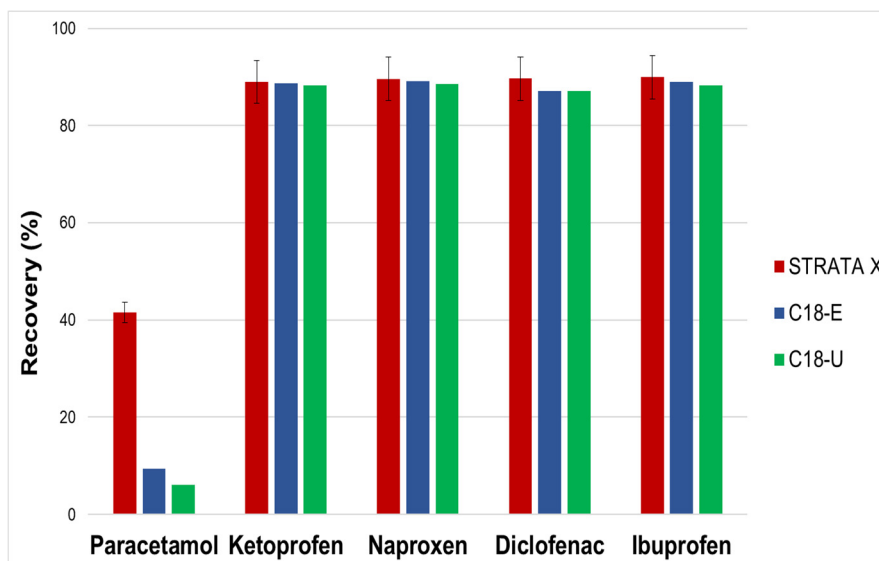


Figure 2. Recovery of studied pharmaceuticals using different SPE cartridges

Influence of pH over the Solid-Phase Extraction. The influence of pH over the SPE recovery was tested at 3 pH levels, such as 3, 4, and 7. The results showed that the most suitable pH is 3, for which both PARA and NSAIDs have the highest extraction recoveries, PARA over 40% and NSAIDs over 80% (Figure 3).

HPLC-PDA VERSUS GC-MS IN THE ANALYSIS OF PARACETAMOL AND NON-STEROIDAL ANTI-INFLAMMATORY DRUGS IN WASTEWATER

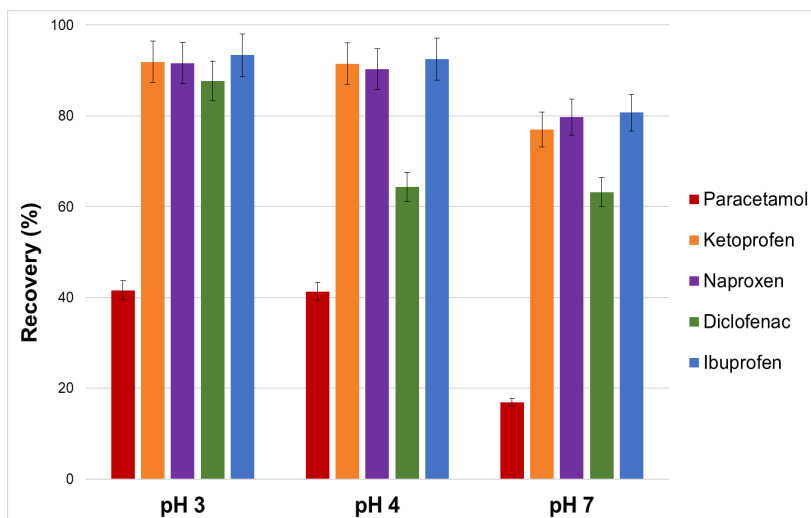


Figure 3. Influence of pH over the recovery of studied pharmaceuticals on Strata X SPE cartridge

Performances of HPLC-PDA and GC-MS-SIM developed methods

For the both chromatographic methods, limit of detection (LOD) and limit of quantification (LOQ) were determined taking into consideration the standard deviation of the response factor (σ) of the detector for each analyte and the slope (S) of each calibration curve. These parameters have been calculated according to equations: $LOD = 3.3 \sigma/S$ and $LOQ = 10 \sigma/S$ [24].

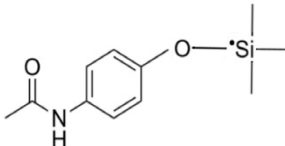
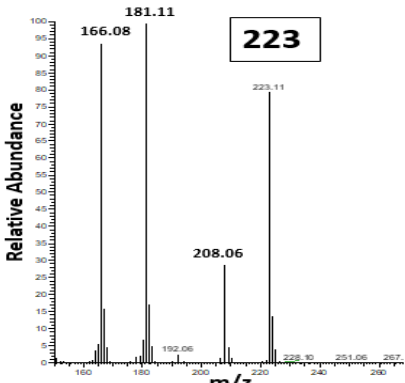
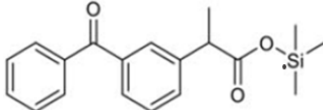
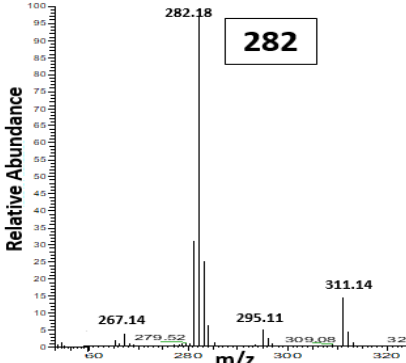
HPLC-PDA method. Linearity (correlation coefficient, R^2) of the method was tested for the concentrations of the studied pharmaceuticals from 10 to 0.25 mg/L. The developed method has good linearity with R^2 over 0.9969, low LODs and LOQs instrument limits in the range of $\mu\text{g/L}$, and relative standard deviation (RSD) below 3%. If we consider that, the pre-concentration factor of the method is 250, the obtained method detection and quantification limits (MDL, MQL) are in the range of ng/L (Table 2).

GC-MS-SIM method. Due to their polarity and instability at high temperature NSAIDs and PARA can be usually analysed by GC only as trimethylsilyl (TMS) derivative compounds. The TMS derivatives molecular formula, molecular ion mass and mass spectra are given in Table 3.

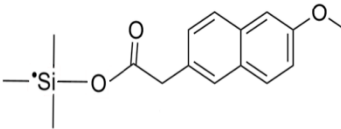
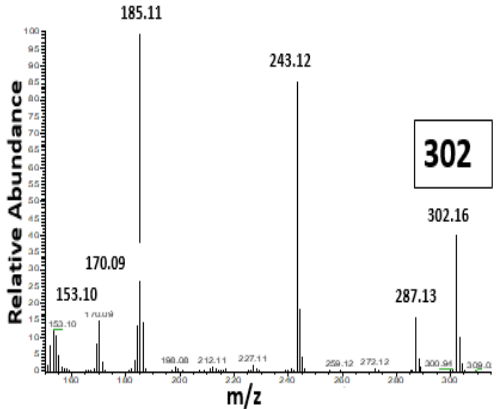
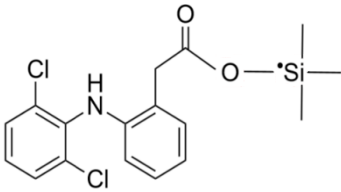
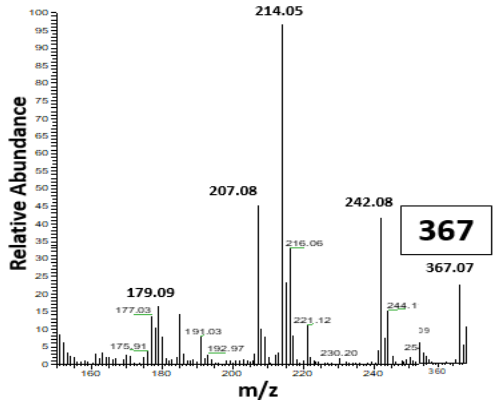
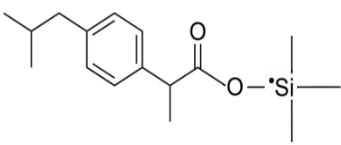
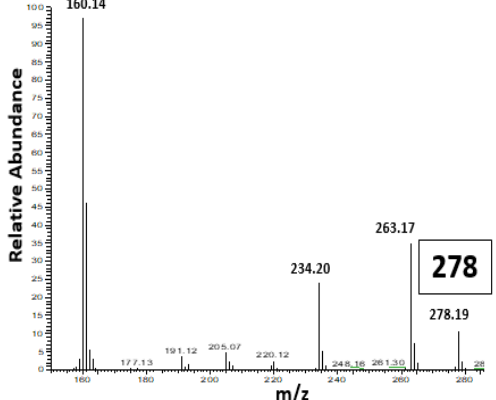
Table 2. Performances of HPLC-PDA method

Analyte	Equation	R ²	SD	Instrument limits		Method limits		Intra-day RSD (%)	Inter-day RSD (%)
				LOD (µg/L)	LOQ (µg/L)	MDL (ng/L)	MQL (ng/L)		
PARA	389956x + 24633	0.9980	1774.6	20	50	80	200	0.89	1.90
KET	79873x - 9553	0.9987	429.2	20	50	80	200	1.30	1.57
NAP	323343x - 12731	0.9984	2545.3	30	80	120	320	1.72	1.99
DIC	158932x - 57580	0.9969	602.3	10	40	40	160	1.76	3.19
IBU	219937x - 54428	0.9969	2019.7	30	90	120	360	2.15	2.82

Table 3. Chemical structure and mass spectra of selected pharmaceutical TMS derivatives

Chemical structure of selected pharmaceutical TMS derivative	Mass spectrum and mass of selected molecular ion
<p>1</p>  <p>TMS Paracetamol</p>	<p>2</p> 
 <p>TMS Ketoprofen</p>	

HPLC-PDA *VERSUS* GC-MS IN THE ANALYSIS OF PARACETAMOL AND NON-STEROIDAL ANTI-INFLAMMATORY DRUGS IN WASTEWATER

Chemical structure of selected pharmaceutical TMS derivative	Mass spectrum and mass of selected molecular ion
<p>1</p>  <p>TMS Naproxen</p>	<p>2</p>  <p>Mass spectrum showing Relative Abundance versus m/z. The base peak is at m/z 185.11. Other significant peaks are at m/z 243.12, 302.16, 170.09, 153.10, and 287.13. The molecular ion peak at m/z 302 is highlighted.</p>
 <p>TMS Diclofenac</p>	 <p>Mass spectrum showing Relative Abundance versus m/z. The base peak is at m/z 214.05. Other significant peaks are at m/z 242.08, 207.08, 179.09, 177.03, and 367.07. The molecular ion peak at m/z 367 is highlighted.</p>
 <p>TMS Ibuprofen</p>	 <p>Mass spectrum showing Relative Abundance versus m/z. The base peak is at m/z 160.14. Other significant peaks are at m/z 263.17, 234.20, and 278.19. The molecular ion peak at m/z 278 is highlighted.</p>

Linearity of the method was tested for the concentrations of the studied pharmaceuticals between 10 mg/L and 0.667 mg/L. Method has a good linearity with R over 0.9872, low LODs and LOQs instrument limits in the range of µg/L, but highest relative standard deviations (RSD) (4.91–12.68%) compared with LC-PDA method. If we consider that, the pre-concentration factor of the method is 5000, the obtained method detection and quantification limits (MDL, MQL) are in the range of ng/L (Table 4).

Table 4. Performances of GC-MS-SIM method

Analyte derivative	Equation	R ²	SD	Instrument limits		Method limits		Intra-day RSD (%)	Inter-day RSD (%)
				LOD (µg/L)	LOQ (µg/L)	MDL (ng/L)	MQL (ng/L)		
PARA-TMS	601089x-627380	0.9902	9097.62	50	150	10	30	5.21	4.91
KET-TMS	148494x-161316	0.9872	1399.07	30	90	6	18	8.08	9.09
NAP-TMS	71359x-59322	0.9925	3137.69	150	440	30	88	8.64	10.23
DIC-TMS	16370x-14843	0.9896	375.96	80	230	16	46	8.68	8.90
IBU-TMS	7831.8x-5449.2	0.9969	319.48	130	410	26	82	12.23	12.68

Table 5. Performance of some methods used for analysis of Paracetamol and NSAIDs in wastewater samples

Analyte	Extraction method	Analysis method	Sensitivity		Ref.
			MDLs (ng/L)	MQLs (ng/L)	
PARA, KET, NAP, DIC, IBU.	SPE (Strata-X)	GC-MS-SIM	PARA: 30 KET: 24 NAP: 10 DIC: 18 IBU: 9	PARA: 90 KET: 71 NAP: 25 DIC: 61 IBU: 22	[9]
PARA, KET, NAP, DIC, IBU.	SPE (Oasis HLB)	GC-MS-SIM	PARA: 7.6 KET: 87.4 NAP: 16.9 DIC: 52.9 IBU: 6.6	PARA: 22.4 KET: 257.1 NAP: 56.5 DIC: 158.7 IBU: 19.5	[17]
PARA, KET, NAP, DIC, IBU.	SPE (Strata-X)	GC-MS-SIM	PARA: 10 KET: 6 NAP: 30 DIC: 16 IBU: 26	PARA: 30 KET: 18 NAP: 88 DIC: 46 IBU: 82	This work
KET, NAP, DIC, IBU.	DLLME-SFO*	LC-UV	KET: 190 NAP: 75 DIC: 140 IBU: 180	KET: 590 NAP: 220 DIC: 420 IBU: 550	[19]
PARA, KET, NAP, DIC, IBU.	SPE (Strata-X)	LC-PDA	PARA: 80 KET: 80 NAP: 120 DIC: 40 IBU: 120	PARA: 200 KET: 200 NAP: 320 DIC: 160 IBU: 360	This work

* Dispersive-liquid-liquid microextraction-solidification floating organic droplet

By comparing our results with the results obtained by other authors worldwide it can be observed that the results are in the same range of sensitivity (Table 5).

Application to real wastewater samples

The two developed methods were applied to the analysis of the selected pharmaceuticals from samples collected in Romania, respectively in wastewater plants (Cluj-Napoca city; Țețchea and Diosig villages in Bihor county), as well as in septic tanks (Turulung and Terebești villages in Satu Mare county).

HPLC-PDA method. The chromatograms obtained were complex, with many different peaks, as it can be seen in Figure 4.

Unexpected compounds co-eluted with pharmaceuticals, making their quantification very difficult. Therefore, SPE-HPLC-PDA method is not suitable for the target pharmaceuticals in wastewater samples.

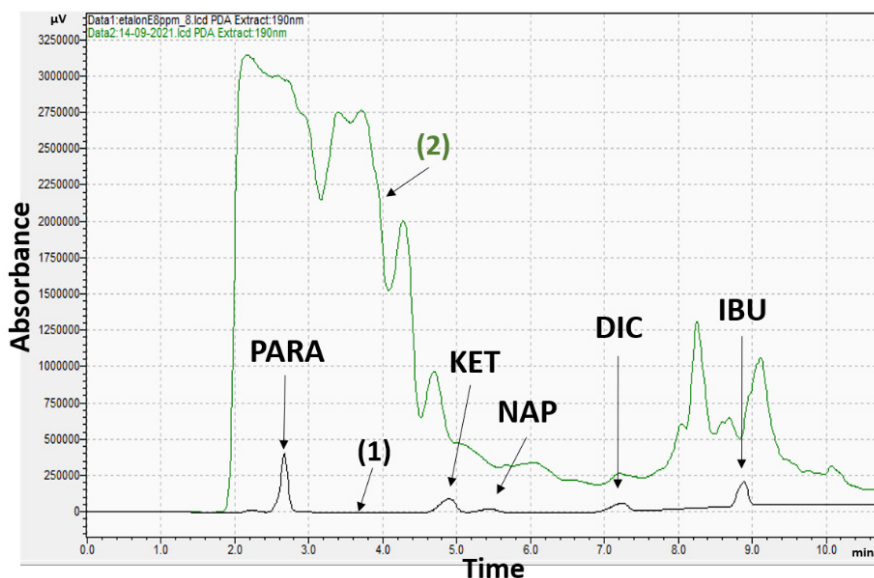


Figure 4. HPLC-PDA chromatograms of studied pharmaceuticals: standards in distilled water (1, black) and wastewater sample (2, green)

GC-MS-SIM method. The selected ion monitoring mode (SIM) allowed the identification of all five pharmaceuticals (Paracetamol, Ketoprofen, Naproxen, Ibuprofen and Diclofenac) as TMS derivatives in wastewater samples (Figure 5).

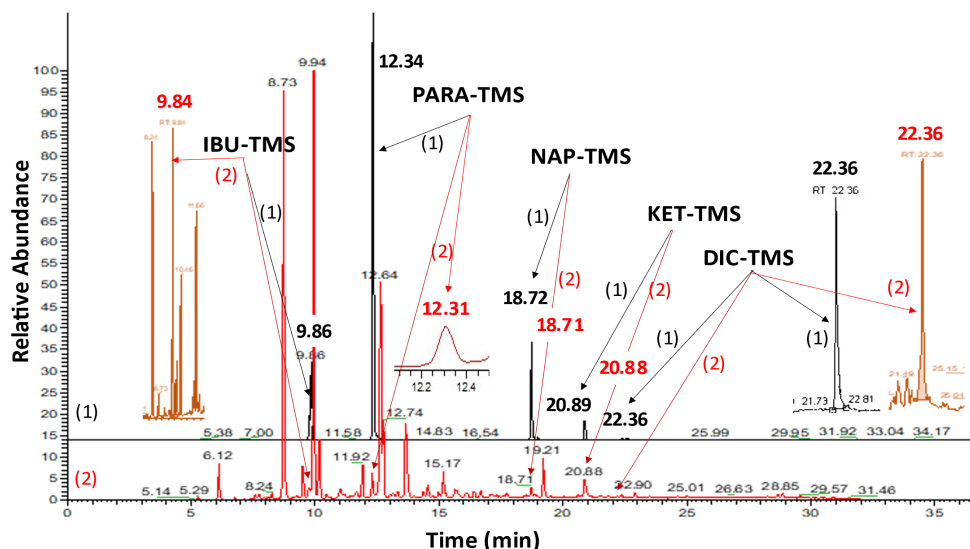


Figure 5. GC-MS-SIM chromatograms of derivatised pharmaceuticals: standard solution (1, black) and wastewater sample (2, red). Details: IBU-TMS (2, red) and PARA-TMS (2, red) in wastewater sample; DIC-TMS in standard solution (1, black) and in wastewater sample (2, red)

The results of analysed wastewater samples showed the presence of the selected compounds in concentration ranged from nd–224.11 ng/L for PARA, from nd–2705.1 ng/L for KET, from nd–1743.4 ng/L for NAP, from nd–16967.8 ng/L for DIC, and from nd–2436.7 ng/L for IBU (Table 6).

Table 6. The concentration of the selected pharmaceuticals in the analysed wastewater samples

Wastewater samples	Found concentration (ng/L)				
	PARA	KET	NAP	DIC	IBU
Cluj-Napoca*	123.19–224.11	567.24–2705.1	440.03–1743.4	351.97–16967.8	1712.26–2436.7
Tețchea*	59.44	318.46	<MQL	68.64	246.82
Diosig*	nd	1986.95	nd	nd	nd
Terebești**	nd	163.61	121.89	89.43	<MQL
Turulung**	nd	nd	nd	nd	nd

*Wastewater treatment plant; **Wastewater from septic tank.

In the samples collected from the wastewater treatment plant, the highest concentrations of the studied pharmaceuticals were found in Cluj-Napoca, while only Ketoprofen was found in Diosig. In the samples collected

from the septic tanks, Ketoprofen, Naproxen and Diclofenac were found in Terebești, while no studied compound was detected in Turulung. Their presence in the septic tank shows their stability during the time and common use of them. Our obtained results are comparable with other studies performed worldwide (Table 7).

Table 7. The concentration of the selected pharmaceuticals analyzed worldwide in wastewater

Analyte (ng/L)					Country	Ref.
PARA	KET	NAP	DIC	IBU		
530.2	nd*	240.0	263.5	280.0	Poland	[6]
7219	4569	7040	2902	6722	Poland	[9]
41.3; 69.1	nd	51.5; 93.8	31.5; 54.6	128.1; 131.5	China	[10]
<MDL	<MDL	240	460	280	Poland	[17]
nd	102–16000	96–35000	47–274	50–150000	Spain	[20]
nd – 224.11	nd – 2705.1	nd – 1743.4	nd – 16967.8	nd – 2436.7	Romania	**

*nd – not detected; **All samples of this work.

CONCLUSIONS

The best recovery for all the pharmaceuticals was obtained by solid-phase extraction on Strata X cartridges.

The GC-MS analysis performed in SIM mode improves the sensitivity and selectivity of the method allowing the simultaneous determination of Paracetamol, Ketoprofen, Naproxen, Ibuprofen and Diclofenac as trimethylsilyl derivatives at ng/L level.

In the analyzed wastewater samples, the concentration of the studied pharmaceuticals range from not detected to hundreds/thousands ng/L depending of the collection point.

The selected pharmaceuticals were found in wastewater samples collected from both sewage systems and septic tanks.

The obtained results show the importance of developing more selective extraction methods as well as the use of detectors of higher selectivity, sensitivity, and specificity for a better quantification of the studied pharmaceuticals in low amounts, even at trace/ultratrace level in wastewaters.

EXPERIMENTAL SECTION

Chemicals

Paracetamol and NSAID standards (>98% purity; Ibuprofen, Ketoprofen, Naproxen, Diclofenac sodium salt) were purchased from Sigma-Aldrich (Steinheim, Germany). The derivatisation agent *N,O*-bis(trimethylsilyl)trifluoroacetamide (BSTFA) with 1% trimethylchlorosilane (TMCS) was purchased from Cerilliant (Texas, USA). Strata X (200 mg/6 mL), Strata C18-U (200 mg/3 mL) and Strata C18-E (200 mg/3 mL) cartridges were purchased from Phenomenex (Torrance, USA). Chromatographic grade solvents (methanol, acetonitrile, *n*-hexane, ethyl acetate, isopropanol), hydrochloric acid (30%), sodium sulphate, and monopotassium phosphate of analytical grade were supplied from Merck (Darmstadt, Germany).

Stock standard solutions of each individual pharmaceutical at 1000 mg/L concentration were prepared in acetonitrile, except diclofenac prepared in methanol. All solutions were stored at 4°C in the dark.

Instrumentation and analytical procedures

Resprep 12 Manifold equipped with Rocker 500 Vacuum Pump (Restek, USA) instrument was used for SPE and Hei-VAP Core evaporator (Heidolph, Germany) for solvent evaporation. The derivatisation of the studied pharmaceuticals was performed with BSTFA with 1% TMCS in a lab oven Memmert UFE 400 (Mettler, Germany).

HPLC analyses were carried out with a LC equipment (SLC-40D) with a photodiode detector (SPD-M40) (Shimadzu, Japan). Instrument control and data acquisition was done with LabSolution software (Shimadzu, Japan). The studied pharmaceuticals were separated on a column Luna C18 (250 x 4.6 mm, 5 µm) (Phenomenex, USA) with a flow rate of 1.0 mL/min at 40°C oven temperature. The injection volume was 20 µL. The gradient elution (acetonitrile and 15 mM aqueous monopotassium phosphate solution) programme was 55% acetonitrile for 4 min, increasing to 83% in 2 min and then held at 83% for 4 min. The specific wavelengths of pharmaceuticals studied using PDA were: Paracetamol – 194 nm, Ketoprofen – 256 nm, Naproxen – 230 nm, Diclofenac – 200 nm, and Ibuprofen – 190 nm.

GC-MS analyses were performed on a Focus GC instrument equipped with DSQ II mass spectrometer (single quadrupole) controlled by a computer running XCalibur software and TriPlus Autosampler (Thermo

Electron Corporation, USA). Column: TR-5MS (30 m x 0.25 mm i.d., 0.25 μ m film thickness; Thermo Fisher Scientific, USA); the carrier gas was Helium (purity 99.999%) at a flow rate of 1.2 mL/min. The column temperature was initially set at 120°C, and then raised with 5°C/min to 275°C, with 1 min hold up time. The GC injection port and transfer line temperatures were kept at 280°C. The mass spectrometer worked in the electron impact mode (70 eV; ion source temperature, 200°C) by scanning from 150 to 400 m/z to obtain full spectra of the studied pharmaceuticals. Their quantification was performed by selected ion monitoring (SIM) mode and comparison of relative retention times.

Our pharmaceuticals were analysed as derivative compounds. Their derivatisation protocol was done with 100 μ L BSTFA with 1% TMCS, for 1h at 100°C, followed by cooling and evaporation under a gentle nitrogen stream and dissolution of the residue extract in 100 μ L of *n*-hexane.

Analysis of studied pharmaceuticals from water samples

Liquid-liquid extraction. A volume of 100 mL of distilled water was introduced in a separation funnel, spiked with 100 μ g of each pharmaceutical, and acidified at pH 3 with hydrochloric acid 30%, followed by the addition and dissolution of 5 g of NaCl salt. The obtained solution was subjected to LLE with 10 mL of solvent extraction (ethyl acetate or *n*-hexane-isopropanol, 3:2 v/v) for 5 min, followed by the separation of funnel content in two phases. This extraction procedure was repeated three times with fresh solvent and the three organic phases were collected, combined and dried with anhydrous sodium sulphate. Then, the extract was evaporated by a rotary evaporator, and finally the residue was dissolved in 2 mL of acetonitrile and analysed by HPLC-PDA.

Solid-phase extraction. Three types of SPE cartridges (C18-U, C18-E and Strata X) were tested. First, they were successively preconditioned with 6 mL of each: distilled water, acetonitrile, and distilled water again. Then, distilled water samples of 100 mL were each spiked with 100 μ g of each pharmaceutical acidified (pH 3), and then passed through the named cartridges at a flow rate of approximately 1 mL/min. Subsequently, the cartridges were dried for 20 minutes under vacuum and then eluted by 4 mL acetonitrile. Each extract was evaporated to near dryness under a gentle stream of nitrogen and then redissolved with 2 mL of acetonitrile for HPLC-PDA analysis.

These two extraction protocols were used to study the extraction recovery of the selected pharmaceuticals from the synthetic water samples.

Analysis of pharmaceuticals from wastewater samples

500 mL of each wastewater sample were acidified at pH 3 with HCl 30%, centrifuged for 5 min at 4000 rot/min to separate the solid particles, and then filtered on 1.6 µm glass fibre filter (Fioroni, France) to remove the smaller particles. Each sample was passed through a Strata X cartridge preconditioned as mentioned before and dried for 20 min under vacuum. The pharmaceuticals of each cartridge were eluted with 4 mL of acetonitrile. Each obtained extract was evaporated under a gentle nitrogen stream.

For HPLC-PDA analysis the residue was dissolved in 2 mL of acetonitrile.

For the GC-MS analysis, the obtained extracts were derivatised as the protocol described previously.

ACKNOWLEDGMENTS

This work was performed in the framework of doctoral studies from the Babeş-Bolyai University, Environmental Science Doctoral School and ESPCI Student Internship at Babeş-Bolyai University. The research leading to these results has received funding from the Norway Grants 2014-2021 under Project contract no. 23 / 2020 (RO-NO-2019-0463). The authors are grateful to Someş Water Company S.A. Cluj-Napoca and also to the public authorities from Terebeşti, Turulung, Ţeţchea and Diosig for providing the wastewater samples.

REFERENCES

1. A. Azzouz; E. Ballesteros; *Sci. Total Environ.*, **2012**, *419*, 208-215.
2. H. Montaseri; P. B. C. Forbes; *TrAC.*, **2018**, *108*, 122-134.
3. T. Mackulak; S. Cernanský; M. Fehér; L. Birosová; M. Gál; *Curr. Opin. Environ. Sci.*, **2019**, *9*, 40-48.
4. S. Esteban; Y. Valcárcel; M. Catalá; M. G. Castromil, *Gac. Sanit.*, **2012**, *26(5)*, 457-459.
5. T. Kosjek, E Heath, A Krbavcic, *Environ. Int.*, **2005**, *31*, 679-685.
6. J Kumirska; A. Plenis; P. Łukaszewicz; M. Caban, N. Migowska; A. Białk-Bielinska, M. Czerwicka; P. Stepnowski; *J. Chromatogr. A*, **2013**, *1296*, 164-178.

7. C. H. Lee; Y. Shin; M. W. Nam; K. M. Jeong; J. Lee, *Talanta*, **2014**, *129*, 552-559.
8. P. Stepnowski; D. Wolecki; A. Puckowski; M. Paszkiewicz; M. Caban; *Sci. Total Environ.*, **2020**, *745*, 140848.
9. M. Caban; K. Mioduszezewska; P. Łukaszewicz; N. Migowska; P. Stepnowski; M. Kwiatkowski; J. Kumirska; *J. Chromatogr. A*, **2014**, *1346*, 107-116.
10. J. Yan; W. Lin; Z. Gao; Y. Ren; *Chemosphere*, **2021**, *279*, 130529.
11. H. Montaseri; P. B. C. Forbes; *TrAC.*, **2018**, *108*, 122-134.
12. K. Wieszczycka; J. Zembrzuska; J. Bornikowska; A. Wojciechowska; I. Wojciechowska; *Chem. Eng. Res. Des.*, **2017**, *117*, 698-705.
13. J. C. G. Sousa; A. R. Ribeiro; M. O. Barbosa; M. F. R. Pereira; A. M. T. Silva, *J. Hazard. Mater.*, **2018**, *344*, 146-162.
14. Y. Chen; Z. Guo; X. Wang; C. Qiu; *J. Chromatogr. A*, **2008**, *1184*, 191-219.
15. L. Nováková; H. Vlcková; *Anal. Chim. Acta*, **2009**, *656*, 8-35.
16. X. Chen; X. Wu; T. Luan; R. Jiang; G. Ouyang; *J. Chromatogr. A*, **2021**, *1640*, 461961.
17. N. Migowska; M. Caban; P. Stepnowski; J. Kumirska; *Sci. Total Environ.*, **2012**, *441*, 77-88.
18. B. Huidobro-López; I. López-Heras; C. Alonso-Alonso; V. Martínez-Hernández; L. Nozal; I. de Bustamante; *J. Chromatogr. A*, **2022**, *1671*, 463006.
19. M. S. Beldean-Galea, R. Klein, M.-V. Coman; *J. AOAC Int.*, 2020, 392-398.
20. T. Martinez-Sena; S. Armenta; M. de la Guardia; F. A. Esteve-Turrillas; *J. Pharm. Biomed. Anal.*, **2016**, *131*, 48-53
21. J. L. P. Pavón; A. M. C. Ferreira; M. E. F. Laespada; B. M. Cordero; *J. Chromatogr. A*, **2009**, *1216*, 6728-6734
22. G. G. Noche; M. E. F. Laespada; J. L. P. Pavón; B. M. Cordero; S. M. Lorenzo; *J. Chromatogr. A*, **2011**, *1218*, 6240-6247.
23. B. Yilmaz; H. Sahin; A. F. Erdem; *J. Sep. Sci.*, **2014**, *37*, 997-1003.
24. International Committee on Harmonization, "Validation of Analytical Procedures: Text and Methodology, Q2(R1), Nov. 2005.
https://www.ema.europa.eu/en/documents/scientific-guideline/ich-q-2-r1-validation-analytical-procedures-text-methodology-step-5_en.pdf
(Accessed December 2022).

KINETICS OF DAPAGLIFLOZIN 10 MG IMMEDIATE RELEASE TABLET IN HEALTHY CAUCASIAN VOLUNTEERS: DOES FOOD INTAKE AFFECT ITS DISPOSITION IN THE BODY?

Monica OROIAN^{a,b}, Ana-Maria VLASE^{c,*},
Adriana MARCOVICI^b, Laurian VLASE^a

ABSTRACT. The aim of the current study was to investigate whether food intake alters the kinetics of dapagliflozin, a modern anti-diabetic agent, after single-dose oral administration of a new 10 mg immediate release tablet. The evaluated formulation was developed and manufactured by Sun Pharmaceutical Industries Limited, India, and the studies were performed in healthy Caucasian subjects. The data obtained during the fasting and fed bioequivalence studies were analyzed to observe the influence of food on the bioavailability and disposition of the evaluated formulation. Although differences were observed between studies concerning some of the main parameters that describe dapagliflozin's disposition (maximum plasma concentration – C_{max} , and the time to reach it - T_{max}), they were proved bioequivalent. The 90% confidence intervals for the evaluated parameters were within the accepted range of 80.00-125.00% for bioequivalence conclusion, therefore the treatments are bioequivalent (dapagliflozin with/without food) and interchangeable. Hence, dapagliflozin can be administered regardless of food intake in diabetic patients.

Keywords: *dapagliflozin, kinetics, Caucasian volunteers, clinical trial, food intake*

^a "Iuliu Hatieganu" University of Medicine and Pharmacy, Faculty of Pharmacy, Department of Pharmaceutical Technology and Biopharmaceutics, 8 Victor Babes str., RO-400012, Cluj-Napoca, Romania

^b Terapia SA – a Sun Pharma Company, Department of Clinical Pharmacology and Pharmacokinetics, 124 Fabricii str., RO-400632, Cluj-Napoca, Romania

^c "Iuliu Hatieganu" University of Medicine and Pharmacy, Faculty of Pharmacy, Department of Pharmaceutical Botany, 23 Marinescu str., RO-400337, Cluj-Napoca, Romania

* Corresponding author: gheldiu.ana@umfcluj.ro



INTRODUCTION

Diabetes affects the lives of millions of people worldwide and represents a constant threat for people's health regardless of social class, region, or race. According to International Diabetes Federation (IDF) and World Health Organization (WHO) by 2045 is predicted that approximately 629.6 million people will be suffering from this condition. Along with cardiovascular disease and cancer, diabetes is one of the top 10 causes of global death [1-4].

In Europe, which according to IDF is the second region in deaths' prevalence caused by diabetes, around 700.000 deaths were reported before the age of 60 out of which 31.274 were recorded only in Romania [4]. In addition, it is estimated that there are more than 58 million people diagnosed with diabetes mellitus (DM) which represents 8.8% of the population from this region with age between 20-79 years old. However, the real silent threat is the alarming number of 22 million cases which remain undiagnosed. Another concern is that in Europe there are approximately 286.000 cases of type I diabetes (T1DM) in children and teenagers and almost 30.000 new cases are registered every year [4,5].

The sodium glucose co-transporter 2 (SGLT2) inhibitors represent a class of drugs which prevent glucose reabsorption from proximal tubules. Dapagliflozin along with canagliflozin and empagliflozin are the main representatives of the SGLT2 inhibitors class which improve both fasting and post-prandial plasma glucose levels [6-8]. These compounds decrease the blood sugar level by excretion of several grams of glucose in urine [9,10].

Dapagliflozin is known by its IUPAC name (2S,3R,4R,5S,6R)-2-{4-chloro-3-[(4-ethoxyphenyl)methyl]phenyl}-6-(hydroxymethyl)oxane-3,4,5-triol. It was classified as a Class III molecule according to Biopharmaceutical Classification system (BCS) as it has a high solubility and low permeability for which the regulatory recommends the conduct of bioequivalence studies under fasting and fed conditions [8,11,12].

Bioavailability is one of the most important properties of a drug defined as the ability to release the active substance so that it reaches the site of action in a sufficient amount to elicit the desired therapeutic effect. More precisely, bioavailability is the rate and extent of absorption of a drug substance from the pharmaceutical form into the systemic circulation [13,14].

As the bioavailability of a drug may be affected by the food intake it is very important to know the drug-food interactions as to increase the efficacy and safety of therapies. It is well known that food may affect the absorption of drugs after oral administration and therefore the active substance's bioavailability and kinetics in the body (also known as disposition) might be affected [15-17]. The type and amount of meal is very important, therefore the regulatory established

standardized conditions for the test meal to be administered in fed clinical studies. More precisely, the test meal must be high-fat, high-calorie (approximately 800-1000 Kcal) [12].

The present study aimed to evaluate the food effect on dapagliflozin's disposition by comparing the results obtained in two bioequivalence studies conducted on healthy Caucasian subjects after administration of the tested drug under fasting and fed conditions.

RESULTS AND DISCUSSION

Subjects

The demographic data of the healthy volunteers who were selected for the bioequivalence studies are shown in Table 1.

Table 1. Demographic characteristics of the subjects included in the studies

Characteristics	Reference period (fasting state)	Test period (fed state)
Number of subjects	38	33
Gender (number) – Men	26	24
– Women	12	9
Age (years) – mean (SD)	29.9 (7.61)	25.9 (5.19)
– range	18-45	18-40
BMI** (kg/m ²) – mean (SD)	23.85 (2.96)	23.28 (3.27)
– range	18.73-28.91	18.67-28.91

*SD – standard deviation; **BMI – body mass index

Kinetic analysis

Mean plasma concentration-time profiles of dapagliflozin from the reference product Farxiga® and from the test product developed by Sun Pharmaceutical Industries Limited, India, when given under fasting or fed state, are presented in Figure 1. For a better visual comparison of the bioavailability of dapagliflozin for reference and test product administered under fasting or fed condition of subjects, the mean plasma concentrations versus time profiles are depicted in Figures 2.

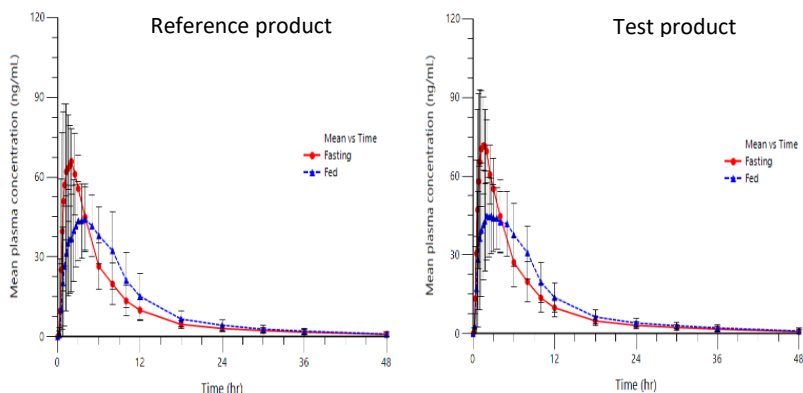


Figure 1. Mean \pm standard deviation (SD) plasma concentration-time curves of dapagliflozin (10 mg, p.o.) administered in fasting state (n=38; represented with red line) or fed state (n=33; represented with blue line) of the reference product Farxiga[®] and of the test product developed by Sun Pharmaceutical Industries Limited, India

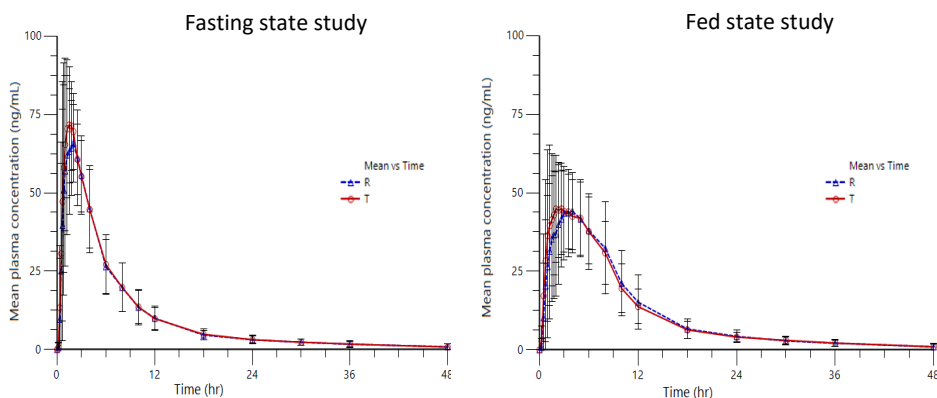


Figure 2. Mean plasma concentration profiles \pm standard deviation (SD) of dapagliflozin after administration of a 10 mg single dose under fasting and fed condition of the reference product Farxiga[®] (with blue line) and of the test product developed by Sun Pharmaceutical Industries Limited, India (with red line)

Table 2 summarizes the main pharmacokinetic (PK) parameters of dapagliflozin, given with or without food in healthy subjects. These parameters describe in detail the kinetics of dapagliflozin given as a single dose by oral administration route. They describe the disposition of the active substance in the body, more precisely they characterize the processes of absorption, distribution, metabolism, and elimination (ADME processes) [18,19].

KINETICS OF DAPAGLIFLOZIN 10 MG IMMEDIATE RELEASE TABLET IN HEALTHY CAUCASIAN VOLUNTEERS: DOES FOOD INTAKE AFFECT ITS DISPOSITION IN THE BODY?

Table 2. Summary of pharmacokinetic (PK) parameters of dapagliflozin after a single dose of 10 mg p.o. administered under fasting or fed state of subjects

PK parameter* (units)	Study period							
	Reference (fasting state)				Test (fed state)			
	Mean	SD	Median	CV%	Mean	SD	Median	CV%
C_{max} (ng/mL)	83.56	28.85	77.32	30.93	59.53	15.59	56.76	26.19
T_{max} (hr)	1.72	0.72	1.75	41.91	3.38	2.13	2.83	62.97
AUC_{0-t} (ng*hr/mL)	488.02	122.39	461.02	25.08	522.01	145.57	501.16	27.89
$AUC_{0-\infty}$ (ng*hr/mL)	491.47	120.30	464.96	24.48	526.05	144.30	508.47	27.43
K_{el} (hr ⁻¹)	0.06	0.03	0.05	49.73	0.07	0.03	0.07	44.34
$T_{1/2}$ (hr)	15.32	8.19	14.40	53.45	12.85	6.25	10.63	48.62
MRT (hr)	11.76	4.48	11.21	38.12	12.84	3.86	12.33	30.04
Cl _F (L/hr)	20.43	4.93	20.77	24.13	19.41	4.91	18.47	25.28
Vd _F (L)	428.69	198.09	391.50	46.21	346.31	157.12	323.48	45.37

*where C_{max} – maximum plasma concentration; T_{max} – time to reach C_{max} ; AUC_{0-t} – area under the plasma vs time curve from time 0 to last determined concentration; $AUC_{0-\infty}$ – area under the plasma vs time curve from time 0 to infinite; K_{el} – first order rate constant of elimination process; $T_{1/2}$ – half life time of given drug; MRT – mean residence time; Cl_F – apparent clearance; Vd_F – apparent volume of distribution

Statistical analysis

The bioequivalence analysis performed is summarized in Table 3. All evaluated pharmacokinetic parameters proved to be bioequivalent between fasting and fed study and therefore dapagliflozin can be administered regardless to food intake.

Table 3. Bioequivalence evaluation of the main PK parameters of dapagliflozin for the fasting and fed clinical trials

Study	Dependent	Units	CI_90_Lower	CI_90_Upper	Ratio_%Ref_	Bioequivalence conclusion*
Fasting	Ln(C_{max})	ng/mL	96.08	115.13	105.17	Bioequivalent
	Ln(AUC_{0-t})	ng*hr/mL	101.02	105.31	103.14	Bioequivalent
	Ln($AUC_{0-\infty}$)	ng*hr/mL	101.19	105.40	103.27	Bioequivalent
	T_{max}	hr	Non-parametric Friedman test			Bioequivalent
Fed	Ln(C_{max})	ng/mL	95.93	112.01	103.66	Bioequivalent
	Ln(AUC_{0-t})	ng*hr/mL	98.84	103.93	101.35	Bioequivalent
	Ln($AUC_{0-\infty}$)	ng*hr/mL	99.05	103.96	101.48	Bioequivalent
	T_{max}	hr	Non-parametric Friedman test			Bioequivalent

*Bioequivalent if Ratio_%Ref_ is in the range 80-125.

Table 4 presents the statistical analysis of the main pharmacokinetic parameters evaluated during both studies. The differences were assessed by using the analysis of variance (ANOVA test) and were considered statistically significant for p value less than 0.05 ($p < 0.05$).

Table 4. Statistical analysis results of mean pharmacokinetic (PK) parameters comparison between Reference period (fasted state) and Test period (fed state) for dapagliflozin

PK parameter	Units	F_stat ^a	p_value ^b
C_{max}	ng/mL	57.47	<0.01
AUC_{0-t}	ng*hr/mL	2.18	0.142
AUC_{0-∞}	ng*hr/mL	2.29	0.132
K_{el}	hr ⁻¹	4.60	0.033
T_½	hr	4.60	0.033
MRT	hr	4.55	0.034
Cl_F	L/hr	1.58	0.211
Vd_F	L	8.96	0.003
T_{max}	hr	Friedman	NS ^c

^aF_stat – statistic factor; ^b $p < 0.05$ statistically significant; ^cNS – statistically non-significant

The adverse events reported by subjects during the bioequivalence clinical trials were carefully monitored and registered. They included increased triglycerides, increased aspartate aminotransferase (AST), increased total bilirubin, vaso-vagal reaction, diarrhea syndrome, and leukocyturia among other side effects. The summary of the adverse events by study period and treatment group are presented in Table 5. None of the reported adverse events posed a threat for the health of the volunteers, neither led to dropout events [15,16].

Table 5. Summary of adverse events reported during both clinical trials

Reported adverse events after dapagliflozin 10 mg administration p.o.	
Reference period (fasting state, 38 subjects)	Test period (fed state, 33 subjects)
- Increased triglycerides	- Vaso-vagal reaction
- Leukocyturia	- Diarrheal Syndrome
- Increased AST	- Vomiting
- Increased total bilirubin	- Increased triglycerides
- positive nitrites in urine	- Leukocyturia
- Decreased platelet.	- Urinary infection
- Leucocytosis	- Haematuria

Drug-food interactions, similar to kinetic drug-drug interaction, can modify a drug's disposition in the body [20-22]. If the later are evaluated as part of post-marketing safety evaluation, the first are investigated prior to market release [23-25]. Food intake may increase or decrease the rate of absorption of a drug product as the content of the meal and ingested amount can change the gastrointestinal transit time and permeability of the drug. The food influences the gastrointestinal motility, the digestive secretions and therefore modifies the bioavailability of the drugs, which can further influence the response to treatment [1,16,26]. Thus, the assessment of interaction between food and drugs represents an important part of development and manufacturing of orally administrated drugs [1,12,13,16,26,27].

Decreased absorption may reduce the efficacy of treatment as in the blood stream will arrive a lower amount from the active substance, while increased absorption may cause adverse reactions. On the other hand, in some cases, food may increase the rate and amount of absorption of an active substance; thus, certain drugs are indicated to be taken after food ingestion. Therefore, it is important to establish the food-effect on the rate and extend of drugs' absorption before concluding the mode of administration [28-31].

The present research aimed to investigate the bioavailability of dapagliflozin and determine the pharmacokinetic parameters after oral administration of 10 mg immediate release formulation under fasting and fed conditions in healthy Caucasian subjects, males and females. The generic product was developed and manufactured by Terapia SA – a Sun Pharma Company and the clinical trials were conducted at the Clinical Pharmacology and Pharmacokinetics Department of Terapia SA, Cluj-Napoca, Romania.

After administration of test and reference product under fasting condition it was observed that the C_{max} (83.56 ± 28.85 ng/mL) was achieved within approximately 2 hours ($T_{max} = 1.72 \pm 0.72$ hours). In comparison, after the administration of the two investigational medicinal products (IMP) under fed conditions the mean value for C_{max} was 59.53 ± 15.59 ng/mL and T_{max} was achieved within approximately 3 hours (3.38 ± 2.13 hours). After food ingestion, the C_{max} decreased with ~28%, whereas T_{max} increased with 96.5%, most probably due to prolonged gastrointestinal transit time. Also, the permeability of dapagliflozin might be affected by food composition, as it belongs to class III according to BCS. Its solubility is high, but the permeability along the gastrointestinal tract is low and the administered food in the fed study was high-fat and high-calorie, as specified by regulatory agencies which validate the guidelines for this type of clinical trials [12]. However, the bioequivalence was concluded for both PK parameters, with parametric or non-parametric tests (see Table 3).

Even though the difference for T_{max} was statistically significant between studies (see Table 4), regulatory guidelines specify it is not clinically relevant [12].

After comparing the mean values obtained for AUC_{0-t} under fasting conditions (488.02 ± 122.39 ng*hr/mL) with the results obtained for AUC_{0-t} after administration of the IMP under fed conditions (522.01 ± 145.57 ng*hr/mL) it was noticed an increase of ~7% which resulted not statistically significant as the p -value was greater than 0.05 (p -value=0.142). A similar increase was observed for $AUC_{0-\infty}$, which also proved to be without statistical significance. Therefore, the bioequivalence was concluded for these PK parameters as well. The total area under the plasma concentration profile versus time is a good indicator of a patient's exposure to a given drug. In this case, the mean plasma concentration profiles of dapagliflozin after administration of a 10 mg single dose under fasting and fed condition of the reference product Farxiga® and of the test product developed by Sun Pharmaceutical Industries Limited, India, were almost superposable, with very small differences (see Figure 2), thus confirming the similar values obtained for AUC_{0-t} and $AUC_{0-\infty}$ in both clinical studies.

The other evaluated PK parameters displayed minor differences between fasting and fed studies. The ANOVA results indicated non-statistical significance of differences for K_{el} , $T_{1/2}$, MRT, Cl_F , and Vd_F (see Table 4). Also, the 90% confidence intervals for these parameters were within the accepted range for bioequivalence, which is 80.00-125.00% (see Table 3).

Similar to these results, no food effect was observed after oral administration of gliclazide, a sulfonylurea medicine also given in DM type 2 [1]. Bioequivalence was proved after statistical analysis of data obtained in two clinical trials conducted on healthy Caucasian subjects, under fasting and fed condition, in which the test product Gliclazide MR developed by Sun Pharmaceutical Industries, India, was evaluated in comparison with the reference product Diamicon MR (Servier, France) [32,33]. A decreased exposure to gliclazide after high-calorie, high-fat meal was observed, as the C_{max} registered a 14% decrease and the $AUC_{0-\infty}$ decreased with 17%. The T_{max} was shortened under fed conditions of subjects with approximately 2% and the K_{el} were comparable, regardless to food intake. However, the minor differences were not statistically significant, and the bioequivalence was concluded for gliclazide, administered with or without food, as in the case of dapagliflozin.

Generic drugs approved on the pharmaceutical market after bioequivalence clinical trials can ease the financial burden of diabetic patients, considering that other comorbidities are associated with DM type 2 which imply complex therapeutic approach with considerable costs.

CONCLUSIONS

The administration of immediate release formulation containing 10 mg dapagliflozin developed by Sun Pharmaceutical Industries, India, was proved bioequivalent with Farxiga[®], AstraZeneca (reference product) in healthy adult Caucasian subjects, males and females, under fasting and fed conditions.

Differences were observed for certain PK parameters, but they were not statistically significant for the two investigational medicinal products and food intake did not affect the overall amount and rate of absorption of dapagliflozin. Therefore, the test and reference product were concluded to be interchangeable and can be administered with or without food in diabetic patients.

EXPERIMENTAL SECTION

Subjects: The data obtained from two bioequivalence studies were considered for evaluation of food effect on the pharmacokinetic profile of dapagliflozin. In the first study were included 38 healthy volunteers and was performed under fasting condition, while in the second study was performed under fed condition, 33 healthy volunteers were selected. Therefore, the presented data correspond to 71 adult subjects, males and females, enrolled in both clinical trials [8,15,16].

The bioequivalence clinical trials were carried out in accordance with the Basic Principles defined in US 21 CFR Part 320, the ICH E6 (R1) (CPMP/ICH/135/95) 'Guideline for Good Clinical Practice' and the principles of the Declaration of Helsinki. The study protocols were approved by the National Agency for Medicines and Medical Devices and Bioethics National Committee of the Medicines and Medical Devices, Romania. Prior to any screening procedures, the volunteers gave their written informed consent for participation in studies. Only healthy subjects who filled all inclusion criteria were further admitted. The two clinical trials were carried out at Clinical Pharmacology and Pharmacokinetics Department of Terapia SA, Romania.

Study design and protocol: Both studies were designed as open-label, balanced, crossover, randomized, single-dose, with two periods. The test product (generic) was developed by Sun Pharmaceutical Industries Limited, India, and the reference product was Farxiga[®] (dapagliflozin) tablets

10 mg manufactured by AstraZeneca Pharmaceuticals, USA. It was defined as test data the results obtained in the fed bioequivalence study and as reference data the results obtained from the fasting study [8,15,16].

For both studies, the washout period between administration of reference and generic product was 7 days to ensure the complete elimination of drugs between study periods and to reduce the risk of carry over effect [15,16].

For the fasting study the blood samples were collected before the administration of drug and at 0.167, 0.33, 0.5, 0.66, 0.83, 1, 1.25, 1.5, 1.75, 2, 2.5, 3, 4, 6, 8, 10, 12, 18, 24, 30, 36 and 48 hours after drug administration [15].

For the fed study the blood samples were collected before the administration of drug and at 0.25, 0.5, 0.75, 1, 1.25, 1.5, 1.75, 2, 2.33, 2.67, 3, 3.5, 4, 5, 6, 8, 10, 12, 18, 24, 30, 36 and 48 hours post-dose [16].

Drug analysis from plasma samples: The total volume of blood collected from each subject during both studies did not exceed 260 mL, including the volume drawn at screening, at the end of study and additional blood collected due to out-of-range laboratory results [15,16].

The collected blood samples were centrifuged at 4000 rpm for 15 minutes under refrigeration at a set temperature of 4°C. The separated plasma was kept at -50°C until analysis [15,16].

A validated HPLC-MS method was used to determine dapagliflozin plasma concentrations [8,15,16].

Pharmacokinetic and statistical analysis: The pharmacokinetic parameters of dapagliflozin during the performed studies were calculated by a non-compartmental analysis method, using Phoenix WinNonlin® version 6.3 (Certara, USA). The statistical analysis of differences registered for PK parameters from both clinical studies was performed with ANOVA test. In addition, the bioequivalence of dapagliflozin treatment given under fasted or fed state of subjects was assessed to highlight the influence of food-intake on the pharmacokinetic profile of the active substance. The analysis was performed as previously detailed [15,16].

Safety evaluation: Throughout both study periods of the fasting and fed bioequivalence studies the safety evaluation was performed, and the summary of adverse events reported are provided in Table 5.

REFERENCES

1. D. Pop; A.-M. Gheldiu; M. Oroian; A. Marcovici; S. Bhardwaj; A. Khuroo; R. Kochhar; L. Vlase; *Acta Med Marisiensis*, **2018**, *64*, 161-168.
2. M.B. Gomes; W. Rathmann; B. Charbonnel; K. Khunti; M. Kosiborod; A. Nicolucci; S.J. Pocock; M.V. Shestakova; I. Shimomura; F. Tang; H. Watada; H. Chen; J. Cid-Ruzafa; P. Fenici; N. Hammar; F. Surmont; L. Ji; *Diabetes Res Clin Pract*, **2019**, *151*, 20-32.
3. A.E. Caballero; *Front Endocrinol (Lausanne)*, **2018**, *9*, 479.
4. International Diabetes Federation (IDF) Diabetes Atlas, 10th edition, 2021. Available at: <https://diabetesatlas.org/data/en/region/3/eur.html>
5. Global Reports on Diabetes, World Health Organization, 2016, ISBN: 978 92 4 156525 7. Available at: <https://www.who.int/publications/i/item/9789241565257>
6. M.A. Abdul-Ghani; R.A. DeFronzo; *Expert Opin Pharmacother*, **2013**, *14*, 1695-1703.
7. M. Isaji; *Kidney Int*, **2011**, *79*, S14-S19.
8. M. Oroian; A. Marcovici; D. Pop; S. Bhardwaj; A. Khuroo; A.-M. Gheldiu; L. Vlase; *Studia UBB Chemia*, **2019**, *LXIV*, 297-308.
9. Y. Tamura; H. Miyagawa; T. Yoshida; H. Chuman; *Biochim Biophys Acta*, **2015**, *1848*, 2799-2804.
10. A. Tahara; T. Takasu; M. Yokono; M. Imamura; E. Kurosaki; *J Pharmacol Sci*, **2016**, *130*, 159-69.
11. R.Z.C. de Meira; A.B. Maciel; F.S. Murakami; P.R. de Oliveira; L.S. Bernardi; *Int J Anal Chem*, **2017**, *2017*, 2951529.
12. Guidance for industry. Food-effect Bioavailability and Fed Bioequivalence Studies. 2002. Available at: <https://www.fda.gov/downloads/drugs/guidancecomplianceregulatoryinformation/guidances/ucm070241.pdf>
13. S.C. Chow; *Wiley Interdiscip Rev Comput Stat*, **2014**, *6*, 304-312.
14. A. Mateus; A. Treyer; C. Wegler; M. Karlgren; P. Matsson; P. Artursson; *Sci Rep*, **2017**, *7*, 43047.
15. M. Oroian; D.I. Pop; A.-M. Gheldiu; S. Bhardwaj; A. Marcovici; A. Khuroo; L. Vlase; *Acta Med Marisiensis*, **2020**, *66*, 30-34.
16. M. Oroian; D.I. Pop; A.-M. Gheldiu; S. Bhardwaj; A. Marcovici; A. Khuroo; L. Vlase; *Farmacia*, **2020**, *68*, 76-81.
17. D.I. Pop; A. Marcovici; M. Oroian; A.-M. Gheldiu; L. Vlase; *Studia UBB Chemia*, **2020**, *LXV*, 187-196.
18. A.-M. Gheldiu; A. Csavdari; M. Achim; L. Vlase; I. Tomuța; D. Muntean; *Studia UBB Chemia*, **2017**, *LXII*, 179-188.
19. A.-M. Gheldiu; D.M. Muntean; I. Cristea; I. Antonescu; R. Chira; C. Ureche; L. Vlase; *Rev Chim (Bucharest)*, **2016**, *67*, 702-705.
20. C. Briciu; M. Neag; D. Muntean; L. Vlase; C. Bocsan; A. Buzoianu; A.-M. Gheldiu; M. Achim; A. Popa; *J Clin Pharm Ther*, **2014**, *39*, 535-540.

21. A.-M. Gheldiu; A. Popa; M. Neag; D. Muntean; C. Bocsan; A. Buzoianu; L. Vlase; I. Tomuta; C. Briciu; *Pharmacology*, **2016**, *98*, 190-198.
22. I. Todor; A. Popa; M. Neag; D. Muntean; C. Bocsan; A. Buzoianu; L. Vlase; A.-M. Gheldiu; C. Briciu; *J Pharm Pharm Sci*, **2016**, *19*, 198-207.
23. A.-M. Gheldiu; L. Vlase; A. Popa; C. Briciu; D. Muntean; C. Bocsan; A. Buzoianu; M. Achim; I. Tomuta; I. Todor; D. Leucuta; M. Neag; *J Pharm Pharm Sci*, **2017**, *20*, 68-80.
24. A.-M. Gheldiu; D.M. Muntean; M. Neag; A. Popa; C. Briciu; L. Vlase; *Studia UBB Chemia*, **2019**, *LXIV*, 153-162.
25. A.-M. Gheldiu; A. Popa; M. Neag; D. Muntean; C. Bocsan; A. Buzoianu; L. Vlase; M. Achim; I. Todor; C. Briciu; *Farmacia*, **2015**, *63*, 453-459.
26. M. Koziolk; F. Carrière; C.J.H. Porter; *Pharm Res*, **2018**, *35*, 55.
27. P.G. Welling; *Annu Rev Nutr*, **1996**, *16*, 383-415.
28. M. Li; P. Zhao; Y. Pan; C. Wagner; *CPT Pharmacometrics Syst Pharmacol*, **2018**, *7*, 82-89.
29. Y. Kawai; Y. Fujii; F. Tabata; J. Ito; Y. Metsugi; A. Kameda; K. Akimoto; M. Takahashi; *Drug Metab Pharmacokinet*, **2011**, *25*, 180-191.
30. K. Sugano; M. Kataoka; C.C. Mathews; S. Yamashita; *Eur J Pharm Sci*, **2010**, *40*, 118-124.
31. A. Karim; M. Slater; D. Bradford D; L. Schwarts; A. Laurent; *J Clin Pharmacol*, **2007**, *47*, 48-55.
32. D.I. Pop; M. Oroian; S. Bhardwaj; A. Marcovici; A. Khuroo; R. Kochhar; L. Vlase; *Clin Pharmacol Drug Dev*, **2018**, *00*, 1-6.
33. D.I. Pop; M. Oroian; S. Bhardwaj; A. Marcovici; A. Khuroo; R. Kochhar; L. Vlase; *Farmacia*, **2018**, *66*, 597-601.

EFFECTS OF PULSED ELECTRIC FIELD ON THE ESTERIFICATION REACTIONS

Ioan-Alexandru UDREA^a, Valentin ORDODI^{a,*}, Cristina PAUL^a,
Cristian STĂNESE^b, Nicolae VASZILCSIN^a

ABSTRACT. The effects of alternative pulsed electric fields on the esterification reactions between acetic acid and different alcohols were investigated in this paper. The aim of this study was the synthesis of some esters using a new and ecological method. Only acetic acid and different alcohols were used as raw materials and an alternative pulsed electric field as accelerator. Also, the enzymatic synthesis of esters was performed in order to draw a conclusion on the effectiveness of the new proposed method. Gas chromatography analysis showed that the esterification was considerably enhanced by an alternative pulsed electric field. The highest amounts of ester were obtained for *n*-propyl acetate, significantly higher than in the case of enzymatic synthesis. The synthesis of *i*-butyl and *i*-amyl acetate using the alternative pulsed electric field shows the formation of lower amounts of ester, probably due to the conformation of the molecule. Using raw materials of natural origin (acetic acid and alcohols obtained, for example, by fermentation) in the presence of an alternative pulsed electric field, natural esters are obtained and they can be used without restrictions in pharma, food, perfume or cosmetic industry.

Keywords: esterification reactions, pulsed electric field, enzymatic synthesis, food industry, natural esters

^a Politehnica University of Timisoara, Faculty of Industrial Chemistry and Environmental Engineering, 6 V. Pârvan Bd., RO-300223, Timisoara, Romania

^b Politehnica University of Timisoara, Faculty of Electrical and Power Engineering, 2 V. Pârvan Bd., RO-300223, Timisoara, Romania

* Corresponding author: valentin.ordodi@upt.ro



INTRODUCTION

In pharma, food, perfume or cosmetic industry, a large number of odors and flavoring compounds are used [1]. Among these, the most commonly products used are esters; they are generally obtained by removing a molecule of water as a result of the reaction between a carboxylic acid and an alcohol or phenol. On the other hand, esters can also be synthesized by Tishchenko reaction or by the addition of a carboxylic acid to an alkene, but there are many other chemical methods that are less used [2, 3]. If esters must be used in pharma and food industry, they are mandatory obtained using enzymes as catalysts, the most preferred being lipases [4]. Also, esters can be obtained using transesterification reaction, or assisted by microwaves, visible light, pulsed electric fields [5 - 10].

There are two ways to obtain natural esters by chemical synthesis, starting from raw materials of natural origin: by chemical reaction using enzymes as catalysts or by chemical reaction using a pulsed electric field as a catalyst [11]. Considering that obtaining esters by enzymatic methods involve high costs, the aim of this study was to apply and test a new esterification method using only acid and alcohol as raw materials, and a rectangular pulsed electric field (20 kHz) as catalyst. The synthesized esters were *n*-propyl acetate, *i*-butyl acetate and *i*-amyl acetate. These three esters were chosen because they have applications in pharma, food industry and in cosmetics [12-14]. In order to draw a conclusion on the effectiveness of the new proposed method using the pulsed electric field as catalyst, the enzymatic synthesis of these esters was performed.

RESULTS AND DISCUSSIONS

n-Propyl acetate synthesis

In Figure 1 (A,B,C), the results obtained in the esterification reaction of acetic acid with *n*-propanol are shown. The reactions were performed in the presence of an alternative pulsed electric field (20 kHz) as catalyst compared with the enzymatic synthesis.

The amount of ester obtained in the case of pulsed electric field synthesis for all 3 molar ratios and at every sampling hour is higher compared to the amount of ester obtained after enzymatic synthesis. The amounts of *n*-propyl acetate obtained after 26 hours using a pulsed electric field as catalyst are 108.8 mg (1:2), 202.2 mg (1:1) and 199.3 mg (2:1), significantly higher than the ones obtained enzymatically: 92.9 mg (1:2), 104.1 mg (1:1)

EFFECTS OF PULSED ELECTRIC FIELD ON THE ESTERIFICATION REACTIONS

and 113.3 mg (2:1). The highest amount of *n*-propyl acetate, 202.2 mg, was obtained when the molar ratio between reactants was 1:1 in the case of synthesis using an alternative pulsed electric field. This result indicates a higher efficiency compared to other molar ratios and the excess of reactants to increase the reaction efficiency is not required.

If the syntheses were performed using excess, either acid or alcohol, significant changes have been observed 26 hours later, especially in the case of pulsed electric field method, so the amount of ester obtained using excess alcohol is around two times lower compared to the quantity obtained in equimolar ratio.

Using an excess of acid, a decrease around 5% was observed; thus, the optimal molar ratio between reactants for the synthesis of *n*-propyl acetate was 1:1.

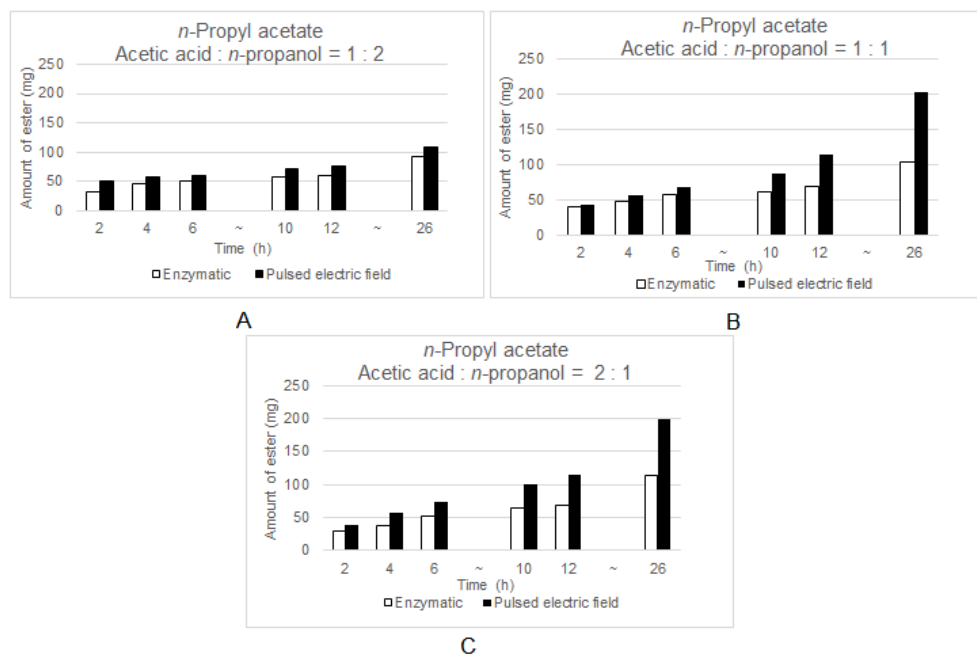


Figure 1 (A,B,C). The amount of *n*-propyl acetate obtained for molar ratio acetic acid : *n*-propanol 1:2, 1:1 and 2:1

For the enzymatic synthesis of *n*-propyl acetate, the optimal molar ratio under the selected reaction conditions is 2:1. In the case of alcohol excess, the amount of ester decreases around 20%, and in the case of the equimolar ratio the amount of ester is about 10% lower than in the case of the optimal molar ratio 2:1.

i-Butyl acetate synthesis

In Figure 2 (A,B,C) the results obtained in the esterification reaction of acetic acid with *i*-butyl alcohol are shown. All reactions were performed in the same conditions as the previous ones.

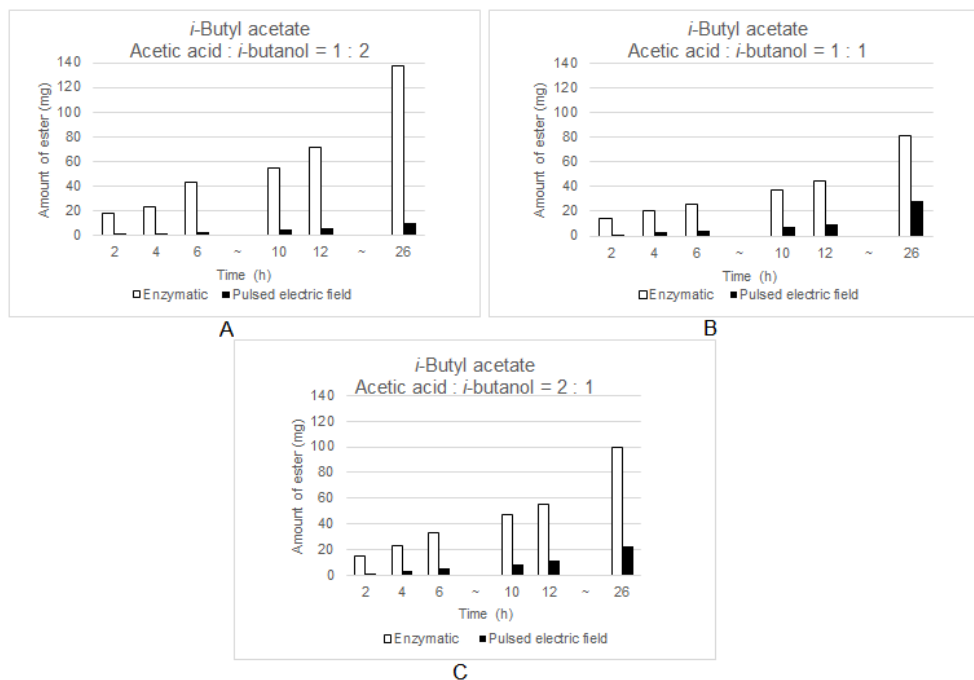


Figure 2 (A,B,C). The amount of *i*-butyl acetate for molar ratio acetic acid : *i*-butanol 1:2, 1:1 and 2:1

It can be observed that in the case of all three molar ratios and at every sampling hour the amount of *i*-butyl acetate obtained using pulsed electric field as catalyst for synthesis is lower compared to the amount of ester obtained enzymatically. The amounts of *i*-butyl acetate obtained after 26 hours using a pulsed electric field as catalysts are 10.5 mg (1:2), 28.1 mg (1:1) and 22.9 mg (2:1), lower than the ones obtained enzymatically: 137.5 mg (1:2), 81.5 mg (1:1) and 99.1 mg (2:1). The highest amount of ester was obtained when the molar ratio between reactants was 1:1 in the case of pulsed electric field synthesis. This result indicates a higher efficiency compared to other molar ratios, with no need for excess reactants to increase the reaction efficiency. If the syntheses were performed using a reactant excess, either acid or alcohol, significant changes are observed after 26 hours, especially in the case of pulsed

electric field method, so the amount of ester obtained using excess alcohol was around three times lower compared to the quantity obtained in equimolar ratio. When an excess of acid was used, it was observed a decrease around 25%; thus, the optimal molar ratio between reactants for the synthesis of *i*-butyl acetate in pulsed electric field was 1:1. The enzymatic synthesis of *i*-butyl acetate proved to be more efficient, the optimal molar ratio under the selected reaction conditions being the molar ratio 1:2. In the case of excess acid the amount of ester decreases around 25% and in the case of the equimolar ratio the amount of ester was about 35% lower compared to the optimal molar ratio (1:2).

i-Amyl acetate synthesis

In Figure 3 (A,B,C), the results obtained in the esterification reaction of acetic acid with *i*-amyl alcohol are shown. All reactions were performed in the same conditions as the previous ones. The synthesis of *i*-amyl acetate by the two presented methods were similar to the reactions of obtaining *i*-butyl acetate, which practically confirms the unfavorable influence of the branched chain on the development of these reactions in the pulsed electric field.

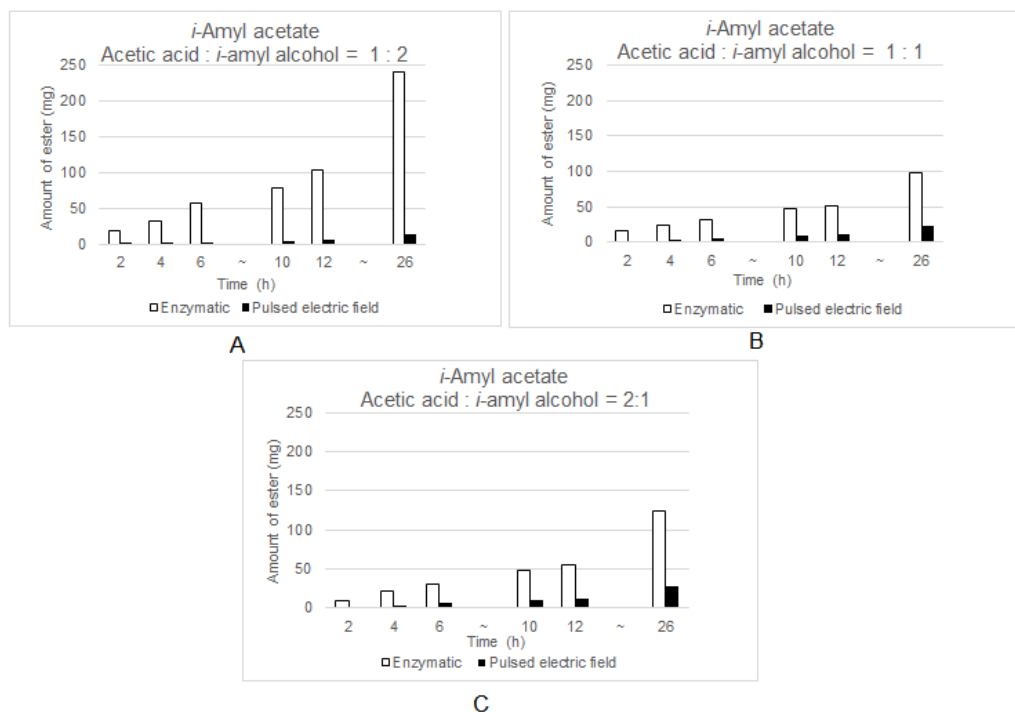


Figure 3 (A,B,C). The amount of *i*-amyl acetate for molar ratio acetic acid : *i*-amyl alcohol 1:2, 1:1 and 2:1

The amounts of *i*-amyl acetate obtained after 26 hours using a pulsed electric field as catalyst are 14.7 mg (1:2), 24.0 mg (1:1) and 27.2 mg (2:1), lower than the ones obtained enzymatically: 239.1 mg (1:2), 99.0 mg (1:1) and 124.1 mg (2:1). The highest amount of ester was obtained when the molar ratio between reactants was 2:1 in the case of pulsed electric field synthesis. If the syntheses were performed using excess of alcohol, significant changes were observed after 26 hours, especially in the case of the pulsed electric field method; therefore, the amount of ester obtained was approximately 2 times lower compared to the amount obtained when the molar ratio was 2:1.

In the case of *i*-amyl acetate synthesis using the reactants in equimolar ratio, it was observed a decrease around 15%, thus resulting that the optimal molar ratio between reactants for the synthesis of *i*-amyl acetate using the pulsed electric field was 2:1.

The enzymatic synthesis of *i*-amyl acetate proved to be more efficient, the optimal molar ratio under the selected reaction conditions being the ratio of 1:2. Using an excess of acid the amount of ester decreases around 50%, and in the case of the equimolar ratio the amount of ester was about 60% lower compared to the optimal molar ratio of 1:2.

It can also be seen that after 12 hours of reaction there is no directly proportional increase in the amount of ester with the number of hours indicating an equilibrium.

CONCLUSIONS

Experimental determinations have shown that the pulsed electric field has an impact regarding the esterification reaction of acetic acid with different alcohols. Due to the orientation of the molecular dipoles in alternative pulsed electric field, the probability of effective collisions with the formation of reactive products is increased. In case of branched alcohols, due to the interactions that manifest themselves between the branched chains, the catalytic effect is less pronounced.

In this study, three esters of acetic acid with linear and branched aliphatic alcohols were synthesized in the presence of a pulsed electric field and enzymatically. The synthesis of some esters using a pulsed electric field as catalysts was demonstrated for the first time, the obtained results being a starting point in the synthesis of "green" esters.

The highest amounts of ester, in the case of pulsed electric field synthesis, were obtained for *n*-propyl acetate, significantly higher than in the case of enzymatic synthesis. The synthesis of *i*-butyl and *i*-amyl acetate in pulsed electric field synthesis shows the formation of lower amounts of ester, probably due to the branched chain of the alcohol.

According to the literature data, a such behavior can be explained taking into consideration the difference between values of the relative polarization of the molecules for the 3 studied alcohols. The greater relative polarization, the more effect of the pulsed electric field is more intense, orienting the alcohol molecules in favorable positions of effective clashes, which materializes by obtaining higher quantities of ester compared to the reactions in which alcohols with lower relative polarizations are used (branched chain alcohols with bigger molecules) [15].

Therefore, starting from raw materials of natural origin, it was demonstrated that natural esters can be obtained using the method presented in this study and it can be used in the food industry because the use of electricity as a catalyst is a natural process, thus it does not have any harmful effect.

On the other hand, flavorings used in the food industry are obtained exclusively enzymatically, which means a higher production cost due to the high price of enzymes as well as the necessary equipment. Therefore, the price of the finished product (flavor) will be higher.

In conclusion, starting from raw materials of natural origin and using as catalyst an alternative pulsed electric field, natural esters can be obtained with a significantly lower production cost than in the case of obtaining esters for the food industry using enzymes as catalysts.

EXPERIMENTAL SECTION

Materials

The reagents used for these studies are commercial and they have been used without further purification: acetic acid (99%, Chimreactiv), *n*-propanol (99%, Merck), *i*-butanol (99%, Merck), *i*-amyl alcohol (99%, Merck), acetone (99%, Merck), decane (99%, Merck), enzyme: lipase *Candida antarctica* - lipase B (Genofocus).

Enzymatic synthesis

In 5 mL Eppendorf tubes predetermined volumes of acetic acid and alcohol (*n*-propanol, *i*-butanol and *i*-amyl alcohol) corresponding to the molar ratios of acid: alcohol = 1:2, 1:1 and 2:1 were added, and then the enzyme *Candida antarctica* lipase B was added, representing 1% of the reaction mass.

The reactions were incubated at 50°C, 1000 rpm and samples were collected at predetermined time intervals: 2, 4, 6, 10, 12 and 26 hours.

Synthesis using a pulsed electric field as catalyst

In a 30 mL glass mini-reactor (figure 4), predetermined volumes of acetic acid and alcohol (*n*-propanol, *i*-butanol and *i*-amyl alcohol) corresponding to the studied molar ratios (acid : alcohol = 1:2, 1:1 and 2:1) were added for a total volume of 25 mL reaction mass. A stainless steel electrode connected to an electronic power amplifier which generates high voltage (5000 V) with a frequency of 20 kHz (rectangular signal), it was inserted inside the glass reactor that on the outside of it is provided with a thin copper sheet sheath that constitutes the external electrode connected to the ground of the device.

The reactions were incubated at 50°C with stirring at 1000 rpm and samples were collected at predetermined time intervals: 2, 4, 6, 10, 12 and 26 hours.

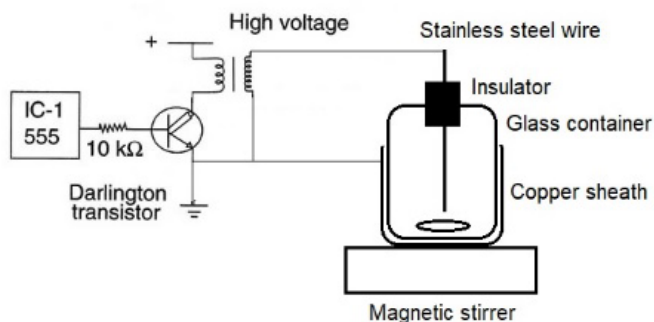


Figure 4. Device used for synthesis of esters using a pulsed electric field.

The amount of esters (mg) obtained for all the reactions (pulsed electric field and enzymatic synthesis) was monitored by flame ionization gas chromatography using acetone as solvent, and decane was used as the internal standard. Chromatographic analyses were performed using a Varian 450-GC chromatograph with autosampler and the parameters used were: injector temperature: 250°C, detector temperature: 300°C, temperature range: from 40°C to 80°C (10°C/min), carrier gas pressure (hydrogen): 10 psi. The mixture (1000 µl) subjected to GC analysis consisted of: 100 µl of reaction mass, 880 µl acetone and 20 µl decane (internal standard).

Confirmation of acetates formation was performed using the classical spectral methods (data not shown):

- Fourier-transform infrared spectra (FT-IR) for the obtained samples were performed using a Bruker Vertex 70 spectrometer (Bruker Daltonics GmbH, Germany) equipped with a Platinum ATR spectrometer, Bruker Diamond Type A225/Q1.

- Mass spectra were recorded with GC-MS Thermo-Scientific TRACE 1310 gas chromatograph, ITQ1100 Ion Trap MS. The parameters used in the GC-MS analysis were: transfer line temperature: 310°C, injector temperature: 250°C, the gas flow was 1ml/min in the reading range 50-500 m/z.

- NMR spectra were recorded with the Bruker FOURIER 300 NMR spectrometer in CDCl₃.

ACKNOWLEDGEMENTS

The financial support and research facilities were offered by Doctoral School of Politehnica University of Timișoara.

REFERENCES

1. D. Baines; N.C. Da Costa; M.L. Dewis; S.Eri; J.Grigo; S.J. Herman; S.B.Jameson; J.Knights; P. Kraft; J.Margetts; L.O'Hare; D.J. Rowe; L.Turin; C.Winkel; M.Zviely; *Chemistry and Technology of Flavors and Fragrances*, D.Rowe, Blackwell Publishing, Oxford, UK, **2004**, pp. 56-82
2. V.V. Rekha; M.V. Ramani; A. Ratnamala; V. Rupakalpana; G.V. Subbaraju; C. Satyanarayana; C. S. Rao; *Org Process Res & Dev*, **2009**, *13*, 769–773
3. T. Seki; T. Nakajo; M. Onaka; *Chem. Lett.*, **2006**, *35*(8), 824-829
4. A. Rajendran; A. Palanisamy; V. Thangavelu; *Braz Arch Biol Technol*, **2009**, *52*, 207-219
5. M. Salaheldeen; A. A. Mariod; M. K. Aroua; S.M.A. Rahman; M. E. M. Soudagar; I.M.R. Fattah; *Catal.*, **2021**, *11*(9), 1121
6. N. R. Khan; V. K. Rathod; *Process Biochem*, **2018**, *75*, 89-98
7. H. Wang; J. Ni; Y. Zhang; *Tetrahedron Lett.*, **2022**, *104*, 154021
8. D. C. Cubides-Roman; V. H. Pérez; H. F. de Castro; C E. Orrego; O. H. Giraldo; E. G. Silveira; G. F. David; *Fuel*, **2017**, *196*, 481-487
9. H. Ligong; D. Xuebao; *JSCUT*, **2011**, *39*(12), 127-131
10. Y. Feng; T. Yang; Y. Zhang; A. Zhang; L. Gai; D. Niu; *Front Nutr.*, **2022**, *9*, 1048632
11. Z. R. Lin; X. A. Zeng; S. J. Yu; D-W. Sun; *Food Bioprocess Tech*, **2011**, *5*, 2637–2645
12. M. C. C. Corradini; R. A. B. Gomes; J. H. H. Luiz; A. A. Mendes; *Chem Eng Commun*, **2016**, *203* (11), 1432-1442

IOAN-ALEXANDRU UDREA, VALENTIN ORDODI, CRISTINA PAUL,
CRISTIAN STĂNESE, NICOLAE VASZILCSIN

13. A. Izci; E. Uyar; E. Izci; *Chem Eng Commun*, **2008**, 196, 56-67
14. A. Wolfson; D. Saidkarimov; C. Dlugy; D. Tavor; *Green Chem Lett Rev*, **2009**, 2, 107-110
15. <https://sites.google.com/site/miller00828/in/solvent-polarity-table>, accessed at 24.02.2023.

THE STUDY OF IONIC INTERACTIONS OF POTASSIUM IODIDE IN THE VEGETABLE OIL-N,N-DIMETHYLFORMAMIDE SOLVENT BY ELECTRICAL CONDUCTIVITY MEASUREMENTS

Syed Muhammad Saqib NADEEM^{a,*}, Rehana SAEED^a

ABSTRACT. The electrical and molar conductivities of potassium iodide solutions in different concentrations of sunflower oil-DMF and corn oil-DMF solvents were measured at temperatures of 303.15, 308.15, 313.15, 318.15 and 323.15 K. The electrical and molar conductivity increased with an increase in temperature while an increase in the concentration of oil in the solvent had a decreasing effect. The electrical conductivity increased while the molar conductivity decreased with an increase in the concentration of potassium iodide in the solution. The limiting molar conductivities of the potassium iodide solution evaluated by the plots of the Debye-Huckel relation were used to determine the strength of ion-ion and ion-solvent interactions. The ion-ion interaction coefficient (A) varied irregularly with temperature while the ion-solvent interaction coefficient (B) increased with temperature in a pattern characteristic of structure-breaking electrolytes. The limiting molar conductivity of potassium iodide solutions obeyed the Arrhenius model of temperature dependence.

Keywords: Vegetable oil; Electrical conductivity; N, N-Dimethylformamide (DMF), Ion-ion interaction; Ion-solvent interaction

INTRODUCTION

Sunflower and corn oil are among the most suitable edible oils due to their cholesterol-controlling ability and consequent prevention of heart diseases.

^a Department of Chemistry, University of Karachi, Room No. 309, 3rd Floor, Karachi-75270, Pakistan

* Corresponding author: smsaqibnadeem@gmail.com



In recent times, vegetable oils have found numerous industrial applications such as base stock for biofuels, lubricants, caulking compounds, anti-corrosion, anti-static agents, pesticides, electrical insulation, epoxies, linoleum backing, and paints [1-11]. The ability of vegetable oils to serve as a carrier for biologically important molecules like vitamins has led to their use in commercial pharmaceutical preparations [12]. The metal-based nanofluids such as water, mineral oils, vegetable oils, and ionic liquids exhibit enhanced electrical conductivity and heat-exchange capacity which has found useful applications in car radiators, refrigerators, solar collectors, aeronautics, and electronic equipment [13]. The chemical inertness and dielectric constant of vegetable oil are critical parameters for its use as a dielectric in electrical devices [14]. The electrically conductive derivatives of vegetable oils have the potential to replace mineral oils as the dielectric medium in transformers, circuit breakers, cables, and capacitors due to their environmental-friendly nature via high biodegradability and high fire point as compared to mineral oils which protect the transformers from fire hazard, and higher moisture affinity which keeps the paper insulation dry and enhances the functional life of transformers [15-17].

The increasing use of vegetable oils in hydraulic fluids, cosmetics, pharmaceuticals, and biofuels has led to extensive research on their various physicochemical properties [18]. The knowledge of ionic interactions that develop upon the addition of electrolytes to vegetable oils due to the change of their inherent bulk structural arrangement is very important for industrial process engineering [19]. Conductometry is a very simple and reliable method for studying the ion-ion and ion-solvent interactions in an electrolyte solution. In the available literature, the electrical conductivity data of polymers, biomolecules and drugs, acids and bases, ionic liquids, and non-nutritional electrolytes are abundant but very little data is published on the electrical conductivity of solutes and solvents of nutritional importance like potassium iodide and vegetable oils [19-29]. The dimethylformamide is used as a solvent because of its solvency for almost all vegetable oils, and inorganic salts. This research work presents the electrical properties and solvation behavior of potassium iodide in sunflower oil-DMF and corn oil-DMF solvents. The main aim of this study is to investigate the electrostatic ionic interactions and structure-making/breaking ability of potassium iodide in the vegetable oil-DMF solvent by applying the Debye-Huckel-Onsager relation. The results are discussed in terms of the structural effects produced by the orientation of ions in the solution and the temperature dependence of the ionic interactions.

RESULTS AND DISCUSSION

The electrical conductivity, molar conductivity, limiting molar conductivity, and ionic interaction coefficients of potassium iodide solutions having concentrations ranging from 1.0 to $9.0 \times 10^{-2} \text{ mol.dm}^{-3}$ were measured in different compositions (1.0%, 2.0%, 3.0%, 4.0%, 5.0% v/v) of sunflower oil-DMF and corn oil-DMF solvents at different temperatures from 303.15 to 323.15 K with a difference of 5 K. The results are tabulated in Tables 1 to 7. The uncertainty in the fundamental experimental results is expressed along with each value.

1. Electrical conductivity (K)

The electrical conductivity of the potassium iodide solution at different temperatures is presented in Tables 1 and 2. The electrical conductivity of the potassium iodide solution is higher in corn oil-DMF as compared to that in sunflower oil-DMF due to its lower viscosity. In a mixed solvent, the electrical conductivity is affected by the ion-solvent interactions, the three-dimensional structure of the solvent, the viscosity and dielectric constant of the solvent, and the solvation of ions [30]. The electrical conductivity increased with an increase in the concentration of potassium iodide and temperature while it decreased with an increase in the concentration of oil in the solution. Potassium iodide is a strong electrolyte and completely dissociates in the relatively polar solvent; vegetable oil-DMF. The increased electrical conductivity at higher concentrations of potassium iodide is due to the increased number of conducting ions in the solution while the increased electrical conductivity at higher temperatures is due to the greater mobility of ions caused by the increased kinetic energy and decreased viscosity of the solution [22,31]. The decrease in electrical conductivity with an increased oil concentration is due to ion-solvent interaction which results in the solvation of ions by the bulky oil molecules and therefore there is less number of free ions available for transportation of electric charge [23]. The effect of potassium iodide concentration is much more pronounced than the concentration of oil because the number of ions is directly related to the charge transferred while the oil molecules cause a decrease in the number of free ions by interacting with ions and hindering their movement.

Table 1. Electrical conductivity of potassium iodide solution in different compositions of sunflower oil-DMF at different temperatures

[KI] x 10 ² (mol.dm ⁻³)	Electrical Conductivity (K) x 10 (mS.cm ⁻¹)				
	303.15 K	308.15 K	313.15 K	318.15 K	323.15 K
	1.0% Sunflower Oil-DMF				
1.0	3.9	4.2	4.5	5.0	5.6
3.0	8.6	8.8	9.1	9.4	9.9
5.0	12.6	12.8	13.0	13.5	14.1
7.0	16.0	16.2	16.5	16.9	17.5
9.0	19.5	19.7	19.9	20.5	21.2
	2.0% Sunflower Oil-DMF				
1.0	3.7	4.0	4.3	4.7	5.1
3.0	8.4	8.6	8.8	9.0	9.4
5.0	12.0	12.5	12.7	13.2	13.6
7.0	15.3	15.7	15.9	16.4	16.9
9.0	18.7	18.9	19.3	19.8	20.5
	3.0% Sunflower Oil-DMF				
1.0	3.2	3.6	3.9	4.3	4.7
3.0	8.0	8.2	8.5	8.8	9.1
5.0	11.5	12.1	12.4	12.8	13.2
7.0	14.7	15.2	15.5	16.0	16.5
9.0	18.2	18.4	18.9	19.3	19.8
	4.0% Sunflower Oil-DMF				
1.0	2.8	3.2	3.5	4.0	4.4
3.0	7.5	7.7	8.1	8.4	8.7
5.0	11.1	11.7	12.0	12.4	12.8
7.0	14.2	14.7	15.1	15.6	16.0
9.0	17.6	17.9	18.5	18.8	19.3
	5.0% Sunflower Oil-DMF				
1.0	2.5	2.8	3.1	3.5	4.0
3.0	7.1	7.3	7.7	8.0	8.3
5.0	10.6	11.2	11.6	12.0	12.3
7.0	13.6	14.2	14.6	15.1	15.6
9.0	17.1	17.4	18.0	18.3	18.8
Note: The uncertainty in the tabulated values is ±0.05 to 0.40%.					

THE STUDY OF IONIC INTERACTIONS OF POTASSIUM IODIDE IN THE VEGETABLE OIL-N,
N-DIMETHYLFORMAMIDE SOLVENT BY ELECTRICAL CONDUCTIVITY MEASUREMENTS

Table 2. Electrical conductivity of potassium iodide solutions in different compositions of corn oil-DMF at different temperatures

[KI] x 10 ² (mol.dm ⁻³)	Electrical Conductivity (K) x 10 (mS.cm ⁻¹)				
	303.15 K	308.15 K	313.15 K	318.15 K	323.15 K
	1.0% Corn Oil-DMF				
1.0	5.0	5.8	6.7	7.8	8.7
3.0	12.5	13.5	14.4	15.3	16.0
5.0	17.7	19.2	20.0	21.0	21.9
7.0	22.7	24.6	25.5	26.5	27.4
9.0	27.5	29.4	30.4	32.3	33.1
	2.0% Corn Oil-DMF				
1.0	4.6	5.3	6.1	7.1	8.0
3.0	12.1	12.9	13.9	14.7	15.3
5.0	17.2	18.5	19.3	20.3	21.1
7.0	22.1	23.7	24.8	25.8	26.6
9.0	26.8	28.6	29.6	30.7	31.4
	3.0% Corn Oil-DMF				
1.0	4.3	4.8	5.5	6.5	7.4
3.0	11.6	12.1	13.3	14.1	14.7
5.0	16.7	17.7	18.6	19.6	20.3
7.0	21.6	22.9	24.2	25.1	25.8
9.0	26.3	27.7	28.8	30.0	30.7
	4.0% Corn Oil-DMF				
1.0	4.0	4.4	5.0	5.8	6.8
3.0	11.1	11.4	12.8	13.3	14.0
5.0	16.2	16.8	17.9	19.0	19.6
7.0	21.1	23.1	23.4	24.5	25.1
9.0	25.8	26.9	28.1	29.2	29.9
	5.0% Corn Oil-DMF				
1.0	3.6	3.9	4.5	5.2	6.1
3.0	10.6	10.7	12.1	12.8	13.3
5.0	15.7	16.1	17.2	18.3	18.9
7.0	20.7	22.5	22.7	23.9	24.4
9.0	25.3	26.1	27.4	28.6	29.2
Note: The uncertainty in the tabulated values is ±0.03 to 0.28%.					

2. Molar conductivity (Λ_m)

The values of molar conductivity are presented in Table 3. The molar conductivity increased with the temperature while it decreased with an increase in the concentration of potassium iodide and oil in the solution [33]. The increase in molar conductance at higher temperatures is due to increased ionic mobility caused by the increased fluidity of the solution [23, 32]. The molar conductivity decreased with an increase in the concentration of potassium iodide in the solution due to a decrease in the number of free ions per unit volume of the solution. The decrease in the number of free ions is due to the ionic association caused by the frequent collision of ions in a concentrated solution. The increase in the concentration of oil in the solution decreased the molar conductivity due to the decreased ionic mobility caused by the viscous oil molecules and increased ion-solvent interactions.

3. Limiting molar conductivity (Λ_m°)

The limiting molar conductivity is the molar conductivity of a solution at infinite dilution and it is the intercept of the plot of the Debye-Huckel-Onsager relation shown in equation 3.1 [32-36].

$$\Lambda_m = \Lambda_m^\circ - [A + B \Lambda_m^\circ] C^{1/2} \quad 3.1$$

Where A and B are the ion-ion and ion-solvent interaction coefficients respectively as derived from the molar conductivity values of the potassium iodide solution. The unit of Λ_m and A is $\text{S}\cdot\text{cm}^2\cdot\text{mol}^{-1}$, B has units of $\text{S}^{-1}\cdot\text{cm}^2\cdot\text{mol}$, and C is expressed in $\text{mol}\cdot\text{dm}^{-3}$. The values of limiting molar conductivity are presented in Table 4 while a representative plot of the Debye-Huckel-Onsager relation is shown in Figure 1.

4. Ion-ion and ion-solvent interactions

The ion-ion and ion-solvent interactions were evaluated from a modified form of the Debye-Huckel-Onsager relation presented in equation 3.2 [35-37].

$$\Lambda_m = \Lambda_m^\circ - \left[\left\{ (82.4/(DT))^{1/2} \eta_o + \{ 8.2 \times 10^5 / (DT)^{1/2} \} \Lambda_m^\circ \right\} C^{1/2} \right] \quad 3.2$$

THE STUDY OF IONIC INTERACTIONS OF POTASSIUM IODIDE IN THE VEGETABLE OIL-N,
N-DIMETHYLFORMAMIDE SOLVENT BY ELECTRICAL CONDUCTIVITY MEASUREMENTS

Table 3. Molar conductivity of potassium iodide solution in different compositions of oil-DMF solvent at different temperatures

[KI] x 10 ² (mol.dm ⁻³)	Molar Conductivity (Λ_m) (S.cm ² .mol ⁻¹)									
	303.15	308.15	313.15	318.15	323.15	303.15	308.15	313.15	318.15	323.15
	K	K	K	K	K	K	K	K	K	K
	1.0% Sunflower Oil-DMF					1.0% Corn Oil-DMF				
1.0	39.0	42.0	45.0	50.0	56.0	50.0	58.0	67.0	78.0	87.0
3.0	28.7	29.3	30.3	31.3	33.0	41.7	45.0	48.0	51.0	53.3
5.0	25.2	25.6	26.0	27.0	28.2	35.4	38.4	40.0	42.0	43.8
7.0	22.9	23.1	23.6	24.1	25.0	32.4	35.1	36.4	37.9	39.1
9.0	21.67	21.9	22.1	22.8	23.6	30.6	32.7	33.8	34.9	36.8
	2.0% Sunflower Oil-DMF					2.0% Corn Oil-DMF				
1.0	37.0	40.0	43.0	47.0	51.0	46.0	53.0	61.0	71.0	80.0
3.0	28.0	28.7	29.3	30.0	31.3	40.3	43.0	46.3	49.0	51.0
5.0	24.0	25.0	25.4	26.4	27.2	34.4	37.0	38.6	40.6	42.2
7.0	21.9	22.4	22.7	23.4	24.1	31.6	33.9	35.4	36.9	38.0
9.0	20.8	21.0	21.4	22.0	22.8	29.8	31.8	32.9	34.1	34.9
	3.0% Sunflower Oil-DMF					3.0% Corn Oil-DMF				
1.0	32.0	36.0	39.0	43.0	47.0	43.0	48.0	55.0	65.0	74.0
3.0	26.7	27.3	28.3	29.3	30.3	38.7	40.3	44.3	47.0	49.0
5.0	23.0	24.2	24.8	25.6	26.4	33.4	35.4	37.2	39.2	40.6
7.0	21.0	21.7	22.1	22.9	23.6	30.9	32.7	34.6	35.9	36.8
9.0	20.2	20.4	21.0	21.4	22.0	29.2	30.8	32.0	33.3	34.1
	4.0% Sunflower Oil-DMF					4.0% Corn Oil-DMF				
1.0	28.0	32.0	35.0	40.0	44.0	40.0	44.0	50.0	58.0	68.0
3.0	25.0	25.7	27.0	28.0	29.0	37.0	38.0	42.7	44.3	46.7
5.0	22.2	23.4	24.0	24.8	25.6	32.4	33.6	35.8	38.0	39.2
7.0	20.3	21.0	21.6	22.3	22.9	30.1	33.0	33.4	35.0	35.9
9.0	19.6	19.9	20.6	20.9	21.4	28.7	29.9	31.2	32.4	33.2
	5.0% Sunflower Oil-DMF					5.0% Corn Oil-DMF				
1.0	25.0	28.0	31.0	35.0	40.0	36.0	39.0	45.0	52.0	63.0
3.0	23.7	24.3	25.7	26.7	27.7	35.3	35.7	40.3	42.7	44.3
5.0	21.2	22.4	23.2	24.0	24.6	31.4	32.2	34.4	36.6	37.8
7.0	19.4	20.3	20.8	21.6	22.3	29.6	32.1	32.4	34.1	34.9
9.0	19.0	19.3	20.0	20.3	20.9	28.1	29.0	30.4	31.8	32.4

Note: The uncertainty in the tabulated values is ± 0.14 to 0.51%.

Table 4. Limiting molar conductivity of potassium iodide solution in sunflower oil-DMF and corn oil-DMF at different temperatures

Concentration of Solvent (%v/v)	Limiting Molar Conductivity (Λ_m°) ($S.cm^2.mol^{-1}$)				
	303.15 K	308.15 K	313.15 K	318.15 K	323.15 K
	Sunflower Oil-DMF				
1.0	45.68 ± 0.6	49.38 ± 0.6	53.22 ± 0.6	59.16 ± 0.7	66.54 ± 0.8
2.0	43.61 ± 0.5	47.32 ± 0.6	50.88 ± 0.6	55.51 ± 0.7	60.36 ± 0.7
3.0	37.49 ± 0.5	42.33 ± 0.5	46.01 ± 0.6	50.86 ± 0.6	55.66 ± 0.7
4.0	32.40 ± 0.4	37.18 ± 0.5	40.94 ± 0.5	47.02 ± 0.6	51.85 ± 0.6
5.0	28.61 ± 0.3	32.19 ± 0.4	35.97 ± 0.4	40.88 ± 0.5	46.82 ± 0.6
	Corn Oil-DMF				
1.0	59.20 ± 0.7	68.77 ± 0.8	80.09 ± 1.0	94.36 ± 1.1	104.30 ± 1.3
2.0	54.36 ± 0.7	62.54 ± 0.8	72.80 ± 0.9	85.05 ± 1.0	96.06 ± 1.2
3.0	50.36 ± 0.6	55.96 ± 0.7	65.30 ± 0.8	77.53 ± 0.9	88.55 ± 1.1
4.0	46.35 ± 0.6	50.28 ± 0.6	59.16 ± 0.7	68.53 ± 0.8	80.91 ± 1.0
5.0	41.15 ± 0.5	43.77 ± 0.5	52.63 ± 0.6	61.08 ± 0.7	72.04 ± 0.9

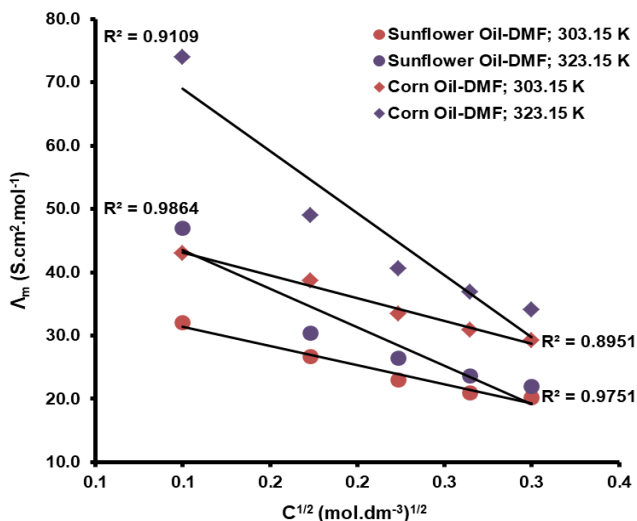


Figure 1. A plot of the Debye-Huckel-Onsager relation at different temperatures

THE STUDY OF IONIC INTERACTIONS OF POTASSIUM IODIDE IN THE VEGETABLE OIL-N,
N-DIMETHYLFORMAMIDE SOLVENT BY ELECTRICAL CONDUCTIVITY MEASUREMENTS

The unit of Λ_m is $S.cm^2.mol^{-1}$, η has units of Pa-s, T has units of K, and C is expressed in $mol.dm^{-3}$. The values of viscosity of the solvent are presented in Table 5 while the ion-ion and ion-solvent interactions evaluated from the Debye-Huckel-Onsager equation are presented in Table 6. The value of A is positive under all experimental conditions indicating significant ion-ion interaction in potassium iodide solution. The ion-ion interaction in the corn oil-DMF is higher as compared to sunflower oil-DMF due to low viscosity which allows free movement of ions and ionic collisions. The variation of the ion-ion interaction due to temperature is rather irregular due to multiple contributing factors such as viscosity, degree of dissociation, and concentration of potassium iodide [38]. The ion-solvent interaction is a specific and additive property of the ions of a strong electrolyte at a given temperature and is strongly influenced by the nature of the solvent [39]. DMF is a dipolar aprotic solvent in which the cation (K^+) is strongly solvated while anion (I^-) is poorly solvated [40,41]. By viewing the two resonating forms of DMF, it is realized that the probability of interaction between the positively charged nitrogen atom and the I^- ions is considerably less due to the steric hindrance whereas the negatively charged oxygen atom is much more available to interact with the K^+ ions for their solvation. There is very less possibility of solvent-solvent interactions due to the very dilute nature of potassium iodide solution which may produce DMF-DMF dimers [41-43].

Table 5. The viscosity of the solvent at different temperatures

Concentration of Solvent (%v/v)	Viscosity x 10 ⁴ (η_0) (Pa-s)				
	303.15 K	308.15 K	313.15 K	318.15 K	323.15 K
	Sunflower Oil-DMF				
1.0	13.03 ± 0.31	12.16 ± 0.29	11.41 ± 0.27	10.63 ± 0.26	9.83 ± 0.24
2.0	13.16 ± 0.32	12.26 ± 0.29	11.50 ± 0.28	10.70 ± 0.26	9.95 ± 0.24
3.0	13.32 ± 0.32	12.37 ± 0.30	11.60 ± 0.28	10.73 ± 0.26	10.04 ± 0.24
4.0	13.43 ± 0.32	12.46 ± 0.30	11.66 ± 0.28	10.88 ± 0.26	10.14 ± 0.24
5.0	13.49 ± 0.32	12.56 ± 0.30	11.80 ± 0.28	10.96 ± 0.26	10.36 ± 0.25
	Corn Oil-DMF				
1.0	7.17 ± 0.17	6.27 ± 0.15	5.75 ± 0.14	5.31 ± 0.13	4.84 ± 0.12
2.0	7.52 ± 0.18	6.87 ± 0.17	6.34 ± 0.15	5.71 ± 0.14	5.14 ± 0.12
3.0	7.85 ± 0.19	7.40 ± 0.18	6.76 ± 0.16	6.24 ± 0.15	5.75 ± 0.14
4.0	8.01 ± 0.19	7.64 ± 0.18	7.29 ± 0.18	6.78 ± 0.16	6.26 ± 0.15
5.0	8.37 ± 0.20	7.88 ± 0.19	7.39 ± 0.18	6.96 ± 0.17	6.59 ± 0.16

The value of B is positive and increased with the increase in temperature. The ion-solvent interaction in the sunflower oil-DMF is stronger as compared to corn oil-DMF due to the higher viscosity of sunflower oil. The ion-solvent interaction also varied with the concentration of oil in the solvent because it affects the viscosity and electrical conductivity of the potassium iodide solution. The ion-solvent interaction is a measure of the effective solvodynamic volume of solvated ions, the charge density and geometry of ions, and the induced structural effects due to the ionic interactions. The dissolved ions attract the solvent molecules per their charge density and disturb the natural three-dimensional structure of the bulk solvent by wrenching out the solvent molecules from the three-dimensional solvent structure. This ion-solvation process results in the formation of ion-molecule clusters of large solvodynamic radii and decreases the limiting molar conductivity of the electrolytes [44]. The limiting molar conductivity is a measure of the solute-solvent interactions [35]. As the temperature is increased, the limiting molar conductivity of the ions increases due to the increased kinetic energy of the ions and decrease in the viscosity of the solvent but at the same time, the formation of ion-molecule clusters produces a decreasing effect on the limiting molar conductivity of the ions. An increase in the limiting molar conductivity with the temperature indicates that the increment due to the increase in temperature has outweighed the decrement due to the formation of ion-molecule clusters. The ion-solvent interaction decreased with the increase in the concentration of oil in the solvent due to decreased ionic motion. A useful parameter to interpret the ion-solvent interactions is the Walden product; $\Lambda_m^\circ \eta_o$ [45]. The Walden product increased with the increase in temperature confirming that the effect of electrical conductivity has more dominant than the effect of the viscosity of the solvent (Table 7). The first derivative of B concerning temperature (dB/dT) is used as a criterion for the structure-making or the structure-breaking ability of the electrolyte in the vegetable oil-DMF solvent [46].

The increase of B with temperature shows that dB/dT is positive and potassium iodide behaves as a structure-breaker in the vegetable oil + DMF solvent. The same conclusion has been obtained by the viscometric analysis of the ionic interactions of KI in the vegetable oil-DMF solvent [47]. The viscometric studies have reported that the potassium iodide also behaves like a structure-breaker in dimethylacetamide-water mixtures, N-formylmorpholine-water, ethylene glycol, glycerol, and urea [48-51].

THE STUDY OF IONIC INTERACTIONS OF POTASSIUM IODIDE IN THE VEGETABLE OIL-N,
N-DIMETHYLFORMAMIDE SOLVENT BY ELECTRICAL CONDUCTIVITY MEASUREMENTS

Table 6. The ion-ion and ion-solvent interactions of potassium iodide solution at different temperatures by the Debye-Huckel equation

Concentration of Solvent (%v/v)	Temperature (K)				
	303.15 K	308.15 K	313.15 K	318.15 K	323.15 K
	A (S.cm ² .mol ⁻¹)				
	Sunflower Oil-DMF				
1.0	5.9952	6.3738	6.7366	7.1724	7.6988
2.0	5.9391	6.3233	6.6856	7.1315	7.6037
3.0	5.8678	6.2671	6.6268	7.1076	7.5408
4.0	5.8197	6.2218	6.5938	7.0128	7.4612
5.0	5.8612	6.1688	6.5145	6.9616	7.3021
	Corn Oil-DMF				
1.0	10.9028	12.3573	13.3782	14.3759	15.6508
2.0	10.3854	11.2831	12.1286	13.3610	14.7307
3.0	9.9591	10.4734	11.3715	12.2356	13.1718
4.0	9.7601	10.1510	10.5520	11.2435	12.0959
5.0	9.3333	9.8303	10.4063	10.9622	11.4933
	B (S ⁻¹ .cm ² .mol)				
	Sunflower Oil-DMF				
1.0	1.7459	1.8730	1.9818	2.1177	2.2479
2.0	1.7309	1.8457	1.9518	2.0565	2.1427
3.0	1.4660	1.6761	1.7966	1.9364	2.0478
4.0	1.1861	1.4531	1.6011	1.8371	1.9701
5.0	0.9398	1.1721	1.3674	1.6007	1.8294
	Corn Oil-DMF				
1.0	1.5018	1.6647	1.8943	2.1046	2.2116
2.0	1.3642	1.5378	1.7714	1.9886	2.1438
3.0	1.2362	1.3713	1.6062	1.8746	2.0663
4.0	1.0812	1.2211	1.4566	1.6900	1.9650
5.0	0.8108	0.9185	1.2429	1.4898	1.7989

Table 7. The Walden product of potassium iodide solutions at different temperatures

Concentration of Solvent (%v/v)	Walden Product x 10 ² (S.cm ² .mol ⁻¹ .Pa-s)				
	303.15 K	308.15 K	313.15 K	318.15 K	323.15 K
	Sunflower Oil-DMF				
1.0	5.9535	6.0041	6.0732	6.2927	6.5406
2.0	5.7372	5.7991	5.8500	5.9370	6.0071
3.0	4.9922	5.2341	5.3374	5.4581	5.5855
4.0	4.3503	4.6308	4.7728	5.1140	5.2590
5.0	3.8605	4.0435	4.2447	4.4788	4.8526
	Corn Oil-DMF				
1.0	4.2426	4.3129	4.6026	4.9438	5.0429
2.0	4.0903	4.2957	4.6141	4.8557	4.9346
3.0	3.9506	4.1414	4.4143	4.8346	5.0871
4.0	3.7110	3.8390	4.3094	4.6488	5.0623
5.0	3.4444	3.4507	3.8874	4.2500	4.7436

5. Temperature dependence of limiting molar conductivity

The temperature dependence of limiting molar conductivity was evaluated by using the Arrhenius relation shown in equation 3.3 [35].

$$\Lambda_m^{\circ} = A e^{-E_a/RT} \quad 3.3$$

Where A is the pre-exponential factor, Λ_m° is the limiting molar conductivity in units of S.cm².mol⁻¹, T is the absolute temperature of the potassium iodide solution in kelvin, R is the universal gas constant having the value of 8.314 J.K⁻¹.mol⁻¹ and E_a is the activation energy in units of J.mol⁻¹. A plot of the Arrhenius equation is presented in Figure 2. The straight lines with correlation coefficients of 0.978 to 0.999 are indicative of a directly proportional relationship between the limiting molar conductivity of potassium iodide solution with temperature. The energy of activation was positive (15.169 to 19.925 kJ in 1.0% to 5.0% sunflower oil-DMF and 23.418 to 23.623 kJ in 1.0% to 5.0% corn oil-DMF). The energy of activation for the ionic conductance increased with the increase in the concentration of oil in the solvent which perfectly complements the simultaneous decrease in the limiting molar conductivity and its increase with the increase of the temperature.

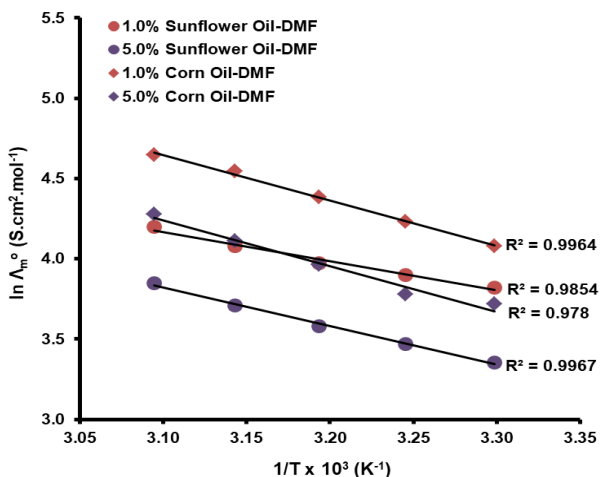


Figure 2. The dependence of limiting molar conductivity of potassium iodide solution on temperature

6. Interrelationship of viscosity and electrical conductivity

There is a significant interrelation between the viscosity and electrical conductivity of electrolyte solutions [30,50]. The interrelationship of viscosity and electrical conductivity was evaluated by the graphical analysis presented in Figure 3. The straight lines with a correlation coefficient of 0.96 indicate a directly proportional relationship between the viscosity and electrical conductivity of potassium iodide solution in the vegetable oil-DMF solvent at different temperatures.

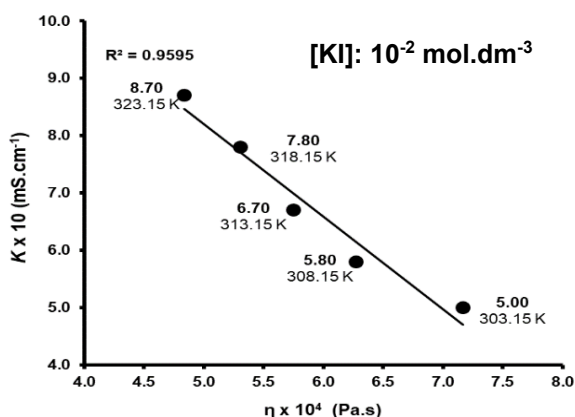


Figure 3. A plot of electrical conductivity vs viscosity of potassium iodide solution in 1.0% corn oil-DMF solvent

CONCLUSION

The potassium iodide solution exhibited higher electrical conductivity in corn oil-DMF as compared to sunflower oil-DMF due to lower viscosity. The electrical conductivity and molar conductivity increased with the increase in temperature while a decrement was observed with the increase in the concentration of oil in the solution. The electrical conductivity increased while molar conductivity decreased with the increase in the concentration of potassium iodide. The ion-ion and ion-solvent interaction coefficients indicated the presence of significant ion-ion and ion-solvent interactions in the potassium iodide solution. The value of B increased with the increase of temperature so that dB/dT is positive and potassium iodide behaves as a structure-breaker in the oil-DMF solvent. A directly proportional relationship exists between the viscosity and electrical conductivity of the potassium iodide solution.

EXPERIMENTAL SECTION

The potassium iodide (99.98% pure solid salt) of RDH, Germany, and dimethylformamide (99.99% pure solvent) of Lab-Scan, Thailand was used with any further processing. The sunflower oil and corn oil were extracted from dried, dehulled, and powdered oil seeds obtained from Empress Market, Karachi, and filtered before use to remove any suspended particles. The 1.0%, 2.0%, 3.0%, 4.0%, and 5.0% v/v sunflower oil-DMF and corn oil-DMF to be used as the solvent was prepared by mixing the required amount of oil and DMF. Potassium iodide solutions with concentrations ranging from 1.0×10^{-2} to $9.0 \times 10^{-2} \pm 1.06 \times 10^{-5}$ mol.dm⁻³ were prepared in different concentrations of the solvent. The volume measurements were done by calibrated glassware having a tolerance of ± 0.1 cm³ whereas a digital electronic weighing balance (BL-150S, Sartorius, Germany) having a least count of ± 0.0001 g was used for mass determination. The electrical conductivity of potassium iodide solutions was measured by a digital conductivity meter (Jenway 4510) with a least count of 0.01 mS.cm⁻¹, uncertainty of ± 0.001 mS.cm⁻¹, and cell constant of 0.99 cm⁻¹. The density of potassium iodide solutions was measured at different temperatures by an R.D. bottle of 10.0 cm³ whereas the viscosity of the solutions was measured by recording their time of flow between the two specified marks of an Ostwald viscometer (Technicominal constant 0.1 cSt/s capillary ASTM D 445) by using a calibrated stopwatch with the least count of 0.01 s (CBM Corporation, Japan). A thermostatic water bath (YCM-01, Taiwan) was used to maintain the desired temperature. The observations were recorded in triplicate.

REFERENCES

1. W. B. W. Nik; F. N. Ani; H. H. Masjuki; S. G. E. Giap; *Ind. Crops Prod.* **2005**, *22*, 249-255.
2. R. Saeed; S. Masood; S. M. S. Nadeem; *Int. J. Chem.*, **2012**, *4*, 28-36.
3. C. K. Ling; M. M. Aung; M. Ryung; L. C. Abdullah; H. N. Lim; I. S. M. Noor; *ACS Omega* **2019**, *4*, 2554-2564.
4. M. A. Husin; S. M. Tahir; *IOP Conf. Series: Journal of Physics: Conf. Series* **2018**, *1083*: 012052.
5. I. O. Igwe; *Ind. Crops Prod.*, **2004**, *19*, 185-190.
6. R. Ceriani; F. R. Paiva; C. B. Goncalves; E. A. C. Batista; A. J. A. Meirelles; *J. Chem. Eng. Data* **2008**, *53*, 1846-1853.
7. L. A. Quinchia; M. A. Delgado; C. Valencia; J. M. Franco; C. Gallegos; *Ind. Crops Prod.*, **2010**, *32*, 607-612.
8. S. Z. Erhan; *National Center for Agricultural Utilization Research, Wiley*, Illinois, **2005**.
9. K. M. Doll; B. K. Sharma; *J. Surf. Det.*, **2011**, *14*, 131-138.
10. S. Roy; *J. Biofuels* **2017**, *8*, 49-52.
11. A. Biswas; A. Adhvaryu; D. G. Stevenson; B. K. Sharma; J. L. Willet; S. Z. Erhan; *Ind. Crops Prod.*, **2007**, *25*, 1-7.
12. E. Zahir; R. Saeed; M. A. Hameed; A. Yousuf; *Arab. J. Chem.*, **2017**, *10*, 3870-3876.
13. A. A. Minea; *Nanomaterials* **2019**, *9*, 1592-1613.
14. M. Spohner; *Acta Polytechnica* **2012**, *5*, 100-105.
15. K. Lakrari; M. El-Moudane; I. Hassanain; I. Ellouzi; S. Kitane; M. A. El-Belghiti; *Global J. Food Sci. Tech.*, **2013**, *7*, 404-407.
16. M. S. Vichcencu; A. Ciuriuc; L. M. Dumitran; *U.P.B. Sci. Bull. Series C* **2013**, *75*, 171-182.
17. R. Rochdi; K. Lakrari; I. Hassanain; S. I. Alaoui; M. Belgharza; F. Elmakhoukhi; E. H. El-Azzouzi; M. A. El Belghiti; *Adv. Environ Bio.*, **2012**, *8*, 1218-1221.
18. M. N. Roy; R. Chanda; R. K. Das; *Phys. Chem. Liq.*, **2012**, *50*, 557-578.
19. R. K. Das; M. N. Roy; *Phys. Chem. Liq.*, **2014**, *52*, 55-77.
20. J. Rouabeh; L. M'barki; A. Hammami; I. Jallouli; A. Driss; *Heliyon* **2019**, *5*, e01159.
21. S. Saravanan; S. Rajesh; R. Palani; *Res. Rev: J. Pure. Appl. Phys.*, **2014**, *2*, 1-8.
22. R. Saxena; S. C. Bhatt; *Adv. Mat. Sci. Eng.*, **2018**, Article ID 1738612.
23. S. M. S. Nadeem; S. M. R. Ullah; *Ionics* **2020**, *26*, 2927-2940.
24. H. Kabir; R. K. Nath; M. K. Hossain; M. K. M. Z. Hyder; *Oriental J. Chem.*, **2018**, *34*, 196-202.
25. S. Seki; K. Hayamizu; S. Tsuzuki; K. Takahashi; Y. Ishino; M. Kato; E. Nozaki; H. Watanabe; Y. Umabayashi; *J. Electrochem. Soc.*, **2018**, *165*, 542-546.
26. V. K. Dakua; B. Sinha; M. N. Roy; *Phys. Chem. Liq.*, **2007**, *45*, 549-560.

27. F. U.Nwokobia; G. A. Coockey; A. A. Abia; *IOSR J. Appl. Chem.*, **2015**, *8*, 35-41.
28. N. H. El-Hammamy; A. I. Kawana; H. A. El-Araby; *J. Chem. Pharm. Res.*, **2016**, *8*, 693-703.
29. S. A. Ismaili; M. Belgharza; I. Marmouzi; H. Saaid; S. Kitane; M. A. El-Belghiti; *Der Pharma Chemica* **2015**, *7*, 294-296.
30. X. Wang; C. Tang; B. Huang; J. Hao; G. Chen; *Energies*, **2018**, *11*, 487-517.
31. R. Saeed; S. Masood; S. M. R. Ullah; *Int. J. Pharma. Chem. Sci.*, **2012**, *1*, 1591-1605.
32. G. F. Durrani; M. K. Baloch; G. Hameed; *J. Chem. Soc. Pak.*, **2004**, *26*, 191-197.
33. R. Saeed; F. Uddin; H. Sultan; *Phys. Chem. Liq.*, **2007**, *45*, 313-321.
34. M. Surekha; H. R. Shivakumar; V. Padpu; *J. Chem. Pharma. Sci. JCHPS Special Issue* **2018**, *1*, 47-52.
35. E. A. Gomaa; R. T. Rashad; *Chem. Sci. J.*, **2018**, *9*, 1-6.
36. K. G. Lawrence; A. Sacco; A. D. Giglio; A. Dell'Atti; *J. Chem. Soc. Faraday Trans.*, **1989**, *1 85*, 23-32.
37. P. Boskovic; V. Sokol; P. A. Ante; J. Giljanovic; *Int. J. Electrochem. Sci.*, **2014**, *9*, 3574-3587.
38. J. Mazurkiewicz; P. Tomasik; *Monatshefte fur Chemie* **1982**, *113*, 1253-1262.
39. D. S. Gill; A. Sharma; M. S. Chauhan; A. N. Sharma; J. S. Cheema; *Electrochim. Acta* **1985**, *30*, 151-153.
40. C. Zhang; Z. Ren; L. Liu; Z. Yin; *Mol. Simulation* **2013**, *39*, 875-881.
41. X. Chen; X. Zhang; H. Li; Q. Zhang; *Batteries & Supercaps* **2019**, *2*, 128-131.
42. C. S. Solanki; S. Tripathy; M. Tripathy; U. N. Dash; *E-J Chem.*, **2010**, *7*, 223-230.
43. V. P. Walden; *Zeitschrift fur anorganische und allgenseine Chemie* **1920**, *113*, 85-97 (1920).
44. S. Thirumaran; K. Sathish; *Res. J. Chem. Sci.*, **2011**, *1*, 63-71.
45. S. M. S. Nadeem; R. Saeed; *Chem. Papers* **2021**, *76*, 3387-3400.
46. N. P. Singh; M. M. Singh; P. K. Tikoo; *Aust. J. Chem.*, **1977**, *30*, 2303-2305.
47. S. F. Al-Azzawi; E. I. Allos; *J. Chem. Eng. Data* **1992**, *37*, 158-162 (1992).
48. K. Crickard; J. Skinner; *J. Phys. Chem.*, **1969**, *73*, 2060-2062.
49. S. Phang; *Aust. J. Chem.*, **1972**, *25*, 1575-1578.
50. D. Kumar; A. Singh; P. S. Tarsikka; *J. Food. Sci. Tech.*, **2013**, *50*, 549-554.

SYNTHESIS, CHARACTERIZATION AND BIOLOGICAL ACTIVITY OF SCHIFF AND AZO-SCHIFF BASE LIGANDS

Alhagie JADAMA^a, Seda YUKSEKDANACI^{b,*},
Demet ASTLEY^a, Ihsan YASA^c

ABSTRACT. Schiff and azo-Schiff base derivatives were synthesized, identified and evaluated for their antimicrobial and antifungal activities against gram-positive bacteria, gram-negative bacteria and fungi such as *Escherichia coli*, *Pseudomonas aureginosa*, *Staphylococcus aureus*, *Bacillus cereus*, *Salmonella typhimurium*, *Saccharomyces cerevisiae* and *Candida albicans*. Chiral amides (**2a-e**) were synthesised by using D-Phenylglycine, L-Phenylalanine, L-valine, L-isoleucine and L-methionine. Experimental studies include the use of chiral amide derivatives (**2a-e**) of the five amino acids to synthesize the Schiff and azo-Schiff base derivatives of amides (**3a-e**, **4a-c** and **4e**). The structures of the compounds were determined by spectroscopic analyses (FTIR, ¹H-NMR, ¹³C-NMR) and elemental analysis. Among the tested compounds, compound **3b** and **3d** were found to show the most potent inhibitory action against Gram positive and Gram negative bacteria.

Keywords: Schiff base, azo-Schiff base, amino acid, amide, biological activity

INTRODUCTION

Schiff base, named after Hugo Schiff, is a compound with the nitrogen atom connected to an aryl or alkyl group and functional group that contains a carbon-nitrogen double bond. And, azo compounds bear the functional group diazenyl R-N=N-R with R being an aryl or alkyl substituent.

^a Department of Chemistry, Faculty of Science, Ege University, Izmir, Turkey

^b Department of Occupational Health and Safety, Faculty of Health Sciences, Uşak University, Uşak, Turkey

^c Department of Biology, Faculty of Science, Ege University, Izmir, Turkey

* Corresponding author: seda.yuksekdanaci@usak.edu.tr



Azo-Schiff base derivatives show various biological activities that include antibacterial [1-4], antifungal [5] and anticancer [6-8]. For example diazenyl chalcones derivatives showed good activity against *E. coli*, *S. enterica*, *B. Subtilis* and *A. fumigatus* [9]. Azo-linked salicylidenic Schiff bases have been tested for their antimicrobial activity and 4-((*E*)-(4-((*E*)-phenyldiazenyl)phenylimino) methyl) benzene-1,2,3-triol showed antimicrobial activity against *K. pneu-moniae*, *E. cloacae*, *E. coli*, *B. megaterium*, *S. aureus*, *M. luteus*, *M. smegmatis*, *P. aeruginosa* [10]. In another study, azo-Schiff base derivatives were synthesized via condensation of salicylaldehyde derivatives with thiosemicarbazide. These azo-Schiff base compounds exhibited antimicrobial activity against *B. Subtilis*, *S. aureus*, *E. coli* and *P. aereuginosa* [11]. In another study by the same group, azo-Schiff base compounds were synthesized by reacting 5-phenyl azo salicyldehyde derivatives with *o*-amino phenol. The synthesized compounds also exhibited very high antimicrobial activity against *P. aeruginosa* [12]. *E*-5-((4-nitro phenyldiazanyl) quinoline-8-ol has been tested for its antimicrobial activity and was found to have high antimicrobial effect against multi-drug resistant bacteria [13]. Slassi et al. synthesized imidazole based azo-Schiff base derivatives and evaluated their antifungal activity against selected fungi species. The synthesized derivatives showed good antifungal activity against *S. spiospermum*, *A. fumigatus*, and *C. albicans* [14].

In this study, D-Phenylglycine, L-Phenylalanine, L-valine, L-isoleucine and L-methionine were used for the synthesis of chiral amide derivatives (**2a-e**). The synthesized chiral amides derivatives were reacted with 2-hydroxy-1-naphthaldehyde and (*E*)-2-hydroxy-5-(phenyl diazenyl) benzaldehyde for the synthesis of Schiff base (**3a-e**) and azo-Schiff base compounds (**4a-c**, **4e**).

RESULTS AND DISCUSSION

Chemistry

In this study, five Schiff base and four azo-Schiff base amino acid derivatives were synthesized, characterized and investigated for their biological activities. D-Phenylglycine, L-Phenylalanine, L-valine, L-isoleucine and L-methionine were used as starting materials for the synthesis of amide structures (**2a-e**) (Scheme 1). For the synthesis of Schiff base derivatives (**3a-e**) 2-hydroxy-1-naphthaldehyde was used in methanol under reflux for 4 hours (Scheme 2). The yields of the products vary between 84 to 94 %.

(*E*)-2-hydroxy-5-(phenyldiazenyl) benzaldehyde was used for the synthesis of azo-Schiff base derivatives (**4a-c**, **4e**) (Scheme 3) and the yields for these products varied between 61 to 85 %. The structure of the final products was determined by using spectroscopic analyses (FTIR, ¹H-NMR, ¹³C-NMR) and elemental analysis methods.

The FTIR spectra of the Schiff base derivatives (**3a-e**) showed characteristic bands for OH, C=N and C=O vibrations. Schiff bases show a absorption band due to O-H vibrations between 3557-3400 cm⁻¹. In the FTIR spectra, Schiff bases exhibit bands at approximately 1690 and approximately 1670 cm⁻¹ that are assignable to vibrations of C=N and C=O stretchings (Table 1).

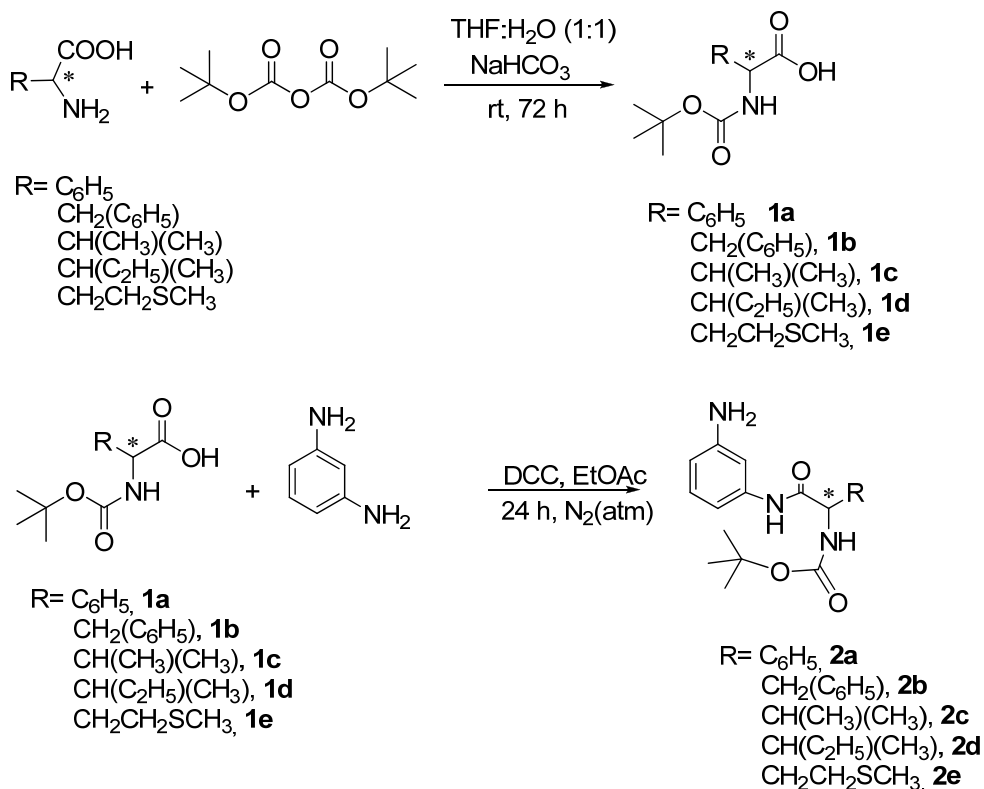
When the ¹H-NMRs of Schiff base derivatives (**3a-e**) are analyzed, we see that -OH protons are observed at 15.33, 15.68, 15.32, 15.31 and 15.29 ppm, respectively. The imine protons of the same compounds also gave signals at 9.21, 9.59, 9.30, 9.36 and 9.21 ppm, respectively.

When the ¹³C-NMR spectra of the Schiff base derivatives (**3a-e**) are examined, the signals observed in the range of 172-169 ppm belong to the carbonyl groups, and the peak observed around 155 ppm belongs to the imine carbon. The chiral amino acid carbons of the same compounds also gave signals at 59.71, 57.11, 61.25, 60.22 and 54.62 ppm, respectively.

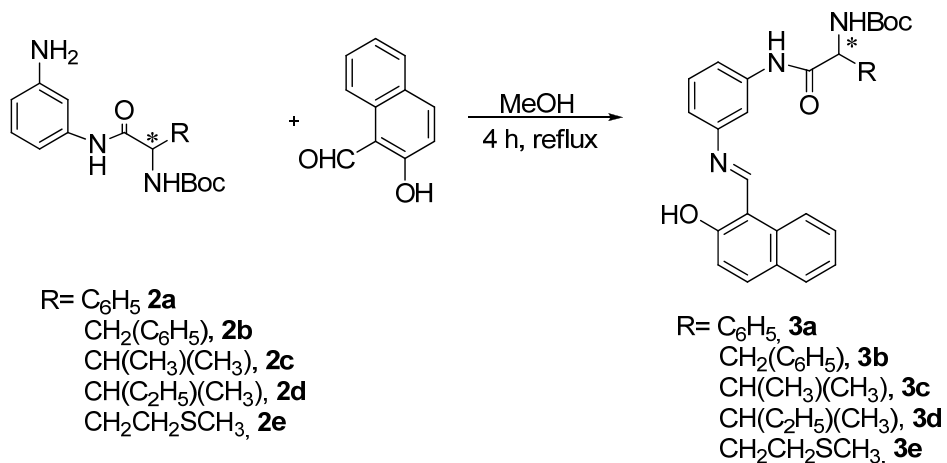
The FTIR spectra of the azo-Schiff base derivatives (**4a-c, 4e**) showed characteristic bands for OH and NH vibrations. Azo-Schiff bases (**4a-c, 4e**) showed a absorption band due to O-H vibrations 3312, 3312, 3474 and 3474 cm⁻¹, respectively. And also Azo-Schiff bases showed a absorption band due to N-H vibrations 3228, 3327, 3263 and 3272 cm⁻¹, respectively (Table 1).

When the ¹H-NMRs of azo-Schiff base derivatives (**4a-c, 4e**) are analyzed, we see that -OH protons are observed at 13.78, 13.69, 13.72 and 13.69 ppm, respectively. The -CH protons in the amino acid structure are observed at 5.88, 5.62, 5.59 and 5.68 ppm, respectively. The imine protons of the same compounds also gave signals at 9.20, 8.95, 9.24 and 9.21 ppm, respectively.

When the ¹³C-NMR spectra of the Schiff base derivatives (**4a-c, 4e**) are examined, the signals observed in the range of 171.26-156.30 ppm belong to the carbonyl groups, and the peak observed around 162 ppm belongs to the imine carbon. The chiral amino acid carbons of the same compounds also gave signals at 59.52, 56.86, 61.20 and 54.52 ppm, respectively.

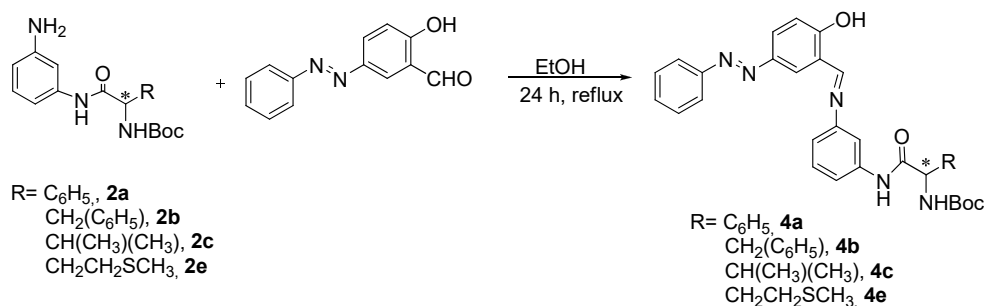


Scheme 1. Synthesis of chiral amide derivatives



Scheme 2. Synthesis of Schiff base derivatives

SYNTHESIS, CHARACTERIZATION AND BIOLOGICAL ACTIVITY OF SCHIFF
AND AZO-SCHIFF BASE LIGANDS



Scheme 3. Synthesis of azo-Schiff base derivatives

Table 1. Selected stretching frequencies of the synthesized final products (cm⁻¹)

Compound	O-H	N-H	C=N	C=O	Ar. C-H	Ar. C=C	Alp. C-H
3a	3436	3315	1690	1663	2970	1525	2853
3b	3557	3328	1688	1660	3031	1527	2876
3c	3400	3316	1690	1668	3055	1505	2872
3d	3485	3330	1688	1662	2960	1526	2830
3e	3480	3301	1682	1672	3055	1546	2919
4a	3212	3328	1690	1669	3055	1598	2852
4b	3212	3327	1690	1673	3056	1599	2853
4c	3474	3263	1695	1628	3059	1544	3025
4e	3474	3272	1694	1673	3059	1544	2936

Biological Activity

The evaluated biological activities of all synthesized compounds (**3a-e**, **4a-c**, **4e**) were tested for their minimum inhibitory concentrations (MIC) (µg/ml) against the gram negative bacteria *E. coli*, *P. aureginosa* and *S. typhimurium*, gram positive bacteria *B. cereus*, and *S. aureus*, and fungi *S. cerevisiae* and *C. Albicans* and compared with the standard drugs Gentamicin and Tetracycline.

Compounds **3a**, **3b**, **3d**, **3e**, **4a** and **4e** showed an inhibitory effect on the Gram negative bacterium *P. aureginosa* (0.19 µg/ml). The effect of the six compounds listed in the smallest MIC value indicates the sensitivity of *P. aureginosa* to these compounds, and therefore its potential to be used for antimicrobial purposes in cases where *P. aureginosa* is targeted with additional studies. It was observed that *E. coli* was generally resistant to synthesized compounds tested in the study (**3a-e**, **4a-c**, **4e**). Except compound **3e** (1.56 µg/ml), MIC values were determined as 6.25 µg/ml and above for the rest. In the *in vitro*

antimicrobial activity determination of all compounds, *S. aureus* exhibit resistance to all derivatives, except for compound **3d** (0.39 µg/ml) and compound **3b** (0.19 µg/ml). A strong antimicrobial effect against *B. cereus* was not detected in the compounds synthesized in the study. *S. typhimurium* was sensitive to the compound **3d** (0.39 µg/ml). And *S. cerevisiae* was sensitive to the compound **3b** (1.56 µg/ml). Compounds **3a**, **3b**, and **3c** showed an inhibitory effect on the pathogenic yeast *C. albicans*. Among the all synthesized compounds used in the MIC test, compounds **3b** and **3d** were observed to have broad spectrum (Gram positive and Gram negative) antimicrobial activity. According to our findings, compounds **3b** and **3d** have the potential to be candidates for new antimicrobials. A detailed comparison of antimicrobial activities of all synthesized derivatives and the standard drugs used for activity comparison is summarized in the MIC table (Table 2).

Table 2. MIC values of Schiff and azo-Schiff base derivatives against bacteria and *C. fungi* (µg/ml)

Compound	<i>E. coli</i>	<i>P. aureginosa</i>	<i>S. aureus</i>	<i>B. cereus</i>	<i>S. typhimurium</i>	<i>S. cerevisiae</i>	<i>C. albicans</i>
3a	12,5	0,19	12,5	25	12,5	6,25	6,25
3b	12,5	0,19	0,19	12,5	6,25	1,56	6,25
3c	12,5	12,5	50	50	50	25	6,25
3d	6,25	0,19	0,39	50	0,39	25	25
3e	1,56	0,19	25	50	25	25	25
4a	12,5	0,19	50	50	50	25	12,5
4b	12,5	25	50	50	50	12,5	12,5
4c	25	50	50	50	25	12,5	12,5
4e	25	0,19	25	50	25	12,5	12,5
Gentamicin	1,56	1,56	0,39	0,39	0,39	25	25
Tetracycline	3,125	25	0,78	1,56	1,56	25	12,5

CONCLUSIONS

Schiff base and azo-Schiff base amino acid derivatives (**3a-e**, **4a-c**, **4e**) were synthesised and evaluated for their antimicrobial and antifungal activities against *Escherichia coli*, *Pseudomonas aureginosa*, *Staphylococcus aureus*, *Bacillus cereus*, *Salmonella typhimurium*, *Saccharomyces cerevisiae* and *Candida albicans*. The synthesised Schiff and azo-Schiff base derivatives show different activity against the test organisms. Compounds **3b** and **3d** seem to show better results with different test organisms compared with the other synthesised compounds.

EXPERIMENTAL SECTION

Materials

The Perkin Elmer Spectrum 100 FTIR Spectrometer was used for infrared spectra studies. All reagents were obtained from Merck, Sigma-Aldrich and Alfa Aesar. Melting points were recorded with an electro thermal digital melting points apparatus. TLC analyses were carried out on precoated aluminium plates and column chromatography was performed on Silica gel 60 F254 (Merck). UV active components were observed under the UV lamp for TLC. ¹H-NMR and ¹³C-NMR spectra were recorded using 400 MHz Varian NMR spectrometer.

General procedure for the synthesis of *N*-(*tert*-butoxycarbonyl)-amino acid (1a-e)

The protection reaction of amine groups was carried out with the same method as in our previous publication [15]. A mixture of di-*tert*-butyl dicarbonate (1.1 equiv) in 40 ml tetrahydrofuran was added to a mixture of an amino acid (1 equiv) and sodium bicarbonate (4 equiv) dissolved in 40 ml of water. The reaction mixture was continued for 72 hours until completion at room temperature. Completion of the reaction was confirmed by TLC (Hexane/EtOAc 1:1) and the remaining THF was evaporated. 2M HCl was added to pH 2 and water layer extracted with EtOAc (4×20ml), dried with sodium sulfate and concentrated in vacuo to give the desired product. D-Phenylglycine, L-phenylalanine, L-isoleucine, L-Valine and L-methionine were obtained in 86%, 87%, 93%, 89 % and 85% yields respectively.

General procedure for the synthesis of *N*-(*tert*-butoxycarbonyl)-amino acid-benzene-1,2-diamine (2a-e)

N-(*tert*-butoxycarbonyl)-amino acids (1 equiv) and *m*-phenylenediamine (1 equiv) were dissolved in 12 ml EtOAc with stirring at room temperature. A solution of *N,N*-dicyclohexylcarbodiimide (1 equiv) dissolved in 8 ml EtOAc was added in drops for 20 mins to the preceding mixture and the reaction was allowed to complete at room temperature for 6 hours. Upon completion, it was filtered and filtrate was washed twice with citric/tartaric acid solution 5% w/w and evaporated to dryness. The residue was purified by SiO₂ gel column chromatography (DCM/EtOAc 2:1) to give the desired compounds.

tert-Butyl 2-(3-aminophenylamino)-2-oxo-1-phenylethylcarbamate (2a)

White solid, yield: 82%, mp: 101-103 °C, IR (KBr, cm⁻¹): 3321, 3010, 2924, 2855, 1668, 1494, 1164. ¹H-NMR (400 MHz, CDCl₃) δ (ppm): 8.65 (s, 1H, NH), 7.47 (d, *J*=5.6 Hz, 2H, Ar-H), 7.29 (d, *J*= 6.2 Hz, 3H, Ar-H), 6.95 (d,

$J=7.9$ Hz, 1H, Ar-H), 6.91 (d, $J=7.6$ Hz, 1H, Ar-H), 6.70 (d, $J=7.0$ Hz, 1H, Ar-H), 6.32 (d, $J=7.6$ Hz, 1H, Ar-H), 6.11 (s, 1H, NH), 5.54 (s, 1H, CH), 3.58 (bs, 2H, NH₂), 1.41 (s, 9H, 3xCH₃). ¹³C-NMR (100MHz, CDCl₃) δ (ppm): 169.08, 155.69, 147.19, 138.52, 137.56, 132.43, 130.91, 129.49, 128.93, 128.35, 127.35, 111.29, 110.14, 106.93, 80.44, 59.12, 28.35. Anal. calc. for C₁₉H₂₃N₃O₃: C, 66.84; H, 6.79; N, 12.31. Found: C, 66.80; H, 6.77; N, 12.28.

***tert*-Butyl 1-(3-aminophenylamino)-1-oxo-3-phenylpropan-2-ylcarbamate (2b)**

White solid, yield: 75%, mp: 145-147 °C, IR (KBr, cm⁻¹): 3433, 3322, 3292, 3026, 2964, 2925, 2852, 1691, 1661, 1523, 1162. ¹H-NMR (400 MHz, CDCl₃) δ (ppm): 7.31-7.25 (m, 3H, Ar-H), 7.19 (t, $J=7.7$ Hz, 1H, Ar-H), 6.97 (d, $J=8.2$ Hz, 1H, Ar-H), 6.92-6.88 (m, 2H, Ar-H), 6.68 (d, 1H, $J=8.4$ Hz, Ar-H), 6.26 (dd, 1H, $J=7.9$ Hz, $J=1.3$ Hz, Ar-H), 5.03 (s, 1H, CH), 4.33-4.28 (m, 1H, NH), 3.33 (s, 2H, NH₂), 3.23 (s, 1H, NH), 2.98 (dd, $J=13.6$ Hz, $J=4.4$ Hz, 1H, CH_{2b}); 2.91 (t, $J=10.0$ Hz, 1H, CH_{2a}); 1.30 (s, 9H, 3xCH₃). ¹³C-NMR (100MHz, CDCl₃) δ (ppm): 170.80, 170.29, 155.78, 149.43, 139.94, 138.44, 129.68, 129.32, 128.43, 126.67, 109.88, 107.74, 105.48, 78.48, 58.74, 38.00, 28.60. Anal. calc. for C₂₀H₂₅N₃O₃: C, 67.58; H, 7.09; N, 11.82. Found: C, 67.52; H, 7.06; N, 11.80.

***tert*-Butyl 1-(3-aminophenylamino)-3-methyl-1-oxobutan-2-ylcarbamate (2c)**

White solid, yield: 86%, mp: 119-122 °C, IR (KBr, cm⁻¹): 3312, 3047, 2969, 2933, 2874, 1667, 1614, 1164. ¹H-NMR (400 MHz, CDCl₃) δ (ppm): 8.84 (s, 1H, NH), 6.95 (t, $J=7.9$ Hz, 2H, Ar-H), 6.79 (d, $J=7.1$ Hz, 1H, Ar-H), 6.34 (d, $J=7.5$ Hz, 1H, Ar-H), 5.70 (d, $J=8.7$ Hz, 1H, CH), 4.16 (s, 1H, NH), 3.63 (s, 2H, NH₂), 2.13 (d, $J=6.7$ Hz, 1H, CH(CH₃)₂), 1.40 (s, 9H, 3xCH₃), 0.99 (t, $J=6.8$ Hz, 6H, 2xCH₃). ¹³C-NMR (100MHz, CDCl₃) δ (ppm): 170.94, 156.41, 147.13, 138.75, 129.46, 111.05, 110.22, 106.90, 79.90, 60.96, 31.15, 28.34, 19.32. Anal. calc. for C₁₆H₂₅N₃O₃: C, 62.52; H, 8.20; N, 13.67. Found: C, 62.50; H, 8.22; N, 13.62.

***tert*-Butyl 1-(3-aminophenylamino)-3-methyl-1-oxopentan-2-ylcarbamate (2d)**

White solid, yield: 85%, mp: 130-131 °C, IR (KBr, cm⁻¹): 3310, 2966, 2933, 2877, 1664, 1528, 1164. ¹H-NMR (400 MHz, CDCl₃) δ (ppm): 8.77 (s, 1H, NH), 6.96 (t, $J=7.6$ Hz, 2H, Ar-H), 6.79 (d, $J=7.0$ Hz, 1H, Ar-H), 6.35 (d, $J=7.5$ Hz, 1H, Ar-H), 5.62 (d, $J=8.7$ Hz, 1H, CH), 4.18 (s, 1H, NH), 3.63 (s,

2H, NH₂), 1.91 (s, 1H, CH_{2a}-CH₃), 1.61 (s, 1H, CH_{2b}-CH₃), 1.40 (s, 9H, 3xCH₃), 1.21-1.12 (m, 1H, CH-CH₃), 0.98 (d, *J*=6.8 Hz, 3H, CH₃), 0.89 (t, *J*=7.6 Hz, 3H, CH₃). ¹³C-NMR (100MHz, CDCl₃) δ (ppm): 170.94, 156.35, 147.10, 138.73, 129.47, 111.03, 110.19, 106.85, 79.99, 60.01, 37.23, 28.33, 24.94, 15.50, 11.05. Anal. calc. for C₁₇H₂₇N₃O₃: C, 63.53; H, 8.47; N, 13.07. Found: C, 63.49; H, 8.49; N, 13.07.

***tert*-Butyl 1-(3-aminophenylamino)-4-(methylthio)-1-oxobutan-2-ylcarbamate (2e)**

White solid, yield: 64%, mp: 77-80 °C, IR (KBr, cm⁻¹): 3311, 3047, 2977, 2928, 2869, 1667, 1615, 1165. ¹H-NMR (400 MHz, CDCl₃) δ (ppm): 8.86 (s, 1H, NH), 6.98 (t, *J*=8.0 Hz, 2H, Ar-H), 6.76 (d, *J*=7.5 Hz, 1H, Ar-H), 6.36 (d, *J*=7.7 Hz, 1H, Ar-H), 5.80 (d, *J*=7.5 Hz, 1H, CH), 4.49 (d, *J*=6.0 Hz, 1H, NH), 3.65 (bs, 2H, NH₂), 2.59 (t, *J*=7.3 Hz, 2H, S-CH₂), 2.14-2.09 (m, 1H, CH-CH_{2a}), 2.06 (s, 3H, S-CH₃), 2.02-1.95 (m, 1H, CH-CH_{2a}), 1.40 (s, 9H, 3xCH₃). ¹³C-NMR (100MHz, CDCl₃) δ (ppm): 170.53, 156.19, 147.20, 138.64, 129.60, 111.24, 110.09, 106.78, 80.32, 54.31, 31.94, 30.26, 28.33, 15.31. Anal. calc. for C₁₆H₂₅N₃O₃S: C, 56.61; H, 7.15; N, 12.42. Found: C, 56.59; H, 7.18; N, 12.40.

General procedure for the synthesis *N*-(*tert*-butoxycarbonyl)-amino acid-2- hydroxy-1-naphthaldehyde (3a-e)

N-(*tert*-butoxycarbonyl)-amino acid-benzene-1,3-diamine (1 equiv) was dissolved in 15 ml methanol. An equimolar amount of 2-hydroxy-1-naphthaldehyde was added to the above mixture under reflux for at least 4 hours with the addition of a trace amount of acetic acid. The reaction was monitored with TLC (DCM/EtOAc 2:1). The reaction mixture was cooled down upon completion, filtered and crystallized from ethanol to obtain the desired product.

(*R,E*)-*tert*-Butyl-2-(3-((2-hydroxynaphthalen-1-yl)methyleneamino)phenylamino)-2-oxo-1-phenyl ethylcarbamate (3a)

Orange solid, yield: 84%, mp: 201-203 °C, IR (KBr, cm⁻¹): 3436, 3315, 2970, 2925, 2853, 1690, 1663, 1525, 1171. ¹H-NMR (400 MHz, CDCl₃) δ (ppm): 15.33 (s, 1H, OH), 9.21 (s, 1H, N=CH), 9.07 (bs, 1H, Ar-H), 8.17 (d, *J*=8.2 Hz, 1H, Ar-H), 7.69 (d, *J*=9.2 Hz, 1H, Ar-H), 7.62 (d, *J*=7.8 Hz, 1H, Ar-H), 7.58 (d, *J*=8.2 Hz, 2H, Ar-H), 7.49 (s, 1H, Ar-H), 7.41-7.34 (m, *J*=7.4 Hz, 3H, Ar-H), 7.29 (d, *J*=7.4 Hz, 1H, Ar-H), 7.25 (d, *J*=8.6 Hz, 1H, Ar-H), 7.15 (d, *J*=8.9 Hz, 1H, Ar-H), 6.95 (d, 1H, *J*=9.0 Hz, Ar-H), 6.86 (d, *J*=6.3 Hz, 1H,

Ar-H), 5.80 (d, $J=6.8$ Hz, 1H, CH), 5.58 (bs, 1H, NH), 1.44 (s, 9H, $3\times\text{CH}_3$). ^{13}C -NMR (100MHz, CDCl_3) δ (ppm): 172.17, 169.17, 164.94, 156.20, 153.74, 144.42, 139.20, 137.02, 136.54, 133.43, 129.72, 129.19, 128.84, 128.04, 127.54, 127.06, 124.48, 123.38, 122.76, 119.23, 118.59, 117.23, 116.58, 109.98, 108.67, 81.01, 59.71, 28.34. Anal. calc. for $\text{C}_{30}\text{H}_{29}\text{N}_3\text{O}_4$: C, 72.71; H, 5.90; N, 8.48. Found: C, 72.68; H, 5.93; N, 8.46.

(*S,E*)-tert-Butyl-1-(3-((2-hydroxynaphthalen-1-yl)methyleneamino)phenylamino)-1-oxo-3-phenyl propan-2-ylcarbamate (3b)

Orange solid, yield: 86%, mp: 206-208 °C, IR (KBr, cm^{-1}): 3557, 3303, 3328, 3031, 2978, 2876, 1688, 1660, 1527, 1160. ^1H -NMR (400 MHz, DMSO-D_6) δ (ppm): 15.68 (s, 1H, OH), 10.17 (s, 1H, NH), 9.59 (s, 1H, N=CH), 8.43 (d, $J=8.4$ Hz, 1H, Ar-H), 7.92 (d, $J=9.2$ Hz, 1H, Ar-H), 7.78 (d, $J=7.8$ Hz, 1H, Ar-H), 7.72 (s, 1H, Ar-H), 7.55 (t, $J=7.8$ Hz, 1H, Ar-H), 7.49 (d, $J=4.7$ Hz, 1H, Ar-H), 7.42 (d, $J=4.8$ Hz, 2H, Ar-H), 7.35 (t, $J=7.7$ Hz, 3H, Ar-H), 7.29 (t, $J=7.2$ Hz, 2H, Ar-H), 7.20 (d, $J=7.2$ Hz, 1H, Ar-H), 7.13 (d, $J=8.0$ Hz, 1H, Ar-H), 6.98 (d, $J=9.1$ Hz, 1H, CH), 4.34 (bs, 1H, NH), 3.03 (d, $J=10.0$ Hz, 1H, Ar- CH_{2b}), 2.86 (t, $J=10.8$ Hz, 1H, Ar- CH_{2a}), 1.31 (s, 9H, $3\times\text{CH}_3$). ^{13}C -NMR (100MHz, DMSO-D_6) δ (ppm): 171.54, 171.18, 155.89, 144.68, 140.51, 138.33, 137.46, 133.55, 130.45, 129.68, 129.49, 128.60, 128.50, 127.11, 126.76, 123.96, 122.63, 120.56, 117.76, 114.94, 112.35, 108.86, 78.60, 57.11, 37.90, 28.61. Anal. calc. for $\text{C}_{31}\text{H}_{31}\text{N}_3\text{O}_4$: C, 73.06; H, 6.13; N, 8.25. Found: C, 73.10; H, 6.14; N, 8.23.

(*S,E*)-tert-Butyl-1-(3-((2-hydroxynaphthalen-1-yl)methyleneamino)phenylamino)-3-methyl-1-oxo butan-2-ylcarbamate (3c)

Orange solid, yield: 91%, mp: 175-177 °C, IR (KBr, cm^{-1}): 3400, 3316, 3055, 2965, 2929, 2872, 2400, 1690, 1668, 1640, 1505, 1162. ^1H -NMR (400 MHz, CDCl_3) δ (ppm): 15.32 (s, 1H, OH), 9.30 (s, 1H, N=CH), 9.09 (s, 1H, Ar-H), 8.04 (d, $J=7.2$ Hz, 1H, Ar-H), 7.65 (d, $J=9.1$ Hz, 1H, Ar-H), 7.57 (d, $J=5.8$ Hz, 2H, Ar-H), 7.42 (t, $J=7.2$ Hz, 1H, Ar-H), 7.24 (t, $J=6.3$ Hz, 2H, Ar-H), 7.12 (s, 1H, Ar-H), 6.94 (d, 1H, $J=8.9$ Hz, Ar-H), 6.85 (s, 1H, NH), 5.62 (d, $J=8.3$ Hz, 1H, CH), 4.26 (s, 1H, NH), 2.21 (d, $J=5.4$ Hz, 1H, CH- $(\text{CH}_3)_2$), 1.45 (s, 9H, $3\times\text{CH}_3$), 1.10 (d, $J=6.2$ Hz, 6H, $2\times\text{CH}_3$). ^{13}C -NMR (100MHz, CDCl_3) δ (ppm): 171.98, 171.23, 156.89, 153.57, 144.45, 139.24, 136.95, 133.33, 129.71, 129.13, 128.02, 127.01, 123.36, 122.67, 119.11, 117.29, 116.41, 110.09, 108.60, 80.48, 61.25, 30.98, 28.38, 19.38, 18.63. Anal. calc. for $\text{C}_{27}\text{H}_{31}\text{N}_3\text{O}_4$: C, 70.26; H, 6.77; N, 9.10. Found: C, 70.27; H, 6.74; N, 9.07.

***tert*-Butyl (2*S*,3*S*)-1-(3-((*E*)-(2-hydroxynaphthalen-1-yl)
methyleneamino)phenylamino)-3-methyl-1-oxopentan-2-
ylcarbamate (3d)**

Orange solid, yield: 94%, mp: 197-200 °C, IR (KBr, cm⁻¹): 3485, 3330, 2960, 2926, 2830, 1688, 1662, 1526, 1174. ¹H-NMR (400 MHz, CDCl₃) δ (ppm): 15.31 (s, 1H, OH), 9.36 (s, 1H, N=CH), 9.08 (s, 1H, Ar-H), 8.04 (d, *J*=8.4 Hz, 1H, Ar-H), 7.64 (d, *J*=9.0 Hz, 1H, Ar-H), 7.57 (d, *J*=8.6 Hz, 2H, Ar-H), 7.43 (t, *J*=7.2 Hz, 1H, Ar-H), 7.27-7.22 (m, 2H, Ar-H), 7.10 (t, *J*=7.2 Hz, 1H, Ar-H), 6.94 (d, *J*=9.1 Hz, 1H, Ar-H), 6.84 (d, *J*=8.5 Hz, 1H, NH), 5.62 (d, *J*=8.5 Hz, 1H, CH), 4.30 (s, 1H, NH), 1.97 (d, *J*=5.6 Hz, 1H, CH-CH₃), 1.44 (s, 9H, 3xCH₃), 1.34-1.24 (m, 2H, CH₂), 1.08 (d, *J*=6.7 Hz, 3H, CH-CH₃), 0.95 (t, *J*=7.4 Hz, 3H, CH₂-CH₃). ¹³C-NMR (100MHz, CDCl₃) δ (ppm): 171.92, 171.40, 156.87, 153.53, 144.44, 139.26, 136.91, 133.33, 129.70, 129.11, 128.02, 127.01, 123.35, 122.65, 119.12, 117.23, 116.46, 109.96, 108.59, 80.47, 60.22, 37.13, 28.38, 25.16, 15.57, 10.92. Anal. calc. for C₂₈H₃₃N₃O₄: C, 70.71; H, 6.99; N, 8.84. Found: C, 70.67; H, 6.95; N, 8.80.

**(*S*,*E*)-*tert*-Butyl-1-(3-((2-hydroxynaphthalen-1-yl)
methyleneamino)phenylamino)-4-(methylthio)-1-oxobutan-2-
ylcarbamate (3e)**

Orange solid, yield: 92%, mp: 156-158 °C, IR (KBr, cm⁻¹): 3480, 3301, 3055, 2978, 2919, 1682, 1672, 1546, 1165. ¹H-NMR (400 MHz, CDCl₃) δ (ppm): 15.29 (s, 1H, OH), 9.21 (s, 1H, N=CH), 9.13 (s, 1H, Ar-H), 8.02 (d, *J*=7.3 Hz, 1H, Ar-H), 7.67 (d, *J*=7.2 Hz, 1H, Ar-H), 7.60 (d, *J*=7.5 Hz, 2H, Ar-H), 7.44 (app. t, *J*=6.2 Hz, 1H, Ar-H), 7.27 (d, *J*=8.4 Hz, 2H, Ar-H), 7.20 (s, 1H, Ar-H), 6.94 (s, 2H, Ar-H+NH), 5.71 (s, 1H, CH), 4.57 (s, 1H, NH), 2.66 (t, *J*=6.3 Hz, 2H, S-CH₂), 2.21 (s, 1H, CH-CH_{2b}), 2.11 (s, 4H, S-CH₃+CH-CH_{2a}), 1.45 (s, 9H, 3xCH₃). ¹³C-NMR (100MHz, CDCl₃) δ (ppm): 170.80, 156.55, 153.88, 144.87, 139.13, 136.99, 133.28, 129.89, 129.19, 128.08, 127.10, 123.47, 122.53, 119.03, 118.60, 117.48, 116.54, 110.58, 108.68, 80.80, 54.62, 31.63, 30.41, 28.38, 15.43. Anal. calc. for C₂₇H₃₁N₃O₄S: C, 65.70; H, 6.33; N, 8.51. Found: C, 65.67; H, 6.31; N, 8.47.

**General procedure for the synthesis *N*-(*tert*-butoxycarbonyl)-
amino acid-phenyldiazenyl salicylaldehyde (4a-c, 4e)**

N-(*tert*-butoxycarbonyl)-amino acid-benzene-1,3-diamine (1 equiv) were dissolved in 35 ml ethanol. An equimolar amount of phenyldiazenyl salicylaldehyde (1 equiv) was added to the above mixture under reflux for at least 24 hours with the addition of a trace amount of acetic acid. The reaction

was monitored with TLC (DCM/EtOAc 2:1). The reaction mixture was cooled down upon completion, filtered and crystallized from ethanol to obtain final product.

***tert*-Butyl-(*R*)-2-(3-((*E*)-2-hydroxy-5-((*E*)phenyldiazenyl)benzylideneamino)phenylamino)-2-oxo-1-phenylethylcarbamate (4a)**

Orange solid, yield: 70%, mp: 183-185 °C, IR (KBr, cm⁻¹): 3328, 3212, 3055, 2924, 2852, 1690, 1669, 1640, 1598, 1167. ¹H-NMR (400 MHz, CDCl₃) δ (ppm): 13.78 (s, 1H, OH), 9.20 (s, 1H, N=CH), 8.59 (s, 1H, Ar-H), 7.95 (app d, *J*=5.6 Hz, 2H, Ar-H), 7.88 (d, *J*= 8.0 Hz, 2H, Ar-H), 7.59 (d, *J*=9.1 Hz, 2H, Ar-H), 7.53 (t, *J*=8.0 Hz, 3H, Ar-H), 7.46-7.42 (m, 1H, Ar-H), 7.39-7.33 (m, 3H, Ar-H), 7.23 (d, *J*=7.7 Hz, 1H, Ar-H), 7.16 (t, *J*=7.6 Hz, 1H, Ar-H), 7.06 (d, *J*=9.4 Hz, 1H, Ar-H), 6.86 (d, *J*=6.9 Hz, 1H, NH), 5.88 (d, *J*=7.2 Hz, 1H, CH), 5.64 (d, *J*=5.5 Hz, 1H, NH), 1.48 (s, 9H, 3xCH₃). ¹³C-NMR (100MHz, CDCl₃) δ (ppm): 169.33, 164.19, 162.01, 162.00, 156.30, 152.56, 147.52, 145.39, 139.01, 139.00, 136.45, 130.45, 129.50, 129.15, 129.04, 128.81, 128.27, 127.56, 127.31, 122.65, 118.68, 118.31, 118.11, 117.71, 111.56, 81.01, 59.52, 28.42. Anal. calc. for C₃₂H₃₁N₅O₄: C, 69.93; H, 5.69; N, 12.74. Found: C, 69.95; H, 5.67; N, 12.75.

***tert*-Butyl-(*S*)-1-(3-((*E*)-2-hydroxy-5-((*E*)phenyldiazenyl)benzylideneamino)phenylamino)-1-oxo-3-phenylpropan-2-ylcarbamate (4b)**

Orange solid, yield: 85%, mp: 191-193 °C, IR (KBr, cm⁻¹): 3327, 3212, 3056, 2984, 2926, 2853, 1690, 1673, 1640, 1599, 1519, 1164. ¹H-NMR (400 MHz, CDCl₃) δ (ppm): 13.69 (s, 1H, OH), 8.95 (s, 1H, N=CH), 8.52 (s, 1H, Ar-H), 7.98 (d, *J*=8.7 Hz, 1H, Ar-H), 7.89 (d, *J*=7.0 Hz, 3H, Ar-H), 7.54 (s, 1H, Ar-H), 7.52 (t, *J*=7.2 Hz, 2H, Ar-H), 7.45 (d, *J*=7.3 Hz, 1H, Ar-H) 7.27 (app d, *J*=3.7 Hz, 4H, Ar-H), 7.18 (s, 2H, Ar-H), 7.08 (d, *J*=8.7 Hz, 1H, Ar-H), 6.91 (s, 1H, Ar-H), 5.62 (d, *J*=6.7 Hz, 1H, CH), 4.74 (bs, 1H, NH), 3.23 (dd, *J*=13.3 Hz, *J*=6.1 Hz, 1H, CH_{2a}), 3.13 (dd, *J*=13.4 Hz, *J*=8.1 Hz, 1H, CH_{2b}), 1.42 (s, 9H, 3xCH₃). ¹³C-NMR (100MHz, CDCl₃) δ (ppm): 170.61, 164.03, 163.12, 162.18, 156.39, 152.53, 151.62, 147.92, 145.40, 138.75, 136.51, 130.50, 129.68, 129.24, 129.05, 128.74, 128.07, 127.52, 127.03, 122.64, 121.72, 118.66, 118.45, 118.05, 117.84, 111.91, 80.73, 56.86, 38.66, 28.35. Anal. calc. for C₃₃H₃₃N₅O₄: C, 70.32; H, 5.90; N, 12.43. Found: C, 70.34; H, 5.91; N, 12.41.

***tert*-Butyl-(S)-1-(3-((*E*)-2-hydroxy-5-((*E*)-phenyldiazenyl)benzylideneamino)phenyl amino)-3-methyl-1-oxobutan-2-ylcarbamate (4c)**

Orange solid, yield: 61%, mp: 172-174 °C, IR (KBr, cm⁻¹): 3474, 3263, 3059, 3025, 2984, 1695, 1628, 1544, 1164. ¹H-NMR (400 MHz, CDCl₃) δ (ppm): 13.72 (s, 1H, OH), 9.24 (s, 1H, N=CH), 8.54 (s, 1H, Ar-H), 7.92 (t, *J*=7.9 Hz, 2H, Ar-H), 7.87 (d, *J*=7.5 Hz, 2H, Ar-H), 7.59 (s, 1H, Ar-H), 7.49 (t, *J*=7.0 Hz, 2H, Ar-H), 7.44 (d, *J*=7.0 Hz, 1H, Ar-H), 7.28 (d, *J*=7.6 Hz, 1H, Ar-H), 7.16 (t, *J*=6.8 Hz, 1H, Ar-H), 7.05 (d, *J*=8.6 Hz, 1H, Ar-H), 6.87 (d, *J*=6.8 Hz, 1H, NH), 5.59 (d, *J*=8.5 Hz, 1H, CH), 4.26 (app t, *J*=7.6 Hz, 1H, NH), 2.19 (d, *J*=6.8 Hz, 1H, CH(CH₃)₂), 1.47 (s, 9H, 3xCH₃), 1.10 (d, *J*=6.2 Hz, 6H, 2xCH₃). ¹³C-NMR (100MHz, CDCl₃) δ (ppm): 171.26, 164.09, 162.00, 156.85, 152.53, 147.69, 145.35, 138.96, 130.44, 129.58, 129.02, 128.15, 127.36, 122.63, 118.66, 118.33, 118.05, 117.66, 111.63, 80.48, 61.20, 30.95, 28.41, 19.41, 18.70. Anal. calc. for C₂₉H₃₃N₅O₄: C, 67.55; H, 6.45; N, 13.58. Found: C, 67.54; H, 6.43; N, 13.52.

***tert*-Butyl-(S)-1-(3-((*E*)-2-hydroxy-5-((*E*)-phenyldiazenyl)benzylideneamino)phenyl amino)-4-(methylthio)-1-oxobutan-2-ylcarbamate (4e)**

Orange solid, yield: 64%, mp: 182-184 °C, IR (KBr, cm⁻¹): 3474, 3272, 3059, 3024, 2936, 1694, 1673, 1544, 1184. ¹H-NMR (400 MHz, CDCl₃) δ (ppm): 13.69 (s, 1H, OH), 9.21 (s, 1H, N=CH), 8.58 (s, 1H, Ar-H), 7.96 (t, *J*=9.0 Hz, 2H, Ar-H), 7.87 (d, *J*=7.4 Hz, 2H, Ar-H), 7.60 (s, 1H, Ar-H), 7.49 (t, *J*=7.4 Hz, 2H, Ar-H), 7.44 (t, *J*=7.2 Hz, 1H, Ar-H), 7.32 (d, *J*=7.7 Hz, 1H, Ar-H), 7.23 (t, *J*=7.6 Hz, 1H, Ar-H), 7.06 (d, *J*=8.8 Hz, 1H, Ar-H), 6.93 (d, *J*=7.2 Hz, 1H, NH), 5.68 (d, *J*=7.7 Hz, 1H, CH), 4.59 (d, *J*=7.0 Hz, 1H, NH), 2.68 (t, *J*=7.2 Hz, 2H, S-CH₂), 2.25-2.17 (m, 1H, CH-CH_{2b}), 2.12 (s, 3H, S-CH₃), 2.09-2.02 (m, 1H, CH-CH_{2a}), 1.46 (s, 9H, 3xCH₃). ¹³C-NMR (100MHz, CDCl₃) δ (ppm): 170.81, 164.03, 162.24, 156.56, 152.51, 147.98, 145.40, 138.89, 130.49, 129.74, 129.04, 128.12, 127.45, 122.62, 118.67, 118.41, 118.07, 117.71, 111.99, 80.80, 54.52, 31.57, 30.38, 28.39, 15.41. Anal. calc. for C₂₉H₃₃N₅O₄S: C, 63.60; H, 6.07; N, 12.79. Found: C, 63.62; H, 6.04; N, 12.77.

Biological Activity

The biological activities of the target compounds were carried out to ascertain the minimum inhibitory concentrations (MIC µg/ml) of derivatives against the gram negative bacteria *E.coli* (ATCC 12228), *P. aureginosa* (ATCC 27853) and *S. typhimurium* (CCM 5445), gram positive bacteria *B.*

Cereus (ATCC 6633), and *S. aureus* (ATCC 6538-P); fungi *S. cerevisiae* (ATCC 9763) and *C. Albicans* (ATCC 10239). All strains were stored as frozen stocks containing 30% glycerol at -2 °C. Stock strains were cultured on TSA (Tryptic Soy Agar) plates prior to experiment. For the determination of MIC values, double strength MHB (Mueller Hinton Broth) medium was inoculated and left to incubate at 37 °C overnight. The experiment was carried out in 96 microplate wells according to the method reported as standard (Clinical and Laboratory Standards Institute, 2011). All products (**3a-e**, **4a-c**, **4e**) whose antimicrobial activity was determined on the strains in the MIC test were prepared in 10% DMSO solution.

The stock concentration of all antimicrobial compounds was set at 100 µg/ml. Fresh cultures of standard strains were prepared to have 0.5 McFarland turbidity. 50 µl of bacterial suspensions were transferred to each well. Then, each antimicrobial compound solution to be tested was added to the wells in a volume of 50 µl. Positive and negative control groups were formed into microplate wells 11 and 12, respectively. Only the relevant test microorganism was transferred to the positive controls and only the relevant antimicrobial compound to the negative controls. The prepared microplates were left to incubation at 37 °C for 24 hours. After the incubation, the activities of the antimicrobial compounds in the wells were evaluated according to the lack of turbidity, which indicates the inhibition of test bacteria, and the formation of red color when 1% TTC solution was dropped. The concentration of the compound in the end wells with no turbidity and red color formation observed was accepted as the MIC values for the microorganism concerned. Antimicrobial activities of the all compounds tested were determined by the MIC (Minimum inhibitory concentration test) and 50 µg/ml was realized as 0.19 µg/ml.

ACKNOWLEDGMENTS

This research has been supported by Ege University Scientific Research Projects Coordination Unit (Project number: 21656).

REFERENCES

1. W. A. Zoubi; A. A. S. Al-Hamdani; , S. D. Ahmed; Y. G. Ko; *Appl. Organometal. Chem.*, **2018**, 32, 3895-3910
2. S. Slassi; A. El-Ghayoury; M. Aarjane; K. Yamni; A. Amine; *Appl. Organometal. Chem.*, **2020**, 34, 5503-5512
3. M. S. Kasare; P. P. Dhavan; B. L. Jadhav; S. D. Pawar; *Chemistry Select*, **2019**, 4, 10792–10797

SYNTHESIS, CHARACTERIZATION AND BIOLOGICAL ACTIVITY OF SCHIFF
AND AZO-SCHIFF BASE LIGANDS

4. M. Gulcan; S. Özdemir; A. Dündar; E. İspir; M. Z. Kurtoğlu; *Anorg. Allg. Chem.*, **2014**, *640*, 1754-1762
5. A. Kakanejadifarda; V. Khojasteha; A. Zabardastia; F. Azarbari; *Org. Chem. Res.*, **2018**, *4*, 210-226
6. H. M. Hessoon; F. F. Karam; *Egypt. J. Chem.*, **2022**, *65*, 327-334
7. K. J. Al-Adilee; S. R. Hasan; *IOP Conf. Ser.: Earth Environ. Sci.*, **2021**, *790*, 12031-12051
8. P. A. Channar; A. Saeed; D. Shahzad; F. A. Larik; M. Hassan; H. Raza; Q. Abbas; S. Seo; *Chem. Biol. Drug Des.*, **2018**, *92*, 1692-1698
9. H. Kaur; J. Singh; B. Narasimhan; *BMC Chemistry*, **2019**, *13*, 1-19
10. E. İspir; *Dyes and Pigment*, **2009**, *82*, 13-19
11. M. S. Refat; I. M. El-Deen; Z. M. Anwer; S. El-Ghol; *J. Coord. Chem.*, **2009**, *10*, 1709-1718
12. M. S. Refat; I. M. El-Deen; R. R. Amin; S. El-Ghol; *Toxicol. Environ. Chem.*, **2010**, *92*, 1093-1110
13. I. N. Witwit; Z. Y. Motaweq; H. M. Mubark; *J. Pharm. Sci. & Res.*, **2018**, *10*, 3074-3083
14. S. Slassi; A. Fix-Tailler; G. Larcher; A. Amine; A. El-Ghayoury; *Heteroat. Chem.*, **2019**, *2019*, 1-8
15. E. Isik; D. Astley; S. Yuksekdanaci; I. Yasa; *Lett. Drug Des. Discov.*, **2020**, *17*, 1372-1379.

COMPARATIVE STUDY OF TWO COMMERCIAL STONEWARE PASTES FOR PLASTIC SHAPING BY POTTERY WHEEL

Réka BARABÁS^a, Oana CADAR^b, Liliana BIZO^{c,*}

ABSTRACT. Two commercial stoneware pastes traditionally used to produce ceramic objects were evaluated. The objective was the comparative characterization of the pastes and to find the most suitable to obtain fine ceramic objects using the pottery wheel. Both ceramic pastes were characterized by X-ray powder diffraction (XRPD), particle size analyses (laser diffraction) and thermal analyses (thermogravimetry-TG, its derivative-DTG, and differential thermal analysis-DTA). The technological properties like linear drying and firing shrinkage, moisture content and plasticity were also determined. The results showed that both pastes have appropriate properties making them suitable for plastic shaping by pottery wheel. In addition, the stoneware paper clay paste is “greener” due to its content of cellulose fibers which can come even from recycled paper.

Keywords: *traditional ceramics, commercial stoneware, XRPD, TG-DTG-DTA, drying and firing shrinkage, moisture content, plasticity, potter’s wheel*

INTRODUCTION

Traditional ceramics refers to ceramic products that are produced from unrefined clay and combinations of refined clay and powdered or granulated non plastic minerals. Often, traditional ceramics is used to refer to ceramics in which the clay content exceeds 20 % [1, 2]. The major ceramic

^a Babeş-Bolyai University, Faculty of Chemistry and Chemical Engineering, Department of Chemistry and Chemical Engineering of Hungarian Line of Study, 11 Arany Janos str., RO-400028, Cluj-Napoca, Romania

^b INCDO-INOE 2000, Research Institute for Analytical Instrumentation, 67 Donath str., RO-400293, Cluj-Napoca, Romania

^c Babeş-Bolyai University, Faculty of Chemistry and Chemical Engineering, Department of Chemical Engineering, 11 Arany Janos str., RO-400028, Cluj-Napoca, Romania

* Corresponding author: liliana.bizo@ubbcluj.ro



categories are earthenware, stoneware and porcelain. Stoneware bodies are composed of modified secondary clays, fired to high temperatures of 1200 to 1300 °C to produce a vitrified, hard, and durable ceramic. It is made from clay but is more durable than other kinds of pottery and earthenware. The porosity of stoneware is < 3 % and colours include white, buff, grey and black. Stoneware has a reputation for being easy to use, is generally quite plastic, workable, and versatile. Some stoneware clay feels quite smooth and silky to use. However, if it is added grog or sand, it can feel coarser and grittier. Grog is clay that has previously been fired and then crushed; it comes in different particle sizes, and it's usually added to clay to give it a different texture and reduce the shrinkage of the piece [3].

The main phases in ceramics technology are: (I) preparation of the ceramic mass; (II) shaping; (III) drying; (IV) firing; and (V) finishing the product. Many shaping/forming methods are used for ceramic products, and these can be grouped into three basic categories: powder compaction (dry pressing, hot pressing, cold isostatic pressing, etc.), casting (slip casting, gel casting, electrophoresis casting, etc), plastic forming (extrusion, injection molding, etc.) [4]. In case of the traditional ceramics there are some manual shaping methods, which belongs to the plastic forming, like: pinching, coiling, or using a potter's wheel [5, 6]. There is a wide variety of clays on the market for potter's wheel and all have their own properties that make them suitable than others for specific projects. Given the fact that in the technology of artisanal ceramics there are several shaping methods, the question arises, which of the commercial clays is the most suitable for shaping on the potter's wheel?

In this study, two commercial stoneware pastes with different compositions were compared. The first studied paste was a Stoneware B17C (noted S1) (Valentine Clays Ltd, Stoke-on-Trent, UK) [7]. This paste is a blend of selected low iron clays providing an ideal background for a decorative approach to stoneware ceramics. Silica sand makes it excellent for throwing, too [7]. The second one, PCL stoneware paperclay (noted S2) (SIO-2®, Esparreguera-Barcelona, Spain) [8], consists of a mixture of clay and cellulose fibers. The cellulose fibers in paperclay can come from either new or recycled paper pulp, derived from plants such as cotton, hemp, flax, linen, or trees [9]. By adding paper to the clay potters the number of defects could be reduced. Because paperclay is so strong at the greenware stage, it can be used in a technique called "raw glazing". In addition, the stoneware paper clay body with 30% impalpable grog (up to 80 Mesh) is formulated for artistic ceramics and it is unique for modelling, due to its exceptional plasticity [8]. It is especially suitable for making impossible shapes with difficult drying. The presence of paper fibers inside avoids formation of cracks and problems of deformations and leads PCL clay to surprising artistic possibilities [8].

Since the knowledge of a material's properties is the basis of materials science and is a necessity in the development of viable technical solutions, the objective of this work was the characterization of two commercial stoneware pastes and to find the most suitable to obtain fine ceramic objects by plastic shaping using pottery wheel. The properties which have been considered in the present study are drying or firing shrinkage, moisture content and plasticity. Moreover, XRPD and TG-DTG-DTA analysis were employed to determine the mineralogical composition, before and after firing, and thermal behavior of the studied stoneware pastes.

RESULTS AND DISCUSSION

Particle size distribution (PSD) analyses

The particle size distribution (PSD) in a ceramic body has a significant impact on the packing efficiency, which in turn, influences the size and shape of pores, the shrinkage behavior and microstructure development [10]. The PSD of the S1 and S2 stoneware pastes in suspension were analyzed by laser diffraction and the results are given in Figure 1(a, b). It can be observed from Figure 1(a) that S1 shows a wide trimodal distribution presenting three maximum points, which are centered at around 0.15, 3 and 30 μm , respectively. For the S2 sample (Figure 2(b)) the results show a narrow distribution with fractions ranged from 0.01 and 0.03 μm . The results for PSD analyses are summarized on Table 1.

As visible from the results, the S2 paste contains finer particles, with a mean value of 0.021 μm , whereas larger particles were found for the S1 paste, with a mean value of 2.382 μm . It is known that the finer the particles, the larger the surface they can expose to water and, consequently, the higher the plasticity.

Mineralogical composition

The mineralogical transformations which take place during the firing process are very important for establishing the final properties of the ceramic products. Consequently, the mineralogical transformations caused by firing, of two different compositions used in the formulation of ceramic pastes have been studied by XRPD. Figure 2 (black line) shows the XRPD pattern of the S1 ceramic paste.

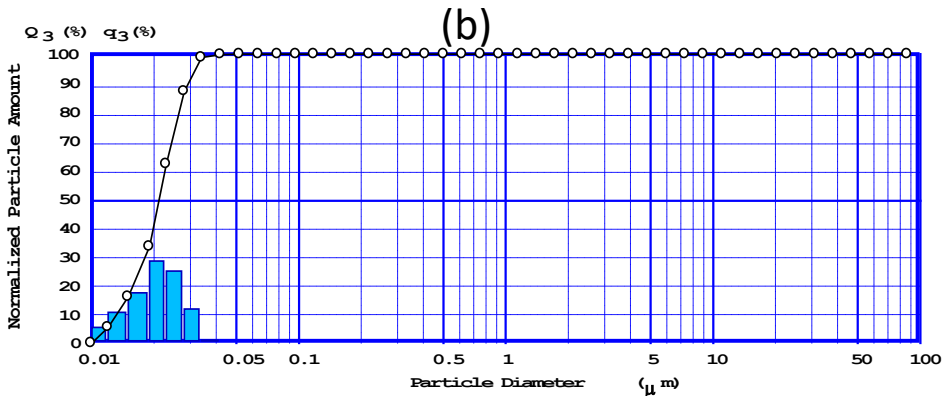
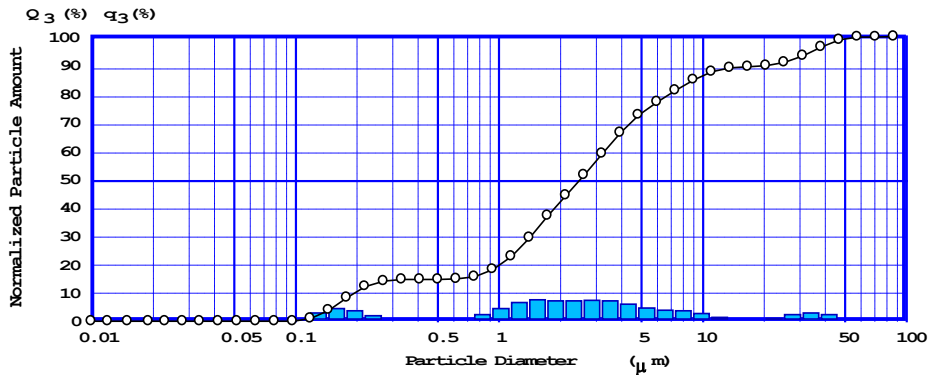


Figure 1. PSD of S1 and S2 stoneware samples.

Table 1. The results of PSD analyses performed on S1 and S2 stoneware pastes

Sample ID	Median D (μm)	Modal D (μm)	Mean V (μm)	SD*	D ₂₅ (μm)	D ₅₀ (μm)	D ₇₅ (μm)
S1	2.503	1.562	2.382	0.640	1.227	2.503	5.433
S2	0.021	0.021	0.021	0.126	0.017	0.021	0.025

* SD-standard deviation

COMPARATIVE STUDY OF TWO COMMERCIAL STONEWARE PASTES
FOR PLASTIC SHAPING BY POTTERY WHEEL

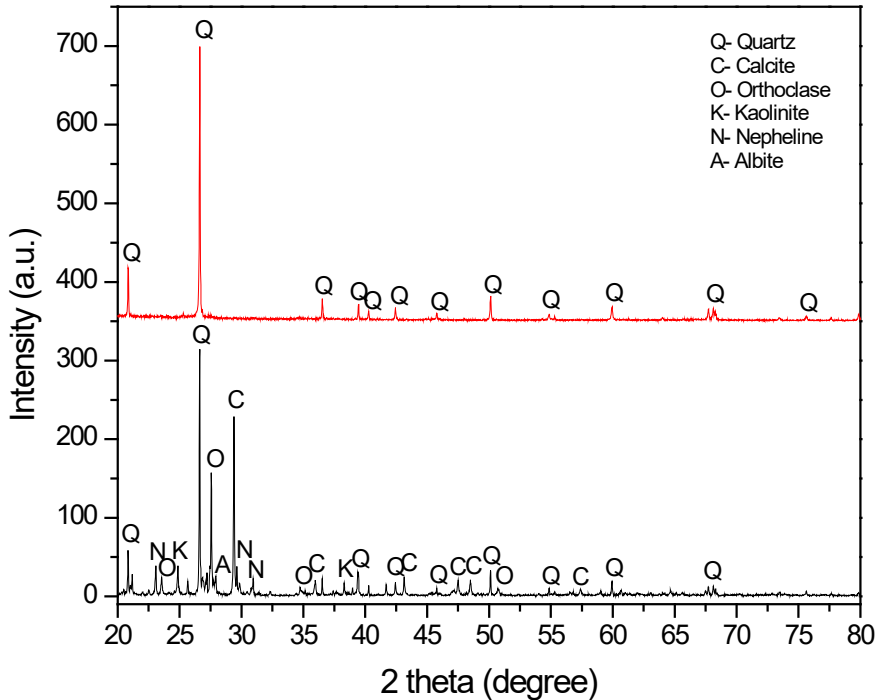


Figure 2. XRPD patterns of S1 sample (black) before and (red) after thermal treatment at 1260 °C.

The sample is mainly constituted of quartz (SiO_2), calcite (CaCO_3), orthoclase (KAlSi_3O_8), albite ($\text{NaAlSi}_3\text{O}_8$). The main clay mineral is kaolinite ($\text{Al}_2\text{O}_3 \cdot 2\text{SiO}_2 \cdot 2\text{H}_2\text{O}$). In addition, some traces of nepheline ($(\text{Na},\text{K})\text{AlSiO}_4$) were also identified. The XRPD diffractogram of the ceramic body fired at 1260 °C is shown in Figure 2 (red line). After firing the crystalline phase identified was quartz (SiO_2).

Jordán et al. stated before that the sintering temperature for firing ceramic pastes exceeds the energy threshold of the reactivity of the materials and produces a series of reactions and transformations that lead to the formation of new phases and the disappearance of others [11].

In Figure 3 are shown the XRPD patterns of the S2 ceramic paste before (black line) and after firing (red line) at 1320 °C. In this case the sample is mainly constituted of quartz (SiO_2), and kaolinite ($\text{Al}_2\text{O}_3 \cdot 2\text{SiO}_2 \cdot 2\text{H}_2\text{O}$). The XRPD diffractograms of the ceramic bodies sintered at 1320 °C are shown in Figure 3. After firing the identified phases were quartz (SiO_2), and mullite.

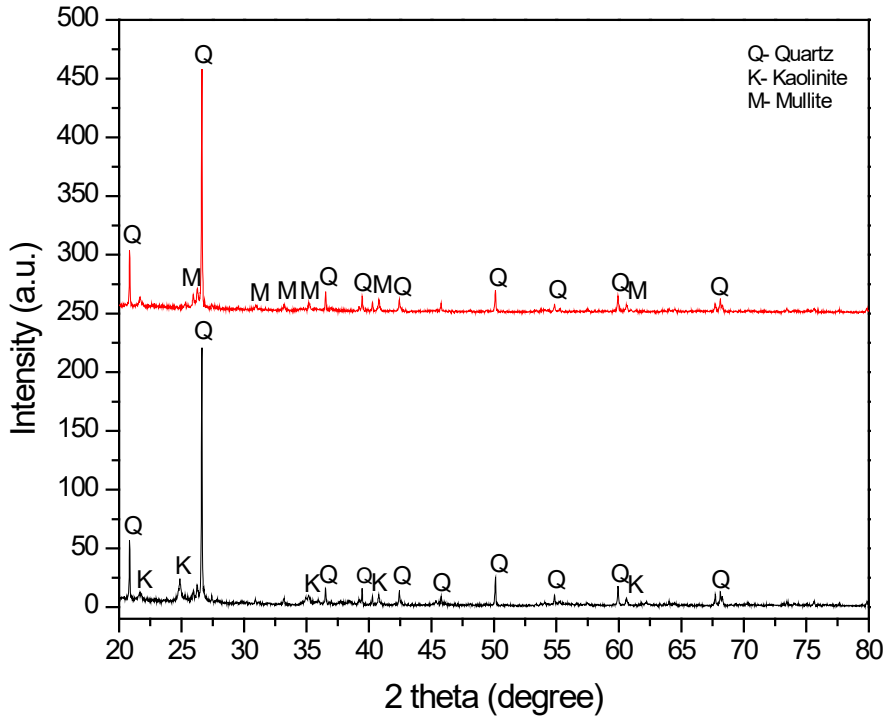


Figure 3. XRPD patterns of S2 sample (black) before and (red) after thermal treatment at 1260 °C.

It was previously demonstrated that mullite ($\text{Al}_2\text{O}_3 \cdot 2\text{SiO}_2$ to $2\text{Al}_2\text{O}_3 \cdot \text{SiO}_2$) is an important crystalline phase which is desirable to be present in ceramics, due to its properties like low thermal expansion and thermal conductivity, creep resistance and high temperature stability [12]. In addition, quartz is known to prevent warping of the fired materials [13].

Thermal analyses

Generally, during the firing process, a series of intercrystalline and extracrystalline reactions take place like: (I) dehydroxylation of clay minerals and the consequent formation of pseudo-amorphous products (such as metakaolinite from kaolinite dehydroxilate product); (II) crystallisation of primary mullite from pseudo-amorphous products with a consequent segregation of a silica rich amorphous phase; (III) formation of an alkaline melt originating from the melting of feldspar; (IV) viscous sintering, or vitrification, in which the viscous melt fills up the pores in the body under the

COMPARATIVE STUDY OF TWO COMMERCIAL STONEWARE PASTES
FOR PLASTIC SHAPING BY POTTERY WHEEL

influence of capillary forces so that a dense body is obtained; (V) partial decomposition of quartz due to instability in the presence of the alkaline melt; (VI) crystallisation of secondary mullite [14].

Thermal behavior of the S1 stoneware is presented in Figure 4, where the obtained TG, DTG and DTA curves are displayed. Through the obtained data, information about the presence of hygroscopic water, chemical water, carbonates (calcite), decomposition of organics, solid phase transformation and polymorphic changes can be obtained by their characteristic endothermic or exothermic responses at different temperature ranges [15-17]. For S1 ceramic paste ~ 20 wt% of mass loss corresponding to surface water (30-100 °C) can be observed. The chemical water mass loss (200-500 °C) was around ~ 1 wt%.

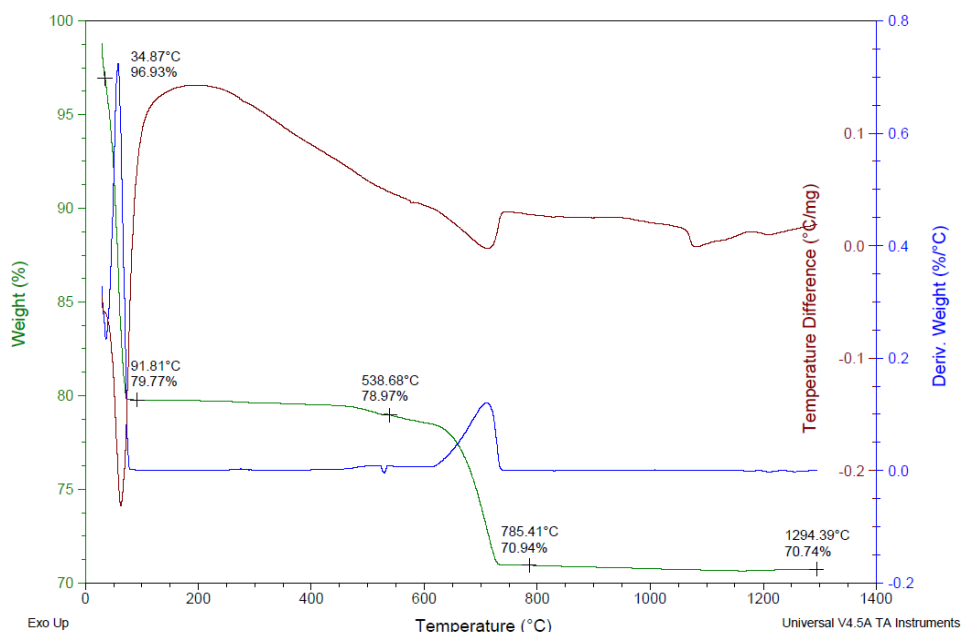


Figure 4. Thermogravimetry (TG- green), its derivative (DTG-blue) and differential thermal analysis (DTA- red) curves of S1 stoneware paste.

The $\alpha \rightarrow \beta$ quartz transformation for the S1 paste was observed in the DTA curve, with the small endothermic minimum at 570 °C [18]. Above ~ 600 °C, the decomposition of calcite started, corresponding to the endothermic peak with the minimum in the DTA curve at 700 °C (Figure 4), overlapping

with the dehydroxylation processes of clay minerals also occurring at these temperatures. Upon heating up to 1300 °C, the total mass loss for the S1 paste was ~ 20 %. The total mass loss was 29.26%.

Figure 5 revealed the results of thermal analysis for the S2 ceramic paste. The mass loss corresponding to surface water (25-100 °C) can be observed; this was ~ 14.73 wt%. The chemical water mass loss (400-600 °C) was around ~ 4.5 wt%. As temperature increased (~ 985 °C) the primary mullite formation process was evidenced by means of a small exothermic peak, and finally, secondary mullite formation, usually detected by a couple of exothermic small peaks in the 1100-1240 °C range was scarcely detected in the studied S2 paste. For the S2 paste the total mass loss was 20.52%.

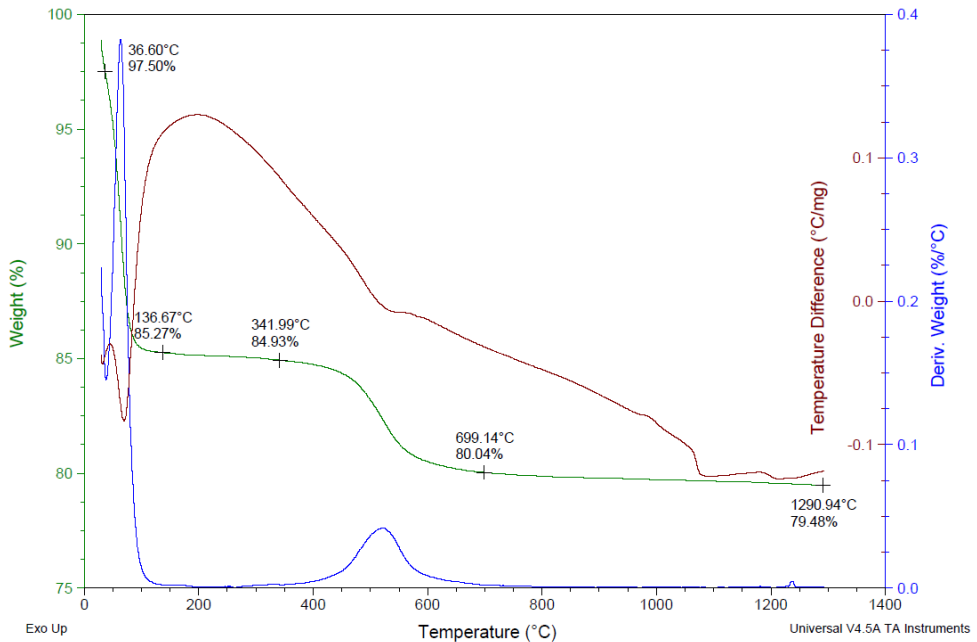


Figure 5. Thermogravimetry (TG- green), its derivative (DTG-blue) and differential thermal analysis (DTA- red) curves of S2 stoneware paste.

Plasticity measurements

Plasticity is the outstanding property of clay-water systems. The shaping of ceramic products by plastic processes is based on the plasticity of the mass, therefore it is important to know it. Mineralogical composition,

particle size distribution, organic substances and additives can affect the plasticity of clays. Several measuring techniques and devices, like Atterberg, Pfefferkorn, stress/strain curves, indentation, and rheological measurements, are the most used techniques to determine the optimal water content in a clay body required to allow this body to be plastically deformed by shaping [14-19]. In this work the Pfefferkorn method was chosen to evaluate the plasticity of the S1 and S2 stoneware masses. This method is widely accepted in practice and was originally developed for soft silicate ceramic materials [19]. Despite the advance in the theory of the plasticity and the methods of measurement, a common procedure for all types of materials does not exist. The Pfefferkorn method is currently used in routine controls owing to the low cost of the equipment used and the short time required for the tests [20, 21].

In our case the plasticity index was found to be 46.18 for S1 and 52.65 for S2 paste, respectively. Afterwards, the following conclusion should be drawn, both S1 and S2 stoneware pastes present an average impact deformation height, between 4 and 1.25. Regarding the plasticity index, both types of pastes, S1 and S2 are ceramic materials with superior plasticity, the plasticity index is over 30 [22]. Plasticity is not a physical property, but is the result of many properties of clay materials, such as: the size and shape of the material particles, the cohesion between them, the swelling capacity in water, the shrinkage when drying, etc.

Moisture content determination

Plastic raw materials can retain large amounts of water in the form of moisture. For this reason, is necessary to know the humidity to make certain corrections to the manufacturing recipes in case the raw materials are no longer dried before. The moisture content obtained from the analyzes are as follows: 16.85% for S1 and 22.10% for S2 stoneware paste, respectively. Ceramic pastes represent a mixture of solid raw materials with water, the percentage of water varying between 18 and 24% and are used for ceramic household products, tiles, and refractory products whose shaping process involves plastic shaping. The obtained results confirm the fact that the S2 stoneware paste has the necessary humidity to be shaped by plastic processes, such as the potter's wheel.

Drying and firing shrinkages determination

The purpose of this test was to obtain values of shrinkage after drying and firing of stoneware bodies. The drying shrinkage of raw materials and ceramic masses consists in reducing the dimensions of the shaped product

by eliminating the water absorbed on the surface of the particles, in the pores and capillaries of the product. During firing the matrix densifies and shrinkage continues, more vitreous bodies shrink more. The fired shrinkage (shrinkage from dry to fired) is a thus comparative indicator of the degree of vitrification.

The linear shrinkage, LS (%), of dried (LDS) and fired (LFS) samples has been determined by means of the following equation [22]:

$$\text{LDS} = (L_0 - L) / L \times 100 \quad (1)$$

$$\text{LFS} = (L - L_1) / L \times 100 \quad (2)$$

where L_0 , L and L_1 are the diameter (mm) of the green, dried, and fired specimens respectively. Finally, the total shrinkage was calculated, as the sum of the drying and firing shrinkage. The linear shrinkage values obtained for five specimens were averaged for each determination.

LDS for S1 and S2 samples shows similar values of 5.6% and 5.5%, respectively. For S1 the LFS was found to be 7.84, whereas S2 has 6.65%. Finally, the total shrinkage was 13.44% for S1 and 12.15% for S2. With the help of the above experimental data, we concluded that S1 and S2 stoneware samples have high total shrinkage (12÷17%). However, the total shrinkage of a smooth, plastic clay body can be as high as 15%. The most important parameters which affect shrinkage and characteristics of final product are the particle size distribution, chemical and mineralogical composition of raw materials, temperature, and sintering time [23]. In our case, both pastes are recommended to be used to obtain ceramic objects by plastic shaping. Anyway, the clay materials for the ceramic industry with high total shrinkage are not recommended for use in the case of products with a flat shape and narrow dimensional tolerances, due to the large deviations from the nominal dimensions, when fired in industrial furnaces with temperature gradients [22].

CONCLUSIONS

The following conclusions can be drawn from the physical, chemical, mineralogical, and technological characteristics of the studied ceramic pastes:

From the analysis of the results, it appears that the S2 paste has a higher plasticity. This may be due to the higher kaolinite content, which promotes mullite formation on firing and confers plasticity on the green paste facilitating shape-forming operations.

COMPARATIVE STUDY OF TWO COMMERCIAL STONEWARE PASTES
FOR PLASTIC SHAPING BY POTTERY WHEEL

The mineralogical analysis shows that the S2 ceramic paste after firing contains mullite, which is desirable due to its important properties like low thermal expansion, creep resistance and high temperature stability.

The PSD results show that the S2 paste is composed of much finer constituent particles, with a narrow particle size distribution (PSD).

In conclusion, although both pastes are commercially available and are currently used, according to scientific analyzes and through a careful comparison, we can state that S2 paste is more favorable for processing on the potter's wheel. As we mentioned before, a main advantage is the fact that this paste contains cellulose fibers which can come either from new or recycled paper pulp, making this “greener” than the other ceramic paste.

EXPERIMENTAL SECTION

Materials and methods

Materials

The two types of stoneware used in the experiments are: *Stoneware B17C* (Valentine Clays Ltd, Stoke-on-Trent, UK, sample name: S1) [7] and *PCLI stoneware paper clay* (SIO-2®, Esparreguera-Barcelona, Spain, sample name: S2) [9], respectively.

Methods

The stoneware pastes were characterized from both the chemical-physical and the technological viewpoints using different techniques, as follow.

Particle size distribution (PSD)

Particle size analysis by laser diffraction was performed with a micro and nanoparticle analyzer SALD-7101 (Shimadzu, Japan). The samples were dispersed in a water medium to form a suspension and drawn into the size analyzer. The particles aggregation was reduced using treatment with ultrasounds.

X-ray powder diffraction (XRPD)

The mineralogical composition of the samples before and after firing was determined by XRPD. Pellets of 10 cm diameter were obtained by manual pressing of the paste using a metallic mold. After pressing, the green

ceramic bodies were dried for 24 hours at 105 °C and heat treated in a laboratory furnace at 1260 °C maximum temperature for 20 min. This maximum temperature corresponds to temperature used during firing of industrial ceramic objects.

Prior to analysis, the samples were air-dried and gently ground with the aid of mortar and pestle into powdery form. The crystalline phases were identified using a Bruker D8 Advance (Germany) diffractometer, operating at 40 kV, 40 mA with CuK α radiation ($\lambda = 1.54060 \text{ \AA}$). Scans were conducted from 10 to 80° with a scan rate of 2°/min.

Thermal analysis

Thermoanalytical measurements were conducted on an SDT Q600 (USA) device from T.A. Instruments. Data on thermogravimetry (TG), its derivative (DTG), and differential thermal analysis (DTA) curves, were simultaneously acquired under the following measurement conditions: heating from laboratory temperature to 1300 °C, at a heating rate of 10 °C/min, under normal air atmosphere, using alumina crucibles.

Plasticity determination

The Pfefferkorn method previously described [22] was used to evaluate the plasticity of the two stoneware masses. The Pfefferkorn plastic meter used for the determination is a modified Vicat apparatus in which the needle has been replaced with a metal disc. A defined sample with a diameter of 33 mm and an initial height of 40 mm, produced manually was deformed by a free-falling plate with a mass of 1.192 kg, diameter of 120 mm and 7.5 mm thickness. This measurement was taken with bodies of varying moisture content. The ratios of deformation or the impact deformation heights (H_0 - initial height; H_f - final height) were plotted against the moisture content. From the linear fit of determined points for the two types of pastes, S1 and S2, which express the relation between moisture and impact deformation heights, the corresponding moisture at 3.3 impact deformation height, was found. These represents the Pfefferkorn's plasticity index, the moisture (%) which corresponds to a normal plasticity.

Linear drying and firing shrinkage

The principle of the method consists in marking on the green shaped samples some indentations at a well-established distance and measuring the same distance after drying. Our specimens are made in a mold with a removable bottom in the form of a cube, with a side of 50 mm. The test pieces are marked with two diagonal lines, on which a mark is placed 25 mm from the point of intersection, and then were subjected to a process of gradual drying in an oven. Further, after drying, the samples were heat treated in the furnace at a temperature of 900 °C, for 1-2 h. After firing, the distance between the marks was measured and the firing shrinkage was calculated.

Moisture analyses

The moisture content was determined using the AGS120 Moisture Analyzer (Scientific Industries, NY, USA) which is an electronic device used for quick and precise determination of material humidity upon the basis of weight loss during drying of its small sample (thermo-gravimetric method).

ACKNOWLEDGMENTS

The authors R.B. and L.B. acknowledge the financial support of Partnership for the transfer of innovative technologies and advanced materials in visual arts industry (production, conservation, restoration) - TeMATIC-Art, Project co-financed by FEDR through Competitiveness Operational Programme 2014 – 2020, Funding contract: 14/01.09.2016. The support from SC Bio Nera Plant SA, partner in the project, is also highly acknowledged.

REFERENCES

1. Kirk Othmer; *Kirk-Othmer Encyclopedia Of Chemical Technology*, 4th ed.; Volume 5, 1992, John Wiley & Sons, New York.
2. F. Ullmann; W. Gerhartz; Y. S. Yamamoto; F. T. Campbell; R. Pfefferkorn; J. F. Rounsaville; *Ullman's Encyclopedia Of Industrial Chemistry*, 5th ed.; Volume A6, 1985, VCH, Weinheim, Federal Republic of Germany.
3. The Pottery Wheel, Available online: <https://thepotterywheel.com/types-of-clay-for-pottery/> (accessed on 12 January 2023).
4. C. B. Carter; M. G. Norton, *Ceramic Materials (Shaping and Forming)*. 2007, Springer, New York.
5. Eternal Tools. *Ceramics: A Complete Guide*, Available online: <https://www.eternaltools.com/blog/ceramics> (accessed on 12 January 2023)
6. C. B. Carter; M. G. Norton, *Ceramic Materials: Science and Engineering*, 2013, Springer, New York.
7. <https://valentineclays.co.uk/product/stoneware-b17c/> (accessed on 12 January 2023)
8. J. Bennett, Studio Potter, Available online: <https://studiopotter.org/beginning-your-exploration-fiber-clay> (accessed on 12 January 2023).
9. <https://www.sio-2.com/gb/> (accessed on 12 January 2023).
10. M. U. Taskiran; N. Demirkol; A. Capoglu; *J. Eur. Ceram. Soc.*, **2005**, 25, 293–300.
11. M. M. Jordán, A. Boix, T. Sanfeliu, C. de la Fuente, *Appl. Clay Sci.*, **1999**, 14, 225-234.
12. C. Baudin, in *Encyclopedia of Materials: Technical Ceramics and Glasses*, **2021**, Editor-in-Chief: Michael Pomeroy, Elsevier.

13. W. Ochen, F. Mutonyi D'ujanga, B. Oruru, *Sci. Afr.*, **2021**, *11*, e00648,
14. M. Lassinantti Gualtieri, M. Romagnoli, A. F. Gualtieri, *J. Eur. Ceram. Soc.*, **2011**, *31*(5), 673–685.
15. M. Bayazit, O. Ekinci, *AKU J. Sci. Eng.* **2019**, *19*, 015704, 193-202.
16. L. Maritan, L. Nodari, C. Mazzoli, A. Milano, U. Russo, *Appl. Clay Sci.*, **2006**, *31*, 1-15.
17. R. Palanivel; U.R. Kumar, *Rom. Journ. Phys.*, **2011**, *56*, 195-208.
18. J. Dweck, *J. Therm. Anal. Calorim.* **2008**, *92*, 129–135.
19. F.A. Andrade, H.A. Al-Qureshi, D. Hotza, *Appl. Clay Sci.*, **2011**, *51*(1–2), 1-7.
20. J. H. Van der Velden. *Ziegelind. Int.* **1979**, *32*(9), 532-542.
21. A. M. Querol, *Bol. Soc. Esp. Ceram. Vidr.* **1983**, *22*(5), 285-289.
22. L. Gagea, *Ceramică de laborator. Lucrări și probleme* (in Romanian), Ed. Casa Cărții de Știință, Cluj-Napoca, **2003**.
23. A. Salem; S.H. Jazayeri; E. Rastelli; G. Timellini, *J. Mater. Process. Technol.* **2009**, *209*(3), 1240-1246.

DESIGN AND CONSTRUCTION OF A PROOF-OF-CONCEPT POULTRY LITTER PYROLYSIS PLANT

Daniel E. BOTHA^{a,b,*}, Paul S. AGACHI^{b,c}

ABSTRACT. One of the challenges facing poultry farming is the safe and economical disposal of poultry litter (PL) waste. PL pyrolysis offers a solution and a commercial scale induction heated auger type reactor, was developed into an engineering solution through mathematical modelling, design, and construction. A 1 ton/day proof-of-concept plant was realized to validate laboratory scale experimental results, producing bio-oil, biochar, and gas at typical product yields of >50%, ~20% and <30% respectively. The pyrolysis plant was packaged into a standard ISO-container format, enabling complete fabrication and testing in a production line, whereafter it can be shipped to any remote location via road, rail, or sea freight, ready to operate by the turn of a key at arrival. With the addition of a heavy fuel oil (HFO) or gas-powered generator, the unit can operate self-sustainably as a stand-alone unit.

Keywords: *Auger Reactor, Poultry Litter Pyrolysis, Waste to Energy, Circular Economy, End-of-Waste*

INTRODUCTION

Poultry Litter (PL) is an agricultural waste product of poultry farming which is distributed over large geographic areas and is currently an untapped renewable resource [1]–[4]. Pyrolysis of PL has the potential to convert this waste product into high value products, i.e., bio-oil, a renewable fuel, electricity and biochar, a soil enhancer. Due to the distributed nature of the PL [3], it is necessary to package the pyrolysis plant into a scale that would service

^a *Pyro Carbon Energy Pty Ltd, BIUST Technology Park, Palapye, Botswana*

^b *Botswana International University of Science and Technology, Palapye, Botswana*

^c *Babeş-Bolyai University, 11 Arany Janos str., RO-400028, Cluj-Napoca, Romania*

* *Corresponding author: daniel.botha@pyrocarbonenergy.com*



single poultry farms or clusters of farms if they are in close proximity. The ideal scale was determined to be at a PL feed rate of 5 metric tons per day [5]. Furthermore, the plant is packaged into a standard 12m ISO-container format [6] for easy transport in any mode (road, rail, or sea freight) to any remote site. This concept has the added benefit of allowing complete fabrication in workshop conditions, including full functional factory testing before dispatch. Scalability is completely linear by deploying parallel units at any site.

The poultry litter (PL) pyrolysis plant is a continuous process (see Figure 1) that accepts loads of PL into a load hopper. The PL is first dried to remove excess moisture, whereafter it is fed into the reactor. In the reactor, the PL is subjected to high temperatures where volatile (VM) matter is released and separated from the residual material (biochar). The biochar is then cooled in the char cooler before it is discharged and packaged. The VM is cooled, and the condensable fraction is collected in a knock-out drum while the non-condensable (permanent) gases, which are typically rich in methane and other light hydrocarbons are consumed in real time in a dual fuel power generator. In poultry farming the bird houses need to be kept warm at night. The excess heat produced in the plant is recovered and used to heat up bird houses at night.

A proof-of-concept plant with a PL feed rate of 1 metric ton per day (TPD) was designed and constructed at Botswana International University of Science and Technology (BIUST). The purpose of this plant was to (a) validate laboratory-scale experimental results on commercial scale, and (b) demonstrate manufacturability in a containerized format.

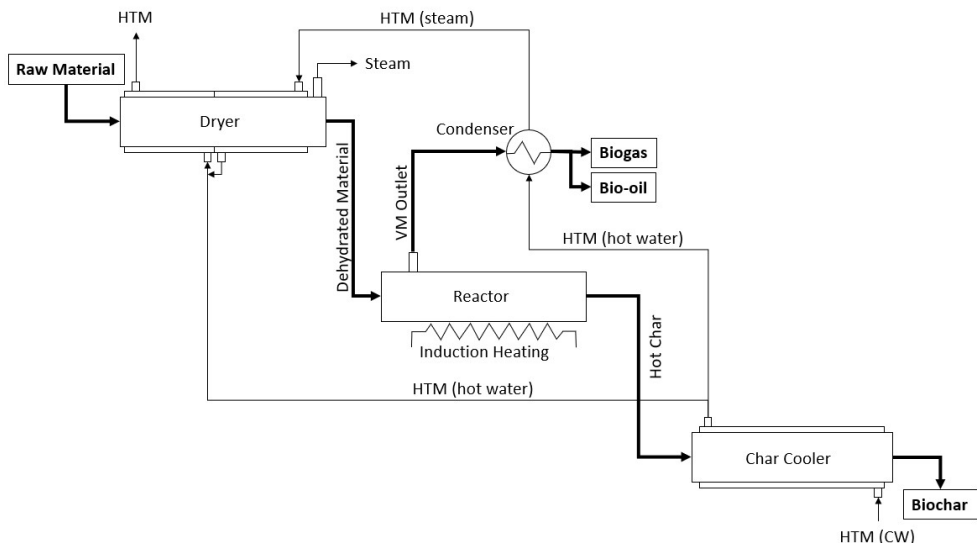


Figure 1. Process Overview

DESIGN

The following parameters were defined as design basis for the proof-of-concept plant:

- Ambient temperature range: 0°C to 40°C
- Pyrolysis temperature range: 400°C to 600°C
- Maximum process pressure: 40kPa
- Raw material: Broiler Poultry Litter
- Maximum raw material feed rate: 1 metric ton per day

For poultry litter (PL), which has a high wood shavings content (mixed with poultry manure), a CEMA material classification code from [7] can be adopted as 21E45HLUVY, i.e.:

- Average bulk density: 338 kg/m³ (21 lbs/ft³)
- Size: E (Irregular)
- Flowability: 4 - Free flowing (but can be slightly sluggish at times)
- Mildly Abrasive: 5 – Index 1-17
- Miscellaneous: HLUVY (Decomposes, Very Dusty, Hygroscopic, Interlocks, Mats or Agglomerates, Light and Fluffy)

The thermochemical breakdown of the PL takes place in the auger reactor where an induction heater is used to heat up its shell. VM is drawn off from the reactor before the heating zone, thereby inducing a counter-current flow of volatiles and immediate evacuation of the VM to minimize the residence time. The reactor shell can be heated to temperatures between 250 °C and 600°C and is controlled using a PID controller. The residence time of the solid residue (char) in the reactor is determined by the auger flight pitch and the rotational speed of the auger.

The reactor operation can be described using a classical Plug Flow Reactor (PFR) reaction, transport, and heating model. Pyrolysis processes are in general extremely complex to solve due to the thousands of reactions taking place and are very difficult to formulate, and the complex composition of PL, which is a mixture of feces (a function of the chicken feed) and bedding (which can be straw, wood shavings, amongst others), is mainly organic matter (85%) and very heterogenous. However, this endothermic reaction can be simplified to produce two pseudo components, i.e., VM and char:



The auger pyrolysis reactor very closely resembles the classical plug flow reactor (PFR) type [8] as shown in Figure 3. PFRs can be solved by approximating each infinitely small volume, dV , as a Continuous Stirred-tank Reactor (CSTR) [9] as shown in Figure 4 and integrating the system of equations over the total length of the reactor.

If each infinitesimal element (with thickness dz) of the PFR represents a small batch reactor which progresses along the PFR from position $z=0$ to $z=L$, then, with certain assumptions, experimental data can be utilized to model the steady state production of the reactor. Applying the experimental results from the batch reactor at the corresponding temperatures along the PFR will enable the modelling of the resulting cumulative production of the PFR.

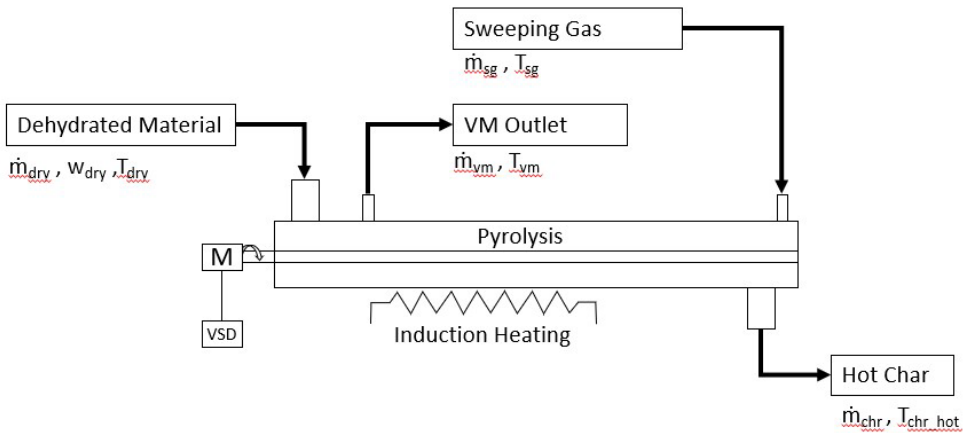


Figure 2. The mathematical model parameters of the reactor.

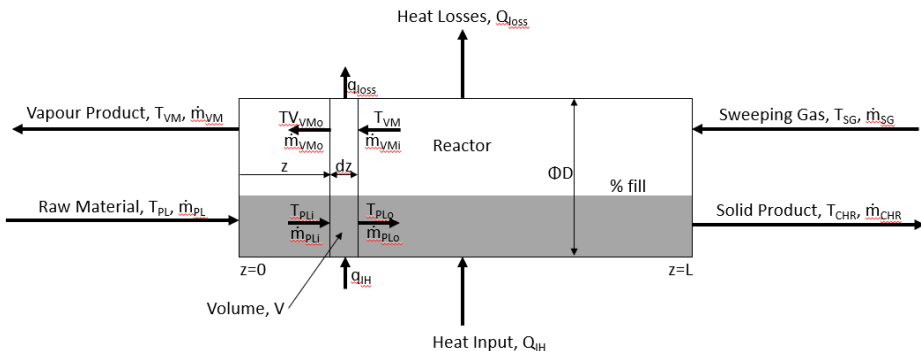


Figure 3. Pyrolysis reactor modelled as a plug flow reactor

DESIGN AND CONSTRUCTION OF A PROOF-OF-CONCEPT POULTRY LITTER PYROLYSIS PLANT

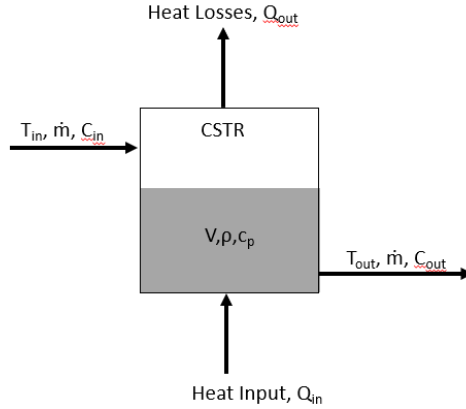


Figure 4. Infinitesimal volume, dV , representing a length of dz of the PFR, which is approximated as a CSTR

The kinetics and thermodynamics of the process are described in [8], [10], [11] and equations (2) and (3) are the similar equations for the pyrolysis reactor which are adapted from 3.9 and 3.13 from [13, pp. 67–70].

$$\frac{\partial}{\partial z}(v\rho c_p T) + \frac{4K_T}{D}(T_{stm} - T) = \frac{\partial}{\partial z}\left(k_T \frac{\partial T}{\partial z}\right), \quad (2)$$

Where v is the velocity of the material in the dryer,
 ρ is the average density of the material,
 c_p is the average specific heat of the material,
 T is the temperature of the material in the dz element,
 K_T is the heat transfer coefficient from the induction heating coil to the material through the dryer's wall,
 D is the auger diameter of the dryer, and
 k_T heat diffusion coefficient in the solid material.

$$D_w \frac{\partial^2 w}{\partial z^2} - \frac{\partial}{\partial z}(v w) = 0, \quad (3)$$

Where v is the velocity of the material in the dryer,
 w is the moisture content of the solid material, and
 D_w is the mass diffusion coefficient of water in the material.

The material entering the CSTR consists of a mixture of solid material and volatile matter (VM). The percentage (by mass) of VM can be equated to the “concentration”, C , of product formed in classical CSTR theory, starting with zero at $z=0$ and increasing to its final value at $z=L$. The assumptions made are as follows:

- Steady state conditions are considered.
- The volume and density in the CSTR remain constant (i.e., the fill % does not vary at any given position, z , in the reactor).
- The sweeping gas is inert and only acts as a carried gas for the VM.
- The sweeping gas flow rate and composition does not significantly alter the results. In practice, as volatiles are produced, they join the sweeping gas stream and therefore the sweeping gas flow rate and composition vary along the length of the PFR. The batch reactor does not take these effects into account.
- The mass flow rate is considered constant.

For a CSTR the mass balance is given in equation (4) and for VM, equation (5) can be derived in terms of mass flow in [kg/s] and concentration in mass%.

$$\text{input} + \text{generation} = \text{accumulation} + \text{output} \quad (4)$$

$$\dot{m} \cdot C_{in} + r \cdot dV = \frac{dC_{out} \cdot \rho \cdot V}{dt} + \dot{m} \cdot C_{out} \quad (5)$$

Where: \dot{m} is the mass flow rate in [kg/s] of the material through the CSTR, dV is the volume of the CSTR in [m³] and ρ the density of the material in [kg/m³],
 $\rho \cdot V = m_{VM}$ is the mass in [kg] of material accumulated in the reactor,
 C_{in} and C_{out} are the concentrations in [mass %] of the VM at the inlet and outlet respectively, and
 r is the rate of reaction in [kg/(m³·s)] and is defined as:

$$r = -k(T) \cdot (C_{VM})^m \quad (6)$$

Where: m is the order of reaction, and

$$k(T) = k_0 \cdot e^{\frac{-E_a}{R \cdot T}} \quad (7)$$

Where: k_0 is the pre-exponential factor in [s⁻¹],
 E_a is the activation energy in [kJ/kmol],

R is the gas constant equal to 8314 [kJ/(kmol·K)], and
 T is the temperature in [K].

With the assumptions of constant volume and density and rearranging:

$$\frac{dc_{out}}{dt} + \frac{\dot{m} + k(T) \cdot V}{\rho \cdot V} C_{out} = \frac{\dot{m}}{\rho \cdot V} C_{in} \quad (8)$$

Being in standard form, the differential equation (8) can be re-written and integrated both sides [14] to yield equation (9):

$$C_{out}(t) = e^{-\frac{\dot{m}+k(T) \cdot V}{\rho \cdot V} t} \left(\int e^{\frac{\dot{m}+k(T) \cdot V}{\rho \cdot V} t} \cdot \frac{\dot{m} \cdot C_{in}}{\rho \cdot V} dt + C_1 \right) \quad (9)$$

Simplification of equation (9) results in the general solution [14] for the output production of VM in mass percentage for an infinitesimal volume of the reactor:

$$C_{out}(t) = \left(\frac{\dot{m} \cdot C_{in}}{\dot{m} + k_0 \cdot V \cdot e^{\frac{-E_a}{R \cdot T}}} + C_1 \cdot e^{-\frac{\dot{m}+k_0 \cdot V \cdot e^{\frac{-E_a}{R \cdot T}}}{\rho \cdot V} t} \right) \quad (10)$$

Where C_1 , k_0 and E_a are unknown constants.

With difficulties to determine the order of reaction, m , the rate constant, $k(T)$, the energy of activation, E_a , and the preexponential factor, k_0 , the kinetics of this reaction is a wild guess at best. On the other hand, experimental data can be obtained for pseudo-component yields of batch pyrolysis processes, which then can be used to determine the values of the unknown constants. An experimental approach could therefore be taken, but this falls out of the scope of this work and is a subject of further research and studies.

The heat balance, equation (11), adapted from equation 3.13 from [9] is:

$$\begin{aligned} \frac{\partial}{\partial z} (\dot{m} c_p T_z + \eta q_{IH}) + \frac{4K_T}{D} (T_z - T_{shell}) \\ = \frac{\partial}{\partial z} (k_T \frac{\partial T_z}{\partial z}) \end{aligned} \quad (11)$$

Where: \dot{m} is the mass flow rate of the PL through the reactor in [kg/s],
 ρ is the density of the PL in [kg/m³],
 T_z is the temperature of the PL at distance z in [K]

T_{shell} is the temperature of the shell in [K],
 k_T is the Fourier diffusion coefficient in $[\frac{W}{mK}]$,
 K_T is the transfer coefficient through the reactor shell in $[\frac{W}{m^2K}]$,
 D is the diameter of the reactor shell in [m],
 q_{IH} is the heat input via the induction heater in [W/m], and
 η is the overall efficiency of the induction heating system,

Heat generated per unit volume by eddy currents (Foucault's currents), q_{IH} in [W/kg], can be calculated [15] as:

$$q_{IH} = \frac{\pi^2 \cdot B_p^2 \cdot t_r^2 \cdot f^2}{6 \cdot \rho_r \cdot \delta_c \cdot L_c} , \quad (12)$$

Where: B_p is the peak magnetic field in [T],
 t_r is the thickness of the reactor shell in [m],
 f is the frequency in [Hz],
 ρ_r is the resistivity of the reactor shell material in [$\Omega \cdot m$],
 δ_c is the density of the reactor material in [kg/m^3], and
 L_c is the length of the coil in [m]

This indicates that the temperature can be controlled using the quantity of electricity delivered to the heating coil, q_{IH} , and the overall efficiency, η . Both heating rate and residence time are important parameters for PL conversion, and these depend on the mass flow and power delivered.

The plant's main material flow path consists of 5 auger sections, i.e., the Feeder, Dryer, Reactor (having two sections within), and Cooler, which are all inclined at an angle of 15° to allow for a compact design in a containerized configuration. The Feeder auger rotational speed determines the feed rate into the system and also acts as a plug to limit the back flow of steam produced in the dryer. For this reason, full loading (i.e., 95%) is chosen for this section. Free moisture is removed in the Dryer where the auger loading is reduced to 15% to allow free passage for steam to be evacuated from the feed material. The first stage of pyrolysis in the Reactor (which operates in the fast pyrolysis regime) is characterized by high heating rates, high volumes of vapor produced, and low vapor residence times. Therefore, the loading in this stage is also chosen as 15% to allow efficient evacuation of these vapors. The bulk of devolatilization occurs in this stage. In the second stage of the Reactor, char is held at the final temperature where final devolatilization takes place. Here longer residence time is required, and low

DESIGN AND CONSTRUCTION OF A PROOF-OF-CONCEPT POULTRY
LITTER PYROLYSIS PLANT

loading is not essential. In order to maximize the residence time, the pitch is minimized with consequential maximum loading of 95%. A low loading of 15% is chosen for the final auger (i.e., the Cooler) to maximize the contact surface area between the hot char and the cold shell. The auger design (summarized in Table 1) yields residence times of 3.77 min in the Feeder, 3.11 min in the dryer, 1.38 min in the first stage of the Reactor (where fast pyrolysis takes place), 19.62 min in the second stage of the Reactor (where final devolatilization occurs) and 21.40 min in the Cooler, giving a total processing time of less than one hour.

Table 1. Auger design calculations using an Excel® spreadsheet

AUGER CALCULATIONS			Equipment				
Parameter	Units	Source	Feeder	Drier	Reactor(a)	Reactor(b)	Cooler
Feed Material			Raw PL	Raw PL	Dry PL	Char	Char
Bulk material density	kg/m ³	Specified	338	338	338	335	335
	lb/ft ³	Converted	21.1	21.1	21.1	20.9	20.9
Feed Rate	TPD	Specified	2.0				
	TPD	Calculated		2.0	1.8	0.7	0.6
	kg/h	Converted	83.333	83.333	75.000	30.000	27.000
	m ³ /h	Calculated	0.247	0.247	0.222	0.090	0.081
	m ³ /min	Converted	0.004	0.004	0.004	0.001	0.001
	cm ³ /min	Converted	4109	4109	3698	1493	1343
	ft ³ /h	Converted	8.707	8.707	7.836	3.163	2.846
	lb/hr	Calculated	183.7	183.7	165.3	66.1	59.5
Conversion	%	Specified	0%	10%	60%	10%	0%
Auger diameter (D)	mm	Specified	207.480	207.480	207.480	207.480	207.480
	in	Converted	8.169	8.169	8.169	8.169	8.169
Pitch (P)	mm	Calculated		104		28	
	mm	Specified	50	105	120	28	150
		Lookup	1/4 Pitch	1/2 Pitch	1/2 Pitch	1/4 Pitch	3/4 Pitch
	mm	Lookup	51.870	103.740	103.740	51.870	155.610
	in	Converted	1.969	4.134	4.724	1.102	5.906
Pitch Capacity Factor (CF ₁)		Calculated	0.24	0.51	0.58	0.13	0.72
Loading		Selected	95%	15%	15%	95%	15%
		Calculated		14.8%	15.0%	94.1%	15.0%
Type of Flight		Specified	Standard	Cut&Folded	Cut&Folded	Cut&Folded	Cut&Folded
Flight Capacity Factor (CF ₂)		Lookup	1.000	1.100	1.100	1.300	1.100
Mixing Paddles per Flight		Specified	None	4	4	4	4
Mixing Paddle Capacity Factor (CF ₃)		Lookup	1.00	1.32	1.32	1.32	1.32
Equivalent Capacity Factor (CF)		Calculated	0.240987083	0.734817814	0.839791787	0.23157895	1.04973973
Inclination Angle	degrees	Specified	15	15	15	15	15

Having defined and designed the main material flow path, all other equipment (including heat exchangers, pumps, valves, piping and instruments) were designed and specified). A comprehensive 3-dimensional solid model was created using Solid Edge® software (refer to Figure 5). A complete set

of fabrication drawings were extracted from this model and the required material was procured.

A comprehensive financial model of the PL pyrolysis plant was also created using Excel® which allowed manipulation of the process and financial parameters that drive the capital expenditure (CAPEX), operational expenditure (OPEX) and revenue streams. The financial model uses appropriate financial parameters (e.g., loan size, interest rate, inflation rate, etc.) and calculates financial metrics (e.g., IRR, ROI, payback, etc.) which are used to determine financial feasibility of a project. The model was used to create scenarios which were used in several sensitivity analyses.

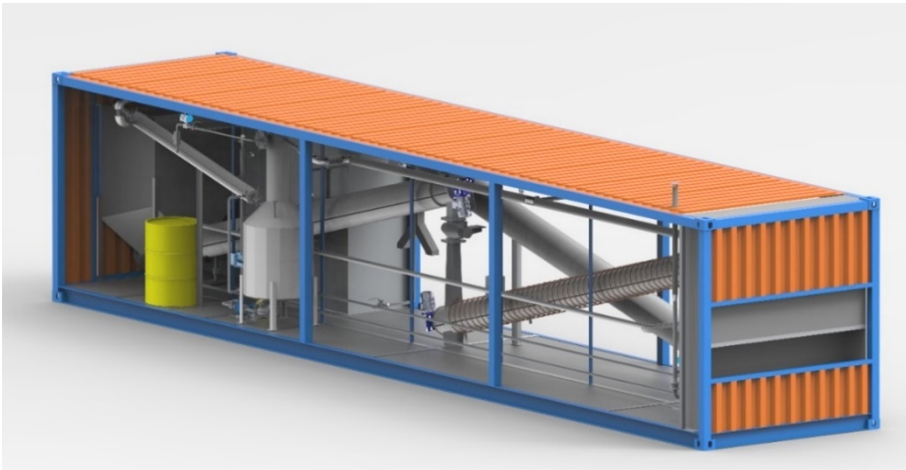


Figure 5. 3-dimensional model of the plant (created with Solid Edge®)

CONSTRUCTION AND COMMISSIONING

After preparing the site the proof-of-concept plant was constructed from the set of drawings which were prepared using Solid Edge® software. The support structure was fabricated first, after which the augers (feeder, reactor, and char cooler) were fabricated (Figure 6) and installed into the structure. Next, followed the installation of the process equipment (knock-out drum, pumps, and heat exchangers), after which all piping was fabricated and installed with the valves (see Figure 7).

Instrumentation was installed after mechanically completing the construction and electrical and instrument cabling was routed from the field devices to the electrical and control panel (Figure 8).

DESIGN AND CONSTRUCTION OF A PROOF-OF-CONCEPT POULTRY LITTER PYROLYSIS PLANT



Figure 6. Main process equipment



Figure 7. Knock-out drum, heat-exchangers, valves, pumps, and piping.



Figure 8. Electrical and control system panel

The capital expenses for this 1TPD proof-of-concept plant were about \$170,000 while a full scale 10 TPD plant is estimated at \$1,684,525 and including for working capital allowance, the total start-up expenses are estimated at \$ 919,205. With a plant lifetime of 20 years, the lifetime operation expenses are calculated at \$24,424,964 with a lifetime revenue of \$72,667,125. The business case assumes a loan amount of \$919,205 at an interest rate of 100% resulting in a total interest of \$307,628 due. The result of this is an IRR of 40% with a NPV of \$1,214,671, a ROI of 28% and a payback period of 3.54 years.

The plant was successfully commissioned and was able to operate at a shell temperature of 500°C and a feed rate of 0.25 metric tons per day (Figure 9). The induction heating system, however, was not yet performing well and further optimization is required in the electro-magnetic coupling between the induction coil and the reactor shell. However, the induction heating system is capable of heating the reactor shell to the pyrolysis range of temperatures between 400°C and 600°C in less than one hour, which is acceptable for start-up. With improvement in the heating system the startup time is expected to be significantly reduced.

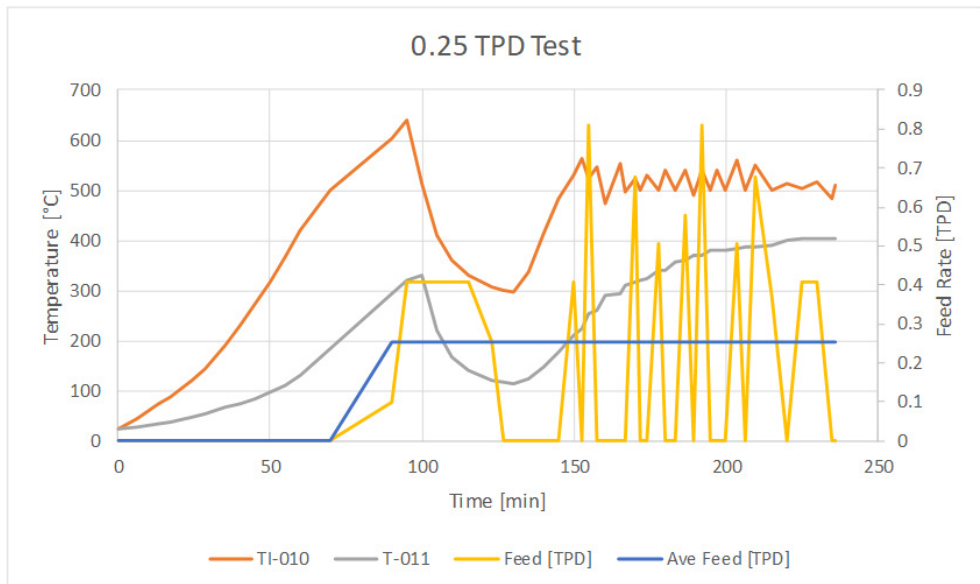


Figure 9. Plant commissioned and operating at 500°C

CONCLUSIONS

While further optimization of the electro-magnetic coupling between the induction coil and reactor shell is necessary to achieve production at full scale, the design and construction of the proof-of-concept plant was successful in demonstrating that this technology can be implemented at a scale suitable for deployment in proximity of typical commercial poultry farms, thereby addressing the challenge of waste disposal. This concept facilitates the drive towards End-of-Waste by converting agricultural waste into energy and other valuable products. By packaging the plant into the standard 12m ISO-Container format (Figure 10), and performing performance tests at BIUST, it is demonstrated that the plant can be completely built and tested within a production workshop and then shipped to any remote destination via road, rail, or sea freight modes.



Figure 10. The completed proof-of-concept plant, ready for transport (via road, rail or sea freight) and deployment in any remote location.

ACKNOWLEDGMENTS

With much gratitude we would like to recognize the contributions of many people and organizations to the successful execution of this project, including the Botswana Innovation Fund (BIF), BIUST, Pyro Carbon Energy, and colleagues.

REFERENCES

1. J. Adewole, S. Akintoye, and K. Olayinka, *African J Poultry Farming*, **2017**, *5*(4), 192–203.
2. J. C. Moreki, *Livestock Research for Rural Development*, **2010**, *22*(5), 89.
3. J. C. Moreki, *Int. J. Agric. Technol.*, **2011**, *7*(6), 1579–1587.
4. J. C. Moreki and T. Keaikitse, *Int. J. Curr. Microbiol. App. Sci* **2013**, *2*(7), 240–248.
5. D. E. Botha and P. S. Agachi, *Bull. Rom. Chem. Eng. Soc.*, **2022**, *9*(1), 103–121.
6. International Organization for Standardization, “Series 1 freight containers — Specification and testing — Part 1: General cargo containers for general purposes,” ISO 1496-1, **2013**.
7. CEMA, “Screw Conveyor Catalog & Engineering Manual.” CEMA, **2004**, pp. 1–8.
8. F. J. Sanchez Careaga, A. Porat, L. Briens, C. Briens, *Can. J. Chem. Eng.*, **2020**, *98*(11), 2417–2424.
9. P. S. Agachi, M. V. Cristea, E.P. Makhura, “Basic Process Engineering Control, 2 Edition, De Gruyter GmbH, Berlin, Boston, **2020**, pp. 67-78.
10. S. Kim and F. Agblevor, *Waste Manag.*, **2007**, *27*, 135–140.
11. J. H. Jo, S. S. Kim, J. W. Shim, Y. E. Lee, and Y. S. Yoo, *Energies*, **2017**, *10*(8), 1–14.
12. P. S. Agachi and M. V. Cristea, Basic Process Engineering Control. Berlin, Boston: De Gruyter, **2014**.
13. “First Order Linear Differential Equations.” [https://www.sfu.ca/math-coursenotes/Math158Course Notes/sec_first_order_homogeneous_linear.html](https://www.sfu.ca/math-coursenotes/Math158Course%20Notes/sec_first_order_homogeneous_linear.html) (accessed Feb. 13, **2023**).
14. P. S. Agachi, V. M. Cristea, and E. P. Makhura, Basic Process Engineering Control. Berlin, Boston, **2020**.
15. I. G. Harvey, “Induction heating” A-to-Z Guid. to Thermodyn. Heat Mass Transf. Fluids Eng., **2011**.

RADIOCARBON DATING OF THE HISTORIC GRAND BAOBAB OF MAHAJANGA, MADAGASCAR

Adrian PATRUT^{a,b*}, Roxana T. PATRUT^a,
Laszlo RAKOSY^c, Ileana Andreea RATIU^{a,b}, Pascal DANTHU^d,
Jean-Michel LEONG POCK TSY^e, Karl F. Von REDEN^f

ABSTRACT. The article reports the AMS (accelerator mass spectrometry) radiocarbon investigation of the historic Grand Baobab of Mahajanga. The largest African baobab of Madagascar exhibits a cluster structure, which consists of 6 fused ordinary stems and of 3 small binding stems. Two samples were collected from the largest stem and from a primary branch, out of which several tiny segments were extracted and dated by radiocarbon. The oldest dated sample segment had a radiocarbon date of 214 ± 17 BP, which corresponds to a calibrated age of 265 ± 25 calendar years. The dating results indicate that the Grand Baobab of Mahajanga is 275 ± 25 years old.

Keywords: AMS radiocarbon dating, *Adansonia digitata*, dendrochronology, Madagascar, age determination, multiple stems.

INTRODUCTION

The *Adansonia* genus, which belongs to the Bombacoideae, a subfamily of Malvaceae, consists of eight generally recognised species. One species originates from mainland Africa, six are endemic to Madagascar, while another

^a Babeş-Bolyai University, Faculty of Chemistry and Chemical Engineering, 11 Arany Janos, RO-400028, Cluj-Napoca, Romania

^b Babeş-Bolyai University, Raluca Ripan Institute for Research in Chemistry, 30 Fantanele, RO-400294 Cluj-Napoca, Romania

^c Babeş-Bolyai University, Faculty of Biology and Geology, 44 Republicii, RO-400015 Cluj-Napoca, Romania

^d Cirad, UPR HortSys, Montpellier, France

^e Dfgrn-fofifa, Antananarivo, Madagascar

^f NOSAMS Facility, Dept. of Geology & Geophysics, Woods Hole Oceanographic Institution, Woods Hole, MA 02543, USA

* Corresponding author: apatrut@gmail.com



grows only in northern Australia. The African baobab (*Adansonia digitata* L.) is certainly the best-known and widespread among these species. It is endemic to the arid savanna of mainland Africa between the latitudes 16° N and 26° S. The African baobab can also be found on several African islands and outside Africa, in different areas throughout the tropics, where it has been introduced [1-5].

In 2005, we started a complex research project for elucidating several controversial aspects related to the architecture, growth and age of the African baobab. This research relies on AMS radiocarbon dating of tiny wood samples extracted from different areas of big baobabs [6-14]. According to the obtained results, all superlative, i.e., very large and/or old baobabs, are practically multi-stemmed and exhibit preferentially closed or open ring-shaped structures. The oldest specimens were found to reach ages up to 2,500 years [11].

Since 2013 our investigations also include superlative individuals of the three best-known species of Madagascar, i.e., *Adansonia za* Baill. (Za baobab), *Adansonia rubrostipa* Jum. & H. Perrier (Fony baobab) and *Adansonia grandidieri* Baill (Grandidier baobab) [15-20]; each species is represented by over one million individuals. On the northwestern coast of Madagascar, between Diego Suarez and Mahajanga, there are located several thousand African baobabs. One specimen, namely the baobab of Mahajanga, is famous for its very large dimensions [21].

Here we present the investigation and AMS radiocarbon dating results of the historic African baobab of Mahajanga.

RESULTS AND DISCUSSION

The Grand Baobab of Mahajanga and its area. Mahajanga (formerly French Majunga) is a city, an administrative district and important seaport on the northwestern coast of Madagascar. It has a population of 250,000 inhabitants and is the capital city of the Boeny region. Mahajanga has a tropical savanna climate with two distinct seasons, a rainy wet season (from November to mid-April) and a sunny dry season (from mid-April to October). Cyclons can occur during the wet season and may produce considerable damage. The mean annual temperature is 26.3°C and the mean annual rainfall is 1476 mm.

The Grand Baobab of Mahajanga (in French, “le gros baobab de Majunga”) grows on the coast, at around 100 m from the sea. Today, the big baobab is protected by a fence in the centre of a large traffic roundabout, where two waterfront boulevards meet the main boulevard “Avenue of France”. The lower trunk is painted to protect against pests and the surroundings of the tree are concreted.

The historic baobab is the symbol of the whole city, with people usually sitting under it. It also appears on the emblem of Mahajanga.

In earlier times, the baobab was used as a place for announcing news to the community and also as a meeting place. In the 19th century, the baobab marked the site for public executions. According to tradition, every traveler must walk around the baobab seven times to receive the blessing of the Malagasy ancestors.

Two decades ago, the baobab was hit by a truck and several branches had to be cut. There have been many speculations about the age of the baobab. Usually, it is considered to be between 700 and 1500 years old.

The first photo of the “gros baobab” dates back to 1898, during the French administration (**Figure 1**). According to official measurements, the tree had then a circumference of 14.60 m at a height of 0.70 m above ground.

The GPS coordinates are 15°43.294' S, 046°18.300' E and the altitude is 8 m. In 2013, the big baobab had a height of 15.6 m, the circumference at breast height (cbh; at 1.30 m above mean ground level) was 21.21 m and the overall wood volume of around 180 m³ (**Figures 2 and 3**). The circumference at 0.70 m was 22.72 m. In 2018, the circumference cbh was only 2 cm larger, reaching 21.23 m. The horizontal dimensions of the large canopy, which has several large branches, are 26.6 (NS) x 31.5 (WE) m.

The impressive trunk exhibits a cluster structure, which consists of 6 fused ordinary/common stems, out of which two are very large, and a further 3 smaller binding stems.

At present, the Grand Baobab is in a general state of decline, with several broken and damaged branches. It almost stopped growing during the last decades. The pavement and the intense traffic around the tree probably play an important role in this process.

Wood samples. Two wood samples were collected from the baobab with an increment borer. One sample, labelled MJ-1, with the length of 0.30 m, was collected from the exterior of a large stem, at the height of 1.90 m. A number of two tiny pieces/segments, each 10⁻³ m long (marked a and b), were extracted from determined positions of sample MJ-1. Another sample, labelled MJ-2, with the length of 0.34 m, was collected from a large primary branch, at the height of 2.20 m. Two segments (marked a and b) were extracted from this sample.



Figure 1. The first photograph of the baobab of Mahajanga taken in 1898.



Figure 2. General view of the Grand Baobab of Mahajanga.



Figure 3. The image shows the large trunk of the Grand Baobab surrounded by a fence.

AMS results and calibrated ages. Radiocarbon dates of the four sample segments are listed in Table 1. The radiocarbon dates are expressed in ^{14}C yr BP (radiocarbon years before present, i.e., before the reference year 1950). Radiocarbon dates and errors were rounded to the nearest year.

Calibrated (cal) ages, expressed in calendar years CE (CE, i.e., common era), are also displayed in Table 1. The 1σ probability distribution (68.3%) was selected to derive calibrated age ranges. For two segments (MJ-1b, MJ-2b), the 1σ distribution is consistent with three ranges of calendar years, while for one sample segment (MJ-2a) it corresponds to four ranges. In all these

cases, the confidence interval of one range is considerably greater than that of the others; therefore, it was selected as the cal CE range of the segment for the purpose of this discussion.

Table 1. AMS Radiocarbon dating results and calibrated ages of samples collected from the Grand baobab of Mahajanga.

Sample code	Depth ¹ [height ²] (m)	Radiocarbon date [error] (¹⁴ C yr BP)	Cal CE range 1σ [confidence interval]	Assigned year [error] (cal CE)	Sample age [error] (cal CE)
MJ-1a	0.15 [1.90]	-	-	-	>Modern
MJ-1b	0.30 [1.90]	123 [± 16]	1712-1718 [4.3%] 1813-1835 [20.6%] 1885-1925 [43.3%]	1905 [± 20]	120 [± 20]
MJ-2a	0.20 [2.20]	158 [± 18]	1695-1711 [12.3%] 1719-1726 [5.0%] 1836-1883 [22.8%] 1925-... [18.1%]	1869 [± 24]	155 [± 25]
MJ-2b	0.34 [2.20]	214 [± 17]	1672-1680 [9.1%] 1733-1782 [52.8%] 1797-1803 [6.3%]	1757 [± 24]	265 [± 25]

¹ Depth in the wood from the sampling point.

² Height above ground level.

For obtaining single calendar age values of sample segments, we derived a mean calendar age of each sample segment, called assigned year, from the selected range (marked in bold). Sample/segment ages represent the difference between the year 2023 CE and the assigned year, with the corresponding error. Sample ages and errors were rounded to the nearest 5 yr.

For one sample segment (MJ-1a), the age falls after the year 1950 CE, namely the ¹⁴C activity, expressed by the ratio ¹⁴C/¹²C, is greater than the standard activity in the reference year 1950. Such values, which correspond to negative radiocarbon dates, are termed greater than Modern (>Modern). In such cases, the dated wood is young, being formed after 1950 CE.

This approach for selecting calibrated age ranges and single values for sample ages was used in all our previous articles on AMS radiocarbon dating of large and old angiosperm trees [6-20, 22-26].

Dating results of sample segments. The sample MJ-1, with a length of only 0.30 m, was collected from a large stem. The diameter in the sampling direction is about 3.10 m, corresponding to radius of 1.55 m, which is also the distance to the theoretical pith of this stem. As mentioned, the wood of segment MJ-1a which originates from a depth of only 0.15 m, was formed after the year 1950. The segment MJ-1b, from a depth of 0.30 m, had a radiocarbon date of 123 ± 16 BP, which corresponds to a calibrated age of 120 ± 20 calendar yr. The sample MJ-1 was too short to provide significant information about the true age of the baobab. We also collected two samples from another stem, which were even shorter. This demonstrates that the stems have large hollow parts, very probably due to the state of decline of the baobab.

The sample MJ-2, with a length of 0.34 m, was extracted from a primary branch. The branch diameter in the sampling direction is 0.72 m. The segment MJ-2a, from a depth of 0.15 m, had a radiocarbon date of 158 ± 18 BP, which corresponds to a calibrated age of 155 ± 25 calendar yr. The segment MJ-2b from a depth of 0.34 m, which is also the sample end, had a radiocarbon date of 214 ± 17 BP corresponding to a calibrated age of 265 ± 25 calendar yr.

Age of the Grand Baobab of Mahajanga. The age of the baobab can be determined by extrapolating the age of the oldest dated segment, i.e., MJ-2b, to the calculated centre of the branch from which it originates. The sample segment MJ-2b, with an age of 265 ± 25 yr, was extracted from a distance of 0.34 m from the sampling point. The calculated centre of the branch is located at 0.36 m from the sampling point. These values indicate that the Big Baobab of Mahajanga is up to 300 yr old; more precisely, its age is of 275 ± 25 years.

This age value is in good agreement with the circumference measurements made over time, namely 14.60 m (at a height of 0.70 m) in 1898, 20.60 m (at 1.50 m) in 1979, 20.70 m (at 1.50 m) in 2011, 21.21 m (at 1.30 m) in 2013 and 21.23 m (at 1.30 m) in 2018. The mentioned values show that the Grand Baobab grew very fast when it was young, due to the sandy soil on limestone rock and also to the very high annual rainfall. The values also show that the Grand Baobab almost stopped growing at least over the last four decades and is probably close to the end of its life cycle.

We should mention that, at a distance of around 200 m, in a yard behind the MCB bank, grows another very large African baobab (GPS coordinates $15^{\circ}43.292'$ S, $046^{\circ}18.672'$ E). It also has a cluster structure and is composed of 10 fused stems (**Figure 4**). This baobab has a height of 18.1 m and a circumference cbh of 20.05 m.



Figure 4. The photograph shows the second largest baobab of Mahajanga.

CONCLUSIONS

The research presents the AMS radiocarbon investigation results of the historic Grand Baobab of Mahajanga, Madagascar. The baobab has a cluster structure and consists of 6 fused ordinary stems and 3 smaller binding stems. Two wood samples were collected from a large stem and from a primary branch, which were dated by radiocarbon. The oldest dated sample segment had a radiocarbon date of 214 ± 17 BP, which corresponds to a calibrated age of 265 ± 25 calendar years. The dating results indicate that the Grand Baobab of Mahajanga is 275 ± 25 years old. It can be stated that the historic baobab of Mahajanga started growing around the year 1750 CE.

The baobab of Mahajanga is in a state of decline and measures should be taken to avoid further degradation of the tree.

EXPERIMENTAL SECTION

Sample collection. The wood samples were collected with a Haglöf CH 800 increment borer (0.80 m long, 0.0054 m inner diameter). A number of four segments of the length of 10^{-3} m were extracted from predetermined positions along the wood samples. The segments were processed and investigated by AMS radiocarbon dating.

Sample preparation. The acid-base-acid pretreatment method was used for removing soluble and mobile organic components [27]. The pretreated samples were combusted to CO₂ by using the closed tube combustion method [28]. Next, CO₂ was reduced to graphite on iron catalyst [29]. Eventually, the resulting graphite samples were investigated by AMS.

AMS measurements. AMS radiocarbon measurements were performed at the NOSAMS Facility of the Woods Hole Oceanographic Institution (Woods Hole, MA, U.S.A.), by using the Pelletron® Tandem 500 kV AMS system. The obtained fraction modern values, corrected for isotope fractionation with the normalized $\delta^{13}\text{C}$ value of -25‰ , were converted to a radiocarbon date.

Calibration. Radiocarbon dates were calibrated and converted into calendar ages with the OxCal v4.4 for Windows [30], by using the SHCal20 atmospheric data set [31].

ACKNOWLEDGEMENTS

The investigation of the baobab was authorised by the Forestry Direction of the Ministry of Environment, Ecology and Forestry of Madagascar and by the Madagascar National Parks. The research was funded by the Romanian Ministry of Research CNCS-UEFISCDI under grant PN-III-P4-ID-PCE-2020-2567, No. 145/2021.

REFERENCES

1. G.E. Wickens, *Kew Bull.*, **1982**, 37(2), 172-209.
2. D.A. Baum, *Ann. Mo. Bot. Gard.*, **1995**, 82, 440-471.
3. G.E. Wickens, P. Lowe, "The Baobabs: Pachycauls of Africa, Madagascar and Australia", Springer, Dordrecht, **2008**, pp. 232-234, 256-257, 295-296.

4. A. Petignat, L. Jasper, "Baobabs of the world: The upside down trees of Madagascar, Africa and Australia", *Struik Nature*, Cape Town, **2015**, pp. 16-86.
5. G.V. Cron, N. Karimi, K.L. Glennon, C.A. Udeh, E.T.F. Witkowski, S.M. Venter, A.E. Assobadjo, D.H. Mayne, D.A. Baum, *Taxon*, **2016**, *65*, 1037-1049.
6. A. Patrut, K.F. von Reden, D.A. Lowy, A.H. Alberts, J.W. Pohlman, R. Wittmann, D. Gerlach, L. Xu, C.S. Mitchell, *Tree Physiol.*, **2007**, *27*, 1569-1574.
7. A. Patrut, K.F. von Reden, R. Van Pelt, D.H. Mayne, D.A. Lowy, D. Margineanu, *Ann. Forest Sci.*, **2011**, *68*, 93-103.
8. A. Patrut, K.F. von Reden, D.H. Mayne, D.A. Lowy, R.T. Patrut, *Nucl. Instrum. Methods Phys. Res. Sect. B*, **2013**, *294*, 622-626.
9. A. Patrut, S. Woodborne, K.F. von Reden, G. Hall, M. Hofmeyr, D.A. Lowy, R.T. Patrut, *PLOS One*, **2015**, *10(1)*: e0117193.
10. A. Patrut, S. Woodborne, K.F. von Reden, G. Hall, R.T. Patrut, L. Rakosy, J-M. Leong Pock Tsy, D.A. Lowy, D. Margineanu, *Radiocarbon*, **2017**, *59(2)*, 435-448.
11. A. Patrut, S. Woodborne, R.T. Patrut, L. Rakosy, D.A. Lowy, G. Hall, K.F. von Reden, *Nature Plants*, **2018**, *4(7)*, 423-426.
12. A. Patrut, R.T. Patrut, L. Rakosy, D.A. Lowy, D. Margineanu, K.F. von Reden, *Studia UBB Chemia*, **2019**, *LXIV*, *2 (II)*, 411-419.
13. A. Patrut, S. Woodborne, R.T. Patrut, G. Hall, L. Rakosy, C. Winterbach, K.F. von Reden, *Forests*, **2019**, *10*, 983-993.
14. A. Patrut, A. Garg, S. Woodborne, R.T. Patrut, L. Rakosy, I.A. Ratiu, *PLOS One*, **2020**, *15(1)*: e0227352.
15. A. Patrut, R.T. Patrut, P. Danthu, J-M. Leong Pock Tsy, L. Rakosy, D.A. Lowy, K.F. von Reden, *PLOS One*, **2016**, *11(1)*: e146977.
16. A. Patrut, K.F. von Reden, P. Danthu, J-M. Leong Pock Tsy, R.T. Patrut, D.A. Lowy, *PLOS One*, **2015**, *10(3)*: e0121170.
17. A. Patrut, K.F. von Reden, P. Danthu, J-M. Leong Pock Tsy, L. Rakosy, R.T. Patrut, D.A. Lowy, D. Margineanu, *Nucl. Instr. Methods Phys. Res. Sect. B*, **2015**, *361*, 591-598.
18. R.T. Patrut, A. Patrut, J-M. Leong Pock Tsy, S. Woodborne, L. Rakosy, P. Danthu, I.A. Ratiu, J. Bodis, K.F. von Reden, *Studia UBB Chemia*, **2019**, *LXIV*, *4*, 131-139.
19. A. Patrut, R.T. Patrut, J-M Leong Pock-Tsy, S. Woodborne, L. Rakosy, I-A. Ratiu, J. Bodis, P. Danthu, *Studia UBB Chemia*, **2020**, *LXV*, *4*, 151-158.
20. A. Patrut, R.T. Patrut, J-M Leong Pock Tsy, P. Danthu, S. Woodborne, L. Rakosy, I.A. Ratiu, *Forests*, **2021**, *12*, 1258.
21. C. Cornu, P. Danthu, "Baobabs de Madagascar: Guide d'identification illustré", CIRAD, Montpellier, **2015**, pp.16-17.
22. A. Patrut, R.T. Patrut, L. Rakosy, K.F. von Reden, *DRC Sustainable Future*, **2020**, *1(1)*, 33-47.
23. A. Patrut, R.T. Patrut, L. Rakosy, D. Rakosy, I.A. Ratiu, K.F. von Reden, *Studia UBB Chemia*, **2021**, *LXVI*, *1*, 153-163.
24. A. Patrut, R.T. Patrut, L. Rakosy, I.A. Ratiu, D.A. Lowy, K.F. von Reden, *Dendrochronologia*, **2021**, *70*, 125898.

25. A. Patrut, R.T. Patrut, L. Rakosy, I.A. Ratiu, J. Bodis, M.N. Nassor, K.F. von Reden, *Studia UBB Chemia*, **2022**, *LXVII*, 2, 143–153.
26. A. Patrut, R.T. Patrut, L. Rakosy, D. Rakosy, W. Oliver, I.A. Ratiu, D.A. Lowy, G. Shimbii, S. Woodborne, K.F. von Reden, *Forests*, **2022**, 13, 1889.
27. N.J. Loader, I. Robertson, A.C. Barker, V.R. Switsur, J.S. Waterhouse, *Chem. Geol.*, **1997**, 136(3), 313–317.
28. Z. Sofer, *Anal. Chem.*, **1980**, 52(8), 1389-1391.
29. J.S. Vogel, J.R. Southon, D.E. Nelson, T.A. Brown, *Nucl. Instrum. Methods Phys. Res. Sect. B*, **1984**, 5, 289-293.
30. C. Bronk Ramsey, *Radiocarbon*, **2009**, 51, 337-360.
31. A.G. Hogg, T.J. Heaton, Q. Hua, J.G. Palmer, C.S.M. Turney, J. Southon, A. Bayliss, P.G. Blackwell, G. Boswijk, C.B. Ramsey, C. Pearson, F. Petchey, P.J. Reimer, R.W. Reimer, L. Wachter, *Radiocarbon*, **2020**, 62(4), 759-778.

ASSESSMENT OF BIOLOGICAL ACTIVITY OF SELECTED SPECIES MUSHROOMS OF THE ORDER AGARICALES AND BOLETALES

Nevena PRODANOVIĆ^{a,*}, Marijana KOSANIĆ^b, Aleksandar KOČOVIĆ^a, Jovica TOMOVIĆ^a, Emina MRKALIĆ^c, Miroslav SOVRLIĆ^a

ABSTRACT. The aim of this study was to examine the antineurodegenerative, antimicrobial and antioxidant potential and to determine the total phenolics and total flavonoids of acetone extracts of selected mushrooms species (*Suillus luteus*, *Leccinum aurantiacum*, *Agaricus xanthoderma* and *Tricholoma terreum*) belonging to the genera *Boletus* and *Agaricus*. The content of phenolic components in the tested mushroom species varied in the total amount from 94.95 to 147.81 µg PE/mg extract, while the content of flavonoids varied in the range from 2.43 to 23.71 µg RE/mg extract. The tested acetone extracts showed acetylcholinesterase inhibition ranging from 11.49 to 17.46%. The strongest antimicrobial activity for the tested bacteria and fungi was shown by the species *Agaricus xanthoderma*. The antibacterial effect was stronger than the antifungal. Acetone extracts of the tested mushroom species showed moderate antioxidant activity. This study shows that the tested species of mushrooms possess different biological activity and that they can be used as a good source of natural agents are beneficial for human health.

Keywords: mushroom, biological activity, antioxidants

INTRODUCTION

Since ancient times, mushrooms have aroused different interests in people. In the last decades, mushrooms are valuable because of their nutritional value due to the content of high-quality proteins, crude fiber, minerals and

^a University of Kragujevac, Faculty of Medical Sciences, Department of Pharmacy, Kragujevac, Serbia

^b University of Kragujevac, Faculty of Science, Department of Biology, Kragujevac, Serbia

^c University of Kragujevac, Institute for Information Technologies, Department of Science, Jovana Cvijića bb, Kragujevac 34000, Serbia

* Corresponding author: nensyprodanovic@yahoo.com



vitamins [1, 2]. By drying the mushrooms at 40 degrees, the protein content is stable, while other types of heat treatment significantly reduce the protein content. They contain all the essential amino acids of which lysine is the most abundant. In addition to lysine, mushrooms also contain other essential amino acids such as arginine, glutamic acid, aspartic acid and serine [3]. Of the fatty acids, unsaturated fatty acids are largely present in the fruiting bodies of mushrooms, the most common of which is linoleic, while carbohydrates represent from 50% to 60% of the mushrooms content. The most common carbohydrates are pentose (xylose, ribose) and hexose (glucose, fructose, galactose, mannose) [4].

The mineral components of the mushrooms are divided into micro and macro elements that are necessary for the normal functioning of the organism. The group of macroelements includes: K, Na, Mg, P and S, while the group of microelements includes: Cu, Co, Fe, J, Mn, Mo, Zn and Se. The content of macronutrients such as sodium, potassium, and phosphorus is constant, while the content of calcium, magnesium and sulfur varies depending on the composition of the substrate on which the mushrooms grow [5]. Mushrooms are a significant source of vitamins, especially B vitamins, thiamine (B₁) and riboflavin (B₂), pyridoxine (B₆) and niacin (B₃) and ascorbic acid (vitamin C). Mushrooms also contain aromatic ingredients that can spice up and raise the quality of other dishes with their magical vinegar and aroma [6-7].

In addition to their nutritional value, mushrooms are a valuable source of many different biologically active compounds, which is why they are becoming an increasingly popular subject of research [8-9]. Among the biologically active compounds in mushrooms are polysaccharides, terpenoids and alkaloids that exhibit antioxidant, antimicrobial, anticancer, immunomodulatory, anti-inflammatory and antineurodegenerative effects, as shown by numerous studies [10-12]. Many antibiotics are still used today, e.g. such as penicillin, streptomycin, chloramphenicol, and others, just derived from mushrooms [13-14]. A large number of compounds with antioxidant action in mushrooms are found in the fruiting body and mycelium. Antioxidants, synthetic or natural, can have a positive effect on human health by reducing oxidative damage caused by ROS [15-16]. Recently, however, it has been suspected that some of synthetic oxidants such as butylated hydroxytoluene (BHT), tert-butylhydroquinone (TBHQ) and propyl gallate (PG) have toxic and carcinogenic effects [17]. In the search for natural antioxidants, we focused our research on mushrooms, which are a potential source of natural antioxidants.

Today, there is a growing interest in traditional medicine, and an increasing number of researchers are focused on finding new medicines from mushrooms. In this study, we considered the bioactive activity of mushrooms from the genera *Boletus* and *Agaricus*. From the genus *Boletus* we examined

the species *Suillus luteus* and *Leccinum aurantiacum*, and from the genus *Agaricus*, species *Agaricus xanthoderma* and *Tricholoma terreum*. Some species of mushrooms that belong to these genera are known producers of biologically active substances, which is why they are used in the production of antibiotics, organic acids, cheeses and many other products [18-19].

The aim of this study is to describe and identify mushroom samples collected in the nearness of the cities Kragujevac and Niš in the Republic of Serbia and to determine total phenolics and total flavonoids in the acetone extracts of examined mushrooms spectrophotometrically. Also, the aim of the study is to examine the biological activities of mushrooms: antibacterial activity of acetone extract of studied mushrooms species in relation to certain bacterial species, antifungal activity of acetone extracts of studied mushrooms species in relation to certain fungal species, antineurodegenerative activity by determining the degree of inhibition of acetylcholinesterase enzyme activity and to determine the antioxidant activity of extracts (determination of DPPH (1,1-diphenyl-2-picrylhydrazyl) free radical scavenging activity, determination of superoxide anion radicals scavenging activity and total reducing power).

RESULTS AND DISCUSSION

Total phenolic and flavonoid contents

It has been demonstrated that the phenol content of mushrooms extracts depended on the solvent used and its polarity and also shown that the acetone extract gave the highest polyphenol content [20]. The high efficiency of acetone to extract phenolic compounds from samples may be due to its ability to prevent the protein–polyphenol binding, which is insoluble complex, through solvent extraction [21]. It has been postulated that acetone is able to inhibit the formation of the protein–polyphenol complex during extraction, or to break down the interaction between the functional group of polyphenols (^{-}OH) and the carboxyl group of proteins [22].

The total content of phenolic and flavonoid compounds in mushroom extracts is shown in Figure 1. The content of phenolic components in the tested mushroom species varied in the total amount from 94.95 to 147.81 $\mu\text{g PE/mg}$ extract. The highest content of measured phenol is in the species *Suillus luteus* 147.81 $\mu\text{g PE/mg}$ extract. Slightly lower phenol content was observed in *Agaricus xanthoderma* 100.29 $\mu\text{g PE/mg}$ extract. The lowest phenol content was measured in *Tricholoma terreum*. The content of flavonoids in the extracts of the tested mushrooms varied in the range from 2.43 to 23.71 $\mu\text{g RE/mg}$ extract. The highest flavonoid content was measured in *Suillus luteus*

23.71 $\mu\text{g RE/mg extract}$, while the lowest flavonoid content was measured in *Agaricus xanthoderma* 2.43 $\mu\text{g RE/mg extract}$. The difference perhaps could be attributed to genetic factors (different species) [23]. The tested mushroom species showed similar or higher content of flavonoids and phenols than the same species collected in other localities around the world, as well as in relation to other species belonging to the same genus, which is why we expected strong bioactivity of their extracts [24-27].

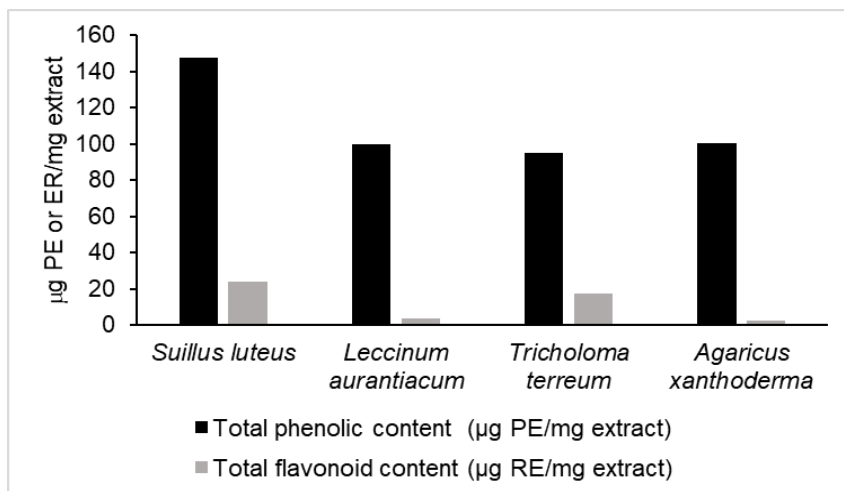


Figure 1. Total phenolic and flavonoid content of tested mushrooms extracts

Inhibition of acetylcholinesterase enzyme activity

Extracts of the studied mushrooms species showed significant potential in inhibiting acetylcholinesterase (AChE) activity compared to the synthetic galantamine inhibitor (Table 1). Acetylcholinesterase activities with these extracts ranged from 11.49 to 17.46%. *Agaricus xanthoderma* extract was the most effective and inhibited acetylcholinesterase activity by 17.46%, while *Suillus luteus* extract was the weakest and inhibited acetylcholinesterase activity by 11.49%.

Despite the fact that the etiology of neurodegenerative disorders, primarily Alzheimer's and Parkinson's disease, has not been fully explained, it is known that there is a reduced level of acetylcholine. The enzyme acetylcholinesterase (AChE) hydrolyzes the neurotransmitter acetylcholine, stopping synaptic transmission. Therefore, AChE inhibitors are considered to be the most effective agents in the treatment of these disorders, since by reducing the activity of this

ASSESSMENT OF BIOLOGICAL ACTIVITY OF SELECTED SPECIES MUSHROOMS
OF THE ORDER AGARICALES AND BOLETALES

enzyme, it helps to restore the level of acetylcholine in cholinergic synapses (28-29). Because synthetic AChE inhibitors are expensive and have a variety of side effects, more and more attention is being paid to finding natural alternative sources. Selected Mushroom species were tested for the first time in terms of inhibition of acetylcholinesterase activity. *Agaricus xanthoderma* extract was the most effective and inhibited acetylcholinesterase activity by 17.46%.

Table 1. Acetylcholinesterase inhibitory activity of tested mushroom extracts in different concentrations

Mushrooms extracts	Inhibition of acetylcholinesterase (%)			
	125 µg/ml	250 µg/ml	500 µg/ml	1000 µg/ml
<i>Suillus luteus</i>	11.49	12.19	15.24	17.45
<i>Leccinum aurantiacum</i>	11.82	13.53	14.20	15.91
<i>Tricholoma terreum</i>	13.13	14.13	15.01	16.71
<i>Agaricus xanthoderma</i>	11.82	14.15	14.20	17.46

Antioxidant activity

The antioxidant activity of the tested extracts was determined through several tests: DPPH free radical scavenging activity, superoxide anion scavenging activity and total reducing power assay. Edible and medicinal mushroom species are a depot of numerous biologically active compounds that individually or in combination with others have significant antioxidant capacity and can be considered potential natural antioxidants [30]. Until now, many researchers have investigated the antioxidant properties of many mushroom extracts from order *Agaricales* and *Boletales* and some of them showed very good antioxidant activity [24, 31-32].

Table 2. The antioxidant activity of examined extracts of mushrooms

Mushrooms extracts	Type of antioxidant activity	
	DPPH IC ₅₀ (µg/ml)	Superoxide anion radical IC ₅₀ (µg/ml)
<i>Suillus luteus</i>	73.41	24.47
<i>Leccinum aurantiacum</i>	107.24	136.08
<i>Tricholoma terreum</i>	142.34	85.24
<i>Agaricus xanthoderma</i>	105.17	116.47

Table 2 showcases the results of DPPH scavenging activity for the examined extracts. The IC₅₀ values of tested extracts ranged from 73.41 to 142.34 µg/ml. The concentration at which 50% of the radicals were neutralized (IC₅₀) was the parameter for comparing antiradical activity (lower IC₅₀ values represent better antiradical activity). Among the examined extracts, the extract of the mushrooms *Suillus luteus* showed the largest DPPH scavenging activity (IC₅₀ = 73.41 µg/ml).

The results of the superoxide anion scavenging activity (Table 2) of the tested extracts showed that the highest activity had the extract of *Suillus luteus* (IC₅₀ = 24.47 µg/ml), while the extract of *Leccinum aurantiacum* showed the lowest activity (IC₅₀ = 136.08 µg/ml).

The reducing power of the tested extracts was dose-dependent (Table 3). The measured values of absorbance in all species ranged from 0.04 to 0.25 (higher value of absorbance indicates stronger reduction power). The strongest reducing capacity was shown by the extract of the fungus *Suillus luteus* (0.3026 at a concentration of 1 mg/ml, 0.1875 at a concentration of 0.5 mg/ml, 0.0864 at a concentration of 0.25 mg/ml, and 0.0522 at a concentration of 125 mg/ml), while the reduction capacity of *Tricholoma terreum* was least pronounced (0.0390 at 1 mg/ml, 0.0318 at 0.5 mg/ml, 0.0265 at 0.25 mg/ml, and 0.0102 at 0.125 mg/ml). The remaining tested species exhibited approximately similar reducing power.

Table 3. Reducing power of examined extracts of mushrooms

Mushrooms extracts	Absorbance			
	125 µg/ml	250 µg/ml	500 µg/ml	1000 µg/ml
<i>Suillus luteus</i>	0.0522	0.0864	0.1875	0.3026
<i>Leccinum aurantiacum</i>	0.0260	0.0510	0.0845	0.1488
<i>Tricholoma terreum</i>	0.0102	0.0265	0.0318	0.0390
<i>Agaricus xanthoderma</i>	0.0318	0.0386	0.0561	0.0813

The degree of strength of antioxidant activity differed in the examined species, which correlates with the amount of phenols present in the mushrooms itself. The tested extracts of mushrooms show strong antioxidant activity against different oxidative systems. The strong antioxidant activity is the result of high total phenolic content of tested extracts, because between the total phenolic content and the antioxidant activity is a positive correlation, and there are reports about it [33-35].

Antimicrobial and antifungal activity

Acetone extracts of the tested species of mushrooms showed different antimicrobial activity according to the tested species of bacteria and fungi. If we take into account the MIC values as well as the number of tested microorganisms in relation to which the antimicrobial effect was found, the highest antibacterial activity was shown by acetone extract of *Agaricus xanthoderma*. The inhibitory effect was manifested in a concentration of 0.78 mg/ml on two tested species of bacteria (*Bacillus cereus* and *Escherichia coli*), in a concentration of 1.56 mg/ml also on two species of tested bacteria (*Bacillus subtilis* and *Proteus mirabilis*), and in a concentration of 3.12 mg/ml per test bacterial species (*Staphylococcus aureus*). The weakest antibacterial activity was shown by *Suillus luteus*, where the MIC was 12.5 mg/ml for one species of tested bacterium (*Bacillus subtilis*), and 25 mg/ml for four species of tested bacteria (*Bacillus cereus*, *Staphylococcus aureus*, *Proteus mirabilis* and *Escherichia coli*) (Table 4).

The strongest antifungal effect was shown by the extract of the *Agaricus xantoderma* where the MIC concentration varied from 3.12 to 12.5 mg/ml. The inhibitory effect was shown at a concentration of 3.12 mg/ml per test fungus (*Candida albicans*), at a concentration of 6.25 mg/ml on three tested fungi (*Geotrichum candidum*, *Penicillium chrysogenum* and *Aspergillus fumigatus*), and at a concentration of 12.5 mg/ml showed an inhibitory effect on two tested fungi (*Trichophyton mentagrophytes* and *Paecilomyces variotii*). The weakest antifungal effect was shown by the extract of the fungus *Tricholoma terreum* where the MIC concentration varied from 12.5 to 25 mg/ml (Table 4).

The antibacterial effect was stronger than the antifungal. Such results could be expected given that numerous studies have shown that bacteria are more sensitive to antibiotics than fungi. The reason for the different susceptibility between fungi and bacteria could be attributed to the different permeability of the cell wall. The cell wall of gram-positive bacteria is made of peptidoglycan (murein) and teichoic acid, and the cell wall of gram-negative bacteria is made of peptidoglycan, lipopolysaccharides and lipoproteins, while the cell wall of fungi contains polysaccharides such as chitin and glucan. Selected species of mushrooms are a possible source of bioactive compounds that have antibiotic activity [36, 37]. The strongest antimicrobial effect was shown by the species *Agaricus xantoderma*.

Table 4. Minimum inhibitory concentration (mg/ml) for mushroom extracts for tested bacterial and fungal strains

Bacterial/fungal strain	Mushrooms species				Control	
	<i>Suillus luteus</i>	<i>Leccinum aurantiacum</i>	<i>Tricholoma terreum</i>	<i>Agaricus xanthoderma</i>	Streptomycin	Ketoconazole
<i>Bacillus subtilis</i> (IPH 189)	12.5	6.25	3.12	1.56	0.016	/
<i>Bacillus cereus</i> (ATCC 11778)	25	25	12.5	0.78	0.016	/
<i>Staphylococcus aureus</i> (ATCC 25923)	25	12.25	12.5	3.12	0.031	/
<i>Escherichia coli</i> (ATCC 25922)	25	25	12.5	1.56	0.062	/
<i>Proteus mirabilis</i> (ATCC 12453)	25	25	6.25	0.78	0.062	/
<i>Trichophyton mentagrophytes</i>	6.25	12.5	25	12.5	/	0.156
<i>Geotrichum candidum</i>	6.25	25	25	6.25	/	0.078
<i>Paecilomyces variotii</i>	6.25	12.5	25	12.5	/	0.156
<i>Fusarium solani</i>	25	25	12.5	25	/	0.156
<i>Candida albicans</i>	3.12	3.12	12.5	3.12	/	0.039
<i>Aspergillus flavus</i>	25	25	25	25	/	0.312
<i>Penicillium chrysogenum</i>	12.5	12.5	12.5	6.25	/	0.312
<i>Aspergillus fumigatus</i>	3.12	12.5	12.5	6.25	/	0.156

CONCLUSIONS

To the best of our knowledge, this study presented for the first time a comparison of biological activity and total phenolic and flavonoid content in mushrooms of the orders *Agaricales* and *Boletales*. The results of biological activity tests show that the extract of *Suillus luteus* has the best antioxidant and antineurodegenerative activity, while the extract of *Agaricus xanthoderma* has the best antibacterial and antifungal activity. Based on the obtained results, it can be concluded that edible mushroom species are a rich source of various biologically active compounds that have significant antimicrobial, antioxidant and antineurodegenerative activity, in addition to their nutritional value, particular aroma and other beneficial properties.

ASSESSMENT OF BIOLOGICAL ACTIVITY OF SELECTED SPECIES MUSHROOMS
OF THE ORDER AGARICALES AND BOLETALES

The discovery of new bioactive metabolites of mushrooms and more detailed studies of the same will enable the discovery of new biologically active agents in the control of various types of diseases, which is of great interest to the human population.

EXPERIMENTAL SECTION

Chemicals/ Reagents

All chemicals and reagents were of analytical grade and were purchased from Sigma Chemical Co. (St Louis, MO, USA), Aldrich Chemical Co. (Steinheim, Germany) and Alfa Aesar (Karlsruhe, Germany).

Plant material

The studied species of mushrooms were collected in the vicinity of Kragujevac and Nis, in the period September-October 2017 (Table 5). Dry mushroom material is kept in the Department of Biology and Ecology, Faculty of Science in Kragujevac. The identification of collected mushrooms was performed using standard herbarium keys [38-40].

Table 5. Examined mushrooms species

Examined mushrooms species	Code	Vicinity	Year of sampling
<i>Suillus luteus</i>	DBFS92	Nis	2017
<i>Leccinum aurantiacum</i>	DBFS93	Nis	2017
<i>Tricholoma terreum</i>	DBFS94	Kragujevac	2017
<i>Agaricus xanthoderma</i>	DBFS97	Kragujevac	2017

Preparation of extracts

The extraction of selected mushroom specimens was performed in the Laboratory for Microbiology and Mycology, Faculty of Science in Kragujevac. The acetone extracts of the studied mushroom species were analyzed. Preparation of acetone extract: Collected mushrooms were firstly dried at room temperature. Dried, main parts (body of mushrooms) of selected mushrooms species were then pulverized and extracted with acetone for 48h at room temperature. The resulting extract was filtered through filter paper (Whatman No. 1) and then evaporated at room temperature to get the dry extract. The obtained acetone extracts were stored at -20 °C, which prevented the possibility of degradation of bioactive molecules. To check

the antibacterial, antifungal, antioxidant, and antineurodegenerative activity, solutions of different concentrations of extracts were obtained by dissolving a certain amount of dry matter in a certain volume of solvent (5% DMSO).

Determination of total flavonoid content

Total flavonoids were determined by the Dovid method (41). The same volume of extract was added to 2 ml of 2% methanolic aluminum (III) chloride solution. After one hour, the absorbance was measured at 415 nm. Based on the measured absorbances, the concentration (μg) of total flavonoids was read from the standard rutin calibration curve, and then the content of total flavonoids in the extract was expressed as rutin equivalent (RE)/mg of extract, according to:

$$\text{Absorbance} = 0.0296 \times \text{total flavonoids } [\mu\text{g (RE)/mg extract}] + 0.0204, \\ (R^2 = 0.9992)$$

Determination of total phenolic content

The total phenolic content in the extracts was determined with Folin-Ciocalteu reagents by the method of Slinkard and Slingleton [42]. The reaction mixture was prepared by mixing 1 ml of extract, 46 ml of distilled water, 1 ml of Folin-Ciocalteu reagent and 3 ml of 2% sodium carbonate solution. After 2 h of incubation, absorbances were measured spectrophotometrically at 760 nm. The standard curve equation was determined by measuring the absorbance of the pyrocatechol concentration series (0.1 - 0.02 mg/ml). The content of the polyphenols was expressed in μg of pyrocatechol equivalents per milligram of dry extract ($\mu\text{g PE/mg dry extract}$), according to:

$$\text{Absorbance} = 0.0021 \times \text{total phenolic } [\mu\text{g PE/mg of extract}] - 0.0092, \\ (R^2 = 0.9934)$$

Inhibition of acetylcholinesterase enzyme activity

The degree of inhibition of acetylcholinesterase activity (AChE) was determined spectrophotometrically using 96-well microtiter plates. The reaction mixture (140 μl 0.1 mM sodium phosphate buffer pH 8.0, 20 μl 5,5-dithiobis-2-nitrobenzoic acid (DTNB), 20 μl extract, 20 μl AChE (5IU) was incubated for 15 min at 25°C. The reaction was initiated by the addition of 10 μl of acetylthiocholine iodide whose hydrolysis was followed by a change in absorption at 412 nm due to the conversion of DTNB to yellow 5-thio-2-nitrobenzoate anion (TNB^-) in an AChE catalyzed reaction 6-15 min after initiation [43]. The degree of AChE inhibition was determined by the formula:

$$\text{Degree of inhibition of AChE activity (\%)} = [(E - S) / E] \times 100$$

where E is the activity of the enzyme without the extract and C is the activity of the enzyme with the extract. The values obtained were compared with a commercial inhibitor, galantamine.

Antioxidant activity

Determination of DPPH free radical scavenging activity

The antioxidant activity of mushroom extracts was determined by a modified (1,1-diphenyl-2-picryl-hydrazyl) DPPH assay [44]. A mixture of methanolic solution of DPPH (concentration 0.05 mg/ml) and mushroom extracts of different concentrations (1, 0.5, 0.25 and 0.125 mg/ml) were incubated at room temperature, in the dark, for 30 minutes. After incubation, absorbance was measured at 517 nm on a spectrophotometer ("Jenway" UK). Ascorbic acid was used as a positive control. The capacity to neutralize free radicals was calculated by the following formula:

$$\text{Neutralization capacity of DPPH radicals (\%)} = [(A_0 - A_1) / A_0] \times 100$$

where A_0 is the absorbance of the negative control and A_1 is the absorbance of the reaction mixture or standard. IC_{50} values (concentration at which 50% of DPPH radicals were neutralized) were calculated from the obtained inhibition values.

Determination of superoxide radical scavenging activity

The effect of the extracts on the superoxide anion radical was determined by the Nishimiki method [45]. The reaction mixture was prepared by mixing 0.1 ml of extract of different concentrations (1, 0.5, 0.25 and 0.125 mg/ml), 1 ml of nitroblue tetrazolium (NBT) solution (156 μ M in 0.1 M phosphate buffer, pH=7.4), 1 ml of NADH solution (468 μ M in 0.1 M phosphate buffer, pH=7.4) and 100 μ l phenazine methosulphate (PMS) solution (60 μ M in 0.1 M phosphate buffer, pH=7.4). After incubation at room temperature for 5 minutes, the absorbance was measured at 560 nm on a spectrophotometer. Ascorbic acid was used as a positive control. The percentage inhibition of superoxide anion radicals was calculated using the following equation:

$$\text{Inhibition of superoxide anion radical (\%)} = [(A_0 - A_1) / A_0] \times 100$$

where A_0 is the absorbance of the negative control and A_1 is the absorbance of the reaction mixture or standard. IC_{50} values (concentration at which 50% of superoxide anion radicals were neutralized) were calculated from the obtained inhibition values.

Total reducing power assay

The total reduction capacity of the extracts was determined by the Oyaizu method (46). Mushroom extract (1ml) of different concentrations (1, 0.5, 0.25 and 0.125 mg/ml) was mixed with phosphate buffer (2.5 ml, 0.2 M, pH=6.6) and potassium ferricyanide (2.5 ml, 1%). Then, the mixture was incubated for 20 min at 50°C, and then 2.5 ml of 10% trichloroacetic acid solution was added. After centrifugation, the supernatant (2.5 ml) was mixed with distilled water (2.5 ml) and 0.1% iron (III) chloride solution (0.5 ml). The absorbance was measured at 700 nm on a spectrophotometer. Ascorbic acid was used as a positive control.

Antibacterial and antifungal activities of extracts of selected mushroom species

Tests of antibacterial activity of extracts of selected mushrooms species were performed against five bacterial species: *Bacillus subtilis* (IPH 189), *B. cereus* (ATCC 11778), *Staphylococcus aureus* (ATCC 25923), (Gram-positive bacteria); *Escherichia coli* (ATCC 25922) and *Proteus mirabilis* (ATCC 12453) (Gram-negative bacteria).

Tests of antifungal activity of extracts of selected mushrooms species were performed in relation to 5 fungal species: *Aspergillus niger* (ATCC 16888), *Candida albicans* (ATCC 10231), *Mucor mucedo* (ATCC 20094), *Penicillium italicum* (ATCC 10454) and *Trichoderma viride* (ATCC 13233). The fungi and bacteria tested come from the American Culture Sample Collection (ATCC).

The sensitivity of microorganisms to acetone extracts of the tested mushrooms species was performed by measuring the inhibition for a given concentration of the extract by determining the minimum inhibitory concentration (MIC) by the microdilution method [47].

In the experiment, 96-well microtiter plates were used to which 100 µl of broth (Müller-Hinton for bacteria and SD for fungi) was added. In the first row, 100 µl of extract of a certain initial concentration was added and a series of double dilutions in the range of 50 to 0.0475 mg/ml was made. Then, 10 µl of a solution of resazurin of prepared growth of 270 mg of resazurin in 40 ml of sterile distilled water was added to all wells. Finally, 10 µl of the appropriate inoculum was added to all wells. After inoculation, the plates were incubated for 24 h at 37°C (bacteria) and 48 h at 27°C (fungi), respectively. MIC was determined visually, by changing the color of resazurin (oxido-reduction indicator for assessing microbial growth). Resazurin is a blue non-fluorescent dye that turns pink fluorescent after reduction of resazurin to resofurin oxidoreductases. The lowest concentration at which there is no discoloration of resazurin is defined as MIC.

ASSESSMENT OF BIOLOGICAL ACTIVITY OF SELECTED SPECIES MUSHROOMS
OF THE ORDER AGARICALES AND BOLETALES

The antibiotic streptomycin was used as a positive control to inhibit bacterial growth, and the antifungal ketoconazole to inhibit fungal growth. A positive control was also set up, which contained a substrate with microorganisms to monitor their unhindered growth. Negative control of the solvent effect was performed in parallel.

ACKNOWLEDGMENTS

This work was supported by the Ministry of Education, Science and Technological Development of the Republic of Serbia (Agreement Nos. 451-03-68/2022-14/200378, 451-03-9/2021-14/200111 and 451-03-9/2021-14/200122). This research was also supported by Science Fund of Republic of Serbia, Grant No. 7743504, Physicochemical aspects of rhythmicity in NeuroEndocrine Systems: Dynamic and kinetic investigations of underlying reaction networks and their main compounds, NES.

REFERENCES

1. P. C. K. Cheung; *Nutr. Bull.*, **2010**, *35*, 292-299.
2. M. E. Valverde; T. Hernández-Pérez; O. Paredes-López. *Int. J. Microbiol.*, **2015**, *2015*, 1-14.
3. P. Kalač. *J. Sci. Food Agric.*, **2013**, *93*, 209-218.
4. S. Prasad; H. Rathore; S. Sharma; A.S. Yadav; *Int. J. Food. Sci. Nutr. Diet.*, **2015**, *4*, 221-225.
5. M. Rudawska; T. Laski; *Food. Chem.*, **2005**, *92*, 499-506.
6. P. Mattila; K. Könkö; M. Euroola; J. M. Pihlava; J. Astola; L. Vahteristo; V. Piironen; *J. Agric. Food Chem.*, **2001**, *49*, 2343-2348.
7. B. Muszyńska; A. Grzywacz-Kisielewska; K. Kała; J. Gdula-Argasińska; *Food. Chem.*, **2018**, *243*: 373-381.
8. J. Rajewska; B. Bałasińska; *Postepy. Hig. Med. Dosw.*, **2004**, *58*, 352-357.
9. W. A. Elkhateeb; G. M. Daba; P. W. Thomas; T. C. Wen; *Egypt. Pharm. J.*, **2019**, *18*, 88-101.
10. S. Saxena; M. Chhibber; I. P. Singh; *Curr. Bioact. Compd.*, **2019**, *15*, 211-231.
11. G. B. Rosa; W. G. Sganzerla; A. L. A. Ferreira; L. O. Xavier; N. C. Veloso; J. da Silva; J. P. Ferrareze, (2020). *Int. J. Med. Mushrooms.*, **2020**, *22*, 931-942.
12. M. Pandimeena; M. Prabu; R. Sumathy; R. Kumuthakalavalli; *Int. Res. J. Pharm. Appl. Sci.*, **2015**, *5*, 16-21.
13. M. Awad; Y. ELâ; R. Aziz; R. Sarmidi; A. Elâ; *J. Teknol.*, **2012**, *59*, 101-111.
14. L. Demain; *Med. Res. Rev.*, **2009**, *29*, 821-842.
15. M. Stajic; J. Vukojevic; A. Knezevic; S. Duletic-Lausevic. I. Milovanovic; *Curr. Top. Med. Chem.*, **2013**, *13*, 2660-2676.
16. I. Mujić; Z. Zeković; Ž. Lepojević; S. Vidović; J. Živković; *J. Cent. Eur. Agric.* **2010**, *11*, 387-392.
17. W. Zhang; B. Li; L. Han; H. Zhang; *Afr. J. Biotechnol.*, **2009**, *8*, 3887-3892.

18. M. Ramos; N. Burgos; A. Barnard; G. Evans; J. Preece; M. Graz; A. C. Ruthes; A. Jiménez-Quero; A. Martínez-Abad; F. Vilaplana; L. Pham-Ngoc; A. Brouwer; B. Van der Burg; M. C. Garrigósa; A. Jiménez; *Food. Chem.*, **2019**, 292, 176-187.
19. M. H. M. Y. Yuswan; J. R. Al-Obaidi; A. Rahayu; S. Sahidan; F. Shazrul; D. Fauzi; *Adv. Biol. Biotechnol.*, **2015**, 6, 320-329.
20. Pk. M. Uddin; R. I. Talukder; M. K. Sarkar; T. Rahman; R. Pervin; M. Rahman; L. Akther; E. A. Zenat; L. Akther; (2019). *Open J. Med. Microbiol.* **2019**, 13, 10-15.
21. L. Jakobek; *Food Chem.*, **2015**, 175, 556–567.
22. E. S. Hwang; N. D. Thi. *Prev. Nutr. Food Sci.*, **2014**, 19, 40–48.
23. D. A. Abugri; W. H. McElhenney; *J. Nat. Prod. Plant. Resour.*, **2013**, 3, 37-42.
24. M. Kosanić, B. Ranković, M. Dašić; *Iran. J. Pharm. Sci.*, **2012**, 11, 1095-1102.
25. J.Zhang; Y Lu; L Zhao; L. A. Wang; (2021). *Int. J. Med. Mushrooms.*, **2021**, 23, 17-26.
26. B. Özaltun; M. Sevindik; *Eur. J. Res.*, **2020**, 6, 539-544.
27. G. Yuvali; D. Onbasli; *Int. J. Environ*, **2021**, 1-12.
28. M. Quik; S. Wonnacott; *Pharmacol. Rev.*, **2011**, 63, 938-966.
29. S. A. Heleno; L. Barros; A. Martins; P. Morales P; V. Fernández-Ruiz; J. Glamoclija; *LWT-Food. Sci. Technol.*, **2015**, 63, 799–806
30. K. Ganesan; B. Xu; *Mol.*, **2018**, 23, 2880.
31. S. Morel; S. Arnould; M. Vitou; F. Boudard; C. Guzman; P. Poucheret; S. Rapior; (2018). *Int. J. Med. Mushrooms.*, **2018**, 20, 20, 13-29.
32. L. Barros; S. Falcão; P. Baptista; C. Freire; M. Vilas-Boas; I. C. & Ferreira; *Food Chem.*, **2008**, 111, 61-66.
33. I. C. F. R. Ferreira; P. Baptista; M. Vilas-Boas; L. Barros; *Food. Chem.*, **2007**, 100, 1511–1516.
34. N. Aoussar; R. Manzali; I. Nattah; N. Rhallabi; P. Vasiljevic; M. Bouksaim; F. Mellouki; *J. Mater. Environ. Sci.*, **2017**, 8, 1968–1976.
35. Y. Choi; S. M. Lee; J. Chun; H. B. Lee; J Lee; *Food Chem.* **2006**, 99: 381–387.
36. S. A. Heleno; L. Barros; A. Martins; P. Morales; V. Fernández-Ruiz; J. Glamoclija; *LWT- Food Sci Technol.*, **2015**, 63, 799–806
37. M. G. Rosenberger; R. Paulert; V. G. Cortez; *Int. J. Med.*, **2018**, 20, 1065-1074.
38. M. Moser; G. Kibby; *Keys to Agarics and Boleti (Polyporales, Boletales, Agaricales, Russulales)*; Transl. Plant, S. London: Roger Phillips, **1983**, pp. 1-535.
39. A. E. Bessette; W. C. Roody; A. R. Bessette; *North American Boletes: A Color Guide to the Fleshy Pored Mushrooms*. Syracuse University Press, Syracuse, NY, **2000**, pp. 1-400.
40. B. Uzelac; *Gljive Srbije i Zapadnog Balkana*. BGV Logik, Beograd, **2009**, 1-462.
41. A. Meda; C. E. Lamien; M. Romito; J. Millogo; O. G. Nacoulma; *Food Chem.*, **2005**, 91, 571–577.
42. K. Slinkard; V. L. Singleton; *Am. J. Enol. Viticult.* **1997**; 28, 49–55.
43. G. L. Ellman; K. D. Courtney; V. Andres; R. M. Featherstone; *Biochem Pharmacol.*, **1961**, 7, 88–95.
44. H. D. Dorman; O. Bachmayer; M. Kosar; R. Hiltunen; *J. Agric. Food Chem.*, **2004**, 52, 762-770.
45. M. Nishikimi; N. A. Rao; K. Yagi; *Biochem. Biophys. Res. Commun.* **1972**, 46, 849–854.
46. M. Oyaizu; *J. Hum. Nutr. Diet.* **1986**, 44, 307–315.
47. S. D. Sarker; L. Nahar; Y. Kumarasamy; *Methods.* **2007**, 42, 321–324.

ESSENTIAL OIL COMPOSITION OF YARROW SPECIES (*ACHILLEA MILLEFOLIUM* L. AND *ACHILLEA WILHELMSII* L.): ANTIOXIDANT AND ANTIBACTERIAL ACTIVITIES OF ESSENTIAL OILS

Bunyamin YILDIRIM^a, Kamil EKICI^b, Mehmet Zeki KOCAK^{c,*}

ABSTRACT. Of the medicinal plants' cosmos, yarrow species (*A. millefolium* L. and *A. wilhelmsii* L.) are of the reputed species due to their phytochemical composition and thereby antioxidant and antibacterial activities. Owing to the high diversity in chemical composition and production of essential oil, the species deserves to be investigated more. In this context, wild yarrow plants were collected in Eastern Anatolia region (Van, Türkiye) and then the dried samples of the plants were subjected to hyd-rodistillation for essential oil extraction. In addition, the essential oils were assayed for their potential antioxidant and antibacterial activities. Gas Chromatography Mass Spectrometry (GC-MS) analysis revealed the presence of 1,8-cineole (75.19%), α -phellandrene (5.53%), P-eugenol (5.53%), camphor (5.45%), α -terpineol (2.09%), β -pinene (1.66%), camphene (1.20%), α -pinene(1.02%) from *A. millefolium* L. However, *A. wilhelmsii* was characterized with menthoglycol (35.84%), 1,8-cineole (34.04%), endo-borneol (9.93%), chrysanthenil acetate (4.76%), thymine (3.66%), terpinene-4-ol (2.33%), camphene (1.66%), and verbenole (1.53%). Regarding scavenging activities of the species, *A. wilhelmsii* exhibited better activity than *A. millefolium*, with a value of 6.5 mM and 4.2 mM Trolox equivalents (TEAC) respectively. With respect to the antibacterial activity against three gram-negative and three gram-positive bacteria, essential oils of both species were compared with standard antibiotic discs (ampicillin and ofloxacin).

Keywords: *Achillea millefolium*, *Achillea wilhelmsii*, Yarrow, Essential oils, Biological activity, GC-MS analysis.

^a Iğdir University, Faculty of Agriculture, Department of Field Crops, Iğdir, Turkey

^b Yuzuncu Yil University, Faculty of Veterinary Medicine, Food Hygiene and Technology, Van, Turkey

^c Iğdir University, Vocational School of Technical Sciences, Department of Herbal and Animal Production, Iğdir, Turkey

* Corresponding author: mehmetzekikocak@gmail.com



INTRODUCTION

Medicinal and aromatic plants have been used for centuries, and are rich valuable natural source of biologically active compounds, being used in traditional medicine for the treatments of various ailments as they possess antioxidant, antimicrobial, anti-inflammatory and antispasmodic activities [1-2]. In addition, the plants were also evaluated in pharmaceutical, sanitary, cosmetics, fragrances, plant protection, agricultural and food industries [2-4]. The genus *Achillea* has a wide range of distribution, and comprises more than 115 species. Most of the species (N=85) are distributed in the British Isles, southern Europe, Asia, Australia and North America [5]. Of those species, yarrow species (*A. millefolium* L. and *A. wilhelmsii* L.) is a widespread rhizomous herbaceous perennial medicinal plant belonging to the Asteraceae family confined to the Northern hemisphere [6-7]. Regarding the species, Turkey (Türkiye) is estimated to be quite rich in *Achillea* species; in addition to, about forty *Achillea* species show a wide distribution in Turkey. The yarrow species is locally named as “civanperçemi, pireotu, yılançiçeği, ormaderen, buyucan, kılıçotu and çoban kirpiği” [8].

Approximately, in the last three decades, a quite number of studies linked to the essential oils from aerial parts or flowers of *Achillea* species have been carried out [6-9-10-11]. Five most abundant monoterpene compounds were 1,8-cineole, camphor, borneol, α - and β -pinenes in the essential oils of *Achillea* species [12]. A study in Turkey revealed that 1,8-cineole was a major component and followed by camphor and borneol in *Achillea* species [13]. The most common essential oils extracted from *A. millefolium* populations were α - and β -pinenes, P-menthane, thujane, pinane, chamazulene, β -caryophyllene, eudesmol, ascaridole and β -oxide [14]. However, *A. wilhelmsii* is rich in sesquiterpenes, lactones, flavonoids and monoterpenoids, which have antimicrobial and antioxidant activities [15-16].

Yarrow is widely used for gastrointestinal disorders in Iranian traditional medicine, and an appetizer, wound healer, diuretic, carminative or menstrual regulator, anti-hemorrhoids and decreasing cholesterol in Turkey [8]. They have a wide range of biological activities including antispasmodic, antiulcer, antioxidant, antibacterial, antifungal, antimicrobial, antihypertensive, anti-hyperlipidemic, vagolytic and antitumoral properties [6-17], and treatment of pain, inflammation, headache, and spasmodic diseases [18]. The hygiene industry utilizes the essential oils of these plants to make skin tender and to treat skin inflammations using cream formulations [17]. Turkey has a rich medicinal and aromatic plant flora that is widely available throughout the country. In this regard, a plethora of reports on those species is available. However, the reports on the species from Eastern Anatolia region are rare.

Due to great differences in the climatic conditions of Eastern Anatolia region rather than other regions of Turkey, we hypothesized that the species of this region would have distinct chemical composition in relation to the species of other regions. The plausible variations in chemical composition would be manifested in their antioxidant and antibacterial activities. To test the hypothesis, we collected yarrow species from the relevant region and extracted the essential oil. Finally, both chemical composition and essential oil content were determined.

RESULTS AND DISCUSSION

Essential oil constituents of *A. millefolium* L. and *A. wilhelmsii* L.

The essential oil compounds identified by Gas Chromatography Mass Spectrometry (GC-MS) analysis of the species were listed in Table 1 along with retention time and percentage of composition. Fifteen compounds from *A. millefolium* and eighteen compounds from *A. wilhelmsii* were identified representing 100% of the total essential oil in the both species. Major components of *A. millefolium* were 1,8-cineole (75.19%), α -phellandrene (5.53%), P-eugenol (5.53%), camphor (5.45%), α -terpineol (2.09%), β -pinene (1.66%), camphene (1.20%) and α -pinene (1.02%). However, main components of *A. wilhelmsii* were menthoglycol (35.84%), 1,8-cineole (34.04%), endo-borneol (9.93%), chrysanthenil acetate (4.76%), thymine (3.66%), terpinene-4-ol (2.33%), camphene (1.66%), and verbenole (1.53%) (Table 1; Fig 1 and 2).

The relative of results, P-eugenol is the main constituent of clove (*Achillea millefolium*). The antimicrobial activity of eugenol is mainly attributed to its phenolic structure and to the hydrophobic character of this compound, facilitating its interaction with the microbial cell envelope. In addition, interfere with microbial virulence, reducing biofilm formation and modulating the expression of target virulence genes in gram-negative pathogens.

As a result of the literature studies, it has been observed that there are great differences in the chemical composition and essential oil components of the species found in different countries. Because of their genetically and chemically polymorphic structure, the essential oil content *Achillea* species could be affected by various factors such as environmental, genotypic, seasonal, soil conditions, developmental stage of plant, harvest time and storage conditions [18]. The main essential oil constituents of *A. millefolium* varied depending on the environmental conditions, locations and genotypes: 1,8-cineole, camphor, borneol, terpinolene, γ -terpinene, thujone, sabinene, cis-chrysanthenol or germacrene D, α -copaene, β -pinene, chamuzulene, p-cymene and methyl eugenol in Iran [19], D-cardinene, limonene, alloaromadendrene in Turkey [1],

1,8-cineole and germacrene-D in Serbia [20], 1,8-cineole, borneol, camphor, chamazulene, β -pinene, nerolidol in Lithuania, 1,8-cineole, β -pinene, β -caryophyllene, chamazulene, sabinene, (E)-nerolidol, guaiol in Estonia [21], camphor, 1,8-cineole, β -pinene, sabinene in Kazakhstan [12].

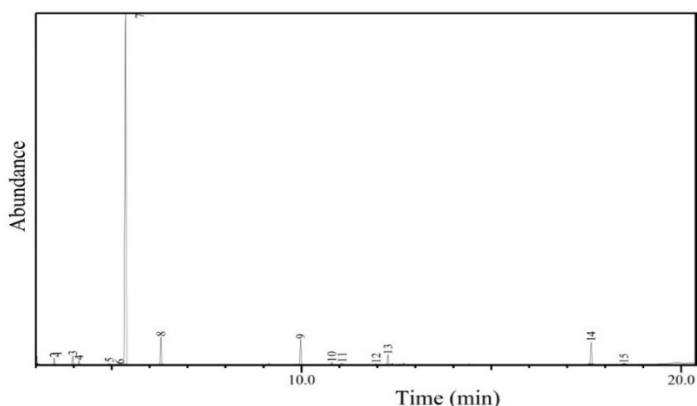


Figure 1. Gas-chromatogram of *Achillea millefolium* essential oils. The peaks correspond to identified compounds: (1) α -Pinene, (2) Camphene, (3) β -Pinene, (4) β -Phellandrene, (5) Terpinolene, (6) Paradiprene, (7) 1,8-cineole, (8) α -Phellandrene, (9) Camphor, (10) Endobornyl acetate, (11) Terpinene-4-ol, (12) δ -Terpineol, (13) α -Terpineol, (14) P-Eugenol, (15) Silaethane.

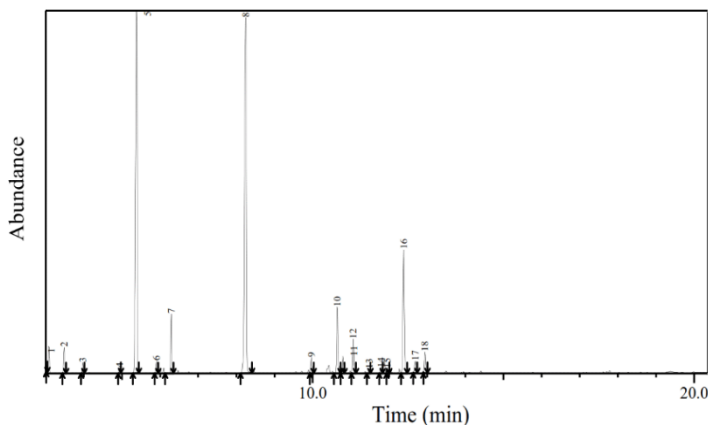


Figure 2. Gas-chromatogram of *Achillea wilhelmsii* essential oils. The peaks correspond to identified compounds: (1) α -Pinene, (2) Camphene, (3) β -Pinene, (4) α -Terpinolene, (5) 1,8-cineole, (6) γ -Terpinene, (7) Thymene, (8) Menthoglycol, (9) Camphor, (10) Chrysanthenil acetate, (11) α -Fenchyl acetate, (12) Terpinene-4-ol, (13) Trans limonene oxide, (14) Isopinocarvol, (15) α -Terpineol, (16) Ascaridole, (17) Endo-borneol, (18) Verbenole.

Table 1. Percentage and retention time of chemical components of essential oils of *Achillea millefolium* L. and *Achillea wilhelmsii* L.

<i>Achillea millefolium</i>				<i>Achillea wilhelmsii</i>			
Peak	Components	Retention Index	Rate (%)	Peak	Components	Retention Index	Rate (%)
1	α -Pinene	868	1.02	1	α -Pinene	868	0.23
2	Camphene	881	1.20	2	Camphene	881	1.66
3	β -Pinene	893	1.66	3	β -Pinene	893	0.65
4	β -Phellandrene	898	0.82	4	α -Terpinolene	919	0.32
5	Terpinolene	919	0.29	5	1,8-Cineole	931	34.04
6	Paradiprene	927	0.13	6	γ -Terpinene	946	0.71
7	1,8-Cineole	931	75.19	7	Thymene	957	3.66
8	α -Phellandrene	957	5.53	8	Menthoglycol	1008	35.84
9	Camphor	1045	5.45	9	Camphor	1045	1.09
10	Endobornyl acetate	1066	0.48	10	Chrysanthenil acetate	1059	4.76
11	Terpinene-4-ol	1068	0.36	11	α -Fenchyl acetate	1062	1.22
12	δ -Terpineol	1087	0.20	12	Terpinene-4-ol	1068	2.33
13	α -Terpineol	1094	2.09	13	Trans limonene oxide	1077	0.29
14	P-Eugenol	1209	5.53	14	Isopinocarvol	1084	0.41
15	Silaethane	1228	0.05	15	α -Terpineol	1094	0.37
16	–	–	–	16	Ascaridole	1103	0.95
17	–	–	–	17	Endo-borneol	1106	9.93
18	–	–	–	18	Verbenole	1108	1.53
Total			100.0				100.0

The essential oil composition of *A. wilhelmsii* were determined as following: 1,8-cineole, camphor, borneol, linalool, carvacrol, α -pinene, camphene, α -thujene, α -terpineol, terpinen-4-ol, thymol, P-cymene, artemisia alcohol, methyleugenol, sabinene, caryophyllene oxide, chrysanthenyl acetate, E-nerolidol, dihydrocarvone [6-15].

After comparing all detected results with values from previous studies, we can confirm the idea that geographic origin has a significant influence on the chemical composition of *Achillea* species. However, it has been declared that climatic and environmental conditions have little effect on essential oils of *Achillea* species [22].

The major aromatic compounds from *A. millefolium* L. and *A. wilhelmsii* was 1,8-cineole (75.19% and 34.04%, respectively) in the present study. The

results indicated 1,8-cineole suppressed human colorectal cancer proliferation by inducing apoptosis suggesting 1,8-cineole would be an effective strategy to treat colorectal cancer [23]. The study of demonstrated antispasmodic and antisecretory activities of 1,8-cineole, and rationalized the traditional use of the plant containing various levels of this terpene in the treatment of gastrointestinal complains such as diarrhea [24].

Antioxidant activity of *A. millefolium* and *A. wilhelmsii* essential oils

Natural antioxidants obtained mainly from herbal materials are effective agents in the prevention of adverse effects of free radicals. Antioxidative effectiveness in natural sources was reported to be mostly due to phenolic compounds, and these compounds have an important role in inhibiting auto-oxidation of the essential oils [8-17]. Trolox equivalent antioxidant capacity (TEAC) or ABTS+ method relies on the reduction of the blue-green cation radical of ABTS. The extent of decolorization, expressed as percentage inhibition of ABTS+, is determined as a function of the concentration and the time, and it is calibrating against Trolox as the reference standard [25]. The concentration of antioxidants that produce the same effect as 1 mM Trolox and ABTS absorbance differences is considered TEAC. In addition, ABTS+ radicals are commonly used as "indicator compounds" for testing hydrogen donating potential and thus antioxidant activity. The indicated method is the most widely used method for the determination of antioxidant activity of plant extracts and Table 2 shows the inhibition of ABTS+ radical by essential oils of yarrow plant species.

The findings of the present study revealed that yarrow essential oils exhibited antioxidant activities but to be distinct according to the species. Although *Achillea millefolium* samples demonstrated slightly well radical scavenging activity against ABTS radicals, *Achillea wilhelmsii* showed good radical scavenging activity against ABTS radicals: *Achillea millefolium* showed 4.2 mM Trolox equivalents activity; however, (Table 2) *Achillea wilhelmsii* has 6.5 mM Trolox equivalents activity [18]. Suggested that essential oils of yarrow species have significant antioxidative effect and scavenging effects are related to camphor and borneol of volatile substances.

Table 2. Radical scavenging activities of essential oils *Achillea millefolium* L. and *Achillea wilhelmsii* L. against ABTS+ radical

Sample	TEAC, mM Trolox (\pm SE, Standard Error)
<i>Achillea millefolium</i>	4.2 \pm 1.4
<i>Achillea wilhelmsii</i>	6.5 \pm 1.6

Antimicrobial activity of *A. millefolium* and *A. wilhelmsii* essential oils

Extracts from aromatic plants, particularly essential oils, are a rich source of biologically active compounds showing antimicrobial properties. Therefore, it is logical to expect a variety of plant constituents in these oils with specific as well as general antimicrobial activity or antibiotic potential [26]. In this study, the potential antimicrobial activity of essential oils from yarrow on the growth of bacteria was investigated. In order to evaluate the antibacterial potential the essential oils from yarrow were screened for activity against three gram-negative (*Pseudomonas aeruginosa*, *Salmonella typhimurium* and *Escherichia coli*) and three gram-positive bacteria (*Staphylococcus aureus*, *Bacillus subtilis* and *Enterococcus faecalis*). The essential oil showed different degrees of inhibitory effect on the growth of tested bacterial strains. The comparison of the antibacterial activity of essential oils of yarrow and two antibiotics (ampicillin and ofloxacin) are presented in Table 3 and Fig 3. The essential oils of yarrow showed lower antimicrobial activities in comparison to the antibiotics according to the inhibition zone.

Table 3. Comparison of antimicrobial activity of *Achillea millefolium* and *Achillea wilhelmsii* essential oils (in μ L) and two antibiotics (ampicillin and ofloxacin) against some pathogens (diameter zones of inhibition, mm)

Pathogens	Antibiotics and Essential oil			
	Ampicillin	Ofloxacin	<i>A. millefolium</i>	<i>A. wilhelmsii</i>
<i>Staphylococcus aureus</i> ATCC 12600	20 – 22	24 – 26	8 – 10	10 – 12
<i>Bacillus subtilis</i> ATCC 6051	25 – 25	30 – 30	10 – 12	11 – 12
<i>Pseudomonas aeruginosa</i> ATCC 10145	22 – 23	26 – 28	10 – 12	11 – 12
<i>Enterococcus faecalis</i> ATCC 29212	26 – 28	20 – 22	12 – 14	14 – 14
<i>Salmonella typhimurium</i> ATCC 25241	22 – 24	24 – 26	8 – 10	12 – 12
<i>Escherichia coli</i> ATCC 11775	26 – 28	26 – 28	8 – 8	9 – 10

Insensitive (-) : diameter of inhibition zones is smaller than 8 mm; Sensitive (+) : diameter of inhibition zones is between 9-14 mm; very sensitive (+ +) : diameter of inhibition zones is between 15-19 mm; Extremely sensitive (+ + +) : diameter of inhibition zones is larger than 20 mm.

Although previous studies indicated that gram-positive bacteria were to be more sensitive to the action of many natural extracts [23], current results revealed there were no significant changes between these two bacteria groups. However, some studies have reported that gram-negative bacteria

are more resistant than gram-positives, due to restricted diffusion of the hydrophobic compounds through the hydrophilic cell wall structure, such as lipo-polysaccharides [27]. Although demonstrated that gram-positive bacterial strains were more susceptible to volatile oils of yarrow plant extracts [6], illustrated gram-negative bacteria more sensitive to *A. wilhelmsii* essential oils. The results of revealed that the essential oils of yarrow species were effective for controlling of certain important gram-positive bacteria, which produces many infectious diseases [27].

Oxygenated monoterpenes like camphor, 1,8-cineole, linaool,-terpinol, 1-terpinen-4-ol, and borneol, which are major compounds in a few essential oils examined were reported to show antimicrobial activity. The oils of the yarrow plant, rich in camphor and 1,8-cineol content, have previously been shown to have effective antimicrobial activities in vitro [28]. It has been shown in another study that thymol and carvacrol essential oils inhibited *Escherichia coli*, *Salmonella enteritidis*, *Salmonella choleraesuis* and *Salmonella typhimurium* bacterial strains [29]. The results of revealed that essential oils of yarrow have a pronounced antioxidative activity [8], but low antimicrobial activity in vitro [27] illustrated that the essential oils of yarrow species were effective for controlling of certain important gram-positive bacteria, which produces many infectious diseases. Essential oils of *A. wilhelmsii* were effective on human pathogens such as *Proteus mirabilis*, *Staphylococcus aureus*, *Serratia marcescens* [30]. The suggested that essential oils of yarrow species have significant antibacterial effect and the presence of chamazulene increased the antibacterial activity of volatile substances [18].

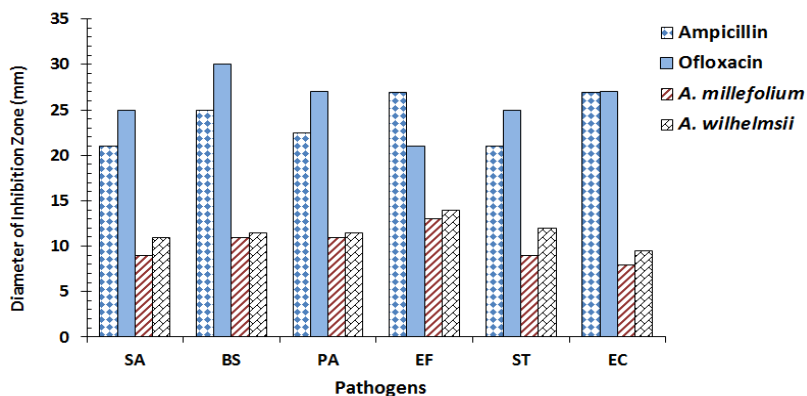


Figure 3. The comparison antimicrobial activity of essential oils of *Achillea millefolium* and *Achillea wilhelmsii* leaves and two antibiotics (ampicillin and ofloxacin) against six bacterial pathogen strains (SA: *Staphylococcus aureus* ATCC 12600, PS: *Bacillus subtilis* ATCC 605, PA: *Pseudomonas aeruginosa* ATCC 10145, EF: *Enterococcus faecalis* ATCC 29212, ST: *Salmonella typhimurium* ATCC 25241, EC: *Escherichia coli* ATCC 11775).

Previous researches revealed that whole essential oils have a greater antibacterial activity than the major components mixed, which suggests that the minor components have a critical function to the antimicrobial activity and may have a synergistic effect [31]. However, it is difficult to attribute the activity of a complex mixture to a single or particular constituent. Possible synergistic and antagonistic effect of compounds in the oil should also be taken into consideration as often-stronger antibacterial effect can be observed with complete essential oils in comparison to single oil components.

CONCLUSIONS

Besides the identified nutritional value, yarrow species can be an interesting source of bioactive compounds. The prominent essential oils content and antibacterial activity of the plant suggest that it may be of important for human health. According to the results, 1,8-cineole, α -phellandrene, P-eugenol, camphor, and α -terpineol were the main compounds of *A. millefolium*, and menthoglycol, 1,8-cineole, endo-borneol, chrysanthenil acetate and thymine were the main compounds of *A. wilhelmsii*. The context, natural essential oils as biological active compounds may also effective, selective, biodegradable and less toxic to environment. This study establishes a relationship between the composition of the oils of the respective plant and their corresponding therapeutic properties. As a result of presented findings, it can be concluded that the essential oils obtained from *A. millefolium* and *A. wilhelmsii* are interesting from a medicinal standpoint because of their antioxidant and antibacterial activities. The results suggest a basis for selection of the plant for further phytochemical and pharmacological investigations. The improving of natural antimicrobials will help to reduce the negative effects of synthetic antibiotics. Finally, further studies are warranted to confirm these results and elucidate the effect of these plants on other biological activities by conducting additional antioxidant and antimicrobial activity assays.

EXPERIMENTAL SECTION

Collection and preparation of plants

The fresh aerial parts of *A. millefolium* L. and *A. wilhelmsii* L. plants were collected from the naturally growing plants on the plateaus and rangelands of Van, Turkey in August 2010. The relative plants collected from located between 38°23'00" N and 43°14'36" E GPS. The taxonomic description of the plant samples collected in the distribution area was made by a plant taxonomist

from the Department of Biology at Yuzuncu Yil University, Van, Turkey. The collected plant materials were air-dried under shade, ground into small pieces, and kept for further analysis.

Chemicals

ABTS, helium tryptic soy broth, 2,2-azinobis (3 ethylbenzothiazoline-6-sulfonicacid) diammonium salt (ABTS) and potassium persulfate were obtained from Sigma-Aldrich. In addition, all other chemicals were of analytical grade.

Antibiotics

For the comparison of the antibacterial activity of essential oils, two antibiotics (ampicillin and ofloxacin; BBL®) were used. Disks are 1/4" in diameter; 50 disks per vial.

Extraction of essential oil

The shade-dried for both plant samples (100g) were subjected to hydro distillation for 3 h using an Clevenger-type apparatus. The both plants oils were extracted with tap water and stored under N₂ atmosphere in a sealed vial until use at 20°C. The yields were based on dry materials of plant samples. After decanting, the obtained essential oils were dried over anhydrous sodium sulfate and after filtration stored in refrigerator at +4°C until tested and analyzed.

Identification of essential oil components

The aerial parts of two plants were shaken sequentially in percolation with N-hexane-ether (1:1,v/v) and methanol for 16 h at room temperature. Samples were sonicated separately for 15 min twice, and then solvents were removed subsequently under reduced pressure by rotary evaporator apparatus. The extracts were weighed and stored in refrigerator at +4°C until the analysis. The essential oils were transferred to the solvent (n-hexane) and after dilution; the desired components were identified by GC-MS. In the preliminary study of the plant species collected beforehand, essential oil components were identified. The best temperature program of essential oils was determined later in GC-MS analysis and the same program was used for all samples.

Gas Chromatography-Mass Spectrometry Analysis

The relevant analyses were carried out on Shimadzu QP2010 brand model gas chromatography quadrupole-mass spectrometry system appropriated with a TRB-WAX column (30 m×0.25 mm film with 0.25 µm thickness). Carrier

gas was helium with a linear velocity of 36.25 cm s^{-1} ; split ratio was 1:50 at a flow rate of 1 mL min^{-1} . The first oven temperature 60°C for 2 min, after that programmed to increase from 60 to 240°C at $10^\circ\text{C min}^{-1}$, and finally held isothermally for 5 min at 240°C . The whole time was 25 min. The injection and ion source temperatures were 240°C . The injection volume was $1 \mu\text{L}$ in the splitless mode. Probably the ionization was with 70 eV. The mass range was from 40 to 300 m/z. The components of essential oils were determined by matching relative retention times and mass spectra with authentic samples from essential oil library data (Nist 27, Wiley, 7 and Nist 147) and by comparing relative retention indices (RRI) with published data [32].

Determination of antioxidant activity

Total antioxidant activity values of *A. millefolium* and *A. wilhelmsii* species were determined as described by [25]. ABTS radical cation (ABTS⁺) was obtained by reacting ABTS⁺ stock solution with 2.45 mM potassium persulfate (final concentration) and allowing the mixture to keep waiting in the dark for 12–16h before use. The radical was stable in this form for more than two days when stored in dark at room temperature. Essential oils of yarrow species were used for antioxidant activity measurement. The ABTS solution was diluted with distilled water to an absorbance of 0.70 ± 0.02 at 734 nm and equilibrated at 30°C . After mixing 2.95 mL of diluted ABTS⁺ solution into 5 mL of antioxidant compounds or Trolox standards in ethanol, the absorbance reading was taken at exactly 30°C 6 minutes after initial mixing. Solvent blanks were run for each assay. Percent inhibition of absorbance at 734 nm was calculated and plotted as a function of antioxidants and Trolox concentration for standard reference data. Total antioxidant activity was expressed as mM Trolox equivalents antioxidant activity (TEAC).

Determination of antibacterial activity

In vitro antibacterial studies were carried out against six bacteria strains: *Staphylococcus aureus* ATCC 12600, *Bacillus subtilis* ATCC 6051, *Pseudomonas aeruginosa* ATCC 10145, *Enterococcus faecalis* ATCC 29212, *Salmonella typhimurium* ATCC 25241, *Escherichia coli* ATCC 11775). The microorganisms were obtained from the Department of Clinical Microbiology, Faculty of Medicine, and Van, Turkey Yuzuncu Yil University. The antibacterial activity of essential oils was tested using the disc diffusion method [33]. Briefly, filter paper disks, 6mm in diameter, were impregnated with $5 \mu\text{L}$ of the essential oils (directly). The bacteria strains were inoculated on tryptic soy agar (Oxoid) for 3–4 h. The density of the cultures was adjusted according to the McFarland 0.5 tube turbidity. Activated microorganisms were spread

on the surface of predetermined Mueller-Hinton Agar (Merck) plates using a sterile swap, and incubated for half an hour. Paper discs (6 mm diameter, Whatman 2017-006) were impregnated with essential oils and transferred onto the Mueller-Hinton agar plates, whose surface had been spread with 0.5 mL of bacterial suspension. Ampicilline and ofloxacin were used as control agents.

The available microorganism species were incubated in the oven at the recommended temperature and time. After the colonies formed around the obtained zone diameter, the inhibition was measured in millimeters with the help of the zone scale. The sensitivity of the bacteria to essential oils and the size of the inhibitory areas were expressed by comparing those [34]. The results were evaluated as follows: zones that were smaller than 8 mm were classified as insensitive, zones 9–14 mm were sensitive, zones 15–19 mm were very sensitive, and those larger than 20 mm were extremely sensitive [35]. All tests were done in duplicate/triplicate and repeated 2/3 times. In addition, the results were expressed as average values.

REFERENCES

1. M.Z. Koçak; M. Karadağ; F. Çelikcan; *J. Agriculture*. **2021**, 4(1), 39-47.
2. W. Ben Bakrim; A. Aghraz; F. Hriouch; M. Larhsini; M. Markouk; K. Bekkouche; G. Dugo; *J. Essent. Oil Res.* **2022**, 1-12.
3. N. Nazar; C. Howard; A. Slater; T. Sgamma; *Plants*. **2022**, 11(1), 137.
4. E. Rahmati; M.H. Khoshtaghaza; A. Banakar; M.T. Ebadi; *Food Sci. Nutr.* **2022**.
5. L. Raudone; J. Radušienė; F. Seyis; F. Yayla; G. Vilckickyte; M. Marksas; C. Cırak; *Plants*. **2022**, 11(3), 447.
6. M. Kazemi; H. Rostami; *Nat. Prod. Res.* **2015**, 29(3), 286-288.
7. M. Popovici; G. Coldea; A. Coste; C. Pop; M. Tămaş; *Farmacia*. **2021**, 69(5), 928-933.
8. F. Candan; M. Unlu; B. Tepe; D. Daferera; M. Polissiou; A. Sökmen; A. Akpulat; *J. Ethnopharmacol.* **2003**, 87(2-3), 215-220.
9. K. H. C. Başer; *Nat. Volatiles Essent. Oils*. **2016**, 3, 1-14.
10. O. Toncer; S. Basbag; S. Karaman; E. Diraz; M. Basbag; *Int J Agric Biol.* **2010**, 12, 527-30.
11. F. P. Turkmenoglu; O. T. Agar; G. Akaydin; M. Hayran; B. Demirci; *Molecules*. **2015**, 20, 11432-11458.
12. N. Farhadi; K. Babaei; S. Farsaraei; M. Moghaddam; A.G. Pirbalouti; *Ind Crops Prod.* **2020**, 152, 112570.
13. I.L. Elisha; F.S. Botha; L.J. McGaw; J.N. Eloff; *BMC Complement Altern. Med.* **2017**, 17(1), 1-10.
14. T. Boris; D. Baričević; F. Batič; *Acta Agric. Slov.* **2021**, 117(2), 1-10.

15. K. Saeidi; M. Moosavi; Z. Lorigooini; F. Maggi; *Ind. Crops Prod.* **2018**, *112*, 274-280.
16. R. Gevrenova; G. Zengin; K.I. Sinan; E. Yıldıztuğay; D. Zheleva-Dimitrova; C. Picot-Allain; S. Dall'Acqua; *Antioxidants.* **2021**, *10(8)*, 1180.
17. C. Cirak; J. Radusiene; L. Raudone; G. Vilkičyte; F. Seyis; M. Marksa; F. Yayla; *S. Afr. J. Bot.* **2022**, *147*, 425-433.
18. C. Barda; M.E. Grafakou; E.M. Tomou; H. Skaltsa; *Sci. Pharm.* **2021**, *89(4)*, 50.
18. F. Rezaei; R. Jamei; R. Heidari; R. Maleki; *Int. J. Food Prop.* **2017**, *20(7)*, 1522-1531.
19. M. Maz; S.Z. Mirdeilami; M. Pessarakli; *J Med Plants Res.* **2013**, *7(16)*, 1063-1069.
20. A. Smelcerovic; M. Lamshoef; N. Radulovic; D. Ilic; R. Palic; *Chromatographia.* **2010**, *71(1)*, 113-116.
21. V. Abdossi; M. Kazemi; *Int. J. Food Prop.* **2016**, *19(8)*, 1798-1808.
22. M. M. Nadim; A.A. Malik; J. Ahmad; S. K. Bakshi; *World J Agric Sci*, **2011**, *7*, 561-565.
23. H.M. Abdallah; S.A. El Awdan; R.F. Abdel-Rahman; A.R.H. Farrag; R.M. Allam; *PloS one.* **2022**, *17(1)*.
24. G. Jalilzadeh-Amin; M. Maham; *Pharm. Biol.* **2015**, *53*, 594-599.
25. R. Re; N. Pellegrini; A. Proteggente; A. Pannala; M. Yang; C. Rice-Evans; *Free Rad. Biol Med.* **1996**, *26(9-10)*, 1231-1237.
26. A. Jafari-Sales; A. Shahniani; R. Fathi; P. Malekzadeh; H. Mobaiyen; F. Rasi-Bonab; *Intern. Med. Med. Investig. J.* **2017**, *2(2)*, 32-36.
27. F.J. Álvarez-Martínez; E. Barrajon-Catalán; J.A. Encinar; J.C. Rodríguez-Díaz; V. Micol; *Micol; Curr. Med. Chem.* **2020**, *27(15)*, 2576-2606.
28. M.A. Açıkgöz; *J. Essent. Oil Res.* **2020**, *32(4)*, 331-347.
29. M. Walczak; M. Michalska-Sionkowska; D. Olkiewicz; P. Tarnawska; O. Warzyńska; *Molecules.* **2021**, *26(9)*, 2723.
30. J. Sharifi-Rad; D. Mnayer; A. Roointan; F. Shahri; S.A.M. Ayatollahi; M. Sharifi-Rad; N. Molaei; *Cell. Mol. Biol.* **2016**, *62(9)*, 75-82.
31. D.L. Miladinović; M.V. Dimitrijević; T.M. Mihajilov-Krstev; M.S. Marković; V.M. Ćirić; *LWT.* **2021**, *136*, 110305.
32. B. Yildirim; A.M. Kumlay; K. Ekici; K.A.P. Rezaeieh; *Ponte.* **2016**, *72*, 159-169.
33. N. Okut; B. Yıldırım; K. Ekici; Ö. Terzioğlu; F. Özgökçe; Yuz. Yil Univ. J. Agric. Sci. **2018**, *28(2)*, 186-191.
34. A.G. Ponce; R. Fritz; C. Del Valle; S.I. Roura; *LWT Food Sci. Technol.* **2003**, *36(7)*, 679-684.
35. M.R. Moreira; A.G. Ponce; C. E. Del Valle; S.I. Roura; *LWT Food Sci. Technol.* **2005**, *38(5)*, 565-570.

COMPARATIVE EVALUATION OF DIFFERENT EXTRACTION METHODS FOR PHYTOCHEMICAL CONTENT AND ELUCIDATION OF MICROSTRUCTURE FROM *MORINGA OLEIFERA* LAM

Hafize DILEK TEPE^{a*}, Fatma DOYUK^a

ABSTRACT. In this study, the effects of three different extraction methods on the antioxidant capacity, phenolic component, volatile organic molecule, and amino acid contents in the leaves of the Moringa (*Moringa oleifera* Lam.) were compared. The amino acid contents were evaluated via liquid chromatography-diode array detection (HPLC-DAD) analysis. In gas chromatography-mass spectrometry (GC-MS) analysis, loliolide and phytol molecules were detected in moringa leaves. Gallic acid, chlorogenic acid, 4-hydroxybenzoic acid, acid, vanillic acid, p-coumaric acid, hesperidin, hyperoside, quercetin, kaempferol were found in high amounts in moringa leaves by liquid chromatography-tandem mass spectrometry (LC-MS/MS) analysis. Tyrosine, glutamic acid, alanine, tryptophan, and L-theanine amino acids were determined by HPLC-DAD analysis. Microstructures images of three extracts were shown with Scanning Electron Microscope (SEM). Element content and mapping were demonstrated by Energy Dispersive X-ray Spectroscopy (EDX). It was found that the best extraction method is MDAE when compared to UBAE and HAE.

Keywords: *Extraction, phenolic compound, amino acid, HPLC-DAD, LC-MS/MS, SEM-EDX.*

INTRODUCTION

Plants and extracts of various parts of them have been used in various treatments in medicine since ancient times. Due to the medicinal bioactive compounds in their structure, they are consumed in various ways

^a Application Science and Research Center (ASRC), Manisa Celal Bayar University, Manisa, Turkey. Email: fatmadoyuk@gmail.com

* Corresponding author: hafize.dilek@hotmail.com



to increase the immunity of the body [1,2]. Qualitative and quantitative studies of bioactive compounds from plant materials mostly rely on the selection of the appropriate extraction method [3,4]. Extraction is the first step of any medicinal plant study and plays a significant and crucial role in the final result and outcome [5]. With the development of modern chromatographic and spectrometric techniques, the determination of bioactive compounds in plants has become easier. However, the extraction method is also effective in the high-yield results obtained in these analyses [6]. An ideal extraction method; should be simple, cheap, fast, and environmentally friendly, and ensure that the desired component is obtained with high efficiency. Efforts to eliminate the problems encountered in classical extraction such as long extraction time, high cost, high purity solvent requirement, the necessity to evaporate large amounts of solvent, low extraction yield, and thermal degradation of temperature-sensitive components [7] have led to the development of new extraction techniques [8]. Methods such as ultrasound-assisted, enzyme assisted, microwave-assisted, pulsed electric field-assisted, homogenizer assisted, supercritical flow, and pressurized liquid extraction have developed as modern extraction methods. Some of these techniques are called 'green techniques' because they comply with the standards set by Environmental Protection Agency, USA [9]. The basic properties sought in extraction techniques developed today are; the use of more reliable chemicals, energy efficiency design, use of renewable raw materials, prevention of pollution, shortened extraction time, low cost, and prevention of accidents [10].

Moringa oleifera Lam. belongs to the *Moringaceae* family and, to date, it represents one of the most important traditional multipurpose food plants [11]. Moringa plants are native to India and Africa and are commonly grown in tropical and arid regions. Thanks to its drought tolerance, the *M. oleifera* tree has spread to other regions, including tropical and subtropical regions. *M. oleifera* is also considered a highly polytropic plant [12]. The seeds, leaves, roots, and even flowers of this plant are fit for both human and animal consumption. The leaves are, in particular, a good source of protein, vitamins, minerals, b-carotene, and antioxidants and have ever been utilized for dietary and medicinal practices [12]. *M. oleifera* has the highest proportion of essential amino acids and significant quantities of minerals when analysed [13]. Several studies have shown that the bioactive components found in the Moringa plant can be used for different industrial and food applications [14, 15, 16]. Intake of essential nutrients and health-promoting phytochemicals increases with the consumption of this plant in humans [17]. The leaves of this plant are used to treat medical conditions such as HIV/AIDS-related symptoms, bronchitis, ulcers, malaria, and fever [18]. It has been confirmed by research that *Moringa oleifera* L. leaf extracts have antioxidant, anti-

hypoglycemic, anti-hypertension, and anti-cancer activities [19,20]. *Moringa Oleifera* Lam. is one of the magical plants considered in many countries of the world due to its high medicinal properties. However, there is still a lot to unleash the potential of *Moringa Oleifera* Lam. by understanding their phytocomponents and variation in extraction due to solvents, understanding their potential properties, and establishing their applications in various fields.

In this study, moringa leaves have been subjected to extraction, and the bioactive compounds from the leaves have been extracted. Three methods were used: microwave digestion, ultrasonic bath, and homogenizer assisted. Methanol was used as a solvent in all three extraction methods. In the obtained extracts, volatile organic compounds, phenolic, and amino acids were determined by chromatographic methods. Images of three different methanol extracts were taken with Scanning Electron Microscopy. In addition, the mineral content of the extracts was shown in the EDS detector of the SEM device by mapping method and their spectra were determined. The antioxidant contents of the extracts were also analyzed. When all analysis data are compared, it was determined which of these three different extraction methods used was more efficient.

RESULTS AND DISCUSSION

Antioxidant Activity Analysis

Antioxidant activities measured in methanol extract of moringa leaves obtained using ABTS, FRAP, and DPPH assays from a single extract were measured three times to test the reproducibility of the assays. Differences were observed according to the three different extraction methods and the results were shown in **Table 1** as TE/g dry weight. According to the FRAP antioxidant activity results, when the microwave-digestion, ultrasound bath, and homogenizer assisted extraction methods were compared, 48.9, 29.3, and 15.65 TE/g DW results were obtained, respectively. In DPPH activity, 64.5, 47.3, and 41.95 TE/g DW results were obtained in these three extractions, respectively. In ABTS activity analysis, 49.25, 34.35, and 16.7 TE/g DW results were obtained in the three extraction methods, respectively. In light of these data, according to the three-antioxidant tests, the highest antioxidant activity was observed in Microwave digestion-assisted extraction. The lowest antioxidant activity was obtained from homogenizer-assisted extraction. It was observed that there was a correlation between the antioxidant capacities of the extracts and the phenolic component results. It was determined that phenolic compounds with strong radical scavenging effects such as Hesperidin, hyproside, and quercetin, especially in microwave decomposition extraction, were higher

than the other extraction methods. Therefore, it could be concluded that its antioxidant capacity was higher than other extractions. Similar to our results, Sreelatha and Padma (2009) reported that they had high antioxidant activity in *moringa* leaves [19].

Table 1. Antioxidant activity results of three extraction methods of moringa leaves

Extraction methods	FRAP mM TE/g DM	DPPH mM TE/g DM	ABTS mM TE/g DM
MDAE	48.9±0.1***	64.5±0.5**	49.25±1.3***
UBAE	29.3±1.17**	47.35±3.5***	34.35±1.2**
HAE	15.65±0.5**	41.95±0.2**	16.7±0.7**

***: P<0.001, **: P<0.05, *: P<0.01, DM: dry mass

As secondary metabolites, phenolic compounds are widely distributed in fruits and vegetables and are considered the main actors in the antioxidant capacity of plants [21]. In a recent study, Castro-López et al. (2017) showed that the extraction method had a strong effect on the recovery of polyphenols from *M. oleifera* leaves [22]. It was determined that the recovery of phenolic compounds was higher especially in the microwave and ultrasonic bath extractions compared to the conventional extraction method, thus corroborating our findings. During microwave extraction, the temperature/microwave energy combination is considered to burst the cell wall, releasing the polyphenols into the extraction solvent more effectively [23].

Phenolic compound identification by LC-MS/MS

The high amount of phenolic component results was given according to MDAE, UBAE and HAE extraction methods, respectively. Gallic acid 9.48, 6.31, 17.47 µg/g DW; protocatechuic acid 22.23, 15.17 and 16.91 µg/g DW; 4-hydroxybenzoic acid 25.61, 21.58, and 21.80 µg/g DW; caffeic acid 21.71, 15.58 and 20.10 µg/g DW; vanillic acid 5.80, 4.50 and 7.25 µg/g DW; p-coumaric acid 12.13, 8.53, and 8,99 µg/g DW; quercetin 24.83, 17.19, and 18.66 µg/g DW; kaempferol 3.82, 3.31, 5.72 µg/g DW were detected (**Table 2**). In particular, the amount of chlorogenic acid, hesperidin, and hyperoside in microwave extraction were 1281.87, 3544.15 and 3070.48 µg/g DW, respectively. Total phenolic component content was obtained as MDAE>UBAE>HAE, respectively. Many researchers have identified the main flavonoids (rutin, hyperoside, kaempferol-3-O-rutinoside, apigenin, quercetin, kaempferol, and D-(+)-catechin) and phenolic acid (chlorogenic acid and rosmarinic acid)

COMPARATIVE EVALUATION OF DIFFERENT EXTRACTION METHODS FOR PHYTOCHEMICAL CONTENT AND ELUCIDATION OF MICROSTRUCTURE FROM *MORINGA OLEIFERA* LAM

from Italy MOLs extracts [24, 25]. In a study by Fombang et al. (2020), it was shown that the antioxidant activity in alcohol extractions of the leaves of the moringa plant is higher than in other parts of the plant [26]. In this context, Vongsak et al. (2015) reported a strong antioxidant activity for isoquercetin, crypto-chlorogenic acid, and astragalins from *M. oleifera* leaves [27]. Several studies have demonstrated that flavonoid compounds including quercetin, kaempferol, and their derivatives possess remarkable antioxidant activities [28]. Quercetin is a powerful antioxidant that can chelate metals, remove free oxygen radicals, and prevent low-density lipoprotein oxidation [29].

Table 2. LC-MS/MS phenolic content of three extraction methods of moringa leaves

Phenolic content (µg/g DW)	MDAE	UBAE	HAE
Gallic acid	9.482±0.09 [*]	6.315±0.10 [*]	17.471±0.22 [*]
Protocatechuic acid	22.23±0.23 ^{**}	15.17±0.34 ^{**}	16.908±0.12 [*]
3-Hydroxytyrosol	9.918±0.05 [*]	7.75±0.15 [*]	6.926±0.11 [*]
3,4-Dihydroxyphenylacetic acid	0.950±0.01 [*]	0.878±0.07	0.936±0.08
(+)-Catechin	0.96±0.51	0.34±0.24	0.49±0.23
Chlorogenic acid	1281.87±62.3 ^{***}	1435.48±73.95 ^{***}	854.35±61.16 ^{***}
2,5-Dihydroxybenzoic acid	0.304±0.05	0.105±0.05	0.217±0.03
4-Hydroxybenzoic acid	25.61±0.30 ^{**}	21.58±0.21 ^{**}	21.798±0.16 ^{**}
(-)-Epicatechin	1.15±0.10 [*]	1.66±0.11 [*]	2.59±0.24 [*]
Caffeic acid	21.709±0.08 ^{**}	15.58±0.14 ^{**}	20.10±0.13 ^{**}
Vanillic acid	5.80±1.27 [*]	4.50±5.61 [*]	7.25±8.61 [*]
Syringic acid	0.17±0.17	0.29±0.16	0.41±0.34
3-Hydroxybenzoic acid	0.29±0.00	0.19±0.19	0.10±0.00
Vanillin	1.810±0.09 [*]	1.12±0.09 [*]	1.412±0.007 [*]
Taxifolin	0.245±0.02	0.404±0.03	2.682±0.01
p-Coumaric acid	12.128±0.21 [*]	8.530±0.22 [*]	8.987±0.25 [*]
Ferulic acid	2.341±0.27 [*]	1.98±0.18 [*]	2.021±0.06 [*]
Luteolin 7-glucoside	1.606±0.02 [*]	1.359±0.03 [*]	1.77±0.25 [*]
Hesperidin	3544.15±11.5 ^{***}	3401.65±30.3 ^{***}	3193.697±40.0 ^{***}
Hyperoside	3070.476±13.4 ^{***}	2791.12±18.07 ^{***}	2574.01±13.0 ^{***}
Rosmarinic acid	0.65±0.92	2.88±0.48 [*]	1.77±0.11 [*]
Apigenin 7-glucoside	2.378±0.02 [*]	2.139±0.16 [*]	2.454±0.22 [*]
2-Hydroxycinnamic acid	0.16±0.03	0.11±0.02	0.15±0.02
Pinosresinol	1.415±0.17 [*]	1.21±0.25	1.110±0.22 [*]
Eriodictyol	0.042±0.01	0.125±0.05	0.690±0.18
Quercetin	24.830±0.61 ^{**}	17.19±0.27 ^{**}	18.66±0.37 ^{**}
Kaempferol	3.82±0.55 [*]	3.31±0.24 [*]	5.72±0.80 [*]
Total Phenolic	8046.09±34.3^{***}	7748.95±42.8^{***}	6764.62±25.5^{***}

***: P<0.001, **: P<0.05, *: P<0.0

Identification of volatile organic molecules by GC-MS

The results obtained in the GC-MS analysis were defined based on their retention time, percentage of similarity and pattern of mass spectra, and its comparison with the data of the library of NIST11.LIB of the National Institute of Standards and Technology (NIST) and among the identified volatile organic compounds, those with similarities over 80% were shown in **Table 3**. As a result of GC-MS analysis in moringa leaves, Palmitic acid.beta.-monoglyceride, loliolide, and phytol were identified in all three extractions. GC-MS volatile organic compounds results were in agreement with the results of a study by Bhalla et al (2021) [30]. In microwave-assisted extraction and homogenizer-assisted extraction, turmerone was also determined. When the extraction methods were compared, 31, 25, and 21 volatile organic compounds were obtained in MDAE, UBAE, and HAE, respectively. The effective extraction process can be accomplished by undergoing the detection, isolation, and characterization of natural antioxidant compounds. Xu et al., (2017) stated that temperature, time, pH, solvent, and concentration of the sample are the factors that affect the efficiency of the extraction method [31]. Besides, the selectivity of the solvent is expressed depending on the chemical structure and the polarity of extracted antioxidant compounds.

Many methods and techniques have been used to reveal the bioactive components of the Moringa plant. New technologies include methods that offer high-quality, high-yield plant extract, and numerous technical or environmental benefits, such as quick processing times and the use of green solvents, during the extraction procedure. It has been found that green solvents can be ideally used to reveal these compounds [32]. In vitro and in vivo, all parts of the *Moringa oleifera* plant extracted with water, methanol, and ethanol showed excellent antioxidant activity, phenolic activity, antiepileptic, anticonvulsant, antidiabetic, antibacterial, and anticancer activity [33, 34, 35] In a study conducted on the *Moringa oleifera* plant, phenolic compound content was obtained higher in ultrasound bath-assisted extraction than in the conventional extraction method. This resulted in less than 45 min in the extraction process to damage the cell walls with an increase in solvent penetration corresponding to a better phenolic compound yield [36]. In addition, another study reported that microwave-assisted extraction was more efficient than traditional extraction methods in producing polyphenolic compounds from various plants, including Moringa leaves [22].

Table 3. GC-MS results from volatile organic molecules of microwave-digestion assisted, ultrasound-bath assisted and homogeniser assisted extractions. Molecules given in the table were chosen based on 85% or higher similarity

Extraction Methods	Identified Molecule (Similarity%)
MDAE	Acetic acid (97.52); Butyric acid, 4-chloro- (gamma-chloro-n-butyric acid) (90.15); 1,2-Cyclopentanedione (93.81); Oxirane, phenyl-(Styrene oxide) (96.52); 4H-Pyran-4-one, 2,3-dihydro-3,5-dihydroxy-6-methyl-(92.59); 4-vinylphenol; p-vinylphenol (93.17); 2-Cyclohexen-1-one, 2-methyl-5-(1-methylethyl)- (Carvone) (95.90); Phenol, 5-methyl-2-(1-methylethyl)- (93.86); Benzeneacetonitrile, 4-hydroxy-(90.13); 2(4H)-Benzofuranone, 5,6,7,7a-tetrahydro-4,4,7a-trimethyl-, (R)- (93.03); (-)-Loliolide (92.31); Pentadecanoic acid, 14-methyl-, methyl ester (92.07); Phytol (91.49); diisooctyl-phthalate (93.93); gamma Tocopherol methyl ether (96.49); Propanoic acid, 2-oxo-, methyl ester (methyl pyruvate) (87.59); n-Hexadecanoic acid (Hexadecanoic acid) (89.79); Palmitic acid .beta.-monoglyceride (88.04)
UBAE	Acetic acid (97.52); Butyric acid, 4-chloro- (gamma-chloro-n-butyric acid) (90.15); 1,2-Cyclopentanedione (93.81); 4H-Pyran-4-one, 2,3-dihydro-3,5-dihydroxy-6-methyl-(92.59); 2-Cyclohexen-1-one, 2-methyl-5-(1-methylethyl)- (Carvone) (95.90); Phenol, 5-methyl-2-(1-methylethyl)- (93.86); 2(4H)-Benzofuranone, 5,6,7,7a-tetrahydro-4,4,7a-trimethyl-, (R)- (93.03); (-)-Loliolide (92.31); Pentadecanoic acid, 14-methyl-, methyl ester (92.07); Phytol (91.49); gamma Tocopherol methyl ether (96.49); Propanoic acid, 2-oxo-, methyl ester (methyl pyruvate) (87.59); n-Hexadecanoic acid (Hexadecanoic acid) (89.79); Palmitic acid .beta.-monoglyceride (88.04); Tetradecane (85.68); Neophytadiene (85.34)
HAE	Acetic acid (97.52); Butyric acid, 4-chloro- (gamma-chloro-n-butyric acid) (90.15); 4H-Pyran-4-one, 2,3-dihydro-3,5-dihydroxy-6-methyl-(92.59); Phenol, 5-methyl-2-(1-methylethyl)- (93.86); 2(4H)-Benzofuranone, 5,6,7,7a-tetrahydro-4,4,7a-trimethyl-, (R)- (93.03); (-)-Loliolide (92.31); Phytol (91.49); 1,2-Ethanediol, monoacetate (94.1); Propanoic acid, 2-oxo-, methyl ester (methyl pyruvate) (87.59); n-Hexadecanoic acid (Hexadecanoic acid) (89.79); Palmitic acid .beta.-monoglyceride (88.04); Hexadecanoic acid, methyl ester (88.97)

Amino acid content by HPLC-DAD

Fourteen amino acid types in moringa leaves were determined by HPLC-DAD. Especially tyrosine, glutamic acid, alanine tryptophan, and L-theanine were determined in very high amounts (**Table 4**). When three different extraction methods were compared, glutamic acid and alanine contents were obtained as 266.6 and 199.4 µg/g DW, respectively, in microwave

digestion-assisted extraction. In ultrasound bath-assisted extraction, L-theanine and phenylalanine contents were obtained as 130 and 53.8 $\mu\text{g/g}$ DW, respectively. The total amino acid contents when the MDAE, UBAE, and HAE extraction methods were compared, were obtained as 977.2, 939.8, and 680.8 $\mu\text{g/g}$ DW, respectively. Moringa leaves have high amounts of crude protein (23.0 to 30.3%) composed of the essential amino acids methionine, phenylalanine, threonine, leucine, valine, histidine, isoleucine, lysine, tryptophan [37,38,39]. The amino acid contents obtained as a result of three different extractions are in agreement with previous studies. Accordingly, *M. oleifera* leaves are a rich source of essential amino acids, often lacking in many vegetables. For example, the contents of lysine (1325 mg/100 g), phenylalanine (1388 mg/100 g), threonine (1188 mg/100 g), leucine (1950 mg/100 g), and valine (1063 mg/100 g) of the dried leaves are higher than those reported for soybeans and beef [40]. In this study, three different extraction methods were applied to the leaves of the moringa plant. The phytochemical components and antioxidant capacities of the obtained methanol extracts were analysed. When the data were compared, it was determined that the best results were in microwave extraction-assisted, ultrasonic bath-assisted, and homogenizer-assisted extraction, respectively.

Table 4. Amino acid contents of three extraction methods of moringa leaves

Amino Acids ($\mu\text{g/g}$) DW	MDAE	UBAE	HAE
<i>Aspartic Acid</i>	6.00 \pm 0.01*	6.60 \pm 0.01*	7.40 \pm 0.11*
<i>Glutamic Acid</i>	266.60 \pm 0.67***	134.00 \pm 0.23***	110.40 \pm 0.25***
<i>Asparagine</i>	12.20 \pm 0.01**	12.60 \pm 0.09**	6.00 \pm 0.07**
<i>Serine</i>	13.00 \pm 0.18**	23.20 \pm 0.20**	17.00 \pm 0.16**
<i>Glutamine</i>	24.80 \pm 0.23**	88.80 \pm 0.31***	65.40 \pm 0.59***
<i>Arginine</i>	31.40 \pm 0.08**	29.40 \pm 0.18**	17.00 \pm 0.18**
<i>Alanine</i>	127.40 \pm 0.53***	126.40 \pm 0.14***	73.60 \pm 0.14***
<i>Tyrosine</i>	199.40 \pm 0.80***	195.20 \pm 0.25***	115.00 \pm 0.37***
<i>Valine</i>	45.80 \pm 0.15***	36.40 \pm 0.08***	30.80 \pm 0.31***
<i>Tryptophan</i>	50.00 \pm 0.47***	33.80 \pm 0.15***	33.60 \pm 0.23***
<i>Phenyl Aniline</i>	37.80 \pm 0.25***	53.80 \pm 0.15***	39.20 \pm 0.17***
<i>Isoleucine</i>	19.80 \pm 0.18**	31.20 \pm 0.01**	21.80 \pm 0.09**
<i>Leucine</i>	25.60 \pm 0.16**	38.40 \pm 0.04**	29.60 \pm 0.13**
<i>L-Theanine</i>	117.40 \pm 0.63***	130.00 \pm 0.45***	114.00 \pm 0.54***
Total Amino acid	977.2\pm0.42	939.8\pm0.28	680.8\pm0.42

***: P<0.001, **: P<0.05, *: P<0.01

Scanning Electron Microscope – Energy Dispersive X-ray Spectroscopy (SEM-EDX) results

According to the SEM results, the images of the three different extractions are different from each other. SEM images of unextracted (before extraction) moringa leaves were also given in figure 1 (d, d1). The results in microwave digestion-assisted extraction are quite interesting when images are taken at 4 μm magnification for each extraction (**Figure 1**). In microwave, digestion assisted extraction images it was observed that there were quite large divergences in leaf morphology. It has been reported and reviewed that microwave irradiation of plant samples leads to intense structural destruction, shrinking of plant parts and irregularities in the plant surface [41]. In the ultrasonic bath-assisted extraction, the leaf epidermis surface was damaged and wrinkling occurred (**Figures 1b, 1b1**). The ultrasonic waves propagate into the liquid, resulting in alternating high-pressure (compression) and low-pressure (rare fraction) cycles. In the rare fraction half-cycle of ultrasonic waves, a vast amount of small vacuum bubbles was generated by the high-intensity ultrasonic waves [42]. This event was followed by cavitation. Cavitation also results in the formation of high-pressure shock wave and the generation of powerful liquid jet that is expelled at the leaf surface [43]. It was observed that there were breaks and deteriorations in the leaf surface morphology in homogenizer-assisted extraction. It can be said that the reason for this is the high rotational speed of the homogenizer device. We can see that it breaks the leaf epidermis tissue due to its high rotation speed (**Figures 1c, 1c1**). Element mapping was done with Energy Dispersive X-ray Spectroscopy (EDX). Carbon (C), oxygen (O), magnesium (Mg), sulphur (S), chloro (Cl), and potassium (K) elements were observed in all three extraction maps (**Figures 2a, 2b, 2c, 2d**). Element detail analyses by EDX detector results were given in **Figures 3a, 3b, 3c, 3d**. Elemental analysis of a specific region was performed for each extraction. The amount of minerals obtained was shown as %. Potassium contents were obtained as MDAE, UBAE, and HAE at 2.25%, 1.05%, and 0.60%, respectively. The lowest carbon content of 54.19% was obtained from MDAE.

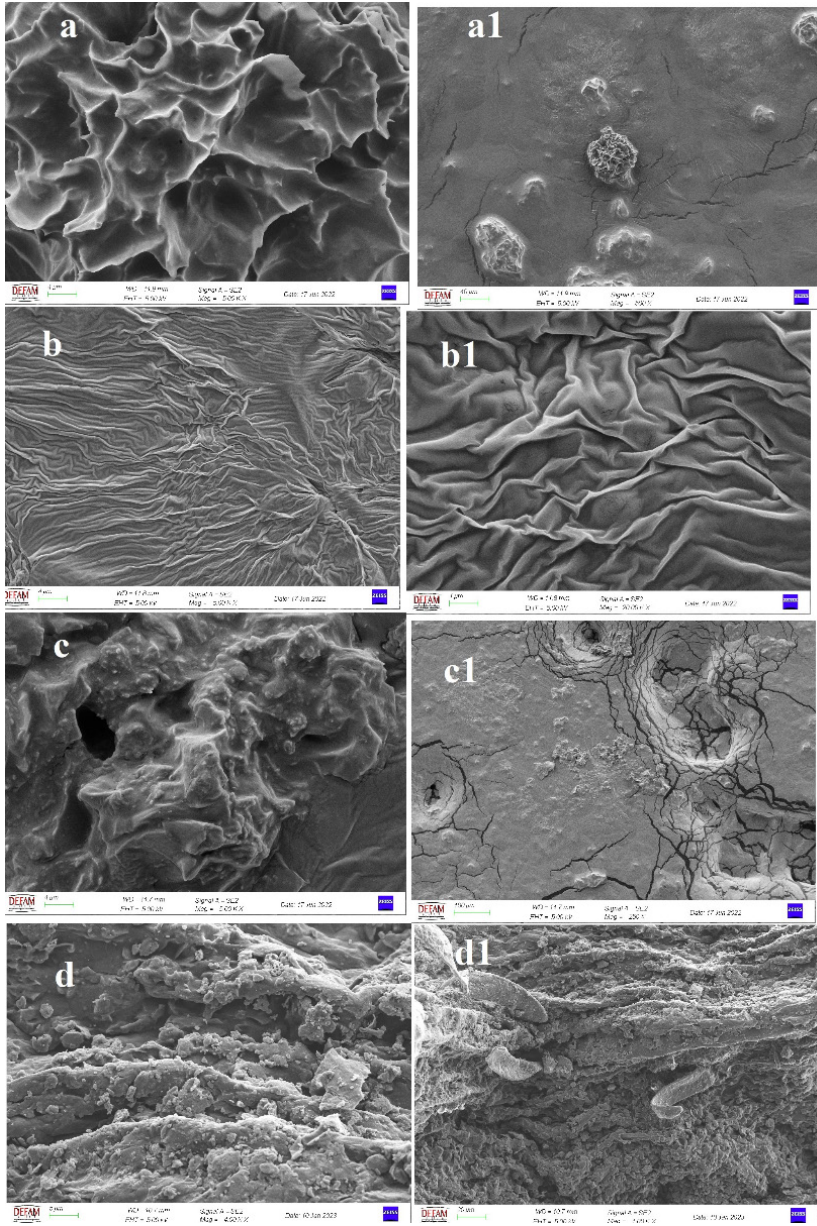


Figure 1. Scanning electron microscope (SEM) images of three plant leaves extractions. a, a1: MDAE, b, b1: UBAE, c, c1: HAE, d, d1: non-extracted/before extraction.

COMPARATIVE EVALUATION OF DIFFERENT EXTRACTION METHODS FOR PHYTOCHEMICAL CONTENT AND ELUCIDATION OF MICROSTRUCTURE FROM *MORINGA OLEIFERA* LAM

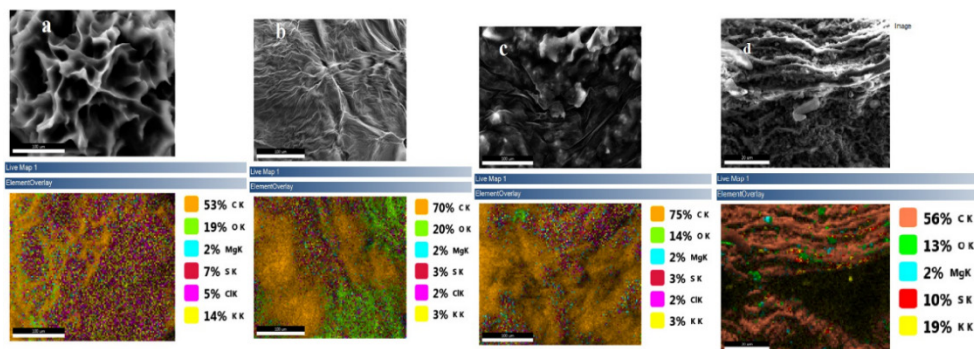


Figure 2. SEM-EDX element mapping results of three plant leaves extractions. a: MDAE, b: UBAE, c: HAE, d: non-extracted/before extraction.

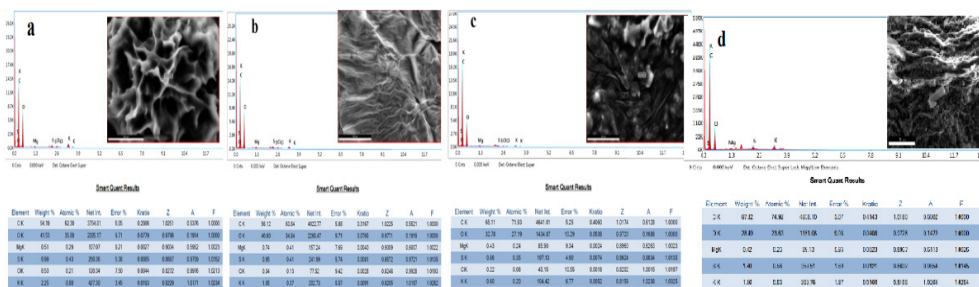


Figure 3. EDX element concentrations (%) of three plant leaves extractions. a: MDAE, b: UBAE, c: HAE, d: non-extracted/before extraction.

CONCLUSION

Extraction is the pre-process that should be done before bioactive component analysis. Today, there are many extraction methods in use. However, it is very difficult to determine an effective extraction method. With an efficient extraction process, product loss, amount of solvent, and wasted time can be minimized. In this study, three different modern extraction methods, microwave decomposition, ultrasonic bath, and homogenizer assisted, were compared. The leaves of *Moringa oleifera*, which is a good source of bioactive compounds, were used as plant material. Phytochemical analyses were carried out with various chromatographic modern devices in the obtained extracts. A detailed determination of the antioxidant capacities and phytochemical

content of moringa leaves after extractions allowed a comparison of extraction efficiency. As a result of three different extractions, differences in phenolic contents and accordingly antioxidant activities were observed. It was found that especially the microwave decomposition method was more effective than other methods and provided the release of phenolic compounds with radical scavenging antioxidant properties. In addition, it has been shown that each extraction creates microstructural differences with SEM images. Thus, it can be said that the selection of the extraction method affects the release of biocomponents as it changes the structure of the plant surface. Especially, a comparison of non-extracted and extracted moringa leaves was demonstrated with SEM images. Specific and distinctive differences were seen in the images obtained. Alanine, glutamic acid, and tyrosine, which are essential organic acids for human health, were determined at high rates in all extractions. However, when the three extractions are compared, it can be said that the effective extraction method is MDAE, UBAE, and HAE, respectively.

The importance of natural products rich in bioactive components is increasing day by day. Therefore, this study may guide similar studies to be conducted in the future.

EXPERIMENTAL SECTION

Chemicals and reagents

Moringa leaves were purchased from an herb market in Manisa city (38.749444°N 28.122778°E), Turkey, in August of 2020. The leaves were washed to remove impurities and then air-dried in the shade before extractions. All standards included chlorogenic acid (>99.0%), D-(+)-catechin (>99.8%), rutin (>99.7%), hyperoside (>99.8%), kaempferol-3-O-rutinoside (>99.7%), astragalin (>99.8%), rosmarinic acid (>99.7%), polydatin (>99.8%), quercetin (>99.8%), apigenin (>99.8%), kaempferol (>99.8%) were purchased from Sigma-Aldrich Chemical Co., Ltd. (St. Louis, Missouri, USA). ABTS (2,2' - Azino-bis (3- ethylbenzothiazoline-6-sulfonic acid) diammonium salt), 1,1-diphenyl-2-picrylhydrazyl (DPPH), 2,4,6-tris(2-pyridyl)-s-triazine (TPTZ), and Trolox (6-hydroxy-2,5,7,8-tetramethylchroman-2-carboxylic acid) were purchased from Sigma-Aldrich Chemical Co., Ltd. (St. Louis, Missouri, USA). Methanol, ethanol, and acetonitrile (≥99.9%, (for HPLC) was obtained from Merck. Amino acid standards 10×1 mL, Sigma/AAS18, Fmoc chloride (FMOC-Cl) (≥% 99.0) from Sigma-Aldrich Chemical Co., Ltd. (St. Louis, Missouri, USA), OPA (o-phthalaldehyde) from Alfa Aesar, Thermo Fisher Scientific Chemicals, Germany.

Extraction methods used for moringa leaves

Microwave digestion-assisted extraction (MDAE)

Dried leaves samples of 0.5 g were weighed, and 20 mL of methanol (100%) was added. Extraction was performed in a Microwave digestion device (Cem, Mars 6 version, NC, USA.), setting the temperature to 55 °C, 15 min ramp, 25 min hold, and 20 min cooling program. The obtained extract solution was filtered. and kept at +4 °C in amber glass vials until the other analysis.

Homogeniser-assisted extraction (HAE)

Dried leaves samples of 0.5 g were weighed, and 20 mL of methanol (100%) was added. Extraction was performed by using an Ultra-turrax (IKA T25, Staufen, Germany) at 5000×g for 3 min at room temperature. The extracts were then centrifuged (Hettich- universal 320, Tuttlingen, Germany) at 10.000×g for 10 min at 4 °C. Finally, the resulting solutions were collected in amber glass containers until the other analysis.

Ultrasound bath-assisted extraction (UBAE)

Dried leaves samples of 0.5 g were weighed, and 20 mL of methanol (100%) was added. Extraction was performed by using an ultrasonic bath device (Wised, Wisd-WiseClean, Germany), for 30 min at 45 °C. The obtained extract solution was filtered and kept at +4 °C in amber glass vials until the other analysis. The percentage yield of extraction was calculated as:

$$\text{Percentage yield} = \frac{\text{weight of dry extract}}{\text{weight of dry plant material}} \times 100\%$$

The percentage yield of microwave digestion-assisted extraction (MDAE): 22.96.

The percentage yield of a homogeniser-assisted extraction (HAE): 17.24.

The percentage yield of ultrasound bath-assisted extraction (UBAE):15.48.

Antioxidant activity assays

The FRAP analysis was performed according to the following procedure with some modifications [44]. The stock solutions included 300 mM acetate buffer (3.1 g $C_2H_3NaO_2 \cdot 3H_2O$ and 16mL $C_2H_4O_2$), pH 3.6, 10 mM TPTZ (2, 4, 6-tripyridyl-s-triazine) solution in 40 mM HCl, and 20mM $FeCl_3 \cdot 6H_2O$ solution.

The fresh working solution mix was prepared as follows: 25 mL acetate buffer, 2.5 mL TPTZ solution, and 2.5 mL $\text{FeCl}_3 \cdot 6\text{H}_2\text{O}$ solution and then warmed at 37°C before use. Leaves extracts (150 μL) were allowed to react with 2850 μL of the FRAP solution for 30 min in a dark condition. Then, absorbance was taken at 593 nm using the spectrophotometer (TECAN, Männedorf, Switzerland). The standard curve was linear between 25 and 600 mM Trolox. Results were expressed in mM Trolox equivalents (TE)/g dry mass (DM).

The DPPH analysis was performed according to the following procedure with minor modifications [45]. The stock solution was freshly prepared by dissolving 24 mg of DPPH in 100 mL of methanol, and then 10 mL of this solution was taken and diluted with 45 mL of methanol. Leaves extracts (150 μL) were allowed to react with 2850 μL of the DPPH solution for 2 h in a dark condition. Then, absorbance was taken at 515 nm using the spectrophotometer (TECAN, Männedorf, Switzerland). The standard curve was linear between 25 and 800 mM Trolox. Results are expressed in mM Trolox equivalents (TE)/g dry mass. In all measurements, additional dilution was needed if the analysis value measured was over the linear range of the standard curve.

For ABTS assay of leaf extracts was performed according to the following method with some modifications [46]. A stock solution containing 7.4 mM ABTS and 2.6 mM potassium persulfate was prepared. The prepared stock solution was kept at room temperature for 12 h and then 1 mL was taken and diluted with 60 mL of methanol before the analysis. Leaves extracts (150 μL) were allowed to react with 2850 μL of the ABTS solution for 2 h in a dark condition. Then, absorbance was taken at 734 nm using the spectrophotometer (TECAN, Männedorf, Switzerland). The standard curve was linear between 25 and 600 mM Trolox. Results were expressed in mM Trolox equivalents (TE)/g dry mass.

Determination of phenolic compounds by LC-MS/MS

Determination of phenolic profiles of leaves extracts, high-performance liquid chromatography-mass spectrometer - mass spectrometer (Agilent 1260 Triple Quadrupole MS/MS) were used. Each analysis was performed with three replications. HPLC column C18 ODS used in the analyses (25x4.6 mmx5 μm) was used. Injection volume for analysis: 2 μL . Water/0.1% formic acid (A), and methyl alcohol (99.9%) (B) was used as a carrier phase. The gradient method is as follows: 3 min 2% B, 6 min 25% B, 10 min 50% B, 14 min 95% B, 17.5 min 2% B. Flow rate: 0.4 mL/min. The identification of compounds was performed in positive and negative modes [47]. LC-MS/MS total ion chromatograms of phenolic compounds were shown in **Figure 4**.

COMPARATIVE EVALUATION OF DIFFERENT EXTRACTION METHODS FOR PHYTOCHEMICAL CONTENT AND ELUCIDATION OF MICROSTRUCTURE FROM *MORINGA OLEIFERA* LAM

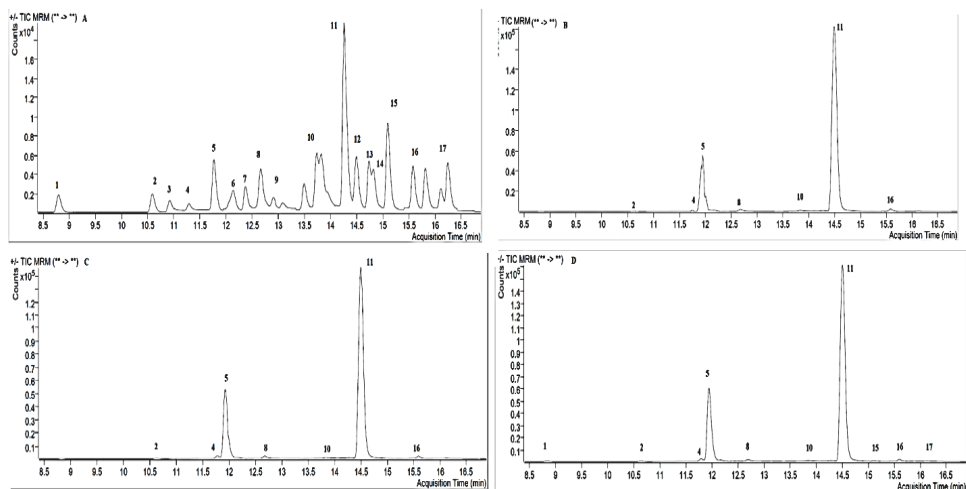


Figure 4. LC-MS/MS total ion chromatograms of phenolic compounds (A: standards, B: MDAE, C: UBAE, D: HAE). 1: Gallic acid, 2: Protocatechuic acid, 3: 3,4-Dihydroxyphenylacetic acid, 4: (+)-Catechin, 5: Chlorogenic acid, 6: 4-Hydroxybenzoic acid, 7: (-)-Epicatechin, 8: Caffeic acid, 9: Vanillic acid, 10: p-Coumaric acid, 11: Hesperidin, 12: Rosmarinic acid, 13: Apigenin 7-glucoside, 14: Pinoresinol, 15: Eriodictyol, 16: Quercetin, 17: Kaempferol

Determination of volatile organic molecules by GC-MS

Volatile molecules in the extract were qualitatively analyzed in electron ionization (EI) mode with Agilent Technology 7890A Gas Chromatography (GC) Mass spectrometer (MS). Chromatographic column Agilent HP-5 MS, capillary column (30 m x 0.25 mm, the film thickness of 0.25 mm). The furnace temperature was started at 40°C, followed by standing for 5 min, then at 5°C min⁻¹ at 280°C and held for 5 min. Helium gas (99.999%) was used as the carrier gas. The constant flow rate is 1.5 mL min⁻¹ and the injector temperature is 250°C. The extract was injected in splitless mode with 1 mL. Interpretation of the mass spectrum was performed according to the National Institute of Standards and Technology (NIST) database. GC-MS total ion chromatograms of volatile organic molecules of the samples were shown in **Figure 5**.

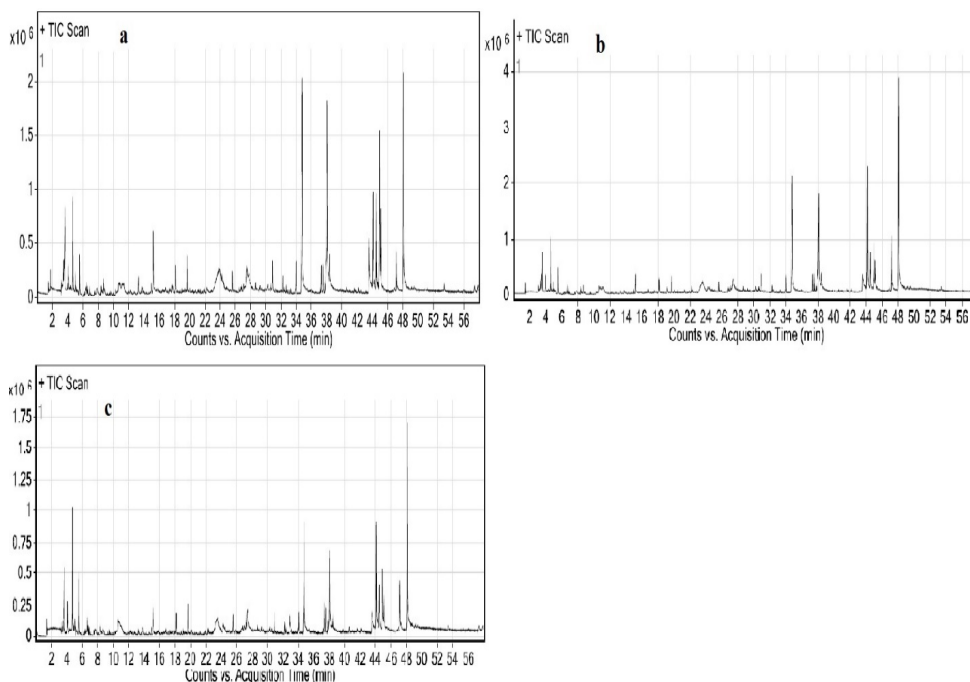


Figure 5. GC-MS total ion chromatograms and acquisition time of volatile organic compounds (a: MDAE, b: UBAE, c: HAE).

Determination of amino acid contents by HPLC-DAD

Derivatisation of samples and amino acid standards

Before HPLC-DAD analysis, amino acid (AA) standards and samples were derivatized using *o*-phthalaldehyde (OPA) for primary AA and 9-fluorenylmethyl chloroformate (FMOC) for secondary AA according to the method of Henderson et al. (2000), modified to optimize the parameters for moringa plant leaves extraction analysis [48]. The derivatization solution was freshly prepared every day as follows: Borate Buffer: 0.4 M in water (pH 9.2), FMOC reagent, 0.2 mg/mL in acetonitrile, OPA reagent, 5 mg dissolved in 0.05 mL of methanol was added 0.45 mL of 0.4 M boric acid buffer (pH=9.5). Then 25 μ L of β -mercaptoethanol was added. Derivatization of amino acids and samples was achieved by preparing a mixture of boric acid buffer/OPA/ amino acid or sample/FMOC (5v/v/v). The mixture was vortexed for 2 min.

HPLC-DAD analysis

HPLC-DAD analysis was performed according to Wang et al. (2010) with some minor changes [49]. Agilent 1200 Infinity series HPLC system (Agilent Technologies, CA, USA) was used for the determination of amino acids. The separation was completed on a Zorbax Eclipse Inertsil ODS-3 column (250x4.6 mm, 5 μ m, Agilent). The temperature of the column oven was set at 40 °C. The mobile phase consisted of methanol /acetonitrile/ water (45/45/10, A) and phosphate buffer (pH 7.5, B). Elution was performed with the following gradient: 0–1.9 min, 100% A; 1.9-18.1 min, 0-58% B; 18.1–18.6 min, 58% B; 18.6–22.3 min, 58-70% B; 22.3–22.4 min, 70-100% B; 22.4–22.6 min, 100% B and 22.6–24 min, 100-0% B. The flow rate was 2.0 ml/min. The DAD was set at 338 nm to monitor the derivatized amino acids. The injection volume was 20 μ L. Except for L theanine amino acid, 13 amino acids could be separated simultaneously with HPLC-DAD. Since the retention times of L- theanine, and tyrosine are the same, a separate chromatogram was created for L-theanine. A standard addition procedure was applied for each amino acid and validation was performed. Chromatograms of amino acids and samples were shown in **Figures 6**, and **7**.

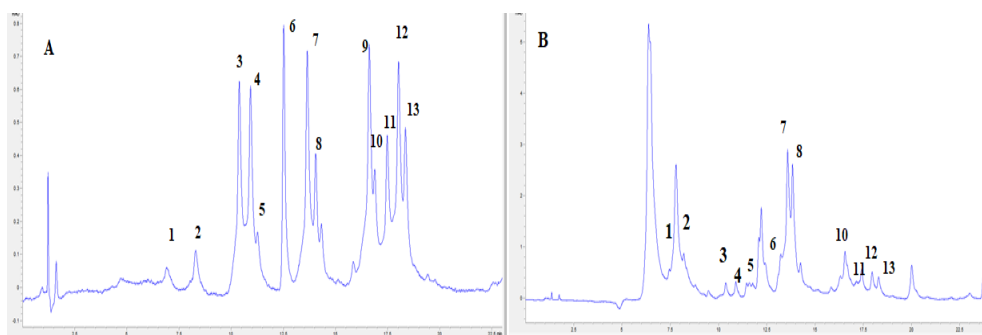


Figure 6 A: HPLC-DAD chromatogram of amino acid standards, B: HPLC-DAD chromatogram of sample (microwave digestion assisted extract). Aspartic acid, 2: glutamic acid, 3: asparagine, 4: serine, 5: glutamine, 6: arginine, 7: alanine, 8: tyrosine, 9: valine, 10: tryptophan, 11: phenylalanine, 12: isoleucine, 13: leucine

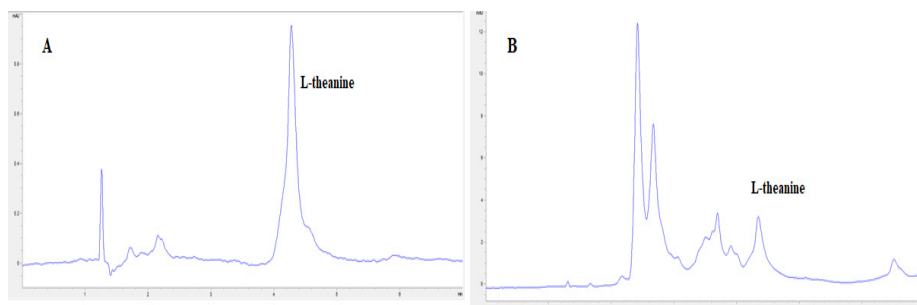


Figure 7. A: HPLC-DAD chromatogram of the standard of L-theanine amino acid, B: HPLC-DAD chromatogram of L-theanine of the sample (microwave digestion assisted extract)

Scanning Electron Microscope – Energy Dispersive X-ray Spectroscopy (SEM-EDX) Analysis

One ml of freshly prepared extracts was dropped onto the carbon band in the sample holder and dried overnight at room temperature. Dried extract samples were coated with an Au-Pd coating device (Leica). Coated samples were viewed on an SEM-GEMINI 500 device. Also, during the analysis, the amount of metal on the surface was determined as a percentage with the EDX detector (Energy Dispersive X-ray Spectroscopy). The metal deposits were visible in the SEM images, and we verified them with the EDX analysis. Working distance (WD) was studied in the range of 2-16 mm, and Electron High Tension (EHT) in the range of 2-5 kw. SE modes were used as a signal. Working conditions were indicated under each SEM image. EDX measurements were taken at a life time of 20 s with a voltage of 20 kV, mapping all elements detectable. For each experimental condition, three EDX measurements were taken.

Statistical analysis

Data were analyzed by two-way analysis of variance (ANOVA) using GraphPad Prism 8.4.2. Means were separated from each other by Bonferroni's multiple comparison tests. All analyses were performed in triplicate.

ACKNOWLEDGEMENTS

This work was supported by the Scientific Research Projects Committee of Manisa Celal Bayar University (Project No: 2020-089). The experiments in the study were carried out at Manisa Celal Bayar University, Application Science and Research Center (ASRC), Turkey.

REFERENCES

1. G.E. El-Ghazali; K.S. Al-Khalifa; G.A. Saleem; E.M. Abdallah; *J. Med. Plants Res.*, **2010**, *4*, 2680–2683.
2. R. Ullah; A.S. Alqahtani; O.M.A. Noman; A.M. Alqahtani; S. Ibenmoussa ; M. Bourhia, *Saudi J. Biol. Sci.*, **2020**, *27*, 2706.
3. S. Sasidharan; Y. Chen; D. Saravanan; K.M. Sundram; L. Yoga Latha; *African J. Tradit. Complement. Altern. Med.*, **2011**, *8*, 1–10.
4. R.M. Smith; *J. Chromatogr. A.*, **2003**, *1000*, 3–27.
5. M.C. Hennion; V. Pichon; *Environ. Sci. Technol.*, **1994**, *28*.
6. S.K. Poole; T.A. Dean; J.W. Oudsema; C.F. Poole; *Anal. Chim. Acta.*, **1990**, *236*, 3–42.
7. F. Chemat; Zill-E-Huma; M.K. Khan; *Ultrason. Sonochem.*, **2011**, *18*, 813–835.
8. J. Azmir; I.S.M. Zaidul; M.M. Rahman; K.M. Sharif; A. Mohamed; F. Sahena; M.H.A. Jahurul; K. Ghafoor; N.A.N. Norulaini; A.K.M. Omar; *J. Food Eng.*, **2013**, *117*, 426–436.
9. <http://www.epa.gov/greenchemistry/>, Pubs/about_gc.html, n.d. Basics of Green Chemistry | US EPA [WWW Document]. URL, <https://www.epa.gov/greenchemistry/basics-green-chemistry> (accessed 10.18.21).
10. C. Wen; J. Zhang; H. Zhang; C.S. Dzah; M. Zandile; Y. Duan; H. Ma; X. Luo; *Ultrason. Sonochem.*, **2018**, *48*, 538–549.
11. F. Anwar; S. Latif; M. Ashraf; A.H. Gilani; *Phytother. Res.*, **2007**, *21*, 17–25.
12. A. Leone; A. Spada; A. Battezzati; A. Schiraldi; J. Aristil; S. Bertoli; *Int. J. Mol. Sci.*, **2016**, *17*, 2141.
13. J. Sabaté; *Am. J. Clin. Nutr.*, **2003**, *78*, 502–507.
14. Y. Cai; L. Wu; X. Lin; X. Hu; L. Wang; *Ind. Crops Prod.*, **2020**, *154*.
15. M.I. Nassar; El-S.A. Aboutabl; D.M. Eskander; M.H. Grace; E.D.A. El-Khrisy; A.A. Sleem; *Pharmacognosy Res.*, **2013**, *5*, 17–21.
16. X. Yang; Q. Wang; ZR. Pang; MR. Pan; W. Zhang; *Pharm. Biol.*, **2017**, *55* (1), 1207–1214.
17. V.P. Singh; A. Arulanantham; V. Parisipogula; S. Arulanantham; A. Biswas; *Eur. J. Nutr. Food Saf.*, **2018**, *8*, 204–214.
18. J.N. Kasolo; G.S. Bimenya; L. Ojok; J. Ochieng; J.W. Ogwal-Okeng; *J. Med. Plants Res.*, **2010**, *4*, 753–757.
19. S.Sreelatha; P.R. Padma; *Plant Foods Hum. Nutr.*, **2009**, *64*, 303–311.
20. B. Vongsak; W. Gritsanapan; Y. Wongkrajang; I. Jantan; *Nat. Prod. Commun.*, **2013**, *8*(11), 1559–1561.
21. N. Tlili; H. Mejri; Y. Yahia; E. Saadaoui; S. Rejeb; A. Khaldi; N. Nasri; *Food Chem.*, **2014**, *160*, 98–103.
22. C. Castro-López; J.M. Ventura-Sobrevilla; M.D. González-Hernández; R. Rojas; J.A. Ascacio-Valdés; C.N. Aguilar; G.C.G. Martínez-Ávila; *Food Chem.*, **2017**, *237*, 1139–1148.
23. B. Kaufmann; P. Christen; *Phytochem. Anal.*, **2002**, *13*, 105–113.
24. L. Pollini; C. Tringaniello; F. Ianni; F. Blasi; J. Manes; L. Cossignani; *Antioxidants*, **2020**, *9*, 277.

25. L. Wu; L. Li; S. Chen; L. Wang; X. Lin; *Sep. Purif. Technol.*, **2020**, *247*, 117014.
26. E.N. Fombang; P. Nobossé; C.M.F. Mbofung; D. Singh; *J. Food Process. Preserv.*, **2020**, *44*, 1–13.
27. B. Vongsak; S. Mangmool; W. Gritsanapan; *Planta Med.*, **2015**, *81*, 1084–1089.
28. S.E. Atawodi; J.C. Atawodi; G.A. Idakwo; B. Pfundstein; R. Haubner; G. Wurtele; H. Bartsch; R.W. Owen; *J. Med. Food*, **2010**, *13*, 710–716.
29. M. Mbikay; F. Sirois; S. Simoes; J. Mayne; M. Chrétien; *FEBS Open Bio* *4.*, **2014**, 755–762.
30. N. Bhalla; N. Ingle; S.V. Patri; D. Haranath; *Saudi J. Biol. Sci.*, **2021**, *28*, 6915–6928.
31. D.P. Xu; Y. Li; X. Meng; T. Zhou; Y. Zhou; J. Zheng; J.J. Zhang; H. Bin Li; *Int. J. Mol. Sci.*, **2017**, *18(1)*, 96.
32. S.Saucedo-Pompa; J.A. Torres-Castillo; C. Castro-López; R. Rojas; E.J. Sánchez-Alejo; M. Ngangyo-Heya; G.C.G. Martínez-Ávila; *Food Res. Int.*, **2018**, *111*, 438–450.
33. S.O. Aisida; N. Madubuonu; M.H. Alnasir; I. Ahmad; S. Botha; M. Maaza; F.I. Ezema; S.O. Aisida; N. Madubuonu; M.H. Alnasir; I. Ahmad; S. Botha; M. Maaza; F.I. Ezema; *Appl. Nanosci.*, **2020**, *10*, 305–315.
34. B.K. Paikra; H.K.J. Dhongade; B. Gidwani; *J. Pharmacopuncture*, **2017**, *20*, 194–200.
35. J.L. Rockwood; B.G. Anderson; D.A. Casamatta; *Int. J. Phytother. Res.*, **2013**, *3*, 2278 – 5701.
36. C. Rodríguez-Pérez; R. Quirantes-Piné; A. Fernández-Gutiérrez; A. Segura-Carretero; *Ind. Crops Prod.*, **2015**, *66*, 246–254.
37. T. A. Aderinola; T.N. Fagbemi; V.N. Enujiugha; A.M. Alashi; R.E. Aluko; *Heliyon*, **2018**, *4(10)*.
38. S.J. Granella; T.R. Bechlin; D. Christ; S.R.M. Coelho; C.H. Paz; *South African J. Bot.*, **2021**, *137*, 110–116.
39. B. Su; X. Chen; *Front. Vet. Sci.*, **2020**, *7*, 53.
40. C. Trigo; M.L. Castelló; M.D. Ortolá; F.J. García-Mares; M.D. Soriano; *Foods*, **2021**, *10*, 311031
41. N. Flórez; E. Conde; H. Domínguez; *J. Chem. Technol. Biotechnol.*, **2015**, *90*, 590–607.
42. S.B. Awad; *Ultrasound Technol Food Bioprocessing*, **2010**, 545–558.
43. C.G. Stephanis; J.G. Hatiris; D.E. Mourmouras; *Ultrason. Sonochem.*, **1997**, *4*, 269–271.
44. I.F.F. Benzie; J.J. Strain; *Anal. Biochem.*, **1996**, *239*, 70–76.
45. W. Brand-Williams; M.E. Cuvelier; C. Berset; *LWT - Food Sci. Technol.*, **1995**, *28*, 25–30.
46. M.B. Arnao; A. Cano; M. Acosta; *Food Chem.*, **2001**, *73*, 239–244.
47. A.C. Gören; S. Çikrikçi; M. Çergel; G. Bilsel; *Food Chem.*, **2009**, *113*, 1239–1242.
48. J.W. Henderson; R.D. Ricker; B. a. Bidlingmeyer; C. Woodward; ; *Amino Acids.*, **2000**, 1–10.
49. L. Wang; R. Xu; B. Hu ; W. Li; Y. Sun; Y. Tu; X. Zeng; *Food Chem.*, **2010**, *123*, 1259–1266.

THERMODYNAMICS OF TEXTILE CATIONIC DYE ADSORPTION ON CLINOPTILOLITE

Goran AMIN^a, Sandra KONSTANTINOVIC^a, Igor JORDANOV^b,
Dragan DJORDJEVIC^{a*}

ABSTRACT. This paper studies the thermodynamics of the adsorption of textile dye on clinoptilolite in order to estimate the potential of this natural material for decolorization. The adsorption of dye in the state of equilibrium in conditions of varying temperature, as well as different models of thermodynamic equilibrium, were analyzed. The most present mineral phase of the adsorbent is the mineral clinoptilolite with a mineral content of about 85% in the tuff. The natural adsorbent, clinoptilolite, originally from Serbia, was characterized by chemical analysis, and dominated by SiO₂ (59.57%). The surface morphology was monitored by electron microscopy. In the research, the concentration of the textile cationic dye (10-110 g·dm⁻³) and the adsorption temperature (293-333 K) were varied, while the amount of clinoptilolite was constant (1 g). To characterize the equilibrium adsorption, the dye removed and the amount of adsorbed dye were calculated. In adsorption thermodynamics, several models have been studied to calculate the most important thermodynamic parameters, free energy change, enthalpy, and entropy change, depending on the choice of thermodynamic equilibrium constant. The activation energy and sticking probability were calculated using a modified *Arrhenius*–type equation.

Keywords: *clinoptilolite, adsorption, textile cationic dye, thermodynamics, free energy change, enthalpy change, entropy change, activation energy*

INTRODUCTION

When dyeing textiles, on average, 50% of the dye is not fixed to the fiber for various reasons. The dye that is not absorbed by the fiber remains as in an aqueous solution and represents waste water, which must be disposed of.

^a Faculty of Technology, Bulevar oslobođenja 124, Leskovac, Serbia

^b Faculty of Technology and Metallurgy, Skopje, North Macedonia

* Corresponding author: drag_64@yahoo.com



Wastewater from the textile industry has a high color, salinity due to electrolytes, then there are acids or alkalis, solids, various compounds, etc. The complex chemical structure of synthetic dyes in water makes their removal difficult. Biological, chemical and physical methods are used for the treatment of wastewater from the textile industry [1-3].

There are a variety of techniques for wastewater treatment, adsorption is relatively acceptable for decolorization and removal of other pollutants due to its economical and simple nature. There are various studies investigating the removal of different colors from aqueous solutions treating different adsorbents: coconut fiber, *Persea americana* nuts activated with phosphoric acid, boron-enriched nanoclay, activated carbon from algae, natural zeolites with a three-dimensional structure, polymer composites of zeolite, heulandite, phillipsite and clay mineral kaolin etc. [4, 5].

Clinoptilolites are, by definition, aluminosilicates of alkaline and alkaline earth cations with a three-dimensional crystal structure [6, 7]. Natural zeolite is abundant in the world and is usually considered a cheap material. There are also synthetic zeolites with high ion exchange and adsorption capacity [8].

In this paper, equilibrium adsorption and thermodynamics of textile cationic dye adsorption on natural zeolite-clinoptilolite were investigated. Practically, it is a process of decolorization of model dyed water, modelled on the waste water that is created after dyeing acrylic textiles with a cationic dye. Clinoptilolite was used as an adsorbent, whose porous particles adsorb cationic dye cations from the aqueous solution onto their surface and into the interior in the process of exchange and interactions. The goal was to obtain information about the probability, nature, predict the direction of possible adsorption mechanisms, the spontaneity of the process, as well as the types of interactions that exist between adsorbate and adsorbent.

RESULTS AND DISCUSSION

The adsorption process continues until a thermodynamic equilibrium is established between the remaining amount of adsorbate in the solution and the amount on the adsorbent. In parallel with the adsorption process, the opposite process takes place, the desorption process, which involves the return of primarily adsorbed molecules/adsorbate ions to the solution. A decrease in the rate of sorption and an increase in the rate of desorption lead to their equalization over time, so at a certain moment a thermodynamic equilibrium occurs in the adsorption system [9].

The state of the surface of each adsorbent depends on the method and conditions of production, and it is the availability of the surface that leads

to the rapid adsorption of organic molecules from aqueous solutions. According to the micrograph in Figure 1 (magnification 30.000 \times), the natural adsorbent used, clinoptilolite, is a powdery material, which has porous particles of various shapes and forms, generally below 10 μm in size. Cubic and spherical morphology is observed for tuff particles. The morphology of clinoptilolite developed through the arrangement of particles in the form of flakes and conglomerates of compact forms.

A similar appearance of the surface morphology of clinoptilolite was also encountered by other authors [10, 11].

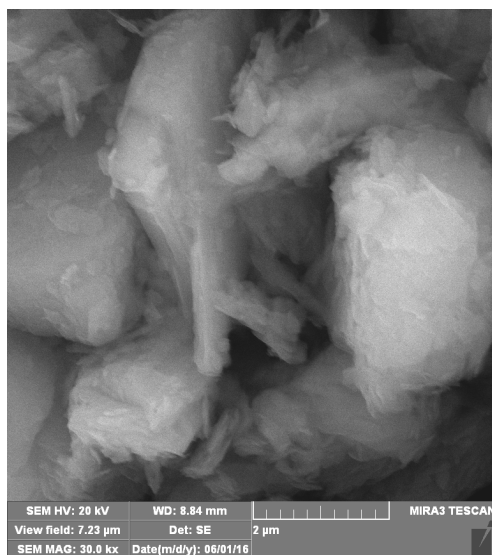


Figure 1. Micrograph of the surface of the applied adsorbent (clinoptilolite)

Chemical analysis revealed that the raw tuff fraction contains SiO_2 , Al_2O_3 , CaO , Fe_2O_3 , K_2O and small amounts of MgO , TiO_2 , Na_2O , MnO , P_2O_5 , SO_3 and Cl . The results are shown in table 1. It is noticeable that silicon cation dominates, which is expected, followed by aluminum, calcium, iron, potassium, etc. cations.

Table 1. Chemical analysis (%) of native clinoptilolite sample

SiO_2	Al_2O_3	CaO	Fe_2O_3	K_2O	MgO	TiO_2	Na_2O	MnO	P_2O_5	SO_3	Cl
59.57	11.25	8.41	3.56	2.02	0.91	0.80	0.21	0.15	0.13	0.05	0.009

Similar chemical composition of clinoptilolite was also found by other researchers [12].

Equilibrium adsorption is of essential importance for the research of the process of removing the dye of the aqueous solution with the help of clinoptilolite, whose ability to interact and exchange cations, enables replacement with other organic or inorganic cations.

The graph in Figure 2 represents the dependence of the %Removal and the amount of adsorbed dye in relation to the change in the initial concentration of the cationic dye for three adsorption temperatures. Dependencies are represented in the form of fitted curves, in order to demonstrate the functionality of the variables. The % removal has a noticeable decrease with increasing C_0 , while it increases with heating of the solution. On the other hand, the amount of adsorbed dye continuously decreases as the C_0 of the cationic dye increases, with the highest numerical values at the highest temperature. Temperature promotes the adsorption of cationic dye on clinoptilolite, so a temperature of 333 K is the best choice in this case.

Increasing the pH value from 2 to 8.5 led to an increase in the adsorption of cationic blue dye on clinoptilolite. Such changes increase the %Removal of the cationic dye from the aqueous solution due to the electrostatic attraction of the dye molecules and the adsorbent surface. This can be attributed to changes in the charge polarity from positive to negative on the clinoptilolite particles. Above a pH value of 8.5, the negative charge density on the surface of the adsorbent decreases, leading to a gradual decrease in %Removal.

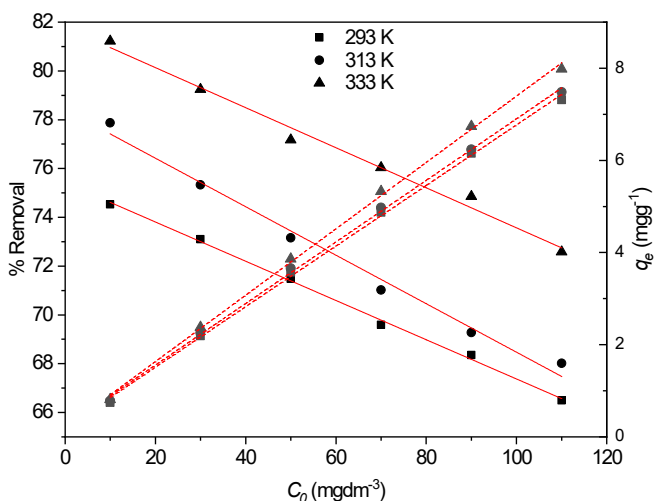


Figure 2. The %Removal (full line) and the q_e (interrupted line) of the cationic dye on clinoptilolite in relation to the initial dye concentration

Figure 3 presents graph of the influence of temperature on the %Removal and q_e . Dependencies are represented in the form of fitted curves, in order to demonstrate the functionality of the variables. In both cases, there is an increase in these parameters, with the fact that the %Removal changes more noticeably. The q_e is less sensitive to temperature changes, which is explained by the fact that it depends on several factors, the concentration of dye and adsorbent, as well as the volume of the adsorption solution. The temperature increases the adsorption, which is associated with the higher energy of the dye molecules, which are mostly in a monomolecular state, with the ability to penetrate more intensively and deeply into the porous structure of clinoptilolite.

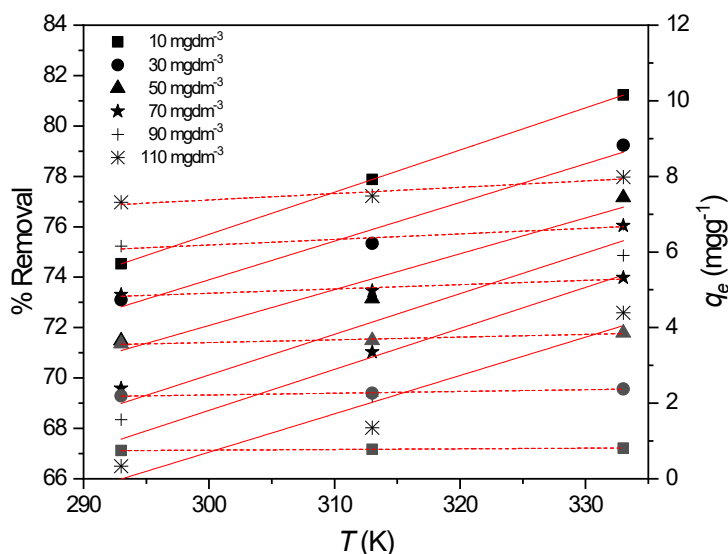


Figure 3. The %Removal (full line) and the q_e (interrupted line) of the cationic dye on clinoptilolite in relation to the change in temperature

Adsorption is a phenomenon that depends on temperature, and the assessment of thermodynamic parameters reflects the feasibility of the process. Temperature has two main effects on sorption, increasing the temperature increases the rate of diffusion of paint molecules through the external boundary layer as well as through the internal pores of the adsorbent particles. The spontaneity of the system is defined by evaluating the change in free energy, there are also changes in enthalpy and entropy, which also define the conditions for the adsorption process, i.e., binding of cationic textile dye cations to clinoptilolite.

Figures 4 and 5 show the dependence of the variable parameters necessary to calculate the distribution and partition coefficient, K_d and K_p , which are used to calculate the thermodynamic equilibrium constant and other thermodynamic parameters. According to the appearance of the straight line after fitting and the distance from the experimental points, high functionality was seen on both graphs, therefore, the results are acceptable and can be used for further calculations and obtaining thermodynamic parameters.

Regarding the way of presenting of distributive and partition coefficient, the graph $\ln(C_s/C_e):C_s$ ($R^2=0.9886-0.9971$) had somewhat better results, in terms of the R^2 value, compared to the graph $\ln(q_e/C_e):C_e$ ($R^2=0.9582-0.9918$), as well as the graph $\ln(q_e/C_e):q_e$ ($R^2=0.9857-0.9971$).

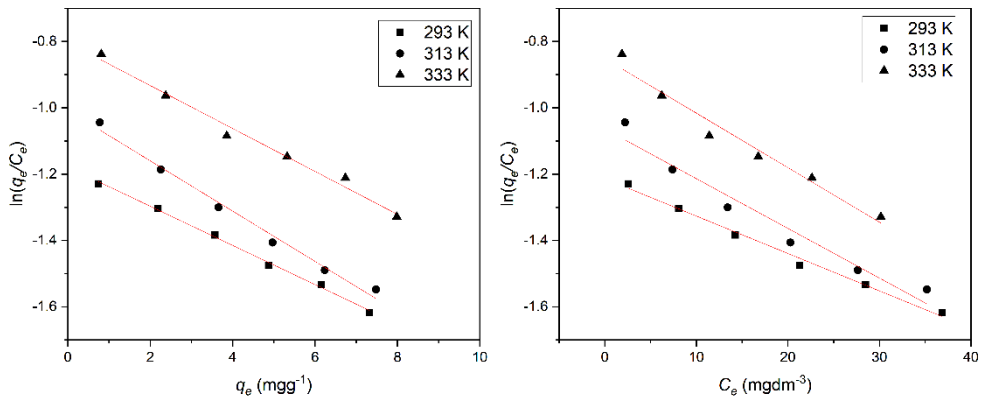


Figure 4. Graphs for calculating the distribution coefficient for the process of sorption of the cationic dye on clinoptilolite

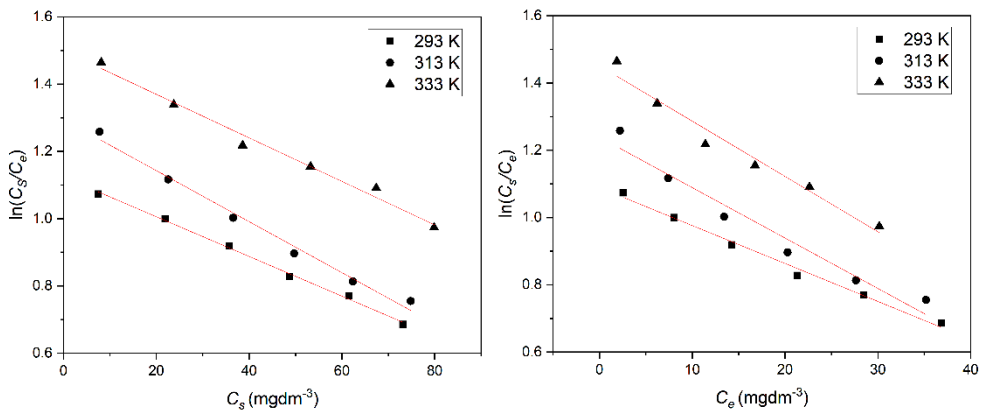


Figure 5. Graphs for calculating the partition coefficient for the process of sorption of the cationic dye on clinoptilolite

Figures 6 and 7 show two graphs that describe $\Delta G : T$ dependencies, through the distribution or partition coefficient. A strong functionality of the fitted lines following the experimental points was observed. Based on these graphs, thermodynamic parameters, enthalpy and entropy of the adsorption process were determined by calculation. In general, the values of ΔG can determine the character of the interactions between the dye molecules and the clinoptilolite, i.e., whether it is physisorption or chemisorption.

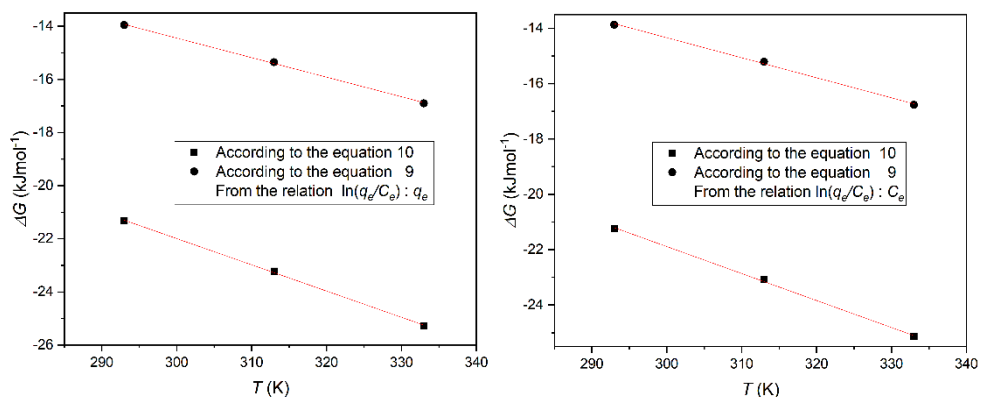


Figure 6. Free energy as a function of temperature (ΔG was calculated by equilibrium constant from the distribution coefficient)

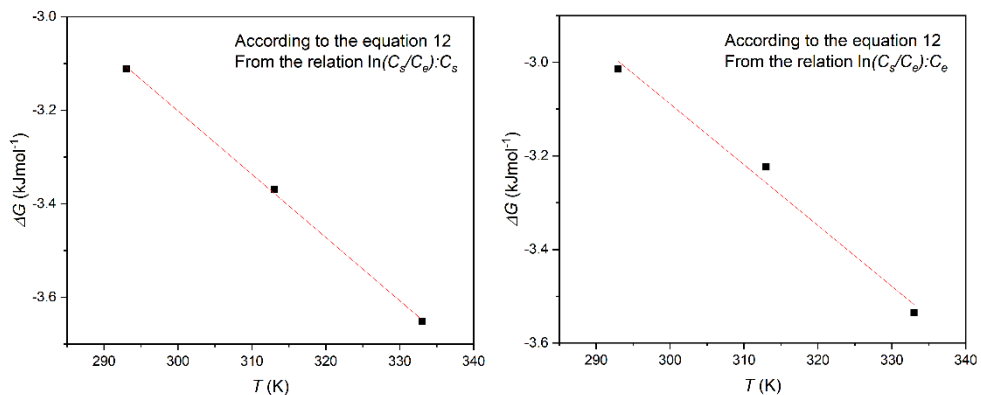


Figure 7. Change in free energy as a function of temperature (ΔG was calculated by equilibrium constant from the partition coefficient)

Table 2 gives numerical data for the basic thermodynamic parameters obtained on the basis of the equilibrium constant, K_{eq} , calculated from the distribution coefficient and the partition coefficient.

Table 2. Thermodynamic parameters for the adsorption of cationic dye on clinoptilolite

Method of calculation	Temp. (K)	ΔG (J·mol ⁻¹)	ΔH (J·mol ⁻¹)	ΔS (J·mol ⁻¹ ·K ⁻¹)	R^2
According to the relation $\ln(C_s/C_e)$: C_s and Equation 12	293	-3.11	0.85	0.013	0.9992
	313	-3.37			
	333	-3.65			
According to the relation $\ln(C_s/C_e)$: C_e and Equation 12	293	-3.01	0.81	0.013	0.9875
	313	-3.22			
	333	-3.53			
According to the relation $\ln(q_e/C_e)$: C_e and Equation 9	293	-13.87	7.38	0.072	0.9980
	313	-15.21			
	333	-16.77			
According to the relation $\ln(q_e/C_e)$: C_e and Equation 10	293	-21.24	7.38	0.098	0.9989
	313	-23.08			
	333	-25.14			
According to the relation $\ln(q_e/C_e)$: q_e and Equation 9	293	-13.95	7.64	0.074	0.9991
	313	-15.35			
	333	-16.9			
According to the relation $\ln(q_e/C_e)$: q_e and Equation 10	293	-21.33	7.64	0.099	0.9995
	313	-23.23			
	333	-25.28			

According to the numerous values for the coefficient of determination, R^2 , in this table, a high dependence of the variables is observed, practically, in all cases, this error parameter is in between 0.9875 and 0.9995. The validity of the results is hereby absolutely accepted.

A slight advantage is given to the distribution coefficient, i.e. the relation $\ln(q_e/C_e)$: q_e , considering $R^2=0.9995$ (according to the equation 10).

The weakest result (according to R^2 , according to the equation 12) was shown by the application of the K_p for calculating the K_{eq} according to the relation $\ln(C_s/C_e)$: C_e , on the basis of which the thermodynamic parameters were obtained.

In best case, ΔG has negative numerous values (-21.33 to -25.28 kJ·mol⁻¹), which indicates the spontaneity of the dye adsorption process at 293, 313 and 333 K. Thus, this confirms the practicality of adsorption, there is a good affinity of dye molecules for the adsorbent, the interaction takes place through physisorption.

It is known that ΔG for physisorption ranges between -20 and 0 $\text{kJ}\cdot\text{mol}^{-1}$, physisorption and chemisorption are in the range of -20 and -80 $\text{kJ}\cdot\text{mol}^{-1}$, while pure chemisorption is in the range from -80 to -400 $\text{kJ}\cdot\text{mol}^{-1}$ [13].

Negative value of ΔG decreases with increasing temperature, which indicates that the sorption process in this case is favorable, spontaneous in nature and more efficient at higher temperatures. The decrease in the value of ΔG with increasing temperature favors the process of exhausting the textile cationic dye to clinoptilolite from an aqueous solution at high temperature.

In best case, the values for the enthalpy change, ΔH , are positive ($7.64 \text{ kJ}\cdot\text{mol}^{-1}$) and reflect the endothermic nature of the sorption process, while the lower value of the required amount of heat characterizes the phenomenon of physisorption. This result can also be an indicator of the occurrence of single-layer adsorption, moreover, physisorption can be explained by the presence of groups on the adsorbate and adsorbent capable of forming electrostatic or ion-exchange compounds [6].

In the most favorable case, positive value of the entropy changes ΔS , ($0.099 \text{ kJ}\cdot\text{mol}^{-1}\cdot\text{K}^{-1}$), corresponds to an increased degree of freedom at the solid/liquid interface, as a result of the adsorption of dye molecules. In this particular case, values for ΔS are approaching zero, i.e., negative values, which confirms the physical adsorption [6].

The graph in Figure 8 serves to determine the sticking probabilities and activation energies. The dependence of the variables on the graph is relatively high, $R^2=0.8906$.

The result obtained for the activation energy in this research ($4.01 \text{ kJ}\cdot\text{mol}^{-1}$) indicates that the adsorption of dye on clinoptilolite takes place through a physical mechanism, which is in accordance with previous results for other thermodynamic parameters. A smaller amount for E_a , assumes that the reactions are relatively fast, the process of adsorption of cationic blue dye on clinoptilolite is endothermic, i.e., the value of E_a suggests that the increase in temperature favored the adsorption of the dye.

From the graph section in Figure 8, the value for the parameter S^* was also obtained. This parameter is defined as a function of the adsorption system that shows the potential of the adsorbate to remain on the adsorbent. A value of S^* between 0 and 1 favors adsorption. In this case, the sticking probability has a value less than unity and slightly greater than zero ($S^*=0.066$), which means that it is a matter of favorable binding of the dye to clinoptilolite.

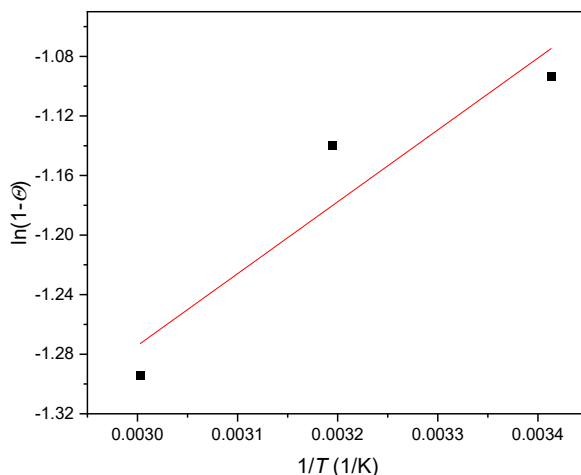


Figure 8. Variation of surface coverage with temperature during the adsorption of cationic dye on clinoptilolite

CONCLUSIONS

The process of textile cationic dye adsorption on clinoptilolite was analyzed by evaluating the thermodynamic parameters that reflect the feasibility of the process. The change of free energy, enthalpy and entropy were calculated based on the equilibrium constant obtained in different ways: from distribution and partition coefficients.

There is a very high functionality of linear regression curves when determining thermodynamic parameters. Accordingly, the results are valid, i.e., adequate and applicable.

The free energy change during adsorption was negative, which corresponds to the spontaneous and dominant physical process of dye sorption onto clinoptilolite. This confirms the feasibility and spontaneous nature of sorption at the applied temperatures, with a good degree of affinity of the dye molecules for the surface of the adsorbent through physisorption.

A positive value for the enthalpy change during dyeing reflects the endothermic nature of the interactions, while a smaller numerical value characterizes the phenomenon of physisorption.

A positive value for the entropy change confirms that it is physical sorption with possible partial participation of chemisorption.

The lower value of the activation energy emphasizes the physical sorption, the reactions are relatively fast, and the increase in temperature promotes the adsorption of the dye.

A numerical value for the sticking probability of less than one suggests favorable binding of the cationic dye to the fibers.

EXPERIMENTAL SECTION

As an adsorbent, natural zeolite, clinoptilolite, from Serbia, was used. The most present mineral phase is clinoptilolite, with a mineral content of about 85% in the tuff.

Before the adsorption experiment itself, clinoptilolite was prepared, which involved repeated washing with distilled water and drying in air.

The research used a triarylmethane class textile blue cationic dye C.I. Basic Blue 5 (Fig. 9), whose molecular formula is $C_{25}H_{28}Cl_2N_2$, the molar mass is $427.41 \text{ g}\cdot\text{mol}^{-1}$. It is mainly used for dyeing and printing textiles. The initial concentrations of this dye in the experiment were defined in relation to the amount of dye of the same type remaining in the water after commercial textile dyeing.

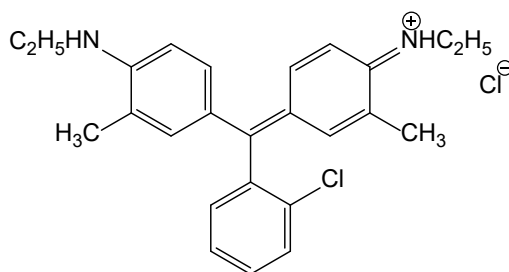


Figure 9. The structure of the applied textile blue cationic dye

Adsorption of a basic (cationic) dye from an aqueous solution was carried out at pH 8.5, in laboratory conditions, in closed reactors, placed on a device with a base rotation of 120 rpm, at 293, 313 and 333 K.

The amount of clinoptilolite in all cases was 1 g, while the solution of constant volume (0.1 dm^3), contained dye with an initial concentration of 10 to $110 \text{ mg}\cdot\text{dm}^{-3}$. The adsorption time, with continuous mixing, was 5–60 min.

X-ray fluorescence spectrometry (XRF) on an ED2000 energy dispersive spectrometer (Oxford Instruments, Great Britain) was used for the chemical composition of the adsorbent.

A scanning electron microscope TESCAN MIRA 3 XMU was used to analyze the surface of the samples.

The apparatus Cary 100 Conc UV-VIS, Varian was used to determine the concentration of the dye in the solution during adsorption (λ_{max} 605 nm).

The %Removal of cationic dye [14] is calculated using the equation:

$$\% \text{Removal} = \frac{C_0 - C_t}{C_0} \cdot 100 \quad (1)$$

where: C_0 ($\text{mg}\cdot\text{dm}^{-3}$) initial concentration of dye (adsorbate); C_t ($\text{mg}\cdot\text{dm}^{-3}$) dye concentration in time t .

The amount of dye adsorbed on the adsorbent [14] was calculated according to the following formula:

$$q_{t,e} = \frac{C_0 - C_{t,e}}{w} \cdot V \quad (2)$$

where: $q_{t,e}$ ($\text{mg}\cdot\text{g}^{-1}$) amount of adsorbed dye in adsorption time (t) and equilibrium time (e); C_0 ($\text{mg}\cdot\text{dm}^{-3}$) initial dye concentration; $C_{t,e}$ ($\text{mg}\cdot\text{dm}^{-3}$) the concentration of the dye in the solution during the adsorption time (t) and equality with time (e); w (g) adsorbent mass; V (dm^3) total volume of solution for adsorption.

The change in free energy, ΔG [4], under equilibrium conditions is defined as follows:

$$\Delta G = -R \cdot T \cdot \ln(K_{eq}) \quad (3)$$

where: K_{eq} - the thermodynamic equilibrium constant (dimensionless quantity); R ($8.314 \text{ J}\cdot\text{K}^{-1}\cdot\text{mol}^{-1}$) gas constant; T (K) temperature.

The relationship between [4] the standard Gibbs free surface energy change, the standard enthalpy change (ΔH) and the standard entropy change (ΔS) is as follows:

$$\Delta G = \Delta H - T \cdot \Delta S \quad (4)$$

From equations (3) and (4) the following equation is obtained:

$$\ln(K_{eq}) = -\frac{\Delta H}{R \cdot T} + \frac{\Delta S}{R} \quad (5)$$

By reviewing the relevant literature, it was found that several different approaches are used to determine K_{eq} . The equilibrium constant can be derived from the distribution coefficient (K_d) and the partition coefficient (K_p). The key fact is that the thermodynamic equilibrium constant should be dimensionless.

K_d and K_p are expressed as follows:

$$K_d = \frac{q_e}{C_e}; \quad K_p = \frac{C_s}{C_e} \quad (6)$$

where: C_s ($\text{mg}\cdot\text{dm}^{-3}$) the equilibrium concentration of the dissolved substance on the adsorbent; C_e ($\text{mg}\cdot\text{dm}^{-3}$) equilibrium concentration of adsorbate in solution.

K_d is obtained by plotting $\ln(q_e/C_e)$ against C_e or q_e [13].

According to this, the coefficient K_d has a dimension, so its translation into a dimensionless quantity is done by multiplying with the density of water (1000) or by multiplying with the number 55.5 and the molar mass of the dye [15, 16], in the second case:

$$K_{eq} \text{ (dimensionless)} = 1000 \text{ (g}\cdot\text{dm}^{-3})\cdot K_d \text{ (dm}^3\cdot\text{g}^{-1}) \quad (7)$$

$$K_{eq} \text{ (dimensionless)} = 55.5 \text{ (mol}\cdot\text{dm}^{-3})\cdot M_w \text{ (g}\cdot\text{mol}^{-1})\cdot K_d \text{ (dm}^3\cdot\text{g}^{-1}) \quad (8)$$

$$\Delta G = -R\cdot T\cdot\ln(1000\cdot K_d) \quad (9)$$

$$\Delta G = -R\cdot T\cdot\ln(55.5\cdot M_w\cdot K_d) \quad (10)$$

where: number 55.5 - the number of moles of water per liter; M_w - molar mass of the dye ($\text{g}\cdot\text{mol}^{-1}$).

The K_p value is obtained by plotting the graph $\ln(C_s/C_e)$ against C_e or C_s and extrapolating to zero [17, 18].

In this case, the partition coefficient agrees with the equilibrium constant, so there was no need to convert it into a dimensionless quantity.

$$K_{eq} \text{ (dimensionless quantity)} = K_p \quad (11)$$

$$\Delta G = -R\cdot T\cdot\ln(K_p) \quad (12)$$

The effect of temperature on adsorbate adsorption can be explained by analyzing the activation energy [19] from the modified *Arrhenius*-type equation:

$$S^* = (1-\theta) \cdot \exp\left(\frac{-E_a}{R\cdot T}\right) \quad (13)$$

where: S^* - the sticking probability and depends on the temperature of the system, E_a ($\text{kJ}\cdot\text{mol}^{-1}$) the activation energy.

Surface coverage (θ) is estimated [19] by the following equation:

$$\theta = \frac{1-C_e}{C_0} \quad (14)$$

where: C_0 ($\text{mg}\cdot\text{dm}^{-3}$) the initial dye concentration.

REFERENCES

1. L. Lara, I. Cabral, J. Cunha, *Sustainability*, **2022**, *14*, 8353.
2. H.B. Slama, A.C. Bouket, Z. Pourhassan, F.N. Alenezi, A. Silini, H. Cherif-Silini, T. Oszako, L. Luptakova, P. Golinska, L. Belbahri, *Appl. Sci.*, **2021**, *11*, 6255.
3. A. Micic, D. Djordjevic, I. Jankovic-Castvan, N. Cirkovic, B. Todorovic, *J. Chem. Soc. Pak.*, **2020**, *42*, 728-736.
4. G. Mersin, U. Acikel, M. Levent, *Chem. Eng. Process.*, **2021**, *169*, 108632.
5. F.O. Kehinde, H.A. Aziz, *J. Environ. Chem. Eng.*, **2016**, *4*, 1242-1247.
6. F. Jafari-zare, A. Habibi-yangjeh, *Chin. J. Chem.* **2010**, *28*, 349-356.
7. J. Yener, T. Kopac, G. Dogu, T. Dogu, *J. Colloid Interface Sci.*, **2006**, *294*, 255-264.
8. R. Hamidi, L. Tai, L. Paglia, M. Scarsella, M. Damizia, P. De Filippis, S. Musivand, B. de Caprariis, *Energy Convers. Manag.*, **2022**, *255*, 115348.
9. Y. Huang, W. Wang, Q. Feng, F. Dong, *J. Saudi Chem. Soc.*, **2017**, *21*, 58-66.
10. G. Mersin, U. Acikel, M. Levent, *Chem. Eng. Process.*, **2021**, *169*, 108632.
11. M. Babazadeh, H. Abolghasemi, M. Esmaili, A. Ehsani, A. Badiei, *Sep. Purif. Technol.*, **2021**, *267*, 118601.
12. T. Farias-Pineira, O. Picazo-Mozo, B. Concepcion-Rosabal, L.C. Menorval, *Rev. Cubana Quím.*, **2018**, *30*, 175-190.
13. T.T.L. Thi, H.S. Ta, K.L. Van, *J. Chem. Res.*, **2021**, *May-June*, 380-394.
14. R. Ullah, J. Sun, A. Gul, S. Bai, *J. Environ. Chem. Eng.*, **2020**, *8*, 103852.
15. A. Gunay, E. Arslankaya, I. Tosun, *J. Hazard. Mater.*, **2007**, *146*, 362-371.
16. M. Ghaedi, F. Karimi, B. Barazesh, R. Sahraei, A. Daneshfar, *J. Ind. Eng. Chem.*, **2013**, *19*, 756-763.
17. J. Perez-Calderon, M.V. Santos, N. Zaritzky, *J. Environ. Chem. Eng.*, **2018**, *6*, 6749-6760.
18. H.N. Tran, S.J. You, A. Hosseini-Bandegharaei, H.P. Chao, *Water Res.*, **2017**, *120*, 88-116.
19. K.M.S. Khalil, W.A. Elhamdy, K.M.H. Mohammed, A.E.A. Said, *Mater. Chem. Phys.*, **2022**, *282*, 125881.

STUDIES REGARDING COPPER IONS REMOVAL FROM WASTEWATERS USING OAK WOOD ASH AND THE EFFECT OF EXHAUSTED ASH AS SOIL AMENDMENT

Giannin MOSOARCA^a, Cosmin VANCEA^{a,*}, Simona POPA^{a,*}, Sorina BORAN^a, Petru NEGREA^a, Maria Elena RADULESCU-GRAD^b

ABSTRACT. In this work it was studied the removal of copper ions from wastewater by adsorption on oak wood ash and the effect of the ash resulting from adsorption process as a soil amendment. The process variables such as pH, contact time and adsorbent dose were optimized for maximum Cu²⁺ removal. It was establishing the mathematical correlation between this factors and the metal ions removal efficiency using specific 3D software. Adsorption process is described by Freundlich isotherm and pseudo-first order kinetic model. The effect of the wood ash, previously used as adsorbent, as soil amendment was studied using barley crop, *Hordeum vulgare* L. The values of the specific parameters: germination percent, plant average length, biomass and relative growth rate proving the beneficial effect of the use of wood ash (resulted from the adsorption process) on plant growth.

Keywords: *Cu²⁺ adsorption; Oak woods ash; Mathematical correlation; Equilibrium; Kinetics; Soil amendment.*

INTRODUCTION

Heavy metal pollution has become one of the most serious environmental problems, in many countries, especially in aquatic environments [1-3]. Unlike most organic pollutants, heavy metals are persistent environmental pollutants and cannot be degraded naturally [4-6].

^a Politehnica University of Timisoara, Faculty of Industrial Chemistry and Environmental Engineering, Bd. V. Parvan No. 6, 300223, Timisoara, Romania

^b "Coriolan Dragulescu" Institute of Chemistry, Romanian Academy, Mihai Viteazu Bd. No. 24, 300223, Timisoara, Romania

* Corresponding authors: cosmin.vancea@upt.ro; simona.popa@upt.ro



Heavy metals are discharged into the environment from different industrial activities and the resulting effluents can contain Cd, Cr, Cu, Co, Pb and Zn. These effluents have been excessively released into the environment and caused serious problems because heavy metals are recognized as major contaminants to plants, animals and human beings [1-6].

Copper is an essential trace element for living organisms. Copper is ubiquitous in the environment and an important trace element in biogeochemical cycles in soils and sediments. However, it becomes extremely toxic when presented at a high concentration. The presence of copper ion in drinking water causes abdominal pain, nausea, and more. Excessive copper intake may be responsible for severe mucosal irritation and corrosion, widespread capillary damage, hemolysis, liver and kidney damage, central nervous system irritation followed by depression, weakness and lethargy [6-11].

Copper and its compounds are widely used in many industries: metallurgy, electrical, electroplating, paper and pigments manufacturing, fertilizer, pesticides, herbicides, tannery. Wastewaters discharged from these industries have contributed to a progressive increase of copper concentrations in environments [6,7,11-13]. Therefore, the copper ions removal from contaminated waters became an important issue for the environmental protection [11].

Several methods, namely chemical precipitation, ion exchange, membrane filtration, electrochemical treatment, biological treatment and hydrogel were currently used to remove Cu^{2+} from aqueous solutions [1-5,7,9,10]. However, these methods have disadvantages and limitations due to high reagents or energy requirements, incomplete metal removal, complex operations, production of high amounts of sludge and unacceptable operating cost [1,2,4,6,14].

In addition to the methods mentioned above, adsorption process is one of the most widely used methods for the removal of metal ions from an aqueous solution. Adsorption is generally preferred due to its high efficiency, simplicity, moderate operational conditions, fast response, the availability of different adsorbents, and its cost effectiveness [1,2,4-6,10,14].

Technical and economic concerns have led to a focus on low-cost adsorbents. These materials include clay minerals, agricultural by-products, some aquatic plants and microorganisms. Industrial solid disposals and agricultural by-products such fly ash, wood ash, lignite, zeolite, clarified sludge, red mud, clay, rice husk ash, fuller's earth, sawdust, cellulose, chitosan, starch, sugarcane bagasse, neem-bark, coconut shell, orange peel, tea leaves have been used to remove heavy metals from wastewaters [1,2,4,14-18].

Wood ash is produce in high quantity every year by combustion of wood in industrial power plant or in home fireplaces [19,20]. It was found that wood ash was a promising adsorbent for the removal of pollutants from waters. [21,22].

An advantage of the adsorption is that it is suitable for mathematical modeling, leading to a better understanding of the factors that influence the process [18].

To the best of our knowledge, only few articles have studied the adsorption of Cu^{2+} on wood ash [23,24], but mathematical correlations between the main factors influencing the adsorption process was not followed.

On the other hand, the adsorption process generates a new waste, exhausted wood ash. The reuse of this material, resulted from copper adsorption, as soil amendment has not yet been reported in the literature.

The first objective of this research was to determine the effect of the solution pH, contact time, and adsorbent doses on the removal of Cu^{2+} from water and to establish a mathematical correlation between these factors and copper ions removal efficiency. In addition, the kinetic and equilibrium parameters of the adsorption process were computed and discussed. The second objective was to reuse wood ash resulted from the copper adsorption process as soil amendment. Therefore, it was studied the effect of wood ash application on a barley crop, *Hordeum vulgare* L.

RESULTS AND DISCUSSION

SEM analysis can be used to characterize the surface morphology of an adsorbent, serving to determine the particles shape and size distribution. Wood ash has a very porous surface, having a relatively uniform dimensional distribution, providing large surface area for Cu^{2+} -surface interaction as it is illustrated in Figure 1a. After adsorption, the surface is saturated, the pores being covered by copper ions (Figure 1b).

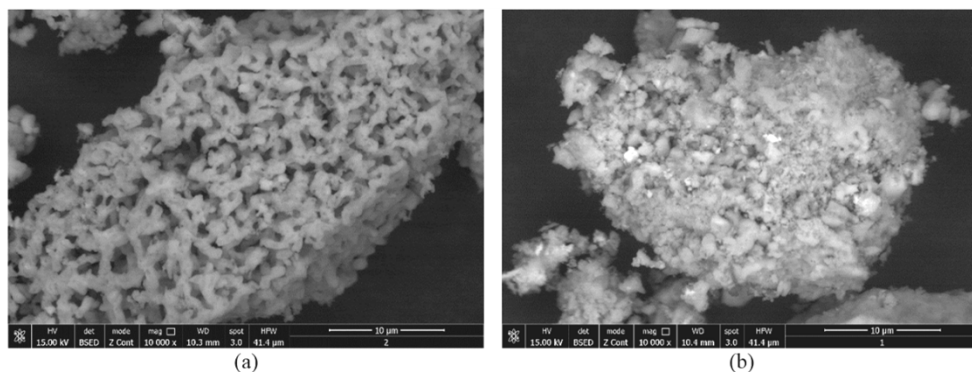


Figure 1. SEM images of wood ash: (a) before and (b) after copper ions adsorption

pH is one of the most important parameter that influence the metal sorption processes, due to its influence on surface properties of the adsorbent and on ionic species chemistry in solution (hydrolysis, complexation by organic and/or inorganic ligands, precipitation, redox reactions) [16,25]. The amount of the adsorbed metal also depends on contact time. In adsorption kinetics this parameter determines the time required to transport adsorbates to the adsorption sites [25,26]. Adsorbent dosage is an important parameter because it determines the adsorption capacity of an adsorbent for a given concentration of the adsorbate [16].

In order to represent a mathematical model between these factors and the copper ions removal efficiency, the experimental data were processed by means of the Table Curve 3D software. In view of choosing the best mathematical model, the following criteria were taken into account: the shape of the response surface, the simplicity of the characteristics mathematical equation and the determination coefficient (R^2) as close as possible to unity [27].

The effects of pH, contact time, wood ash dosage on adsorption process and mathematical correlation between these and the Cu^{2+} removal efficiency are presented in the Figures 2-4.

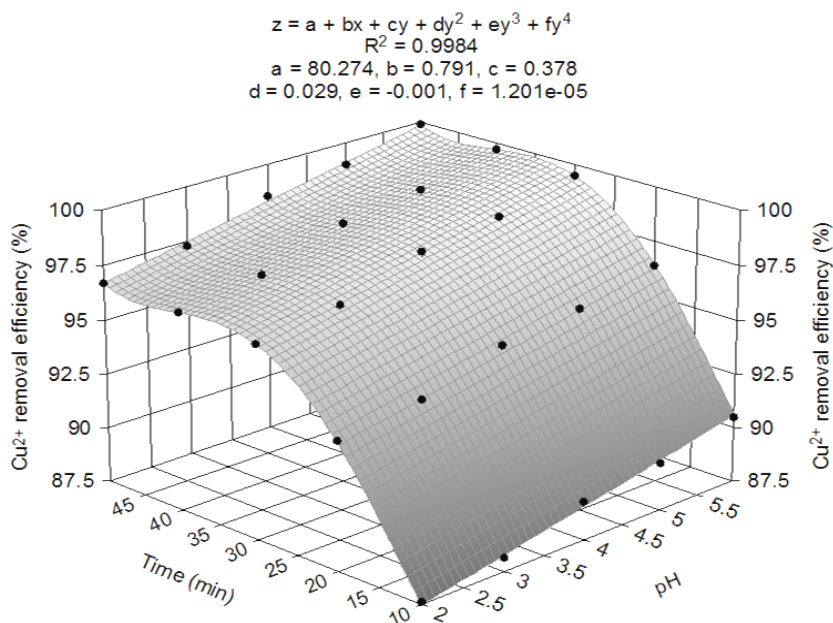


Figure 2. The mathematical correlation between pH, contact time and the copper ions removal efficiency from wastewater using wood ash

STUDIES REGARDING COPPER IONS REMOVAL FROM WASTEWATERS USING OAK WOOD ASH AND THE EFFECT OF EXHAUSTED ASH AS SOIL AMENDMENT

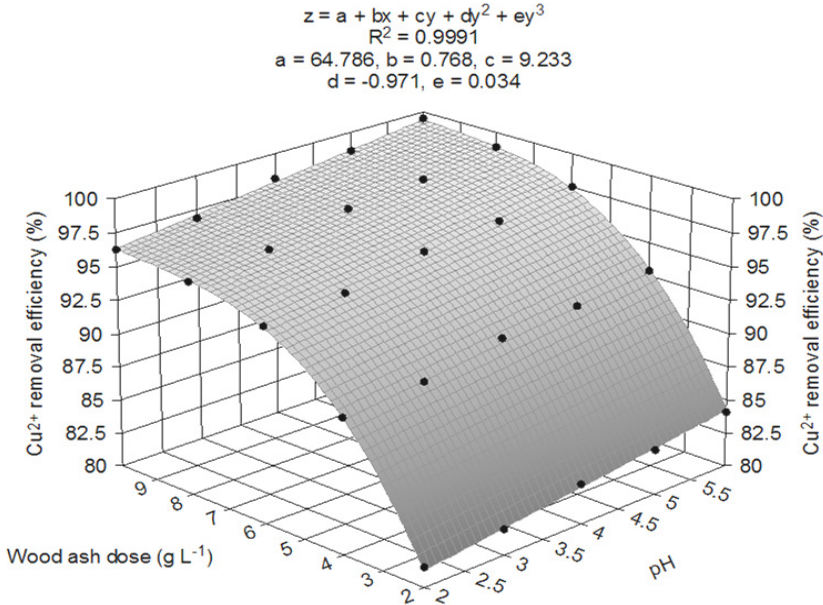


Figure 3. The mathematical correlation between pH, adsorbent dose and the copper ions removal efficiency from wastewater using wood ash

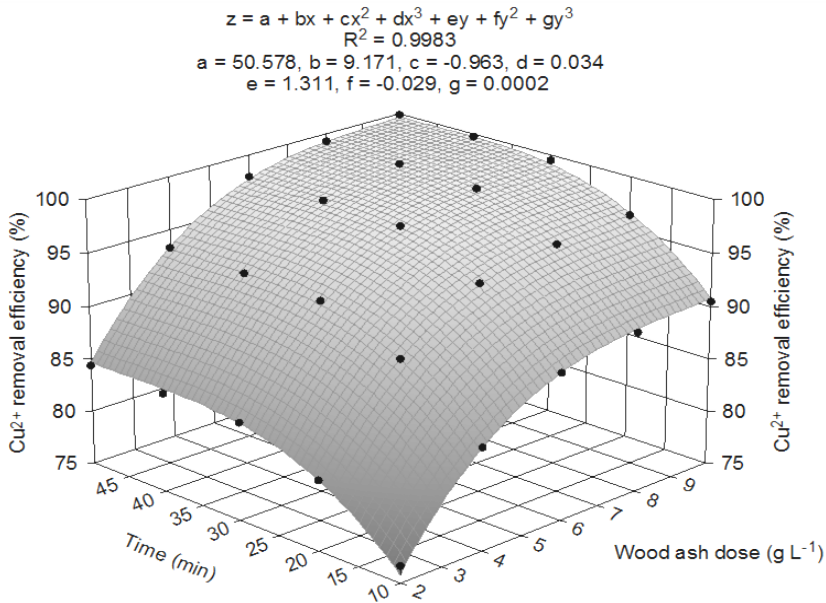


Figure 4. The mathematical correlation between contact time, adsorbent dose and the copper ions removal efficiency from wastewater using wood ash

Due to the high basicity of the used ash, the removal of copper ions varies slightly by increasing the initial pH of the wastewater, reaching the highest value at pH = 6 (Figure 2 and Figure 3). Electrostatic adsorption and precipitation can be involved in the expected mechanism of metal ions removal from aqueous solutions by wood ash [28,29]. At higher pH values, a negatively charged surface sites of the ash favour the adsorption of copper metal ions based on the electrostatic attraction [16,23].

At these pH values, the ash could act as a precipitant agent because of it's alkalization properties. The most important characteristic of the wood ash is the Ca^{2+} content, that generates alkalinity. This means that at higher pH values precipitation could be involved in the mechanism of toxic metal ions removal. Since Ca^{2+} in the ash is present as CaO , it can be assumed that the following reaction occur: $\text{CaO} + \text{H}_2\text{O} + \text{Cu}^{2+} = \text{Cu}(\text{OH})_2 + \text{Ca}^{2+}$ [29].

According to the experimental data, the copper ions removal efficiency increases by increasing the contact time. The effect is more obvious up to 30 minutes, after this time the copper removal yield is practically constant (Figure 2 and Figure 4).

The initial Cu^{2+} adsorption rates are high due to the availability of a large number of vacant surface sites for adsorption or to a higher diffusion rate towards the pores at the beginning of the adsorption process. As the contact time increases further, the available active sites for adsorption are gradually occupied and the driving force is weakened. As a result, the adsorption presents a slower rate, taking a longer time to achieve adsorption equilibrium [5,29].

Along with increasing of the adsorbent dose from 2 to 10 (g L^{-1}) the adsorption efficiency of Cu^{2+} on the wood ash increases gradually until 99.8% (Figure 3 and Figure 4). This phenomenon could be explained by the fact that along with increasing the amount of adsorbent the active surface increase. At initial stages, there is a large number of reactive sites leading to an efficient copper ions removal [7,16].

Adsorption isotherm is very useful in giving information on adsorption behavior, surface properties and adsorbent-adsorbate interactions [30,31].

Figure 5 illustrate the Langmuir, Freundlich and Temkin adsorption isotherms for copper ions adsorption on wood ash. The adsorption isotherms constants and the corresponding error parameters are detailed in Table 1. It was observed that the adsorption is best described by the Freundlich isotherm (highest determination coefficient R^2 and lowest chi-square χ^2 , sum of square error SSE, and average relative error ARE). The adsorption intensity calculated value, $n = 2.13$, is greater than unity, that indicates a favorable adsorption [6].

STUDIES REGARDING COPPER IONS REMOVAL FROM WASTEWATERS USING OAK WOOD ASH AND THE EFFECT OF EXHAUSTED ASH AS SOIL AMENDMENT

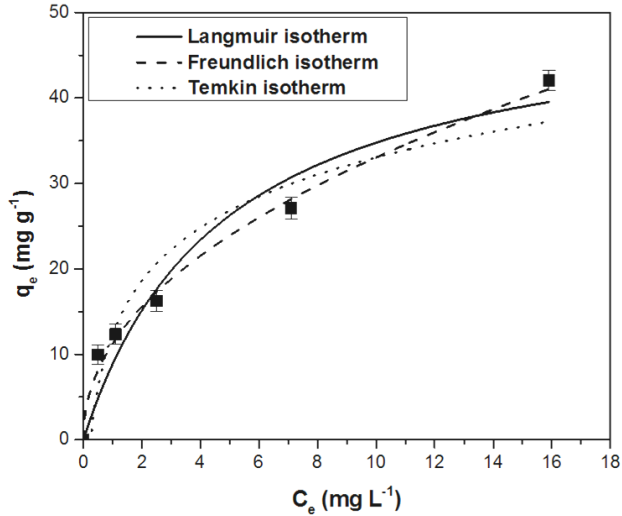


Figure 5. Langmuir, Freundlich and Temkin isotherms for copper ions adsorption on wood ash

Table 1. The adsorption isotherms constants and the corresponding error parameters

Isotherm model	Parameters	Value
Langmuir	K_L ($L\ mg^{-1}$)	0.208 ± 0.031
	q_{max} ($mg\ g^{-1}$)	51.43 ± 4.25
	R^2	0.9542
	χ^2	6.96
	SSE	58.95
	ARE (%)	26.88
Freundlich	K_f ($mg\ g^{-1}$)	11.26 ± 2.74
	$1/n$	0.46 ± 0.05
	R^2	0.9926
	χ^2	0.60
	SSE	8.19
	ARE (%)	8.23
Temkin	K_T ($L\ mg^{-1}$)	3.96 ± 0.47
	b ($kJ\ g^{-1}$)	272.25 ± 16.54
	R^2	0.957
	χ^2	4.33
	SSE	69.11
	ARE (%)	22.74

Kinetic of the adsorption process represents an important aspect because it provides information about the uptake rate and controls the residual time of the entire process. The adsorption rate is influenced by different processes including: transfer of solute to the sorbent surface, diffusion from the surface to the internal sites (surface or pore diffusion) and retention of the adsorbate which can involve sorption, complexation or intraparticle precipitation phenomena [6,30,31].

Figure 6 shows the pseudo-first order, pseudo-second order and Elovich kinetic models for copper ions adsorption on wood ash. The kinetic models constants and the corresponding error parameters are presented in Table 2. The pseudo-first order model best describe the adsorption process. The highest R^2 value and the lowest values for χ^2 , SSE, and ARE were obtained for this kinetic model. Also, the q_e calculated values, $1.71 \text{ (mg g}^{-1}\text{)}$ is in good agreement with the q_e experimentally determined values, $1.70 \text{ (mg g}^{-1}\text{)}$. This model assumes that physisorption limits the adsorption rate of the adsorbate on the adsorbent surface [32].

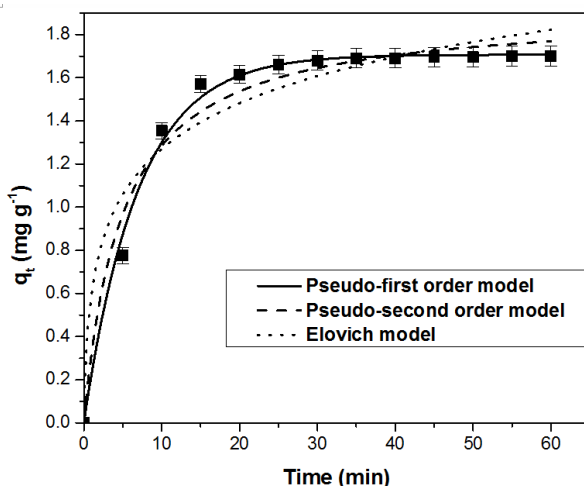


Figure 6. Pseudo-first order, pseudo-second order and Elovich kinetic models for copper ions adsorption on wood ash

The scientific literature mentions that pseudo-first order model also described the adsorption process of some heavy metal ions on different biomasses such as: Cu^{2+} , Cd^{2+} , Pb^{2+} , Zn^{2+} on wood ash [23], Cu^{2+} , Ni^{2+} , Mn^{2+} , Zn^{2+} on agroforestry waste mixtures (fern, rice husk, oak leaves) [33], Cu^{2+} on garden grass [34] and chemically modified Neem (*Azadirachta indica*) sawdust [35], Ni^{2+} on *Peganum harmala*-L seeds [36] and orange peel, pineapple peel, passion fruit wastes [37], Cd^{2+} on natural and modified *Posidonia oceanica* leaves [38].

Table 2. The kinetic models constants and the corresponding error parameters

Kinetic model	Parameters	Value
Pseudo-first order	k_1 (min^{-1})	0.143 ± 0.024
	$q_{e,\text{calc}}$ (mg g^{-1})	1.71 ± 0.08
	R^2	0.9946
	χ^2	0.01
	SSE	0.01
	ARE (%)	1.77
Pseudo-second order	k_2 (min^{-1})	0.106 ± 0.015
	$q_{e,\text{calc}}$ ($\text{g mg}^{-1} \text{min}^{-1}$)	1.91 ± 0.14
	R^2	0.9739
	χ^2	0.06
	SSE	0.08
	ARE (%)	4.85
Elovich	a (g mg^{-1})	3.23 ± 0.54
	b ($\text{mg g}^{-1} \text{min}^{-1}$)	1.85 ± 0.11
	R^2	0.9395
	χ^2	0.14
	SSE	0.18
	ARE (%)	6.69

The general characteristics of the wood ash used in this work (determined in other previously study [25]) were follows: $\text{pH} = 11.7$, $[\text{Ca}^{2+}] = 61980$ (mg kg^{-1} d.m.), $[\text{Mg}^{2+}] = 13310$ (mg kg^{-1} d.m.), $[\text{Na}^+] = 1890$ (mg kg^{-1} d.m.), $[\text{K}^+] = 94293$ (mg kg^{-1} d.m.), $[\text{P}] = 19452$ (mg kg^{-1} d.m.), $[\text{Fe}_{\text{total}}] = 2100$ (mg kg^{-1} d.m.), $[\text{Mn}^{2+}] = 7490$ (mg kg^{-1} d.m.), $[\text{Cu}^{2+}] = 95$ (mg kg^{-1} d.m.).

The wood ash, resulted from adsorption, had the following characteristics: $[\text{Ca}^{2+}] = 34328$ (mg kg^{-1} d.m.), $[\text{Mg}^{2+}] = 7684$ (mg kg^{-1} d.m.), $[\text{Na}^+] = 1193$ (mg kg^{-1} d.m.), $[\text{K}^+] = 53689$ (mg kg^{-1} d.m.), $[\text{P}] = 12281$ (mg kg^{-1} d.m.), $[\text{Fe}_{\text{total}}] = 788$ (mg kg^{-1} d.m.), $[\text{Mn}^{2+}] = 3220$ (mg kg^{-1} d.m.), $[\text{Cu}^{2+}] = 7225$ (mg kg^{-1} d.m.). The pH of this material was alkaline (9.12).

The experimental results show a decrease of the main chemical elements concentrations from the ashes after the adsorption process due to the lixiviation effect. The exhausted wood ash presents a large increase of the copper concentration from 95 to 7225 (mg kg^{-1} d.m) due to the retention of the copper ions.

Also, it can be noted that this exhausted wood ash contains high concentrations of chemicals, useful in plant growth. Calcium and potassium are useful for cell division and formation. Many plants enzymes are activated by potassium, magnesium and manganese. Potassium and phosphorus are involved in protein synthesis and activity. An important role in photosynthesis is held by magnesium, phosphorus and copper. Calcium and manganese increase plant resistance to various diseases. Also, phosphorus and copper have a major function in respiration and reproductive stages [39].

In order to establish the effect of the exhausted wood ash, resulted from cooper adsorption, as a soil amendment, *Hordeum vulgare* L. was used, this plant being a well-known bio-indicator [40,41].

Figure 7 summarizes the percentage of germination for each sample. It can be observed the beneficial effect of the copper ash addition. In the control sample, 82 % (mean) of seeds were germinated. In the samples with ash addition, the germination percentage is higher, reaching up to 95 % when the ash was added as a layer above ground, in the ratio ash : soil = 1: 50.

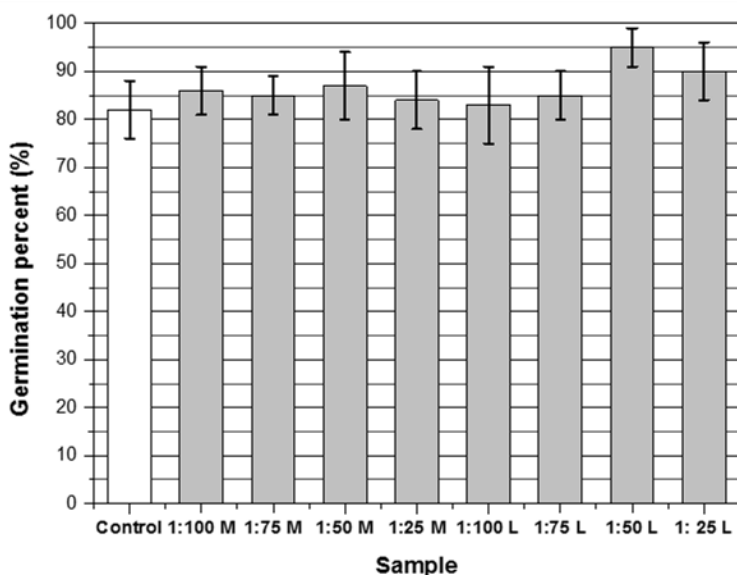


Figure 7. The germination percentage for control and sample with ash addition in both variant studied: soil mixed with ash (M) and ash as a layer above the soil (L) for different ash : soil ratio

Figure 8 presents the average lengths of the plants at 21 days after sowing. The experimental results show the positive effect of the ash addition on length of plants.

STUDIES REGARDING COPPER IONS REMOVAL FROM WASTEWATERS USING OAK WOOD ASH AND THE EFFECT OF EXHAUSTED ASH AS SOIL AMENDMENT

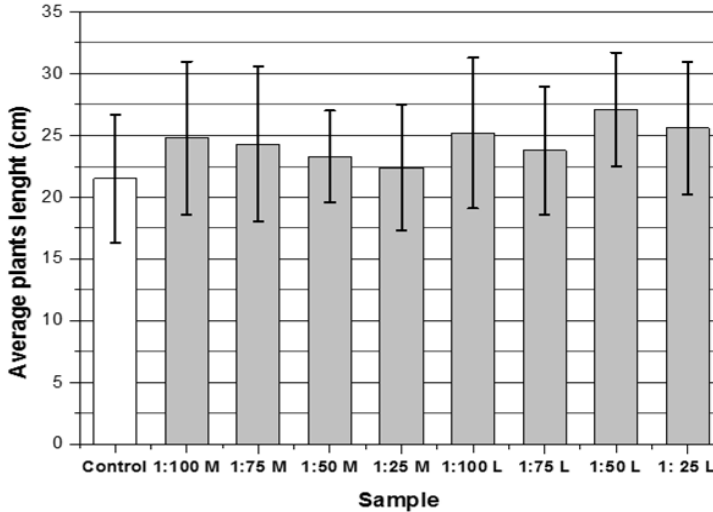


Figure 8. The average lengths of the plants at 21 days after sowing in both variant studied: soil mixed with ash (M) and ash as a layer above the soil (L) for different ash: soil ratio

Another followed parameter was the amount of the obtained biomass. The biomass mean value, after 21 days of sowing is presented in Figure 9.

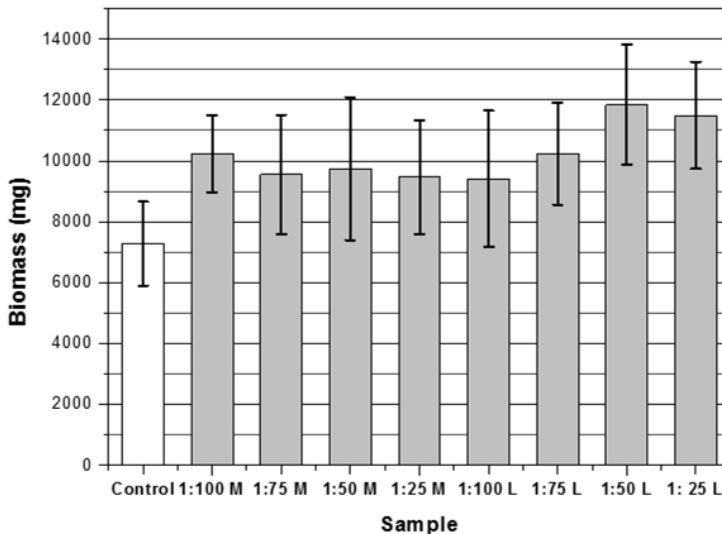


Figure 9. The biomass mean value after 21 days of sowing in both variant studied: soil mixed with ash (M) and ash as a layer above the soil (L) for different ash: soil ratio

Addition of ash leads to an increase of the biomass in all samples. The amount of biomass was higher by 30 - 62 % compared to the control sample. For the samples where the ash was added as a layer above ground, in the ratio ash: soil equals with 1: 50 and 1: 25, were recorded the biomass highest values.

The most used parameter for assessing the growth of plants is relative growth rate [42]. Figure 10 presents the relative growth rate of plants at 21 days after sowing. In all samples containing exhausted wood ash this parameter was higher than the control sample. The wood ash application method, soil mixed with ash (M) and ash as a layer above the soil (L) have no sensible effect upon the relative growth rate of the plants.

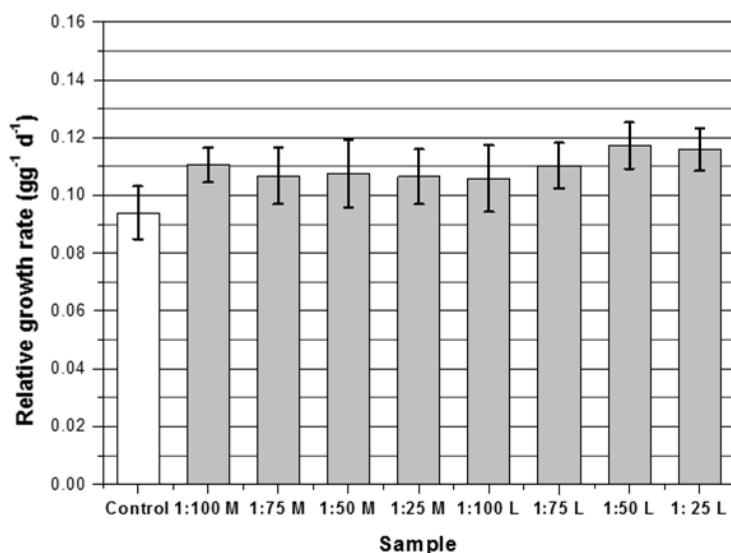


Figure 10. Relative growth rate after 21 days in both variant studied: soil mixed with ash (M) and ash as a layer above the soil (L) for different ash: soil ratio

CONCLUSIONS

Wood ash has a high efficiency in the removal of copper ions from wastewater (more than 99 %). Maximum efficiency was obtained under the following experimental conditions: pH = 6, mixing time 30 minutes and adsorbent dose 10 ($g L^{-1}$). Developed mathematical models that describe the dependence between copper removal efficiency and the main factors that influence the adsorption process have correlation coefficients close to unity.

Adsorption process is best described by Freundlich isotherm and pseudo-first order kinetic model.

The use of exhausted wood ash, resulted from the adsorption process of copper ions from waste water, as soil amendment has a beneficial effect for the barley crop. The germination percent, the plant average length, the amount of biomass and relative growth rate of plants were higher in the samples containing wood ash compared to the control sample. This fact can be explained by the high content of essential elements in the nutrition and development of plants from the ash (calcium, magnesium, potassium, phosphorus and manganese). The copper adsorbed on the ash is, also, a trace element in plant growth. Wood ash application method (soil mixed with ash and ash as a layer above the soil) does not significantly influence the plant development.

EXPERIMENTAL SECTION

Analytical grade reagents (purchase from Merck) were used in experiments. A Cu^{2+} stock solution, $100 \text{ (mg L}^{-1}\text{)}$ was prepared from distilled water and an appropriate quantity of $\text{CuSO}_4 \cdot 5\text{H}_2\text{O}$.

The wood ash for the present assay was derived from the combustion of oak wood (*Quercus robur* L.) in a home fireplace. BET analysis showed that the majority of pores are mesopores [25]. Quanta FEG 250 SEM microscope was employed to analyze the adsorbent surface morphology, before and after adsorption, at 10000x magnitude.

For determination of the general characteristics of the wood ash this material was digested with aqua regia and the concentrations of metals were determined using an atomic absorption spectrophotometer Varian SpectrAA 110 with graphite furnace. The vanadomolybdophosphoric acid method and UV-VIS spectrophotometer (Varian Cary 50) were used for the phosphorous determination. The measure of the wood ash pH, in distilled water ($\text{pH}_{\text{H}_2\text{O}}$), was realized according to USEPA Method 9045D, Soil and waste pH.

The adsorption experiments were carried out in 150 mL Erlenmeyer flasks at room temperature using an M.T.A. 609/A shaker. Mixing intensity was maintained constant throughout the experiments. The batch experiments were conducted at 2 - 6 pH range, contact time between 10 - 60 minutes and adsorbent dose between 2 - 10 (g L^{-1}). The pH was measure with an Ino-lab pH-meter and was adjusted using 0.1 N solutions of NaOH/HCl. After mixing, the samples were filtrated and the copper concentration was determined by atomic absorption spectroscopy.

Three independent replicates were performed for each adsorption experiment. In order to describe the adsorption behavior of Cu^{2+} ions on wood ash, three of the most commonly used adsorption isotherm models were applied to analyze the adsorption data obtained from the experiments, Langmuir, Freundlich and Temkin isotherms.

The non-linear forms of these isotherms models are expressed by the following equations:

$$\text{Langmuir isotherm} \quad q_e = \frac{q_m \cdot K_L \cdot C_e}{1 + K_L \cdot C_e} \quad (1)$$

$$\text{Freundlich isotherm} \quad q_e = K_F \cdot C_e^{1/n_F} \quad (2)$$

$$\text{Temkin isotherm} \quad q_e = \frac{R \cdot T}{b} \cdot \ln(K_T \cdot C_e) \quad (3)$$

where q_e is the amount of adsorbate adsorbed per unit mass of adsorbent; C_e is the equilibrium concentration of the adsorbate; K_L , K_F , and K_T are the Langmuir, Freundlich and Temkin isotherms constants; $1/n_F$ is an empirical constant indicating the intensity of adsorption; R is the universal gas constant; T is the absolute temperature; b is Temkin constant which related to the adsorption heat [43].

Pseudo-first order, pseudo-second order and Elovich kinetic models were applied in order to investigate adsorption process of Cu^{2+} onto the wood ash. The non-linear forms of these kinetic models are expressed by equations:

$$\text{Pseudo-first-order kinetic model} \quad q_t = q_e (1 - \exp^{-k_1 \cdot t}) \quad (4)$$

$$\text{Pseudo-second-order kinetic model} \quad q_t = \frac{k_2 \cdot t \cdot q_e^2}{1 + k_2 \cdot t \cdot q_e} \quad (5)$$

$$\text{Elovich kinetic model} \quad q_t = \frac{1}{a} \ln(1 + a \cdot b \cdot t) \quad (6)$$

where q_e is the equilibrium adsorption capacity, q_t is the adsorption capacity at time t , k_1 and k_2 are the rate constants of pseudo-first-order and pseudo-second-order kinetic models; a is the desorption constant of Elovich model; b is the initial velocity [44].

The proper isotherm and kinetic models was determined using values of determination coefficient (R^2), sum of square error (SSE), chi-square (χ^2) and average relative error (ARE) [43].

The exhausted wood ash, resulted from adsorption, was dried at room temperature and use as soil amendment.

The soil used in experiments was collected from the surface layer of a public garden in Timisoara town and had the following main characteristics: $\text{pH}_{\text{H}_2\text{O}} = 6.7$, sand = 34.2 %, clay = 39.4 %, silt = 26.4 % [25].

Seeds of *Hordeum vulgare* L. (purchase from a local farmer) were surface sterilized with 80% (v/v) ethanol and then were rinsed with distilled water for two to three times. Sterilized seed were kept at room temperature to make them completely dried.

Various wood ash: soil weight ratios have used in the experiment, from 1:100 to 1:25, in two variants, soil mixed with ash (M) and ash as a layer above the soil (L). For a correct analysis of the results, a soil control sample without ash addition was prepared for comparison. For each treatment, three independent replicates were performed.

In order to evaluate the addition effect of the wood ash, the germination percent, plant height, biomass and relative growth rate were determined, after 21 days from *Hordeum vulgare* L. seeds sowing.

Equation (7) was used for the relative growth rate determination:

$$RGR = \frac{\ln W_2 - \ln W_1}{t_2 - t_1} \quad (7)$$

where W_1 is fresh biomass of plants at time one (g), W_2 is fresh biomass of plants at time two (g), t_1 is time one (days) and t_2 is time two (days) [42].

The data consists of the mean values of three replicates. The one-way ANOVA was used in the statistical analysis in order to assess significant differences among the various wood ash: soil ratios. Considering $P < 0.01$ as a significant value, a comparison of mean using the least significant different test was calculated for P-values.

REFERENCES

1. M. G. Ghoniem; M. A. Ben Aissa; F. A. M. Ali; M. Khairy; *Inorganics*, **2022**, *10*, 256.
2. A. B. S. Aguiar; J. M. Costa; G. E. Santos; G. P. Sancinetti; R. P. Rodriguez; *Sustain. Chem.*, **2022**, *3*, 535-550.
3. F. Altaf; S. Ahmed; M. Usman; T. Batool; J. Shamshad; P. Bocchetta; R. Batool; *Processes*, **2021**, *9*, 2120.

4. C. Tejada-Tovar; A. Villabona-Ortiz; R. Ortega-Toro; *Appl. Sci.* **2021**, *11*, 9355.
5. N. Bakhtiari; S. Azizian; S. M. Alshehri; N. L. Torad; V. Malgras; Y. Yamauchi; *Micropor. Mesopor. Mat.*, **2017**, *217*, 173-177.
6. M. Mushtaq; H. N. Bhatti; M. Iqbal; S. Noreen; *J. Environ. Manage.*, **2016**, *176*, 21-33.
7. A. Labidi; A. M. Salaberria; S. C. M. Fernandes; J. Labidi; M. Abderrabba; *J. Taiwan Inst. Chem. E.*, **2016**, *65*, 140-188.
8. T. C. Totito; K. Laatikainen; O. Perea; C. Bode-Aluko; L. Petrik; *Appl. Sci.*, **2021**, *11*, 11912.
9. M. Rapa; A. A. Turcanu; E. Matei; A. M. Predescu; M. C. Pantilimon; G. Coman; C. Predescu; *Materials*, **2021**, *14*, 7187.
10. E. Mosayebi; S. Azizian; *J. Mol. Liq.*, **2016**, *214*, 384-389.
11. P. Kong; J. Wang; *Appl. Surf. Sci.*, **2016**, *389*, 316-323.
12. M. H. Morcali; B. Zeytuncu; A. Baysal; S. Akman; O. Yucel; *J. Environ. Chem. Eng.*, **2014**, *2*, 1655-1662.
13. Q. Wu; J. Chen; M. Clark; Y. Yu; *Appl. Surf. Sci.*, **2014**, *311*, 264-272.
14. N. Demirkiran; *Trans. Nonferrous Met. Soc. China*, **2015**, *25*, 647-653.
15. L. Xia; Y. Hu; B. Zhang; *Trans. Nonferrous Met. Soc. China*, **2014**, *24*, 868-875.
16. A. Ahmad; M. Rafatullah; O. Sulaiman; M. H. Ibrahim; Y. Y. Chii; B. M. Siddique; *Desalination*, **2009**, *247*, 636-646.
17. M. H. Morcali; B. Zeytuncu; A. Baysal; S. Akman; O. Yucel; *J. Environ. Chem. Eng.*, **2014**, *2*, 1655-1662.
18. M. Fouladgar; M. Beheshti; H. Sabzyan; *J. Mol. Liq.*, **2015**, *211*, 1060-1073.
19. M. Fernandez-Delgado Juárez; B. Prahauer; A. nWalter; H. Insam; I.H. Franke-Whittle; *Waste Manage.*, **2015**, *46*, 155-164.
20. E. Oburger; A. Jager; A. Pasch; A. Dellantonio; K. Stampfer; W. W. Wenzel; *Sci. Total Environ.*, **2016**, *544*, 711-721.
21. Y. Guo; C. Zhao; X. Chen; C. Li; *Appl. Energ.*, **2015**, *137*, 26-36.
22. E. Pehlivan; H. Kahraman; E. Pehlivan; *Fuel Process. Technol.*, **2011**, *92*, 65-70.
23. T. Chirenje; L. Q. Ma; L. Lu; *Water Air Soil Poll.*, **2006**, *171*, 301-314.
24. N. Tewari; V. K. Verma; J. P. N. Raj; *J. Sci. Ind. Res.*, **2006**, *65*, 935-938.
25. G. Mosoarca; C. Vancea; S. Popa; S. Boran; C. Tanasie; *J. Chem. Technol. Biotechnol.*, **2020**, *95*, 1781-1789.
26. P. K. Pandey; S. K. Sharma; S. S. Sambhi; *Int. J. Environ. Sci. Tech.*, **2010**, *7*, 395-404.
27. C. Cobzaru; V. Inglezakis; *Environ. Eng. Manag. J.*, **2012**, *11*, 2059-2063.
28. H. Cho; D. Oh; K. Kim; *J. Hazard. Mat. B.*, **2005**, *127*, 187-195.
29. K. Chojnacka; I. Michalak; *Global NEST J.*, **2009**, *11*, 205-217.
30. G. Mosoarca; C. Vancea; S. Popa; M. Gheju; S. Boran; *Sci. Rep.*, **2020**, *10*, 17676.
31. G. Mosoarca; C. Vancea; S. Popa; S. Boran; *Materials*, **2021**, *14*, 5861.
32. B. Liu; H. Luo; H. Rong; X. Zeng; K. Wu; Z. Chen; H. Lu; D. Xu; *Desalin. Water Treat.*, **2019**, *160*, 260-267

33. E. Rosales; L. Ferreira; M. Ángeles Sanromán; T. Tavares; M. Pazos; *Bioresour. Technol.*, **2015**, *182*, 41-49.
34. M. A. Hossain; H. H. Ngo; W. S. Guo; T. Setiadi; *Bioresour. Technol.*, **2012**, *121*, 386-395.
35. S. Sachan; H. Kumar; *Int. J. Sci. Eng. Res.*, **2015**, *6(6)*, 499-504.
36. M. Ghasemi; N. Ghasemi; G. Zahedi; S. R. W. Alwi; M. Goodarzi; H. Javadian, *Int. J. Environ. Sci. Technol.*, **2014**, *11*, 1835-1844.
37. G. L. Dotto; L. Meili; A. K. de Souza Abud; E. H. Tanabe; D. A. Bertuol; E. L. Foletto; *Water Sci. Technol.*, **2016**, *73(11)*, 2713-2721.
38. V. F. Meseguer; J. F. Ortuño; M. I. Aguilar; M. L. Pinzón-Bedoya; M. Lloréns; J. Sáez; A. B. Pérez-Marín; *Environ. Sci. Pollut. Res.*, **2016**, *23*, 24032-24046.
39. F. J. M. Maathuis; E. Diatloff; Roles and Functions of Plant Mineral Nutrients, in *Plant Mineral Nutrients: Methods and Protocols, Methods in Molecular Biology*, F. J. M. Maathuis Eds.; Humana Press, Totowa, USA, **2013**, vol. 953, pp 1-21.
40. S. Aras; S. S. Aydin; D. A. Korpe; C. Donmez; Comparative Genotoxicity Analysis of Heavy Metal Contamination in Higher Plants, in *Ecotoxicology*, G. Begum Eds.; InTechOpen, Rijeka, Croatia, **2012**, pp. 107-124.
41. C. S. Fontanetti; L. R. Nogarol; R. B. de Souza; D. G. Perez; G.T. Maziviero; Bioindicators and Biomarkers in the Assessment of Soil Toxicity, in *Soil Contamination*, S. Pascucci Eds.; InTechOpen, Rijeka, Croatia, **2011**, p 143-168.
42. P. Saha; O. Shinde; S. Sarkar; *Int. J. Phytoremediat.*, **2017**, *19*, 87-96.
43. J. S. Piccin; T. R. S. Cadaval; L. A. A. de Pinto; G. L. Dotto; Adsorption isotherms in liquid phase: Experimental, modeling, and interpretations, In *Adsorption Processes for Water Treatment and Purification*, A. Bonilla-Petriciolet, D. Mendoza-Castillo, H. Reynel-Avila Eds.; Springer, Cham, Switzerland, **2017**, pp. 19-51.
44. G. L. Dotto; N. P. G. Salau; J. S. Piccin; T. R. S. Cadaval; L. A. A. de Pinto, Adsorption kinetics in liquid phase: Modeling for discontinuous and continuous systems, In *Adsorption Processes for Water Treatment and Purification*, A. Bonilla-Petriciolet, D. Mendoza-Castillo, H. Reynel-Avila Eds.; Springer, Cham, Switzerland, **2017**, pp. 53-76.

PROTECTIVE EFFECTS OF ALUMINOSILICATES ON LEAD-ACETATE TOXICITY IN BROILER CHICKENS

Dejan PRVULOVIĆ^{a,*}, Danijela KOJIĆ^b

ABSTRACT. The study examined the effect of dietary supplements of lead acetate (PbA) and/or aluminosilicates (zeolite and montmorillonite) on growth traits, relative organ weights, activity of liver enzymes and activity of enzymes of antioxidant protection and lipid peroxidation in liver, erythrocytes, pancreas and spleen of chickens. Weight gain, feed conversion ratio, relative weights of liver, pancreas and spleen and activity of antioxidative enzymes in pancreas and spleen were not influenced with dietary treatment. Dietary intake of PbA induces oxidative stress and promotes lipid peroxidation in liver and erythrocytes. Activities of liver enzymes (alkaline phosphatase, γ -glutamyltransferase and α -amylase) were influenced by PbA also. Aluminosilicates alone did not provoke any adverse effect and did not disturb normal biochemical and physiological homeostasis in broilers. The combined data showed that chickens fed aluminosilicates received significant protection against the effects of the PbA for most parameters measured.

Keywords: *aluminosilicates; antioxidative enzymes; bentonite; chickens; erythrocytes; lead acetate; liver; montmorillonite*

INTRODUCTION

Lead is one of the well-known ubiquitous non-essential metal poisons in the environment, particularly widespread in industrial areas. Thus, it is obvious that exposure to lead is implicated a broad range of physiological,

^a *University of Novi Sad, Faculty of Agriculture, trg Dositeja Obradovića 8, RS-21000, Novi Sad, Serbia.*

^b *University of Novi Sad, Faculty of Sciences, trg Dositeja Obradovića 3, RS-21000, Novi Sad, Serbia.*

* *Corresponding author: dejanp@polj.uns.ac.rs*



biochemical and behavioral dysfunctions in animals and humans [1,2]. The main sources of exposure are contamination of feed and soil by industrial pollution, agricultural and food processing [3]. Its toxicity is closely related to its accumulation in certain tissues and its interference with the bioelements, whose role is critical for several physiological processes. The most deleterious effect of lead is on erythropoiesis, soft tissues, kidney function, and the central nervous system [4,5]. The extent of which orally administrated lead is absorbed is small. However, due to its slow rate of elimination, harmful levels of lead can accumulate in tissues after prolonged exposure to low quantities [1,6,7]. One of the most important mechanisms suggested for lead toxicity is a disruption in the prooxidant/antioxidant balance and inducing oxidative stress in cells with the generation of highly reactive oxygen species (ROS), such as hydroxyl radical, hydrogen peroxide, superoxide anion and lipid peroxides [3,8].

Aluminosilicates have been the subject of tremendous interest of both scientific and industrial world. They are used on a large industrial and scientific scale for a great variety of processes [9]. Clays and zeolites are hydrated and composed mostly of aluminium and silica and belong to the group of aluminosilicates. Phyllosilicate clays are hydrated, crystalline aluminosilicates containing alkali and alkaline earth cations and have layered structure. Montmorillonite, main constituent of phyllosilicate ore bentonite is trimorphic phyllosilicate formed by a 2:1 condensation of layers with aluminium sandwiched between two layers of silica. Montmorillonite possesses exchangeable sodium or calcium cations and has expandable sheets [10]. Because of accessibility and functional properties, bentonite and similar materials are widely used as a feed additives [11]. Natural zeolites are hydrated aluminosilicate minerals characterized by cage-like structures, with high internal and external surface area, and high cation-exchange capacities. The basic building blocks of natural zeolites are electrostatically charged tetrahedra of silica and aluminium, with the negative charge balanced by alkaline or alkaline earth cations. The stacking of these tetrahedral gives rise to various three-dimensional honeycomb structures containing tunnels or channels of uniform diameter [12]. Zeolites, due to their high ion-exchange capacity, have been used effectively for the prevention of heavy metal toxicity in animals [13].

The goal of present study is to throw the light on the possibilities of feed additive based on natural occurring hydrated aluminosilicates (Antitoxic nutrient-ATN) in preventing or minimizing the oxidative stress induced by chronic administration of lead acetate in chickens.

RESULTS AND DISCUSSION

Growth performance and relative organ weight

Results of body weight gain and feed efficiency in this experiment showed that lead acetate, at this level, alone or in combination with ATN did not manifest adverse effects (Table 1). Body weight was not found to change in any of the treated groups. Growth performance results from our experiment agreed with those of Tangpong and Satarug [14], Sainath et al. [8] and Flora et al. [15] performed on rats. Contrary to these results, studies of some other authors showed that adult treatment with different doses of lead acetate cause a significant decrease in pig's [16] and rat's [17] body weight. These studies suggested that the reduced growth was due to reduced food consumption via lead effects on the satiety set-point. Efficiency of feed utilization was not different among treatments. Also, Biesek et al. [18] and Banaszak et al. [19] found out that the use of halloysite and zeolite (0.5–2% in the feed) had positive effect on growth performance of broiler chickens in long-term experiment.

Table 1. Effect of chronic exposure to lead acetate (Pb) and ATN supplementation on body weight gain and feed conversion ratio of broilers

Body weight gain [g/day]	Experimental group			
	Control	ATN	Pb	Pb + ATN
Day 1-7	13.73 ± 1.14	14.02 ± 0.92	14.22 ± 0.57	13.64 ± 1.08
Day 8-14	27.87 ± 0.87	29.02 ± 1.16	25.45 ± 1.65	29.74 ± 0.78
Day 14-21	49.26 ± 1.65	50.20 ± 2.00	50.24 ± 1.36	47.83 ± 2.16
Feed conversion ratio [kg/kg]	1.60	1.58	1.60	1.57
The data are mean values ± standard error				

The effects of lead acetate and ATN on relative organ weights of poultries are presented in Table 2. No significant changes in the relative weights of liver, pancreas and spleen were observed in control and experimental chickens although animals in ATN-treated groups showed a tendency to have increased weights of measured organs. In our previous experiment broilers fed with addition of ATN in 6-week trial had significantly increased relative weight of spleen and some organs of digestive tract [20]. It is also reported that supplemental clays and zeolites did not significantly affect the relative weights of the liver, pancreas and spleen in poultry [18, 21]. The animals treated with lead acetate alone, or in combination with ATN were comparable to the control.

Table 2. Effect of chronic exposure to lead acetate (Pb) and ATN supplementation on relative organ weights of broilers

Organ	Experimental group			
	Control	ATN	Pb	Pb + ATN
Liver [g/kg]	24.00 ± 2.51	27.22 ± 2.24	25.56 ± 2.27	28.24 ± 3.09
Pancreas [g/kg]	3.31 ± 0.43	3.73 ± 0.40	3.44 ± 0.42	4.02 ± 0.70
Spleen [g/kg]	0.73 ± 0.19	1.00 ± 0.26	0.79 ± 0.20	0.92 ± 0.21
The data are mean values ± standard error				

Enzyme activity and lipid peroxidation in liver

In animal production, different aluminosilicates (clays and zeolites) are used as adsorbents of different toxic substances (mycotoxins, phytotoxins, enterotoxins, heavy metals etc.). Some aluminosilicates have potential to absorb and sequester different organic and inorganic ions and molecules in the lumen of the gastrointestinal tract of animals, favoring their expulsion from the body [22].

The liver plays a major role in lead's metabolism because after lead exposure liver is one of the major organs involved in the storage, biotransformation and detoxification [23]. Lead-induced hepatic damage with, cholestasis and is well-documented. Lead hepatotoxicity manifests itself in portal cellular infiltration, biliary hyperplasia, disorganization of the hepatic cords, cytoplasmic vacuolization and invading of infiltrative inflammatory cells. Chronic lead toxicity affects a range of cellular enzymes particularly those involved in energy production [24].

Table 3. Effect of chronic exposure of lead acetate (Pb) and ATN on liver enzyme activities of broilers

Parameter	Experimental group			
	Control	ATN	Pb	Pb + ATN
ALP [IU/mg protein]	56.10 ^a ± 5.97	51.14 ^a ± 6.35	34.18 ^b ± 2.02	42.08 ^c ± 4.11
ALT [IU/mg protein]	35.72 ^a ± 4.85	37.26 ^a ± 3.77	36.14 ^a ± 1.11	33.57 ^a ± 1.09
GGT [IU/mg protein]	4.69 ^a ± 0.07	3.73 ^{a,b} ± 0.43	3.04 ^b ± 0.28	3.86 ^{a,b} ± 0.39
AMY [IU/mg protein]	9.37 ^a ± 2.50	8.27 ^a ± 1.32	11.85 ^b ± 1.31	11.44 ^b ± 1.56
The data are mean values ± standard error ^{a,b,c} Values without the same superscripts within each row differ significantly ($P < 0.05$) ALP, alkaline phosphatase; ALT, alanine amino transferase; GGT, γ -glutamyltransferase; AMY, α -amylase				

During oxidative stress, which leads to cell damage or organ dysfunction, there is generally an increase in the activity of different enzymes: AST, ALT, ALP, LDH, GGT and others [25]. The serum levels of the enzymes ALT, GGT and ALP are considered as a biomarkers of hepatocyte function [26]. However, levels of this enzymes in serum could be results of metabolic disorders of other organs: heart [27], kidneys [28] or pancreas [29]. Many studies have demonstrated similar results that lead changes the liver function inducing liver fattening and increased activity of serum AST, ALT, ALP and GGT enzymes [23,30,31,32]. Our previous studies demonstrated that dietary inclusion of clinoptilolite or ATN do not affect activity of these serum enzymes in pigs [33,34,35] and broilers [20]. Treatment with lead acetate significantly ($P<0.05$) decreased hepatic ALP and GGT and increased activity of AMY compared with other experimental groups (Table 3). Activity of ALT in liver was not influenced by dietary treatment ($P>0.05$). These results are partially in accordance with those of Abdou and Newairy [32]. They hypothesized that the decrease in activity of hepatic AST, ALT and ALP could be expected to occur associating with the pathology involving necrosis of the liver. This decrement in enzyme activities is mainly due to the leakage of these enzymes from the liver cytosol into the blood stream which gives an indication on the hepatotoxic effect of lead.

The results of this study indicate that lead causes significant changes in oxidative stress in different organs, particularly in erythrocytes and liver which are found to be more vulnerable to lead-induced toxicity. SOD was found to play a major role in the first line of antioxidant defense by catalyzing the dismutation of superoxide anion radicals to form hydrogen peroxide and molecular oxygen. Oxidative stress created by the metal ions favors increased production of superoxide anions [36]. Under oxidative stress, SOD can behave in two different ways: initially and when stress is moderated, the cells act by increasing the SOD activity, but if the stress lasts a long time and favors increased production of ROS, the enzyme is exhausted and its activity falls [37]. In our case, decreased SOD-1 activity observed ($P<0.05$) could be explained by the massive production of superoxide anions, which override enzymatic activity and lead to the fall of its concentration in liver (Table 4). This could be due to a lead-induced copper deficiency. The low activity of SOD-1 could also be due to the inactivation of the enzyme by crosslinking or damage of DNA. Similar results were obtained by Ilesamni et al. [23]. Unlike Sainath et al. [8], Ilesamni et al. [23] and Mehana et al. [30], we did not observed any change in activity of other measured antioxidative enzymes in liver under lead intoxication. Our previous study also demonstrates that oral intake of ATN does not provoke inhibition or stimulation of liver GST in broilers [20, 38].

The oxidative stress has also been implicated to contribute to lead-associated tissue injury in the liver. Our study showed an increase in MDA content ($P<0.05$) in liver of broilers treated with the lead acetate, suggesting an increase in lipid peroxidation in hepatic cells. This result is in agreement with the studies undertaken by other authors [31,32] who recorded an increase in MDA content in the liver of rats subjected to subchronic exposure to lead for a period of several weeks.

Table 4. Effect of lead acetate (Pb) exposure alone and in combination with ATN on the activity of endogenous antioxidant enzymes and lipid peroxidation in the liver of broilers

Parameter	Experimental group			
	Control	ATN	Pb	Pb + ATN
SOD-1 [IU/mg protein]	18.46 ^a ± 0.63	19.56 ^a ± 0.86	15.14 ^b ± 0.69	18.98 ^a ± 0.54
CAT [IU/mg protein]	22.20 ^a ± 1.75	24.05 ^a ± 2.24	25.03 ^a ± 0.94	22.53 ^a ± 0.84
GPx [IU/mg protein]	2.08 ^a ± 0.066	2.14 ^a ± 0.062	2.18 ^a ± 0.071	2.02 ^a ± 0.070
PPx [IU/mg protein]	64.32 ^a ± 3.22	58.19 ^a ± 1.75	62.02 ^a ± 2.20	60.01 ^a ± 1.98
GST [IU/mg protein]	390.08 ^a ± 10.24	376.21 ^a ± 12.38	388.26 ^a ± 11.63	367.14 ^a ± 15.20
LP [nmol MDA/mg protein]	2.05 ^a ± 0.14	1.92 ^a ± 0.09	2.67 ^b ± 0.04	2.07 ^a ± 0.07

The data are mean values ± standard error
^{a,b} Values without the same superscripts within each row differ significantly ($P<0.05$)
SOD-1, superoxid dismutase; CAT, catalase; GPx, guaiacol peroxidase; PPx, pyrogallol peroxidase; GST, glutathion S-transferase; LP, lipid peroxidation

Enzyme activity and lipid peroxidation in red blood cells

The hematological system has been proposed as being important target for lead-induced toxicity. Lead may be rapidly absorbed and reached considerable amount in the blood. Once absorbed, blood lead is transported to the erythrocytes as lead diphosphate [4].

In the present study the decrease in the mean corpuscular hemoglobin concentration ($P<0.05$) of broilers treated with lead acetate may result from the direct and indirect toxic effects of lead acetate (Table 5). These results are in agreement with results of other authors mostly performed on rats [15], mice [39,40] and humans [41]. Lead is known to interfere with heme and hemoglobin synthesis and to affect erythrocyte morphology and survival. Anemia caused during lead poisoning is result of inhibition of heme synthesis and a decreased life span of circulating erythrocytes. This shortening of life span is probably due to the direct toxic effect of lead upon the cell membrane

integrity by inhibiting Na-K-ATPase. Lead, furthermore, interferes with iron utilization for heme formation in the mitochondria, and studies showed that lead competes with iron for the incorporation into red blood cells. Moreover, oxidative stress and free radicals produced in the presence of heavy metals cause changes in the structure and function of Hb, leading to anemia. Anemia observed in lead poisoning is caused also indirectly by the accumulation of δ -aminolevulinic acid [1,36].

The Table 5 shows the activity of antioxidant enzymes SOD-1, CAT, GPx, PPx, and GST in red blood cells. Significant decreases in SOD-1 activity of erythrocytes were recorded in Pb group as compared with control and ATN groups ($P < 0.05$). Activities of all other measured antioxidant enzymes were significantly increased in Pg group of broilers when compared to values of control, ATN and Pb + ATN groups of broilers ($P < 0.05$). The high level of antioxidant enzymes found in this study are consistent with the results of Wang et al. [39] and Tangpong and Satarug [14], who reported increased activity of glutathione peroxidase and decreased activity of SOD in red blood cells of mice after Pb administration.

Table 5. Effect of lead acetate (Pb) exposure alone and in combination with ATN on the hemoglobin concentration, activity of endogenous antioxidant enzymes and lipid peroxidation in the erythrocytes of broilers

Parameter	Experimental group			
	Control	ATN	Pb	Pb + ATN
Hb [g/l]	146.42 ^a ± 3.92	146.10 ^a ± 3.11	105.22 ^b ± 5.54	127.95 ^{a,b} ± 6.65
SOD-1 [IU/mg Hb]	466.08 ^a ± 12.33	489.75 ^a ± 15.45	354.88 ^b ± 12.76	485.45 ^a ± 12.34
CAT [IU/mg Hb]	8.26 ^a ± 0.48	8.12 ^a ± 0.59	10.09 ^b ± 0.29	7.50 ^a ± 0.45
GPx [IU/mg Hb]	6.41 ^a ± 0.24	6.83 ^a ± 0.17	8.44 ^b ± 0.09	6.78 ^a ± 0.19
PPx [IU/mg Hb]	14.40 ^a ± 0.50	15.00 ^a ± 0.48	18.95 ^b ± 0.57	14.80 ^a ± 0.44
GST [IU/mg Hb]	120.05 ^a ± 3.22	133.21 ^a ± 3.46	162.44 ^b ± 3.08	132.97 ^a ± 3.00
LP [nmol MDA/mg Hb]	1.19 ^a ± 0.089	1.41 ^a ± 0.125	2.86 ^b ± 0.088	1.45 ^a ± 0.103
The data are mean values ± standard error				
^{a,b} Values without the same superscripts within each row differ significantly ($P < 0.05$)				
Hb, hemoglobin; SOD-1, superoxid dismutase; CAT, catalase; GPx, guaiacol peroxidase; PPx, pyrogallol peroxidase; GST, glutathion S-transferase; LP, lipid peroxidation				

There was no significant difference in red blood cells MDA concentration of the control and those of the animals treated with ATN or ATN along with Pb, whereas chickens treated with Pb only showed a significant increase in MDA concentration. This agrees with other reports on experimental lead intoxication in mice [14] and rats [42].

Enzyme activities and lipid peroxidation in pancreas and spleen

Literature data about oxidative process in pancreas and spleen of animals under lead toxicity are very limited. Lead is stored in almost all soft tissues, autopsy studies showed that liver is the largest repository of soft tissue lead, followed by the kidney cortex and medulla, and other soft tissues: pancreas, spleen, ovary, adrenal gland, prostate, testis, fat, brain, heart and skeletal muscle [4,40]. Muselin et al. [43] reported that chronic exposure to lead can induce severe lesions in spleen with small necrosis spots. Data presented in Table 6. and Table 7. demonstrate that oral administration of lead acetate or ATN did not provoke oxidative stress or induce activity of antioxidative enzymes in pancreas and spleen of broiler chickens ($P > 0.05$).

Table 6. Effect of lead acetate (Pb) exposure alone and in combination with ATN on the activity of endogenous antioxidant enzymes and lipid peroxidation in the pancreas of broilers

Parameter	Experimental group			
	Control	ATN	Pb	Pb + ATN
SOD-1 [IU/mg protein]	4.14 ^a ± 0.12	4.29 ^a ± 0.21	4.40 ^a ± 0.22	4.31 ^a ± 0.11
CAT [IU/mg protein]	7.55 ^a ± 0.40	7.39 ^a ± 0.21	8.42 ^a ± 0.49	8.56 ^a ± 0.25
GPx [IU/mg protein]	0.36 ^a ± 0.011	0.39 ^a ± 0.020	0.35 ^a ± 0.017	0.40 ^a ± 0.010
PPx [IU/mg protein]	2.66 ^a ± 0.26	2.15 ^a ± 0.13	2.95 ^a ± 0.22	2.32 ^a ± 0.14
LP [nmol MDA mg ⁻¹ protein]	3.26 ^a ± 0.34	2.98 ^a ± 0.06	2.84 ^a ± 0.16	2.56 ^a ± 0.34

The data are mean values ± standard error
^{a,b} Values without the same superscripts within each row differ significantly ($P < 0.05$)
 SOD-1, superoxid dismutase; CAT, catalase; GPx, guaiacol peroxidase; PPx, pyrogallol peroxidase; LP, lipid peroxidation

Table 7. Effect of lead acetate (Pb) exposure alone and in combination with ATN on the activity of endogenous antioxidant enzymes and lipid peroxidation in the spleen of broilers

Parameter	Experimental group			
	Control	ATN	Pb	Pb + ATN
SOD-1 [IU/mg protein]	3.88 ^a ± 0.10	3.67 ^a ± 0.14	3.66 ^a ± 0.14	3.75 ^a ± 0.13
CAT [IU/mg protein]	5.72 ^a ± 0.12	5.12 ^a ± 0.17	5.63 ^a ± 0.17	4.85 ^a ± 0.10
GPx [IU/mg protein]	0.59 ^a ± 0.03	0.63 ^a ± 0.03	0.64 ^a ± 0.02	0.60 ^a ± 0.02
PPx [IU mg ⁻¹ protein]	16.45 ^a ± 1.13	14.25 ^a ± 0.63	11.61 ^b ± 0.83	13.31 ^{a,b} ± 0.82
LP [nmol MDA/mg protein]	2.58 ^a ± 0.05	2.60 ^a ± 0.08	2.37 ^a ± 0.17	2.24 ^a ± 0.17

The data are mean values ± standard error
^{a,b} Values without the same superscripts within each row differ significantly ($P < 0.05$)
 SOD-1, superoxid dismutase; CAT, catalase; GPx, guaiacol peroxidase; PPx, pyrogallol peroxidase; LP, lipid peroxidation

CONCLUSIONS

Results of this study are similar to those from our previous study [44] where we demonstrate that application of ATN in broilers' feed can prevent biochemical alterations in kidneys, brain and duodenum induced by intoxication with lead acetate. Co-administration of natural occurring aluminosilicates (ATN) with lead acetate offers significant protection against lead-induced oxidative stress by inhibiting lipid peroxidation and activating antioxidant defense system in red blood cells and liver of chickens. It has ability to absorb lead in lumen of digestive tract and thus could be used as a supplementary agent in animal feeds.

EXPERIMENTAL SECTION

Chickens and diet

Eighty four 1-day-old, unvaccinated broiler chicks of both sexes were obtained from a commercial hatchery. Individually weighted chicks were divided at random into four groups. There were seven replicates of three broiler chicks for each dietary treatment. The chicks were housed in electrically heated batteries under fluorescent lighting and received a commercial basal diet (maize and soybean meal diet 220 g protein, 13.00 MJ ME kg⁻¹) formulated to contain the National research Council (1994) requirements. Food and water were available *ad libitum* and lighting was continuous.

Experimental design

The experimental design consisted of four dietary treatments: 1. Control: basal diet; 2. ATN: basal diet plus 5.0 g ATN/kg diet; 3. Pb: basal diet plus 500 mg lead acetate/kg diet; 4. Pb + ATN: basal diet plus 500 mg lead acetate plus 5 g ATN/kg. ATN (Antitoxic nutrient) is a fine powder containing mostly zeolitic ore (with > 90% of clinoptilolite) and bentonite (with > 83% of montmorillonite), together with small amounts of activated charcoal (ratio 60:20:1/zeolite:bentonite:charcoal). The experimental protocol was approved by Ethics Committee on Animal Use of the University of Novi Sad.

Blood sampling and slaughter

When the chicks reached 3 weeks of age, the feeding trial was terminated and all broilers were bled by cardiac puncture. Heparin was used as an anticoagulant and non-coagulated blood was used for separation of

erythrocytes. Hemoglobin (Hb) concentration in red blood cells was determined by the cyanmethemoglobin procedure [45]. Blood samples (20 μ L) were mixed with 5 mL Drabkin's solution (0.1% sodium bicarbonate, 0.005% potassium cyanide, and 0.02% potassium ferricyanide) for Hb determination. All 84 broilers were sacrificed by cervical dislocation and liver, spleen, and pancreas were removed and weighted. Homogenates of these organs with phosphate buffer (pH=7.0) were used for further biochemical analysis. Samples were homogenized with using a MiniBatch D-15 homogenizer (MICCRA GmbH, Müllheim, Germany).

Biochemical analysis

Activity of alkaline phosphatase (ALP), alanine aminotransferase (ALT), γ -glutamyltransferase (GGT), and α -amylase (AMY) in liver homogenate were determined on a clinical chemistry analyzer (Microlab 200, Merck) according to the manufacturer's recommended procedure.

The antioxidant enzyme activity of superoxide dismutase (SOD-1), catalase (CAT), guaiacol peroxidase (GPx), pyrogallol peroxidase (PPx), and malondialdehyde (MDA) level was determined from erythrocytes, liver, spleen and pancreas. Glutathione S-transferase (GST) activity was evaluated in erythrocytes and liver homogenate. Protein content in homogenate of liver, spleen, and pancreas were determined according to the method of Bradford [46], using bovine serum albumin as the protein standard. SOD-1 activity was determined in samples according to the method of Mandal et al. [47] slightly modified by measuring its ability to inhibit photochemical reduction of nitro blue tetrazolium (NBT) chloride. The reaction mixture contained 50 mM phosphate buffer (pH 7.8), 13 mM L-methionine, 75 μ M NBT, 0.1mM EDTA, 2 μ M riboflavin and 20 μ L of the enzyme extract. It was kept under a fluorescent lamp for 30 min, and the absorbance was read at 560 nm. One unit of the SOD-1 activity was defined as the amount of enzymes required to inhibit reduction of NBT by 50%. The activity of the enzyme was expressed in IU/mg of protein. The CAT activity was assayed by the method of Aebi [48]. The utilization of hydrogen peroxide by CAT in the samples was measured spectrophotometrically. The decomposition of H_2O_2 was followed as a decrease in absorbance at 240 nm. The enzyme extract (20-100 μ L) was added to the assay mixture containing 1 mL of 50 mM potassium phosphate buffer (pH 7.0) and 10 mM H_2O_2 . GPx activity was measured by following the H_2O_2 depend oxidation of guaiacol at 470 nm [49]. This method consists of an assay of tetraguaiacol - a colored product of guaiacol oxidation in the investigated sample. The enzyme extract (40 μ L) was added to the assay mixture containing 3 mL of 20 μ M guaiacol and 20 μ L of 3 mM H_2O_2 .

The absorbance was recorded at 436 nm. The activity of PPx was measured using pyrogallol as the substrate according to Murtic et al. [50]. This method is based on the measurement of the content of purpurogallin - a product of pyrogallol oxidation. The enzyme extract (20 μ L) was added to the assay mixture containing 3 mL of 180 mM pyrogallol and 20 μ L of 2 mM H₂O₂. The absorbance was recorded at 430 nm. GST activity in samples was evaluated using 1-chloro-2,4-dinitrobenzene (CDNB) as substrate as previously described by Habig et al. [51]. The formation of adduct of GSH-CDNB (2,4-dinitrophenyl glutathione) was monitored by estimation of the increase in absorbance at 340 nm against a blank with a spectrophotometer. The reaction mixture consisted of 33 mM Hepes buffer (pH 7.5), 1.5 mM GSH, 1.5 mM CDBN, and water in a total volume of 1 mL. The activity of the enzymes was expressed in IU/mg of protein.

The MDA level (as a measure of lipid peroxidation (LP) intensity) was analyzed with 2-thiobarbituric acid, monitoring the change of absorbance at 532 nm with the spectrophotometer [47]. The enzyme extract (0.5 mL) was incubated with 2 mL of 20% trichloroacetic acid (TCA) containing 0.5% thiobarbituric acid for 40 min at 95° C. The reaction was stopped by cooling on ice for 10 min and the product was centrifuged at 10.000 \times g for 15 min. The total amount of TBA-reactive substances was expressed as nmol MDA/mg protein.

Statistical analysis

Results were expressed as mean of determinations \pm standard error (SE). Statistical significance was tested by analysis of variance followed by comparison of means by Duncan's multiple range test ($P < 0.05$) calculated using STATISTICA for Windows version 13.0 (StatSoft, Tulsa, OK, USA). Stepwise multiple regression analyses were used to determine correlation among variables.

ACKNOWLEDGMENTS

This work was supported by the Ministry of Education, Science and Technological Development of the Republic of Serbia (grant number 451-03-68/2022-14/200117)

REFERENCES

1. L. Shvachiy; Â. Amaro-Leal; T.F. Outeiro; I. Rocha; V. Geraldese; *Bioogy.*, **2022**, 11, 1164
2. S.M. Shawky; S.G.A. Ramadan; S.H. Orabi; *Int. J. Adv. Res.*, **2014**, 2, 418-429
3. A. Kumar; A. Kumar; M.M.S. Cabral-Pinto; A.K. Chaturvedi; A.A. Shabnam; G. Subrahmanyam; R. Mondal; D.K. Gupta; S.K. Malyan; S.S. Kumar; S.A. Khan; K.K. Yadav; *Int. J. Environ. Res. Public Health*, **2020**, 17, 2179
4. S. Sharma; V. Sharma; R. Paliwal; Pracheta; *Int. J. Biotechnol. Mol. Biol. Res.*, **2011**, 2, 214-221
5. M. Andjelkovic; A. Buha Djordjevic; E. Antonijevec; B. Antonijevec; M. Stanic; J. Kotur-Stevuljevic; V. Spasojevic-Kalimanovska; M. Jovanovic; N. Boricic; D. Wallace; Z. Bulat; *Int. J. Environ. Res. Public Health*, **2019**, 16, 274
6. N. Haleagrahara; S. Chakravarthi; A.B. Kulur; A. Radhakrishnan; *Afr. J. Pharm. Pharmacol.*, **2011**, 5, 923-929
7. M.H. Karimfar; A. Bargahi; D. Moshtaghi; P. Farzadinia; *Iran Red Crescent Med. J.*, **2016**, 18, e22157
8. S.B. Sainath; R. Meena; Ch. Supriya; K. Pratap Reddy; P. Sreenivasula Reddy; *Eniron. Toxicol. Pharmac.*, **2011**, 32, 146-154
9. F.A. Mumpton; *Proc. Natl. Acad. Sci USA*, **1999**, 96,3463-3470
10. N. Stanković; M. Logar; J. Luković; J. Pantić; M. Miljević; B. Babić; A.R. Mihajlović; *Process. Appl. Ceramic.*, **2011**, 5, 97-101
11. S. Kraljević Pavelić; J. Simović Medica; D. Gumbarević; A. Filošević; N. Pržulj; K. Pavelić; *Front. Pharmacol.*, **2018**, 9, 1350
12. T. Suponik; M. Lutyński; *Arch. Min. Sci.*, **2013**, 58, 1263-1278
13. M. Beltcheva; R. Metcheva; M. Topashka-Ancheva; N. Popov; S. Teodorova; J.A. Heredia-Rojas; A.O. Rodriguez-de la Fuente; L.E. Rodriguez-Flores; *J. Bioequiv. Availab.*, **2015**, 7, 12-29
14. J. Tangpong; S. Satarug; *Toxicol. Lett.*, **2010**, 198, 83-88
15. S.J.S. Flora; P. Gautam; P. Kushwaha; *Alcohol Alcoholism*, **2012**, 47, 92-101
16. H. Choi; S.Y. Ji; H. Jo; M. Song; B.G. Kim; *Anim. Biosci.*, **2021**, 1, 102-108
17. H.M. Hassim; A.A. Hassan; *Iraqi J. Vet. Sci.*, **2011**, 25, 1-7
18. J. Biesek; M. Banaszak; K. Kądziołka; S. Wlazlak; M. Adamski; *Sci. Rep.*, **2022**, 12, 20425
19. M. Banaszak; J. Biesek; M. Adamski; *Vet. Res. Comm.*, **2022**, 46, 37-47
20. D. Prvulović; D. Kojić; G. Grubor-Lajšić; S. Košarčić; *Turk. J. Vet. Anim. Sci.*, **2008**, 32, 183-189
21. C.A. Bailey; G.W. Latimer; A.C. Barr; W.L. Wigle; A.U. Haq; J.E. Balthrop; L.F. Kubena; *J. Appl. Poult. Res.*, **2006**, 15, 198-206
22. A. Domato; F. Vianello; E. Novelli; S. Balzan; M. Ganesella; E. Giaretta; G. Gabai; *Front. Vet. Sci.*, **2022**, 9, 998612
23. O.B. Ilesanmi; E.F. Adeogun; T.T. Odewale; B. Chikere; *Environ. Anal. Health Toxicol.*, **2022**, 37, e2022007
24. M.S. El-Neweshy; Y.S. El-Sayed; *Exp. Toxicol. Pathol.*, **2011**, 63, 221-227

25. K. Ognik; M. Krauze; *World. Poult. Sci. J.*, **2016**, 72, 535-550
26. M. Kohsari; M. Moradinazar; Z. Rahimi; Y. Pasdar; E. Shakiba; *BioMed Res. Int.*, **2021**, 2021, 5584452
27. G. Ndrepepa; A. Kastrati; *J. Lab. Precis. Med.*, **2019**, 4, 29
28. H. Ochiai; T. Shirasawa; T. Yoshimoto; S. Nagahama; A. Watanabe; K. Sakamoto; A. Kokaze; *BMC Nephrol.*, **2020**, 21, 471
29. D.C. Diaz T.; W.O. Regino; M.G. Zuleta; *Rev. Col. Gastroenterol.*, **2015**, 30, 475-479
30. E.E. Mehana; A.R.M.A. Meki; K.M. Fazli; *Exp. Toxicol. Pathol.*, **2012**, 64, 291-295
31. R.M. Ahmed; A.K. Mohammed; *World Vet. J.*, **2022**, 12, 323-329
32. H.M. Abdou; A.A. Newairy; *J. Med. Res. Inst.*, **2006**, 27, 295-302
33. D. Prvulović; A. Jovanović-Galović; B. Stanić; M. Popović; G. Grubor-Lajšić; *Czech J. Anim. Sci.*, **2007**, 52, 159-164
34. D. Prvulović; S. Košarčić; M. Popović; G. Grubor-Lajšić; *Cuban J. Agric. Sci.*, **2009**, 43, 59-63
35. D. Prvulović; S. Košarčić; M. Popović; D. Dimitrijević; G. Grubor-Lajšić; *J. Anim. Vet. Adv.*, **2012**, 11, 134-140
36. R. Sivaprasad; M. Nagaraj; J. Varalakshmi; *Hum. Exp. Toxicol.*, **2003**, 22, 183-192
37. Y. Wang; R. Branicky; A. Noë; S. Hekimi; *J. Cell Biol.*, **2018**, 217, 1915-1928
38. D. Prvulović; M. Popović; D. Kojić; G. Grubor-Lajšić; *Studia UBB Chemia*, **2014**, 59, 51-62
39. C. Wang; J. Liang; C. Zhang; Y. Bi; X. Shi; Q. Shi; *Ann. Occup. Hyg.*, **2007**, 51, 563-569
40. T.L. Wang; T.H. Kao; B. Stephen Inbaraj; Y.T. Su; B.H. Chen; *J. Agric. Food Chem.*, **2010**, 58, 12562-12567
41. T. Permpongpaiboon; A. Nagila; P. Pidetcha; K. Tuangmungsakulchai; S. Tantrarongroj; S. Porntadavity; *Hum. Exp. Toxicol.*, **2011**, 30, 1196-1203
42. A.A. Khaki; A. Khaki; *J. Med. Plant Res.*, **2010**, 4, 1492-1495
43. F. Muselin; A. Trif; D. Brezovan; A. Stancu; S. Petrovici; *Lucrări Științifice Medicină Veterinară*, **2010**, 43, 123-127
44. D. Prvulović; D. Kojić; M. Popović; G. Grubor-Lajšić; *Thai J. Vet. Med.*, **2015**, 45, 255-261
45. W.I. Leong; C.L. Bowlus; J. Tallkvist; B. Lonnerdal; *Am. J. Physiol. Gastrointestin. Liver Physiol.*, **2003**, 285, 1153-1161
46. M.M. Bradford; *Anal. Biochem.*, **1976**, 72, 248-254
47. S. Mandal; A. Mitra; N. Malick; *Physiol. Mol. Plant Pathol.*, **2008**, 72, 56-61
48. H. Aebi; *Meth. Enzymol.*, **1984**, 105, 121-126
49. P. Agrawal; M.M. Laloraya; *Biochem. J.*, **1977**, 166, 205-208
50. S. Murtic; R. Oljaca; M.S. Murtic; I. Koleska; A. Muhic; *J. Anim. Plant Sci.*, **2019**, 29, 1664-1672
51. W.H. Habig; M.J. Pabst; W.B. Jakoby; *J. Biol. Chem.*, **1974**, 249, 7130-7139

PARTIAL DESULFURIZATION OF CRUMB RUBBER IN THE PRESENCE OF METALLIC OXIDES

Luiza-Andreea MÎRȚ^a, Dorin BOMBOȘ^{b,c,*}, Simona GHIMIȘ^a,
Mihaela Mariana BOMBOȘ^b, Gabriel VASILIEVICI^a

ABSTRACT. Sulfur has been used for a long time as a vulcanizing agent for polybutadiene and polyisoprene rubber. The presence of sulfur in the used crumb rubber powder reduces its dispersion in the bitumen and favors its separation from the colloidal structure of the bitumen. For this reason, it does not allow the use of this waste to modify the road bitumen. In this paper, the desulfurization of used crumb rubber is studied by reactive adsorption in the presence of metal oxide adsorbents in pulverized form. Metal oxide adsorbents were prepared based on Fe, Cu and a mixture of the two metal oxides with a bimodal particle size distribution and an average particle diameter between 500 and 800 nm, by the sol-gel precipitation method, in the presence of a Pluronic® surfactant. The morphology of the prepared adsorbents was investigated by Dynamic Light Scattering (DLS), Scanning Electron Microscopy (SEM) and nitrogen porosimetry analyses (BET method). The desulfurization of crumb rubber experiments was carried out in a high-pressure Parr stainless steel reactor with electric heating and stirring in an inert gas atmosphere (nitrogen). The conversion in the desulfurization process of vulcanized rubber was influenced both by the size of the adsorbent particles and also by the nature of the adsorbent.

Keywords: *crumb rubber, desulfurization, adsorbents, sol-gel method, metallic oxides*

^a National Institute for Research Development for Chemistry and Petrochemistry-ICECHIM-București, 202 Spl. Independenței, 060021, Bucharest, Romania.

^b ATICA Chemicals SRL, 202 Căzănești str., Râmnicu Vâlcea, 240414, Vâlcea, Romania.

^c Petroleum-Gas University of Ploiești, 39 Bucuresti Blvd., 100680, Ploiești, Romania.

* Corresponding author: bombos.dorin@gmail.com



INTRODUCTION

Numerous methods, adsorbents and catalysts are used to remove sulfur compounds from various products. The usual methods for desulfurization are hydrodesulfurization, extractive desulfurization, oxidative desulfurization, chlorination desulfurization, electrochemical desulfurization, pervaporation desulfurization, alkylation desulfurization, and bio-desulfurization [1-3].

At an industrial level, desulfurization is carried out in the refining processes of petroleum products, through hydrodesulfurization processes on catalysts based on transition metals such as Ni-Mo and Co-Mo. In many recent works [4-14] it was mentioned the need to reduce the high content of sulfur in petroleum products that generate a wide range of problems (poisoning for catalysts, corrosive agents, polluting the environment, etc.).

The hydrodesulfurization process was studied using molybdenum catalysts, promoted with cobalt or nickel, thus obtaining a reduction in the sulfur content. The selection and use of various active catalysts that allow obtaining clean fuels, with as little sulfur content as possible, would be one of the ways to improve fuel quality along with other aspects (the quality of the raw material subjected to desulfurization, working conditions, changes in fuel properties, contamination during transport and delivery to consumers).

Organosulfur compounds react in the presence of a catalyst and are transformed into hydrogen sulfide and organic compounds without sulfur. Standard hydrodesulfurization catalysts are Ni-Mo/Al₂O₃ and Co-Mo/Al₂O₃ [15], but there are several types of guard catalysts or adsorbents available. During hydrodesulfurization, sulfur from organosulfur compounds is transformed into H₂S. The choice of a type of catalyst is dependent on the requirement. In general, Ni-Mo catalysts are used for hydrogenation, while Co-Mo ones are efficient for hydrogenolysis [16]. Hydrotreating conditions usually vary: temperatures from 200 to 425°C and pressure between 1-18 MPa, and the conditions depend on the degree of desulfurization required and the nature of the sulfur compounds in the feed. Aliphatic sulfur compounds are very reactive and can be completely removed during hydrodesulfurization [17].

Desulfurization by adsorption can remove sulfur compounds by physical adsorption or chemisorption [18]. The adsorption process using porous forms of modified adsorbents can be an excellent desulfurization technique. It is expected that the classic adsorption process will present a selective removal of sulfur compounds under normal conditions, which facilitates the control of the process and allows the removal of sulfur compounds at much lower costs. The easy regeneration of the adsorbent material with a minimum of chemical and energetic effort is essential for the use of this technology.

In specialized literature, numerous adsorbents are mentioned, some successful and others unsatisfactory [16, 19]. Adsorbents impregnated with transition metals such as nickel, iron, copper, zinc, palladium are considered effective in removing sulfur compounds. In the studies carried out for numerous separation or purification processes including industrial applications, solid adsorbents were used, such as activated carbon, zeolites, membranes impregnated with silver, polymeric adsorbents, etc. These substances were used due to their large surfaces and good adsorption capacity. The availability for commercial use of numerous adsorbent substances with different adsorption capacities and with various porous structures makes a careful selection of the best variants necessary. The selection of the present adsorbents was made considering polarity interactions to obtain improvements in desulfurization performance [20].

Reactive adsorption [21] is a mixed desulfurization method that combines the hydrodesulfurization process with the adsorption process. In the case of this process, metals are used as catalysts, such as nickel on aluminum oxide or other metal oxides in the presence of hydrogen. The metal catalyst reacts with the sulfur forming metal sulfides and fixes the sulfur on the surface by chemisorption. In the case of this reaction, only sulfur atoms are adsorbed on the adsorbent surface, while molecules of organic compounds are not adsorbed. Desulfurization by reactive adsorption is a promising method, but it has certain shortcomings regarding the removal of sulfur, due to the difficulty in removing sulfur compounds with high resistance to desulfurization, also since the interaction that the compounds have is still not well known with sulfur with an adsorbent surface, which plays a crucial role in their elimination. This implies an improvement of the knowledge regarding the adsorption behavior of different compounds with sulfur on different adsorbent surfaces and the size and effectiveness of new materials used in intensive desulfurization [22].

Studies were carried out to analyze the parameters (temperature, pressure and contact time of the adsorption process) using Ni as a sorbent [23]. The removal of sulfur by means of Ni-based sorbents is in principle feasible both for products with a high content of sulfur and for those with low content. The optimal temperature range for this process is between 200-220°C when a degree of desulfurization < 0.2 ppm is obtained and varies depending on the contact time. Therefore, desulfurization with Ni sorbent is suitable and adaptable for all desulfurization processes [24]. If the process takes place at high temperatures of 200°C, the organic compound must be properly pressurized to avoid evaporation. The determination of the optimal operating conditions demonstrated that the process of desulfurization by adsorption using nickel-based adsorbents is independent of the pressure in the system but is strongly influenced by the contact time and temperature.

Adsorbent desulfurization takes place through the same mechanism as in the case of hydrodesulfurization. The difference between the two processes lies in the supply of hydrogen; during the adsorption process there is an internal supply of hydrogen, while in the case of hydrodesulfurization there is an external supply [21]. Desulfurization by adsorption depends on the ability of a solid sorbent to selectively adsorb organosulfur compounds from petroleum. The efficiency of this method depends on the properties of the adsorbent material: selectivity to organosulfur compounds, hydrocarbon-related compounds, adsorption capacity, durability, and regeneration. There are two approaches that can be considered for desulfurization by adsorption: i) physical adsorption, in case the sulfur compounds are chemically unchanged after separation; ii) reactive adsorption, which involves a chemical reaction between organosulfur compounds and a solid surface sorbent. Sulfur is usually attached to the adsorbent in the form of sulfide. Regeneration of the adsorbent can be done thermally, or by washing the adsorbent deposited on the desorbent. Sulfur is usually removed as H_2S , SO_x or elemental sulfur, depending on the process and the nature of the raw materials [25].

A variety of adsorbent materials have been evaluated for desulfurization such as activated carbon, zeolites, amorphous silica-alumina, and organometallic compounds (MF). Sorbents were evaluated for the desulfurization of model petroleum fractions, raw materials for fluidized bed catalytic cracking, the naphtha fraction from coking and petroleum distillates [26-28]. Despite the studies on desulfurization that were carried out under mild reaction conditions, in the laboratory and in pilot plants, the performances are still insufficient for industrial applications even in the case of the most effective results of the adsorbents.

Sulfur has been used for a long time as a vulcanizing agent for polybutadiene and polyisoprene rubber. The presence of sulfur in the used rubber powder reduces its dispersion in the bitumen and for this reason it does not allow the use of this powder to modify the road bitumen [19, 29]. In this paper, the desulfurization of used rubber powder is studied by reactive adsorption in the presence of metal oxide adsorbents in pulverized form.

RESULTS AND DISCUSSION

The results of the DLS analysis for the synthesized adsorbents are presented in figures 1-3 and Table 1. The adsorbents have a bimodal polydisperse dimensional distribution, with aggregated particles, with reproducible measurements. The FeO adsorbent has the smallest average particle size ($D_m=509$ nm) and the FeO-CuO bimetallic adsorbent has the largest average particle size ($D_m=816$ nm).

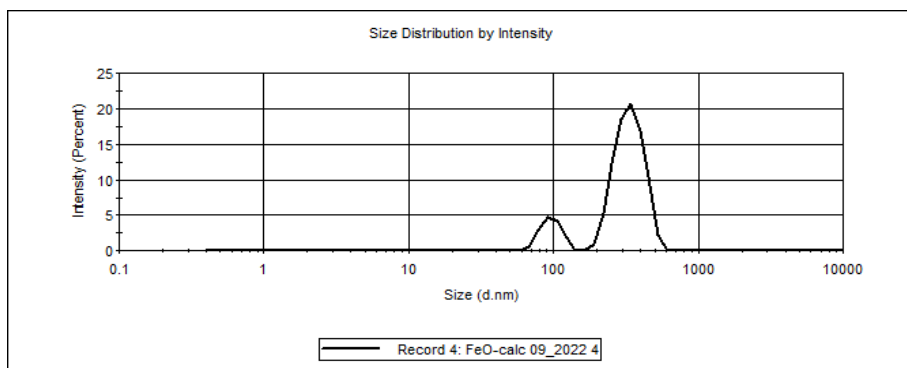


Figure 1. DLS distribution of particle sizes for FeO adsorbent

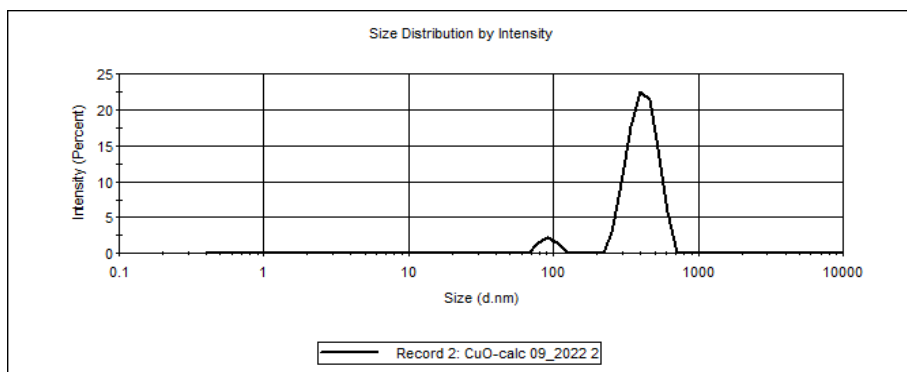


Figure 2. DLS distribution of particle sizes for CuO adsorbent

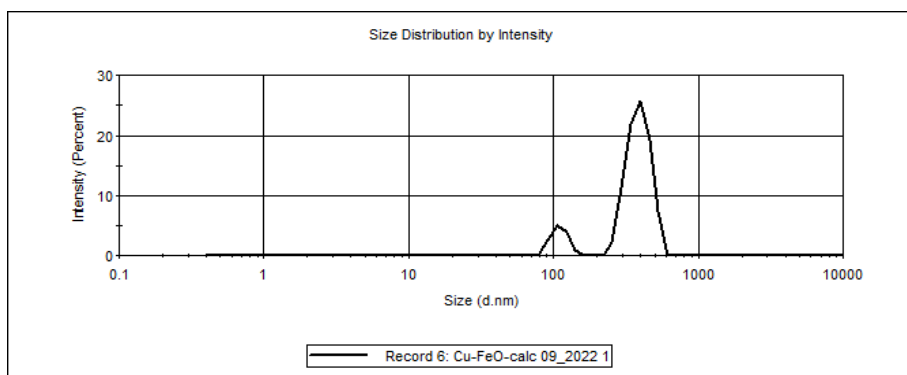


Figure 3. DLS distribution of particle sizes for FeO-CuO adsorbent

Table 1. DLS analysis results for the synthesized adsorbents

Sample	Dm (nm)	Pdl	Peak Intensity (nm)
FeO	509	0.627	P ₁ = 338; P ₂ = 96
CuO	595	0.460	P ₁ = 420; P ₂ = 95
FeO-CuO	816	0.681	P ₁ = 391; P ₂ = 111

The main textural characteristics of the adsorbents are presented in Table 2. The average pore size of the synthesized adsorbents (7.8-20.1 nm) classifies the analysed adsorbents as mesoporous materials.

Table 2. The results of the porosimetry analysis (BET) for the synthesized adsorbents

Sample	Specific surface (m ² /g)	Total pore volume (cm ³ /g)	Average pore diameter (nm)
FeO	30.18	0.1518	20.12
CuO	42.78	0.0084	7.862
FeO-CuO	45.61	0.1161	10.18

The obtained adsorption isotherms and BJH desorption are shown in figures 4-6. The adsorption isotherms are type II, exhibiting an H3-type hysteresis, meaning that they show no adsorption limitation at a high p/p₀ level. This type of isotherm usually appears in the case of particles in the form of plates, having pores in the form of slits [30].

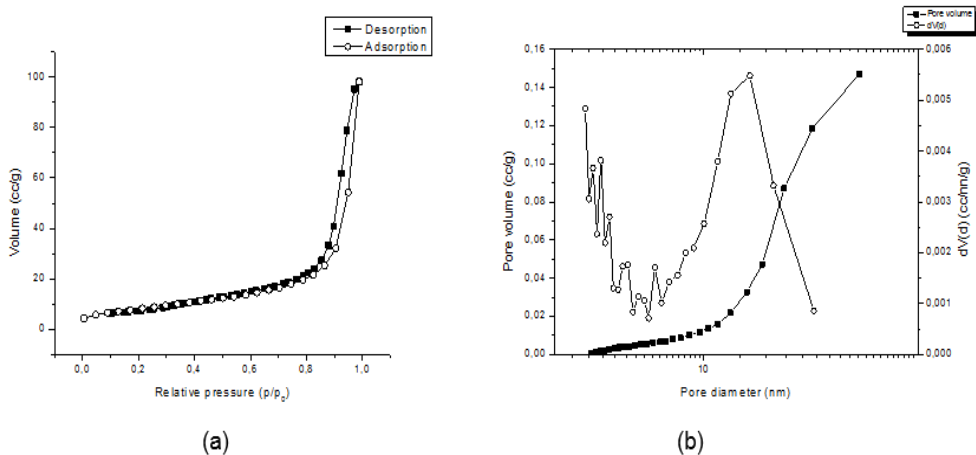


Figure 4. Isotherm (a) and BJH desorption (b) of FeO adsorbent

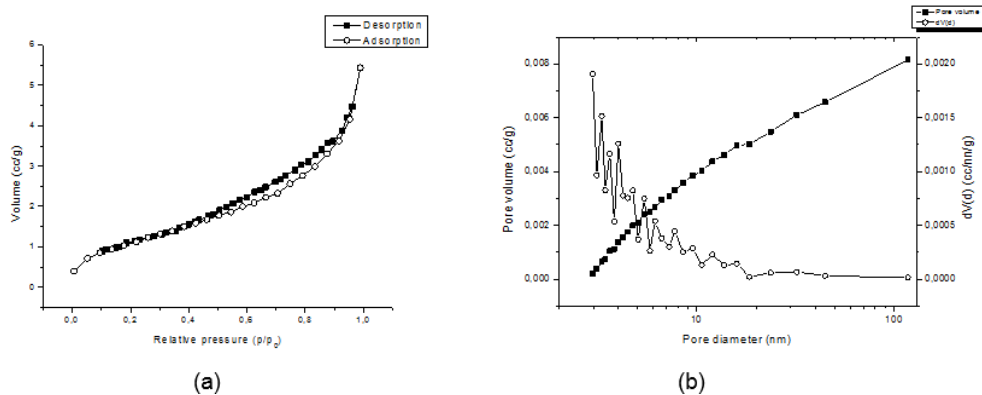


Figure 5. Isotherm(a) and BJH desorption (b) of CuO adsorbent

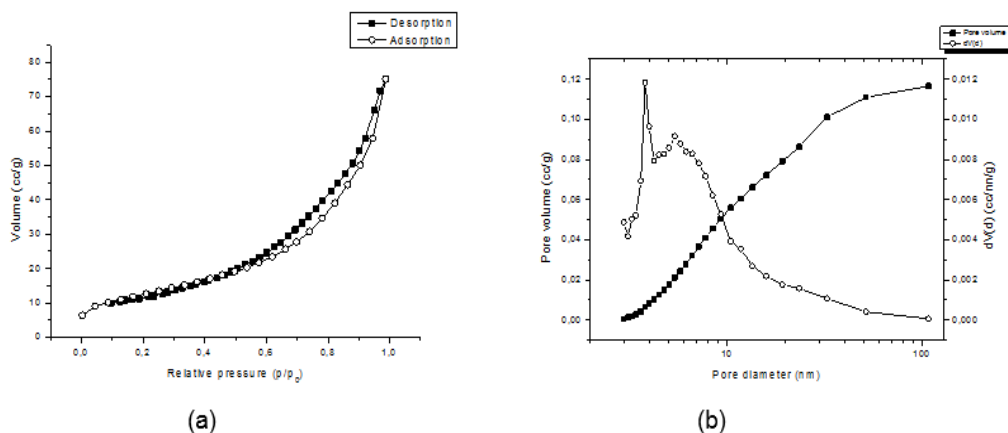
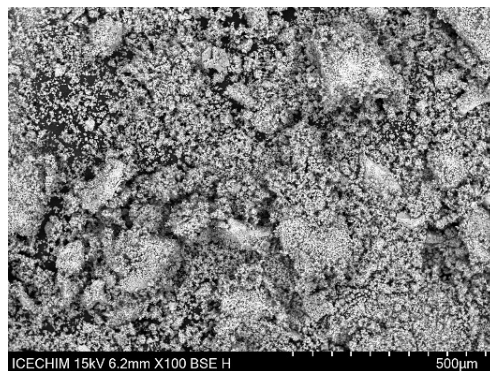
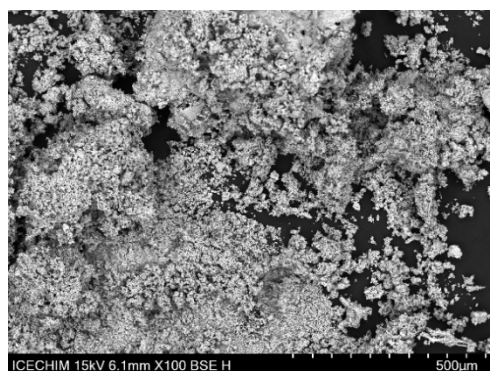


Figure 6. Isotherm (a) and BJH desorption (b) of FeO-CuO adsorbent

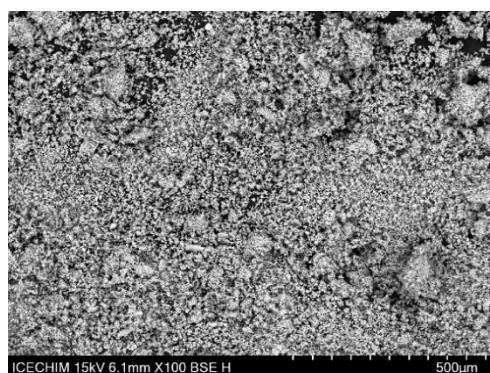
SEM images of adsorbents show a similar morphology of the samples (Figure 7.) with a large distribution of particle dimensions. The particles form dense agglomerations, with the largest aggregate sizes in the case of FeO (Figure 7. (a)).



(a)



(b)



(c)

Figure 7. SEM images of the (a) FeO; (b) CuO; (c) FeO-CuO

Conversion in the desulfurization process of vulcanized crumb rubber in the presence of synthetic adsorbents was calculated with equation (1), based on the total sulfur content of the crumb rubber before and after experiments. The results are presented in Table 3.

Table 3. Conversion of devulcanization of crumb rubber with synthesized adsorbents

Time, h	Conversion, %		
	FeO	CuO	FeO-CuO
0	0	0	0
2	55.13	48.68	42.35
4	81.47	72.02	62.78
6	93.43	87.04	78.64

The highest conversion (93.43%) was obtained with FeO after 6 hours of reaction in the presence of FeO adsorbent, being 6.39% higher than the CuO adsorbent and 14.79% higher than the FeO-CuO adsorbent.

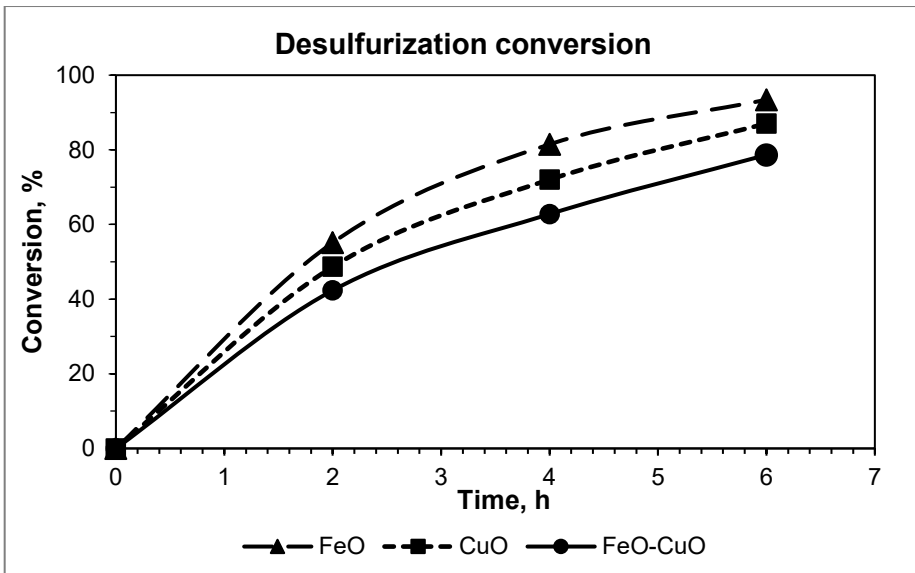


Figure 8. Conversion of crumb rubber desulfurization with synthesized adsorbents

CONCLUSIONS

Metal oxide adsorbents were prepared based on Fe, Cu, and a mixture of the two metal oxides with a bimodal particle size distribution and an average particle diameter between 509 and 816 nm, by the sol-gel precipitation method, in the presence of a Pluronic® surfactant.

The morphology of the prepared adsorbents was investigated by Dynamic Light Scattering (DLS), Scanning, Electron Microscopy (SEM) and nitrogen porosimetry analyses (BET method).

The desulfurization of crumb rubber experiments was carried out in a high-pressure Parr stainless steel reactor with electric heating and stirring in an inert gas atmosphere (nitrogen 5.0).

The adsorbents have a bimodal polydisperse dimensional distribution, with aggregated particles. The FeO adsorbent has the smallest average particle size and the FeO-CuO bimetallic adsorbent has the largest average particle size.

The average pore size of the synthesized adsorbents classifies the analysed adsorbents as mesoporous materials and the adsorption isotherms are type II, exhibiting an H3-type hysteresis, which appears in the case of particles in the form of plates, having pores in the form of slits.

SEM images of adsorbents show a similar morphology of the samples with a large distribution of particle dimensions in which the particles form dense agglomerations, with the largest aggregate sizes in the case of FeO

The conversion in the desulfurization process of vulcanized crumb rubber was influenced both by the size of the adsorbent particles and also by the nature of the adsorbent.

EXPERIMENTAL SECTION

Materials

In the experimental program it was used crumb rubber obtained from waste tires with a bulk density of 418 kg/m³ and an average particle diameter of 0.31-0.80 mm.

All the chemicals were of analytical grade and used as received: Copper (II) nitrate trihydrate (Cu(NO₃)₂·3H₂O) and Iron (III) nitrate nonahydrate (Fe(NO₃)₂·9H₂O) were purchased from Scharlau. Pluronic® P123 was acquired from Sigma Aldrich, absolute ethanol (EtOH) was acquired from Chemical Company (Romania), and Xylene (mixture of o-, m-, p-xylene) was purchased from Chimreactiv SRL (Romania). The 3% hydrogen peroxide solution and sodium carbonate were acquired from Chimreactiv SRL (Romania).

Synthesis of adsorbents

Three adsorbents based on copper and/or iron oxide were prepared by the sol-gel method. The method was adapted from the work of A. Moatti et al. [31] of obtaining catalysts by the sol-gel method. The metal nitrate precursor(s) along with the necessary distilled water is added to a beaker and stirred until the copper and/or iron nitrate is completely dissolved. Ethanol is gradually added over the surfactant (Pluronic®) and stirred until it is completely dissolved in the alcohol, then incorporated with the metal nitrate solution. The resulting mixture is heated to 40°C and stirred continuously for 70 min. The solvent was partially evaporated in a rotary evaporator, and the samples were transferred to an oven and dried at 60°C for 48 h under static conditions. The resulting dried gels were calcined at 400°C for 6 h in an oven at a heating rate of 1°C/min. Table 4 shows the quantities needed to obtain the three adsorbents used in the experimental part.

Table 4. Data required for the preparation of sol-gel adsorbents

Adsorbent code	Reagents	Quantity of the product obtained after the calcination
FeO	20 g Fe(NO ₃) ₂ ·9H ₂ O 0.30 g Pluronic® P123 100 mL EtOH 16 mL distilled water	6.6 g
CuO	20 g Cu(NO ₃) ₂ ·3H ₂ O 0.30 g Pluronic® P123 100 mL EtOH 16 mL distilled water	6.2 g
FeO-CuO	20 g Fe(NO ₃) ₂ ·9H ₂ O 12 g Cu(NO ₃) ₂ ·3H ₂ O 0.48 g Pluronic® P123 150 mL EtOH 26 mL distilled water	7.7 g

Characterization Methods

The morphology of the prepared adsorbents was investigated by Dynamic Light Scattering (DLS), Scanning Electron Microscopy (SEM) and nitrogen porosimetry analyses (BET method).

Measurement System of Particles Dimensions by Dynamic Light Scattering using a Nano ZS Zetasizer (Malvern Inst., UK). The average diameter of the dispersed adsorbents particles and the polydispersity index (PDI) were

calculated using the software of the instrument. The data were obtained as mean values in automatic mode from multiple measurements. For all samples, dilution was made as follows: 0.002 g of the sample dispersed in 25 mL of distilled water. Before being analyzed, the samples were ultrasonicated for 10 minutes in an ultrasound bath.

SEM images were recorded on a Hitachi TM4000plus II equipment with BSE detector, vacuum – conductor; accelerating voltage 15 kV, and magnification 100x. The samples were deposited on carbon tape.

Textural characteristics of the adsorbents (surface area, pore volume, average pore diameter, pore size distribution) were determined on a NOVA 2200e-Quantachrome Analyzer (Quantachrome Instruments, USA). Data processing was performed using NovaWin version 11.03 software. The specific surface area was calculated from the linear portion of the adsorption isotherm using the BET (Brunauer-Emmett-Teller) equation. The total pore volume was estimated from the amount of N₂ adsorbed at the relative pressure $p/p_0 \sim 0.9$. The pore size distribution was obtained from the desorption branch of the isotherm by applying the BJH (Barrett-Joyner-Halenda) method. All samples were initially degassed under vacuum at 160°C, for 4 h.

The total sulfur content (TSC) of crumb rubber was determined by the quartz tube combustion method (Grote method). The principle of the method consists in burning a sample of the product to be analyzed in a quartz tube in a stream of air at a high temperature, over 800°C, when the component elements of the sample are oxidized to carbon dioxide, water, and sulfur dioxide. The resulting combustion gases are bubbled in a 3% hydrogen peroxide solution, transforming sulfur dioxide into sulfuric acid, which is titrated with sodium carbonate solution n/100, in the presence of methyl orange.

Desulfurization experiments

The desulfurization of crumb rubber experiments was carried out in a high-pressure Parr stainless steel reactor with electric heating and stirring in an inert gas atmosphere (nitrogen 5.0). The xylene/crumb rubber/adsorbent mass ratio was 100/3/1. The volume of the reactor is 1 liter, and the reaction mass was 400 mL. The temperature program was heating with 10°C/min up to 280°C and maintaining the temperature for 2, 4 or 6 hours.

After carrying out the desulfurization experiments, the crumb rubber was separated from the solvent by settling. The residual solvent was removed by heating to 80°C in a vacuum oven until constant mass. In order to determine the conversion, the total sulfur content of the crumb rubber was determined before experiments and after the progress of the reaction for each adsorbent (FeO, CuO and Fe-CuO). The conversion was calculated from the total sulfur content of samples after desulfurization using the equation (1):

$$\text{Conversion, \%} = \frac{TSC_i - TSC}{TSC_i} \times 100 \quad (1)$$

TSC_i = initial total sulfur content of crumb rubber;

TSC = total sulfur content of crumb rubber after experiments of desulfurization.

ACKNOWLEDGMENTS

This work was supported by a grant of the Ministry of Research, Innovation and Digitization, CCCDI - UEFISCDI, project number PN-III-P2-2.1-PTE-2021-0552, within PNC DI III.

REFERENCES

1. M.N. Hossain, H. Park, H. Choi; *Catal.*, **2019**, 9(3).
2. M.N. Hossain, M.K. Choi, H.S. Choi; *Catal.*, **2021**, 11(7).
3. H.M. Ashoshan; Memorial University of Newfoundland, **2022**.
4. A. Stanislaus, A. Marafi, M.S. Rana; *Catal. Today*, **2010**, 153(1-2), 1-68.
5. G.I. Danmaliki, T.A. Saleh; *J. Clean. Prod.*, **2016**, 117, 50-55.
6. V.C. Srivastava; *RSC Adv.*, **2012**, 2(3), 759-783.
7. S.P. Hernandez, D. Fino, N. Russo; *Chem. Eng. Sci.*, **2010**, 65(1), 603-609.
8. I. Ali, T.A. Saleh; *Inorg. Chem. Commun*, **2022**, 138, 109237.
9. B.S. Huang, W.F. Yin, D.H. Sang, Z.Y. Jiang; *Appl. Surf. Sci.*, **2012**, 259, 664-670.
10. P.P. Alvisi, V.F.C. Lins; *Eng. Fail. Anal.*, **2011**, 18(5), 1403-1406.
11. J.H. Kim, X. Ma, A. Zhou, C. Song; *Catal. Today*, **2006**, 111(1-2), 74-83.
12. I. Ali, T.A. Saleh; *Appl. Catal. A. Gen.*, **2020**, 598, 117542.
13. T.A. Saleh; *Environ. Technol. Innov.*, **2021**, 24, 101821.
14. T.A. Saleh; *Environ. Technol. Innov.*, **2020**, 20, 101067.
15. H. Topsøe; B.S. Clausen; F. Massoth; *Fuel sci. technol. int.*, **1996**, 11, 1-310.
16. T.A. Saleh; *J. Mol. Liq.*, **2022**, 359, 119340.
17. R. Javadli, A. de Klerk; *Appl. Petrochem. Res.*, **2012**, 1(1-4), 3-19.
18. G.G. Zeelani, S.L. Pal; *Int. J. Sci. Res.*, **2016**, 5(5), 2413-2419.
19. A. Tanimu, K. Alhooshani; *Energy Fuels*, **2019** 33(4), 2810-2838.
20. S.V. Patil, L.G. Sorokhaibam; V.M. Bhandari, D.J. Killedar; V.V. Ranade; *J. Environ. Chem. Eng.*, **2014**, 2, 1495-1505.
21. O. van Rheinberg, K. Lucka, H. Köhne; *J. Power Sources*, **2011** 196(21), 8983-8993.
22. O.V. Golubev, H. Zhou, E.A. Karakhanov; *Russ. J. Appl. Chem.*, **2021**, 94(5), 586-594.

23. C. Sentorun-Shalaby, S.K. Saha, X. Ma, C. Song; *Appl. Catal. B*, **2011**, 101(3-4), 718-726.
24. X. Ma, M. Sprague, C. Song; *Ind. Eng. Chem. Res.*, **2005**, 44, 5768-5775.
25. I.V. Babich; J.A. Moulijn; *Fuel.*, **2003**, 82, 607-631.
26. A.B.S.H. . Salem; *Ind. Eng. Chem. Res.*, **1994**, 33, 336-340.
27. A.B.S.H. Salem; *Chem. Eng. Technol.*, **1997**, 20, 342-347.
28. G.B. Brieva, J.M. Campos-Martin; S.M. Al-Zahrani; J.L.G. Fierro; *Glob. Nest J.*, **2010**, 12, 296-304.
29. M.A. Parvez, M. Al-Mehthel, H.I. Al-Abdul Wahhab, I.A. Hussein; *J. Appl. Polym. Sci.*, **2014**, 131(7).
30. K.S.W. Sing, D.H. Everett, R.A.W. Haul, L. Moscou, R.A. Pierotti, J. Roquerol, T. Siemieniewska; *Pure Appl. Chem.*, **1985**, 57, 603-619.
31. A. Moatti, J. Javadpour; M. Anbia; A. Badiei; *Ceram. Int.*, **2014**, 40(7), 10231-10236.

EXPERIMENTAL LAB-SCALE BIOGAS PRODUCTION BY ANAEROBIC CO-DIGESTION OF AGRICULTURAL RESIDUES AND BREWERY WASTEWATER

Madalina IVANOVICI^{a,*}, Adrian-Eugen CIOABLA^b,
Gabriela-Alina DUMITREL^a, Ana-Maria PANA^a,
Laurentiu-Valentin ORDODI^a

ABSTRACT. As a result of environmental and economic concerns, anaerobic co-digestion process has gained increasing interest as a viable technology for both energy production and waste treatment. In this work, anaerobic co-digestion of agricultural residues (animal slurry and corn grains) and wastewater from a local brewery plant was studied using a laboratory-scale experimental installation. Multiple batch experiments (Tst1-Tst7) were carried out in which the influence of the substrate mixture ratio, the temperature and the purging of N₂ of the reactor on the process was analyzed. Batch anaerobic-digestion experiments were performed at initial pH values between 7.5÷7.9 and at two temperature regimes (termophilic and mesophilic) and the substrates involved in the experiments were characterized using solid biofuels European Standard (EN 14774, EN 14775, EN 14918, EN 15297). The biogas was characterized by determining the CH₄, CO₂, and H₂S fraction over time. The best results were obtained when nitrogen purging was used to minimize the exposure of the substrate mixture to oxygen at an operating temperature of 45°C and a volume ratio of animal slurry to wastewater of 3:1 and 150 g of corn grain. Higher operating temperature and N₂ purging had a positive impact by increasing biogas production and decreasing the H₂S fraction of the total produced gas.

Keywords: *biogas production, agricultural residues, lab-scale experiments, N₂ purging*

^a Politehnica University of Timisoara, Faculty of Industrial Chemistry and Environmental Engineering, 6 Vasile Parvan Blvd., RO-300223, Timisoara, Romania.

^b Politehnica University of Timisoara, Faculty of Mechanical Engineering, 1 Mihai Viteazu Blvd., RO-300222, Timisoara, Romania.

* Corresponding author: madalina.ivanovici@student.upt.ro



INTRODUCTION

Anaerobic digestion (AD) is a versatile process by which various types of organic matter are converted to biogas using technology that may be designed at different scales providing benefits such as energy autonomy, pollution mitigation, and waste valorization. It also sustains economic entities in the agricultural, industrial, and municipal sector due to the fact that it can be adapted to the energy needs and local available renewable resources including waste generated in the aforementioned sectors. The advantages attained by using various types of substrates in the anaerobic digestion have made the anaerobic co-digestion of multiple feedstocks an important research field in improvement of the AD technology [1-3].

In addition to the common types of waste exploited in the anaerobic digestion technology, such as food waste (from industrial and commercial activities, restaurant and household activities), organic fraction of the municipal solid waste, agriculture waste (from harvest activity and animal husbandry and farms), sewage sludge, it has to be mentioned another category of organic waste: wastewaters. The wastewaters with potential use for biogas production are provided mainly from food production and biorefineries (e.g. pulp, paper and biofuels production) sectors and among the wastewaters reported in the scientific literature for the AD process there may be mentioned: brewery wastewater, wastewater from household and personal products, yogurt/cheese whey wastewater, meat processing wastewater, ethanol wastewater, palm oil mill effluent, biodiesel wastewater, seafood processing wastewater, agro-industrial wastewater [4-6]. The high organic load, high biodegradability, microbial presence, low degree of physical and chemical contamination make the wastewater appealing co-substrates for anaerobic digestion. Therefore, the wastewaters can be mixed together with complementary substrates such as other types of wastewaters, animal manure, food waste, lignocellulosic biomass, algae e.g. to improve the nutrient content, C/N ratio and to overcome the toxicity contained in some of the wastewaters for the AD process [5, 6].

The exploitation of wastewater by anaerobic fermentation serves not only as an approach to improve the AD process for biogas production but also as a treatment method for industrial effluents with high organic strength, for which before discharging a purification step is required. In this way, anaerobic co-digestion of wastewaters represents a viable option to diminish considerable source of pollution for the soil, groundwater and atmosphere which contribute to the energy savings of the waste provider industry and to reduce the sludge excess accumulation. Furthermore, AD for wastewater treatment shows economic benefits over aerobic treatment technologies (such

as sequencing batch reactor, activated sludge and aerobic filter) because the demand for some operations such as aeration, sludge disposal, and maintenance of the mechanical device contribute to their operating costs [5, 7-10].

Combinations of wastewaters with solids or semi-solids waste and utilization of slurries are suitable for wet fermentation (low solids anaerobic digestion) in low rate systems: batch, fed-batch and continuous. The most common reactor type for wet fermentation is Continuously Stirred Tank Reactor (CSTR), wherein the retention can be ranged between 2 and 4 weeks [8, 11]. Another type of waste generated in large quantities with serious environmental implication, as in the case of industrial wastewater, is animal manure which contains both bacteria and nutrients, for which improper management can lead to ground water contamination and public health threat. As an alternative to disposal in landfill sites, anaerobic digestion of animal manure is used to maximize the benefits while overcoming the pollution problems. However, due to the low carbon to nitrogen (C/N) ratio, the animal manure is commonly used in mixtures with carbon rich co-substrates such as lignocellulosic biomass to satisfy the anaerobic digestion requirements [12, 13].

In this study, different mixtures of wastewater from brewery with animal slurry and corn grains were used for anaerobic co-digestion lab scale batch experiments to investigate the influence of operating parameters on the process behavior. Hence, variation of the temperature domain, mixture ratios and the exposure to oxygen of the substrates inside the reactor were conducted with an emphasis on studying the modification of the pH in time, the amount of produced biogas and the biogas composition, respectively.

RESULTS AND DISCUSSION

Increased pH values of the mixture are given by the animal manure contained in the mixture which usually contains high concentration of $\text{NH}_4\text{-N}$. In figure 1, it is represented the variation of pH over time for anaerobic co-digestion batch experiments Tst1-Tst7, as presented in Table 2. It can be noticed that the values of the initial pH of the Tst3-Tst7 are between 7.5 and 7.7, wherein the animal slurry to wastewater volume ratio is 3:1 and higher initial pH value (7.9) were recorded for Tst1 and Tst2 where the animal manure to wastewater volume ratio is higher. The optimal pH range for maximal biogas production by anaerobic digestion is 6.5÷7.5, but the pH can be extended to wider ranges such as 6.5÷8.5 depending on the substrate and digestion technology [14, 15]. Still, based on other scientific studies, biogas production decreases at pH values above [16-20]. In figure2 are represented the total amount of biogas, methane and carbon dioxide for each batch experiment presented above in table 1. In the first set of experiments, low concentrations

of methane and carbon dioxide of the total gas are obtained and it can be concluded that the variation of substrate mixture ratio has little impact on the process performances and that the selected operating conditions and the pH control were not favorable for the process. Furthermore, the variation of CO₂ and CH₄ low concentration over time are illustrated in figure 3.

Therefore in the second set of experiment enhanced biogas, methane and CO₂ production were obtained. The best results are attributed to batch experiment Tst7, with a total production of biogas of around 15 liters of which 51% is CH₄ and 31.6% is CO₂.

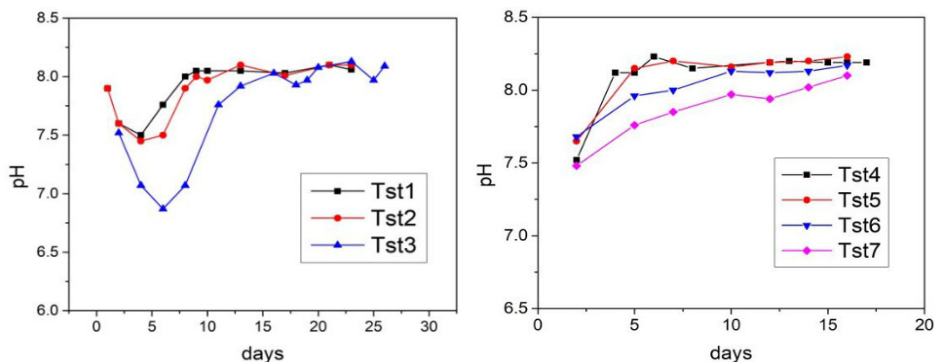


Figure 1. The pH profile in the anaerobic co-digestion batch experiments (Tst1-Tst7)

Comparing the Tst7 with Tst4, it can be noticed that the total amount of biogas, CH₄ and CO₂ for Tst4 was 49.7%, 49.9% and respectively 47.7% lower than in the case of Tst7. These results showed that the use of N₂ purging in order to diminish the suspension mixture exposure to oxygen led to enhanced biogas production.

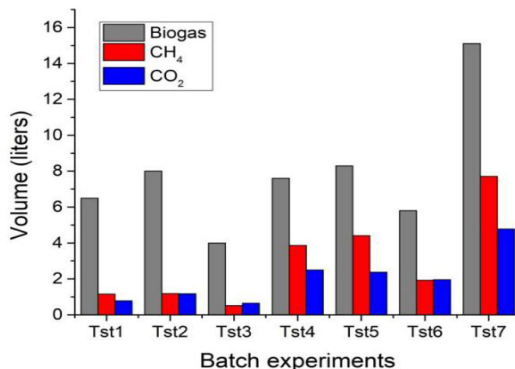


Figure 2. The total amount of produced biogas, methane and carbon dioxide for anaerobic co-digestion batch experiments from Tst1 to Tst7

This can be explained by the oxygen effect on the overall anaerobic digestion process. Based on the scientific literature, hydrolysis (the first stage occurring in the anaerobic fermentation) is carried out in both aerobic and anaerobic condition, whereas the microorganism involved in the following stages (acidogenesis, acetogenesis and methanogenesis) are strictly anaerobic [21, 22]. Higher yields of organic matter conversion were reported in the aerobic hydrolysis, while exposure to surpassing oxygen content lead to oxidation of available soluble carbon into carbon dioxide, reducing the potential conversion into methane. This suggests that too high levels of oxygen have a negative impact on the biogas yields in the anaerobic digestion process [21, 22]. Furthermore, lower pH values were obtained for Tst7 when compared with Tst4, which may imply that higher conversion of the organic substrate into acidic compounds was obtained concomitantly with faster and higher rates methane formation as it is illustrated in figure 3 and figure 5.

Lower operating temperature in Tst6 (37°C) and Tst5 (30°C) led to decreased biogas production, but surprisingly higher in Tst5 than in Tst6. Moreover, lower yield of gaseous mixture consisting of CH₄ and CO₂ of the total produced biogas (around 67%) was attributed to Tst6, while CH₄ and CO₂ gaseous mixture yields in the Tst4, Tst5 and Tst7 were around 83%. Generally, the typical minimum retention time in the anaerobic digestion for mesophilic temperatures is about 30 to 40 days and for thermophilic temperatures it ranges between 15 to 20 days. This fact, corroborated with methane production over the operation time (figure 3 and figure 4), indicates that Tst4 and Tst7 batch experiment correspond to thermophilic behavior, as it is expected. Herein, the maximum methane production was reached between day 4 and day 10 with the methane content of the total biogas in the 55-70% range for Tst7 and between day 7 and day 15 in the 50-65% range for Tst4.

By analogy, evaluating the CH₄ production over time in Tst 6, wherein a different thermal regime was applied, indicates a similar trend of gas production with Tst 4 and Tst 7, with the maximum methane production reached between day 4 and day 9, in the range 42-52%. Otherwise, in the Tst5 batch experiment, methane production reached a maximum plateau for a prolonged period, starting from day 8 to day 17 in the range 60-70%, indicating a slower production rate of biogas in the first 8 days. This trend corresponds to a mesophilic behavior and explains the increased biogas production for Tst5 when compared with Tst6. Figure 4 presents, the evolution of methane, biogas and carbon dioxide production over time as accumulated gases produced for batch experiments Tst4-Tst7, revealing the production ratio of methane and carbon dioxide in relation to biogas.

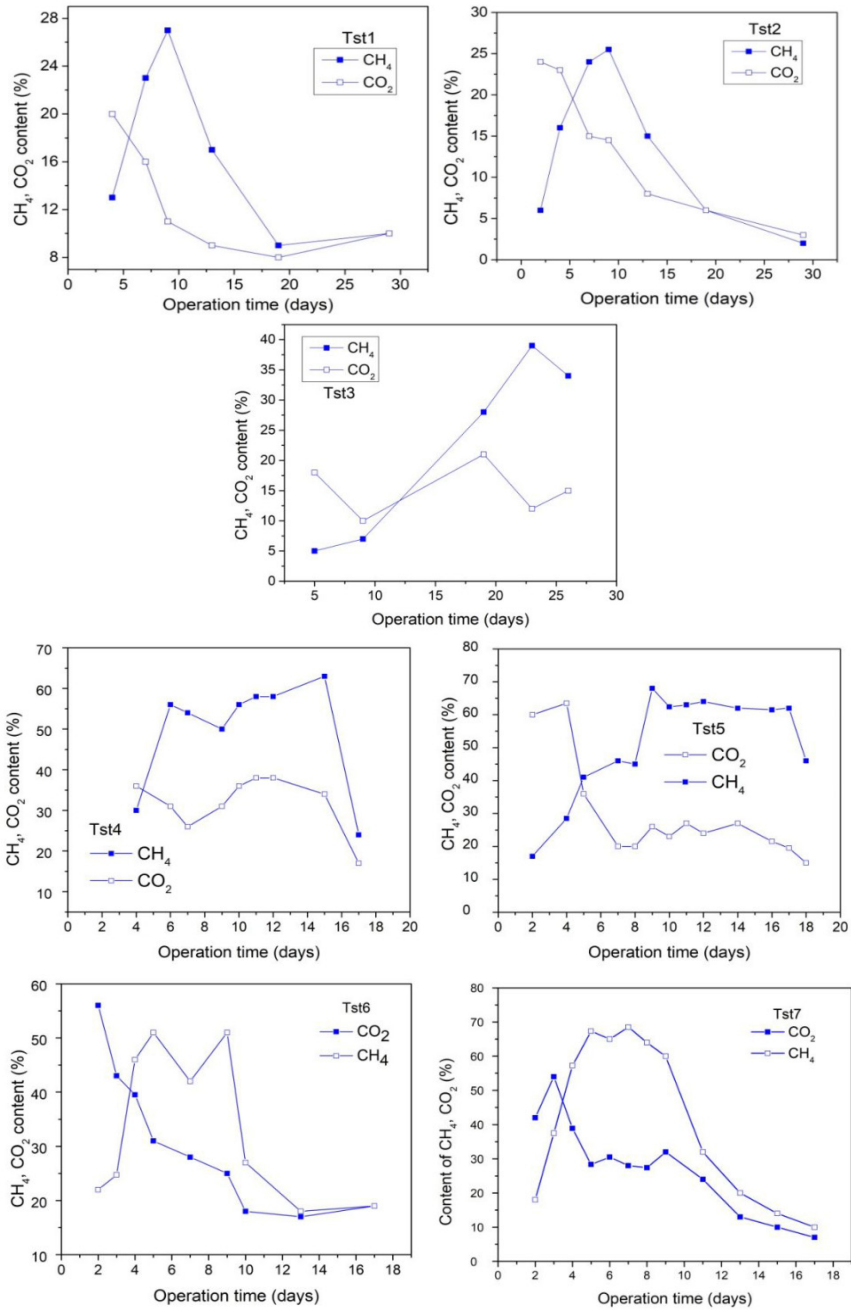


Figure 3. The variation of CH₄ and CO₂ percent of biogas obtained over the operation time of anaerobic co-digestion batch experiments: Tst1-Tst7

EXPERIMENTAL LAB-SCALE BIOGAS PRODUCTION BY ANAEROBIC CO-DIGESTION OF AGRICULTURAL RESIDUES AND BREWERY WASTEWATER

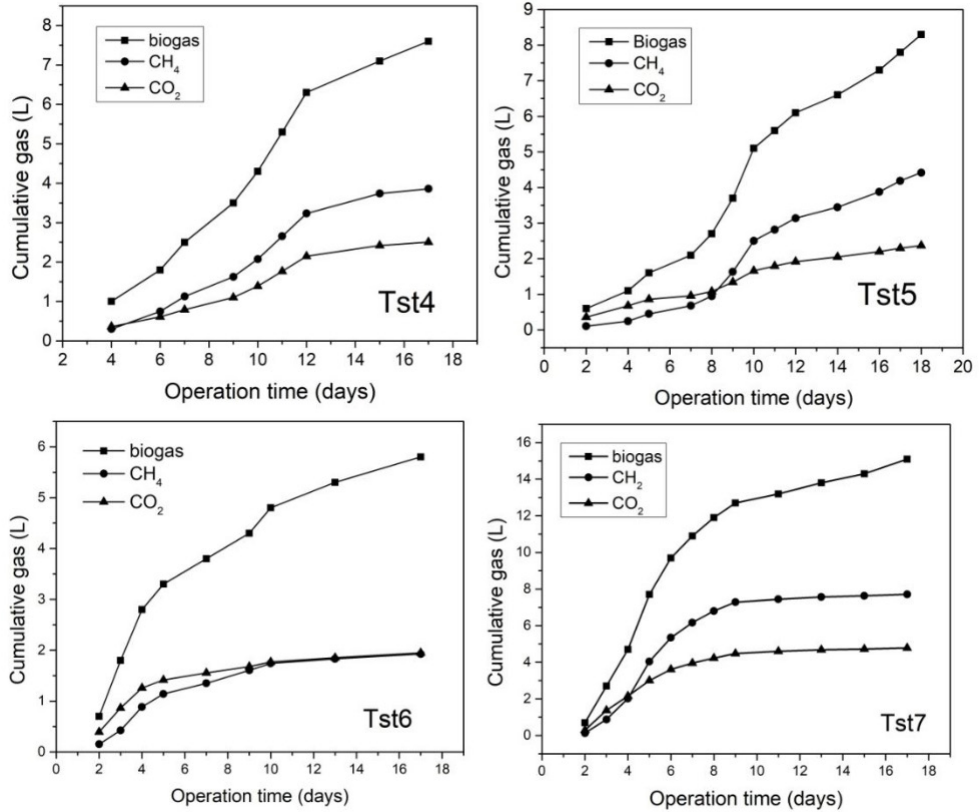


Figure 4. The accumulated gas (biogas, CH₄ and CO₂) obtained in the anaerobic co-digestion batch experiments: Tst4-Tst7

An important aspect in appreciating the anaerobic co-digestion process for biogas production is represented by the content of H₂S of the total biogas. Due to its corrosive action in further biogas utilization technologies, it is desirable to obtain low concentration of H₂S. In table 1, the H₂S content in biogas for batch experiments Tst4-Tst7 are presented.

By assessing the above, it can be noticed that lower H₂S content is obtained during the Tst7 experiment due to the fact that anaerobic co-digestion in case of diminished exposure to oxygen resulted after N₂ purging of the reactor lead to lower activity in sulfur producing microorganisms.

Table 1. Production of H₂S of the total biogas obtained in the second set of batch anaerobic co-digestion experiments

Batch experiment	H ₂ S content (ppm)
Tst4	680
Tst5	300
Tst6	32
Tst7	417

By comparing the Tst5, Tst6 and Tst7, where different temperatures regimes were operated, the H₂S concentration decreases in the following order: Tst7, Tst5 and Tst6 similarly with the biogas, CH₄ and CO₂ concentration which suggests that lower biogas production is correlated with lower CH₄, CO₂ and H₂S production.

CONCLUSIONS

Based on the results obtained in the first set of experiments (Tst1-Tst3), it can be concluded that the animal slurry to brewery wastewater volume ratio of 4:0 and the addition of acid for the pH control contributed to low methane and carbon dioxide yields of the total biogas when compared to the second set of experiments.

The variation of operating temperature in the experiments Tst5-Tst7, while the substrate mixture was the same (the animal slurry to brewery wastewater volume ratio was 3:1 and the mass of corn grain was 150 g), led to different behavior regarding the biogas and methane production. Hence, the best results were obtained for Tst7 batch experiment, wherein the operating temperature is thermophilic (45°C), followed by Tst5 (operated at 30°C) and by Tst6 (operated at 37°C). Also, by analyzing the Tst4 and Tst7 experiments, it was pointed out that the N₂ purging significantly improved the anaerobic co-digestion process by increasing the biogas and methane production by 100%.

EXPERIMENTAL SECTION

Anaerobic co-digestion batch experiments were carried out using lab scale reactors of 5L capacity with automatic stirring and temperature control, as described in a previous study [23]. Multiple batch experiments were

EXPERIMENTAL LAB-SCALE BIOGAS PRODUCTION BY ANAEROBIC CO-DIGESTION OF
AGRICULTURAL RESIDUES AND BREWERY WASTEWATER

conducted wherein different operating parameters including substrates mixture ratios, temperature domain and the working atmosphere were selected in order to investigate the behavior of the process by analyzing the amount of obtained biogas, biogas composition and pH modification. In table 2, there are presented the operating parameters for each batch experiment. The working volume of the reactor was 4 L and the remaining part was left for gas accumulation. For batch experiments Tst3 - Tst7, the headspace of the reactor was purged with N₂ to remove the air containing the oxygen which is considered a toxic agent for the anaerobic digestion due to the inhibiting effect on the anaerobic microorganism (acetogens and methanogens) [24].

Table 2. The operating parameters for the anaerobic co-digestion batch experiments

Batch	Substrate mixture		Temperature [°C]	N ₂ purge	operation time (days)
Experiments code	Animal slurry to brewery wastewater volume ratio	Corn grain [g]			
<i>First set of experiments</i>					
Tst1	4:0	150	35°C	no	26
Tst2	4:0	200	35°C	no	26
Tst3	3:1	150	35°C	yes	26
<i>Second set of experiments</i>					
Tst4	3:1	150	45°C	no	18
Tst5	3:1	150	30°C	yes	18
Tst6	3:1	150	37°C	yes	18
Tst7	3:1	150	45°C	yes	18

Three types of substrates were involved in the experimental investigations: wastewater from brewery factory, animal (cow and chicken) slurry and corn grain (figure 5). The animal slurry was obtained from a local biogas industrial plant (Timișoara, Romania). Therefore, the experimental studies involved in the current work are classified in two sets of experiments. The first set of experiments comprising Tst1-Tst3 were conducted at the same operating temperature and operation time in order to investigate the effect of substrate mixtures and oxygen on the process and the second sets of experiments (Tst4-Tst7), wherein the operation time and substrate mixture were selected to be the same, with the aim of investigating the influence of oxygen and temperature regime. As well, small amounts of acetic acid were added in the reactor for the Tst1-Tst3, whereas no pH adjustments were performed for the Tst4-Tst7. The obtained biogas was collected in sample gas bags and subjected to composition analysis using a portable biogas analyzer (Biogas 5000 Gas Analyzer provided by Geotech). For the first set of experiments, the biogas composition was assessed in terms of CH₄ and CO₂ fraction determination and for the second set of experiments, the analyzed components were CH₄, CO₂ and H₂S.



Figure 5. The anaerobic co-digestion suspension consisted of animal slurry, wastewater and corn grain mixture

As it is presented in table 2, the anaerobic digestion process was carried out at thermophilic (45°C) and mesophilic (30-37°C) temperatures and different operation time were selected (18 and 26 days).

The substrates were subjected to characterization in order to determine the moisture, ash and minor elements content and calorific value (table 3) using solid biofuels European Standard (EN 14774, EN 14775, EN 14918, EN 15297), for the brewery wastewater and animal slurry additional properties (chemical oxygen demand - T_{COD} , orthophosphate - P_T and ammonia - N_T concentration) are presented in table 4.

Table 3. The properties of the substrates based on the European Standards characterization techniques - EN 14774, EN 14775, EN 14918, EN 15297

Substrate	Moisture content (dry basis) [%]	Ash content (dry basis) [%]	Superior calorific power (dry basis) [J/g]	Lower calorific power (dry basis) [J/g]	Minor elements [ppm]				
					Cr	Mn	Ni	Cu	Pb
Corn grain	10.2	1.58	18460	16887	<5	10.0	<5	<5	450
Wastewater from brewery factory	5.1	26.7	17412	16125	<5	102	<5	8.5	<5
Animal (cow and chicken) slurry	8.46	18.7	16699	15444	7.8	-	14	390	<5

Table 4. Additional properties (chemical oxygen demand, orthophosphate, ammonia) of the substrates of high water content

Substrate	T _{CO_D} (mg/L)	N _T (mg/L)	P _T (mg/L)	source
Wastewater from brewery factory	4679- 5118	59.8 – 79.3	21 – 80.2	Local brewery plant
Animal (cow and chicken) slurry	11200÷24000	>1800÷500	>500÷200	[25,26]

REFERENCES

1. E. Uçkun Kiran, K. Stamatelatos, G. Antonopoulou, G. Lyberatos; Production of biogas via anaerobic digestion. In *Handbook of Biofuels Production*, 2nd ed.; R. Luque, C. Sze Ki Lin, K. Wilson, J. Clark Eds.; Woodhead Publishing, **2016**; Chapter 10, pp. 259-301.
2. G. Náthia-Neves, M. Berni, G. Dragone, S.I. Mussatto, T. Forster-Carneiro; *IJEST*, **2018**, *15(4)*, 2033-2046.
3. J. N. Meegoda, B. Li, K. Patel, L. B. Wang; *IJERPH*, **2018**, *15(10)*, 2224.
4. Y. Shen, J. L. Linville, M. Urgun-Demirtas, M. M. Mintz, S. W. Snyder; *Renew. Sust. Energ. Rev.*, **2015**, *50*, 346-362.
5. C. Sawatdeenarunat, C. Wangnai, W. Songkasiri, P. Panichnumsin, K. Saritpongteeraka, P. Boonsawang, S. K. Khana, S. Chaiprapat; Biogas Production from Industrial Effluents, In *Biofuels: Alternative Feedstocks and Conversion Processes for the Production of Liquid and Gaseous Biofuels*, 2nd ed.; A. Pandey, C. Larroche, C.-G. Dussap, E. Gnansounou, S. K. Khanal, S. Ricke Eds.; Academic Press, **2019**; Chapter 23, pp. 779-816.
6. E. Karlsson; *Biogas through Anaerobic Digestion from Waste Streams as a Renewable Transportation Fuel - A Brief Review of Technology*, European Technology and Innovation Platform
https://www.etipbioenergy.eu/images/ETIP_Bioenergy_Biogas_publications_review.pdf.
7. M. Berni, I. Dorileo, G. Nathia, T. Forster-Carneiro, D. Lachos, B. G. M. Santos; *Int. J. Chem. Eng.*, **2014**, 1-8.
8. A. Eusebio, A. Neves, I. P. Marques; *Apl. Sci.*, **2021**, *11(10)*, 4346.
9. A. M. Enitan, J. Adeyemo, F. M. Swalaha, F. Bux; *Environ. Model. Assess.*, **2015**, *20*, 673-685.
10. European Biogas Association, *The role of biogas production from industrial wastewaters in reaching climate neutrality by 2050*.
<https://www.europeanbiogas.eu/wp-content/uploads/2021/04/Paper-The-role-of-biogas-production-from-wastewater-in-reaching-climate-neutrality-by-2050.pdf>.
11. T. Z. D. de Mes, A.J.M. Stams, J.H. Reith and G. Zeeman; Methane production by anaerobic digestion of wastewater and solid wastes. In *Bio-methane & Bio-hydrogen*, J.H. Reith, R.H. Wijffels and H. Barten Eds.; Smiet offset, The Hague, Netherlands, **2003**; Chapter 4, pp. 58-102.

12. S. A. Neshat, M. Mohammadi, G. D. Najafpour, P. Lahijani; *Renew. Sust. Energ. Rev.*, **2017**, 79, 308-322.
13. J. Huang, Z. Yu, H. Gao, X. Yan, J. Chang, C. Wang, J. Hu, L. Zhang; *PLoS One*, **2017**, 12(6), e0178110.
14. N. T. Sibiyi, E. Muzenda, H. B. Tesfagiorgis; *ICGTREEE'2014*, **2014**, 198-201.
15. N. Sawyerr, C. Trois, T. Workneh, V. Okudoh; *IJEPP*, **2019**, 9(2), 105-116.
16. J. M. Triolo, A. J. Ward, L. Pedersen, S. G. Sommer; Characteristics of Animal Slurry as a Key Biomass for Biogas Production in Denmark, In *Biomass Now – Sustainable Growth and Use*, M. D. Matovic Eds.; Intech Open, **2013**; Chapter 12, pp. 307-312.
17. I. S. Ogiehor, U. J. Ovueni; *Int. J. Eng. Res.*, **2014**, 5(1), 62-69.
18. M. Benali, T. Hamad, Y. Hamad; *J. Sustain. Bioenergy Syst.*, **2019**, 9(3), 91-97.
19. G. Ortiz, C. A. Villamar, G. Vidal; *Sci. Agric.*, **2015**, 71(6), 443-450.
20. H. K. Ahn, M. C. Smith, S. L. Kondrad, J. W. White; *Appl. Biochem. Biotechnol.*, **2010**, 160(4), 965-975.
21. D. B. Bernt, L. R. Bakke; *J. Waste Manag.*, **2011**, 4, 1-19.
22. V. Dubrovskis, V. Kotelenecs; *Engineering for Rural Development, Proceedings*, **2014**, 13, 455-458.
23. M. Ivanovici, A. E. Cioabla, D. Lelea, F. Popescu, L. I. Dungan, L. V. Ordodi; *J. Phys.: Conf. Ser.*, **2021**, 1781, 012069.
24. C. Pedizzi, L. Regueiro, I. Rodriguez-Verde, J. M. Lema, M. Carballa; *Bioresour. Technol.*, **2016**, 211, 765-768.
25. C.-A. Villamar, D.-C. Rodríguez, D. López, G. Peñuela, G. Vidal; *WM&R*, **2013**, 31(8), 820-828.
26. O. El bied, M. Kessler, M. A. Terrero, T. Techtali, A. F. Cano, J. A. Acosta; *Agronomy*, **2021**, 11, 2158.

WATER SORPTION, SOLUBILITY AND MONOMER RELEASE OF A FAST POLYMERIZED HEAT-CURING RESIN ENHANCED WITH GRAPHENE SILVER NANOPARTICLES

Cecilia BACALI^a, Marioara MOLDOVAN^b, Stanca CUC^b,
Corina Elena TISLER^{a,*}, Smaranda BUDURU^a

ABSTRACT. Heat-cure denture base resins are the most used materials in denture fabrication for almost a hundred years, because of their favorable characteristics, but they also have some drawbacks that influence the durability and biocompatibility. Over time researchers tried to obtain improvements of the denture materials by adding different types of additives. Water sorption, solubility, and monomer release are among the most important acrylic resins characteristics that influence dentures' durability and biocompatibility. The aim of the present study was to evaluate the effect of graphene silver nanoparticles addition to a commercial heat-curing acrylic resin processed through a fast-polymerization cycle on the water sorption, solubility, and monomer release.

Keywords: *acrylic resin, water sorption, solubility, monomer release, graphene silver nanoparticles.*

INTRODUCTION

Acrylic resins have been used for almost 100 years in denture fabrication without major improvements [1]. Over time, they showed good mechanical and esthetic characteristics, biocompatibility, and low toxicity [2,3] together

^a *Iuliu Hatieganu University of Medicine and Pharmacy, Department of Prosthodontics and Dental Materials, 32 Clinicilor str, 400006, Cluj-Napoca, Romania.*

^b *Department of Polymer Composites, Institute of Chemistry "Raluca Ripan", Babes-Bolyai University, 400294 Cluj-Napoca, Romania*

* *Corresponding author: corina.tisler@yahoo.com*



with easy repairs and low costs. These materials, accessible for the patients, are also convenient for the technicians, which do not need expensive devices in the fabrication process. However, among its shortcomings are some mechanical characteristics such as the brittle nature of the acrylic resins and the low flexural strength that may favor denture fractures and affect durability. The resin surface characteristics and poor antimicrobial activity are factors that favor bacterial adhesion to the denture. Other inconveniences are related to the water sorption, solubility, and monomer release, which can influence the dimensional stability, affecting the material durability [4]. The residual monomer is also related to possible adverse reactions - cytotoxic effects, inflammations of the oral mucosa, and allergic reactions [5]. As regarding the monomer release, although it is well known that in the resin obtention the conversion of the monomer to polymer is not complete [6], it has been demonstrated that fast polymerization methods are associated with higher amounts of residual monomer release compared to the standard polymerization techniques [6,7]. After the polymerization reaction that takes place between the PMMA powder particles and the methyl methacrylate monomer, a certain amount of unpolymerized monomer is always found [7,8].

Some of the acrylic resin characteristics, like water sorption and solubility, need to be improved for better durability and functionality of the acrylic resins [4]. Different materials were added to dental materials over time in order to improve their mechanical behavior and to induce antibacterial properties [9,10,11,12]. Composite materials improved with nanomaterials like graphene oxide showed improved mechanical and physical properties while the weight of the material is just slightly increased [9]. In other studies, antimicrobial effects (*Streptococcus* mutants, *Candida albicans*) were obtained together with improved mechanical properties (flexural strength) when using PMMA composites improved with silver and nano-ZrO. Addition of silver nanoparticles induced antibacterial properties to PMMA to both Gram-negative and Gram-positive bacteria [13,14].

The additives used for the acrylic resin improvements can influence other material properties like water sorption, solubility, and the residual monomer. Water sorption of acrylic resins is determined mainly by the polar properties of the molecules [15] and can be also associated with the porosity of the material [16]. Water sorption, solubility, and monomer release were shown to be influenced by the type of curing method and also by the additives used in the enhanced resins [17,18].

In our country, heat cure resins, such as Superacryl Plus (Spofa Dental) are widely used in removable denture fabrication because of the low costs, ease in processing, and the simple laboratory devices that are needed.

The *aim of this study* is to analyze the effect on the monomer release, solubility, and water sorption of graphene oxide and silver nanoparticles addition to a heat curing resin that was processed in a short curing cycle.

The *null hypothesis* was that there is no difference between the water absorption, solubility, and residual monomer results between the samples of conventional and enhanced heat-curing resin.

RESULTS AND DISCUSSION

Although PMMA resins are used for a long time in the fabrication of removable dentures due to their favorable characteristics, they cannot be considered an ideal material. Many attempts have been made by adding different types of materials in order to improve their mechanical, physical, or chemical properties. The presence of the denture in the oral cavity exposes it to a variety of forces during mastication, while the material is also interacting with oral fluids and different beverages.

Over time, many studies were directed in the research of an ideal material for the denture bases, a material that should have in the same time adequate mechanical, physical, and chemical properties. Various materials, such as fibers and fillers of different types and sizes, have been used to improve the mechanical properties of PMMA [12,19,20] and to enhance its antibacterial activity and biocompatibility. Properties like minimum water absorption, solubility, and low residual monomer are also desired in order to obtain better acrylic resin behavior, durability, and esthetics.

It is well known silver's property to inhibit bacterial growth. Studies demonstrated its biocompatibility and lack or minimal cytotoxicity when used in low concentrations. [10,13]. A lower monomer content can improve material characteristics and also biocompatibility [6].

Graphene has a bidimensional structure of carbon atoms disposed in one – atom thick layer. Graphene oxide can be obtained by graphite oxidation. It has remarkable mechanical properties such as high resistance, flexibility, low weight that permits the material a wide applicability. Mechanical properties of graphene oxide were studied by Forati et al. [9] who demonstrated that small amounts, up to 1%, of graphene oxide, added to polyether sulfone nanocomposite significantly improved the mechanical properties of the material and Kang et al. [21] who found a Young moduli of 695 \pm 50GPa, ultimate tensile strength values 3-33 GPa, while Lee [22] obtained a Young moduli of 1TPa and a breaking strength of 130 GPa, for the graphene monolayer, resulting the strongest material ever measured.

An ideal denture material should have high chemical and thermal stability [15] for better durability and low possibility of side effects. Heat-cure PMMA are the most used materials for denture fabrication [1].

In rapid curing cycles the presence of a low concentration of benzoyl peroxide initiator in the powder and a very small activator dimethyl-p-toluidine in the monomer can reduce the porosity of the acrylic resin [23], and by this way, also the water absorption. In a study that evaluated water sorption and solubility values for self-cured and heat-cured acrylic resins, significant differences were found between mean values of the various acrylic resins, but no correlation was found between the studied properties [15]. The processing methods can influence the water absorption of acrylic resins used in denture fabrication [24].

Superacryl plus is an easy processing, finishing, and polishing heat cure resin, frequently used in our country in complete denture fabrication. It is a modern variant of methacrylate resin, supplied in bicomponent system, powder and liquid, and is recommended for the fabrication of removable denture bases, orthodontic appliances and indirect rebasing of removable dentures. It can be processed, according to the manufacturer, using four types of curing methods: standard polymerization, faster polymerization, fast-boiling polymerization, and polymerization using a pressure polymerizing device. The standard polymerization recommends a total processing time of 2 hours that starts with the flask immersion in cold water, followed by a raising of the temperature to 70 0C and then to 100 0C. The faster polymerization method that was used in our study consists of flask immersion in cold water, followed by a temperature raising to 100 0C, which was then maintained for the next 45 minutes.

A fast-boiling method is also possible, but only for partial dentures; the flask is directly immersed in boiling water, and the temperature (100 0C) is maintained for 45 minutes. The curing method in a pressure polymerizing device is performed in a 10-15 minutes' interval, without flacking, directly on the model, at a pressure of 0.6 MPa and a 100-110 0C temperature; it is though recommended only for small partial dentures. Adverse reactions to this material are possible (methyl methacrylate sensitivity), especially for allergic people. Higher monomer amounts were found in the self-cure resin compared to the heat-cure ones [25]. The level of residual monomer in self-curing denture base materials. The higher amounts of residual monomer can be caused by the graphene oxide inhibitory effect in the polymerization reaction that leads to a lower conversion of the monomer into polymer [26].

1. MMA monomer release

The amount of methyl methacrylate monomer (MMA) was higher when the fillers were added to the studied resin and when the samples were immersed in chloroform, than in simulated saliva, as shown in the **Table 1/Figure 1**.

Table 1. MMA values for MMA release for the M (control), P1(1% G-Ag Np) and P2(2% G-Ag Np) samples stored in chloroform and simulated saliva

MMA -	Chloroform (mg/50ml)	MMA - saliva (ug/g)
M	9.98	0.751
P1	11.268	0.73
P2	12.296	0.66

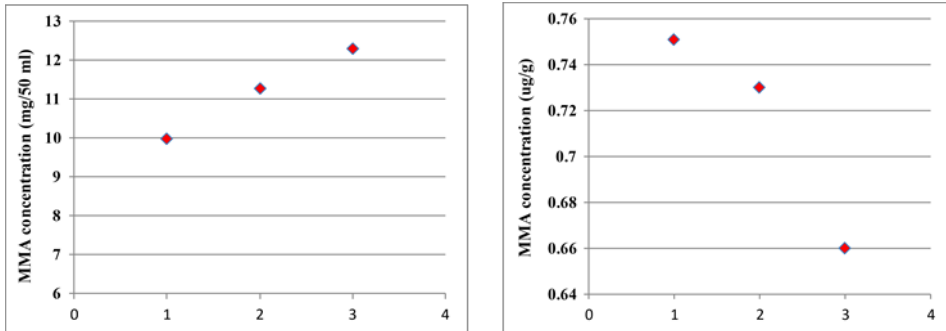


Figure 1. Higher amounts of residual methyl methacrylate monomer (MMA) were obtained for the samples dissolved in chloroform compared to those dissolved in the cell medium solution (figures). The enhanced samples P1 and P2 showed higher values of MMA. Lower amounts of MMA were determined for the samples stored in cell medium.

In the present study the residual MMA was recovered from two types of solvents, cell medium solution, used to simulate *in vivo* conditions [27] and chloroform. The amount of monomer in cell medium solution was lower than that found in the chloroform solution, as a result of methyl methacrylate solubility in chloroform. G-Ag Np addition to PMMA increased the residual monomer dissolved in chloroform solution. The graphene high possibility of interaction may contribute to the incomplete polymerization, due to their interference in the curing process [26].

The amount of the unconverted monomer in the polymerization reaction is important to be assessed because of its possible side effects. The contact with the residual MMA can cause irritations of the skin, dependent on the time of exposure, for the persons which manipulate the material [28], even if they wear dental gloves, as long as vinyl and latex gloves showed monomer permeability [29]. Other adverse reactions concerning the nervous system, headaches, balance disorders and visual disturbances, as a result of vapour inhalation or dermal exposure to methyl methacrylate, were also found [30,31]. The values obtained for MMA resulted from a fast polymerization processing method in this research were higher than those obtained for a self-cure resin in a previous study [32].

Studies showed that a longer curing time can reduce the amount of residual monomer [5]. A 7h immersion in water at 70°C followed by a 1h immersion in water at 100°C are recommended for a maximum conversion of the monomer [33]. The use of microwave polymerization was also showed to reduce the residual monomer content comparing to other polymerization methods [34]. The immersion of the material in water at 37°C for 24 hours is generally recommended after the polymerization reaction in order to reduce the amount of unreacted monomer [35] and also the associated side effects.

2. Water sorption

Water can have in time plasticizing and degradation effects for the dentures, as a consequence of the interaction with the polymer chains and irreversible changes caused in the matrix [4,15]. In the present study, the decrease in water sorption for the higher concentrations of additives may be caused by the filler distribution within the matrix, the lower porosity and the hydrophobic character of graphene. The water sorption seems to be related to the residual monomer, a soluble component of the acrylic resin. Studies show that the processing method [36], the temperature and the time of polymerization reaction can influence the material characteristics (like density, porosity), also the residual monomer, and consequently the water absorption.

The results obtained after the samples storage in distilled water and saliva for 28 days showed a significant weight increase. Higher values of water sorption were obtained for the control sample, both in water and saliva (Table2). A lower water sorption was found for the samples with higher additives content, the lowest value was obtained for the P2 sample. The fillers distribution within the enhanced resin and its lower porosity may have influenced the diffusion of water molecules into the polymeric matrix. No significant variation between samples P1 and P2 were found.

Table 2. Water sorption expressed as weight increase percentage after saliva exposure

Sample	Saliva exposure time	
	7 days	28 days
M	1.24 ± 0.11 ^a	1.49 ± 0.05 ^a
P1	0.94 ± 0.08 ^b	1.31 ± 0.09 ^b
P2	0.81 ± 0.12 ^c	1.26 ± 0.14 ^b

M, PMMA sample; P1, PMMA + 1%GAgNp; P2, PMMA + 2%GAgNp. Different superscript letters indicate statistically significant variation ($p < 0.05$) between the samples

The fast polymerization method may have increased the water sorption, as higher values were obtained than for self-cure resin evaluated in a previous study [32].

3. Solubility

The material weight loss was tested at 37°C during a 28 days interval using two different solvents – water and saliva. The sample mass was weighted after 1, 7, 14, 21, 28 days of immersion [Figure 2].

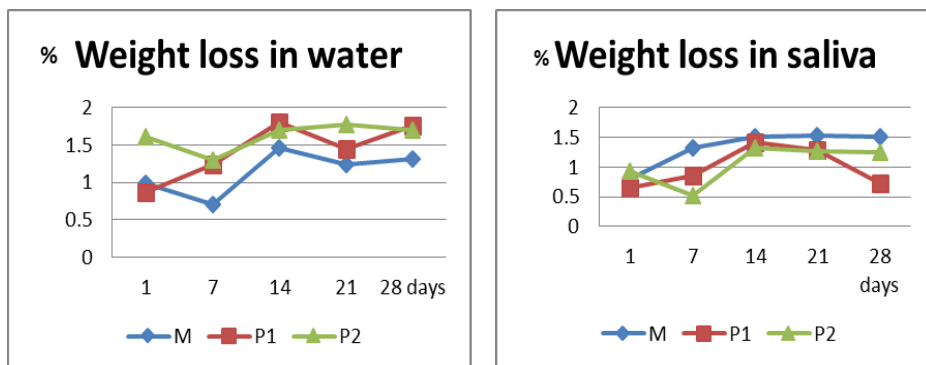


Figure 2. Mean values of weight loss in water and saliva (%) for the control (M) and reinforced samples P1 and P2 after 1, 7, 14, 21, 28 days of immersion

Lower values in terms of weight loss in water were found for the samples with lower content of additives (1%) than for the samples with higher fillers concentration (2%). The control samples (M) showed the lowest weight loss in water, registered after 7 days, from the tested materials. The highest weight loss in water was registered for the P1 sample in the 14th day.

Regarding the weight loss in saliva, the higher values were obtained for the control sample (M), while the enhanced materials (P1, P2) showed slightly lower values. The samples with 2% G-Ag Np showed the lowest weight loss in saliva from the tested samples, registered after 7 days. The highest value for the weight loss in saliva was found for the control sample. Lower values were generally found for the weight loss in saliva than for the solubility in water.

The values were slightly higher than those obtained for a self-cure resin in a previous study [14]. Increased values in solubility can be associated with the higher values of residual monomer and the consequent diffusion of the water and solvent molecules within the resin matrix. The faster polymerization method could cause a lower monomer conversion that can be associated to the higher solubility.

Water sorption and solubility were according to the International Standard Organization (ISO) specifications, which recommend that water sorption should be lower than $32 \mu\text{g}/\text{mm}^3$ for heat-cured or self-cured materials and the loss in mass per unit volume (soluble material) should be lower than $1.6 \mu\text{g}/\text{mm}^3$ for heat-cured and $8.0 \mu\text{g}/\text{mm}^3$ for self-cured materials [37]. There were no correlations between the water sorption and solubility values.

The results obtained in this research are in agreement with the results obtained in other studies on water absorption, solubility and monomer release in acrylic resins [14,15,32].

4. SEM Analyses

Scanning electron microscopy was performed to analyse the surfaces of the samples. Magnification of 500x, 5000x and 10000x were used for capturing conclusive images. The additives have a uniform distribution inside the resin matrix, at both 1% and 2% concentrations. They appear like white areas surrounding the PMMA spheres [Figure 3].

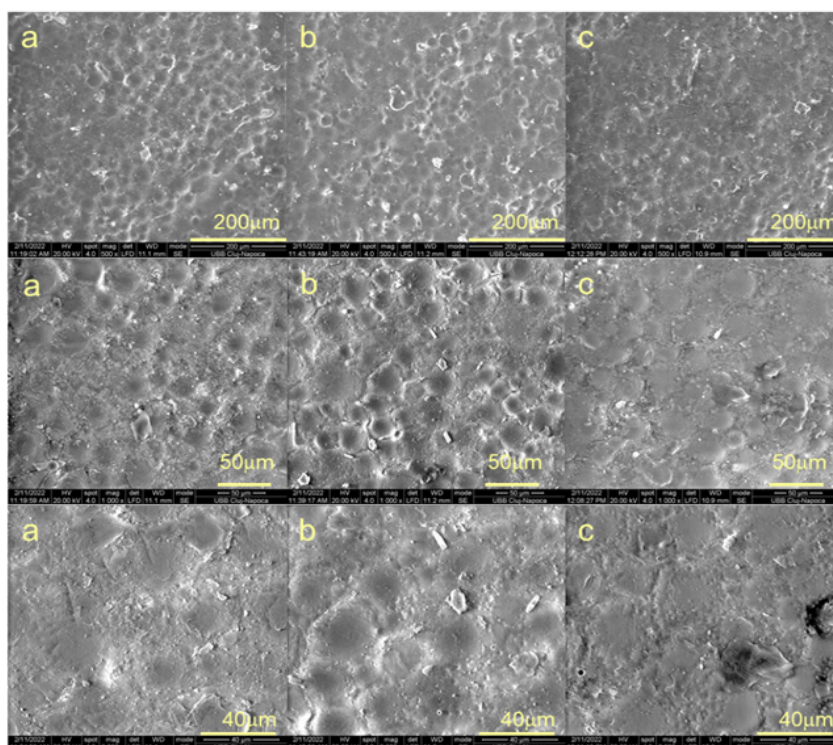


Figure 3. SEM imagines for samples a) M, PMMA; b) P1, PMMA + 1%GAgNp; and c) P2, PMMA + 2%GAgNp.

At the SEM images analysis, a uniform distribution of the additives within the acrylic resin was found, together with a low porosity of the samples. This aspect has a great importance for the material properties, as the higher the homogeneity is present, the lower the water absorption and solubility [38].

The characteristics of new proposed materials are first of all assessed by in vitro investigations, focused on different physical, chemical and mechanical properties [39,40,41].

Limitations. The water sorption and monomer release should also be evaluated for the other Superacryl plus curing methods, in order to evaluate the differences between different polymerization techniques.

CONCLUSIONS

The addition of graphene silver nanoparticles to a commercial heat-cured resin processed by a fast-polymerizing technique show to influence the water sorption, solubility, and monomer release values.

Higher amounts of residual monomer for the enhanced resins in chloroform, but lower in saliva compared to the control samples were found. Lower water sorption values were determined for the samples containing additives (depending on the fillers content) than those of the control samples.

Higher weight loss values in water for the P1 and P2 samples, but lower in saliva compared with M samples were obtained. A uniform distribution of the fillers and a low porosity for the enhanced samples was observed on the SEM images.

The water absorption, solubility, and monomer release values found in the study were in accordance with ISO specifications.

EXPERIMENTAL SECTION

1. Materials

Superacryl Plus (Sofa Dental), a heat-cure commercial acrylic resin used in complete denture fabrication, was used in the study. Addition of 1% and 2% G-AgNp to the resin was performed after the additives' synthesis through Radio-Frequency Catalytic Chemical Vapor Deposition (RF-CCVD) method [11]. Silver nanoparticles were distributed over magnesium oxide (Agx/MgO, where x = 3 wt %) and graphene oxide, using techniques presented in previous studies. The additives were mixed with the denture base resin in

95% ethyl alcoholic solution, at room temperature, under continuous stirring, for 30 minutes and then dried in the oven at 40°C. A methane flow rate of 80 mL/min was used [42]. The reaction interval was 60 minutes [43].

2. Sample preparation

Three study groups (M, P1, P2) were established, each of them containing ten samples, obtained using the faster polymerization method. The first group, M, contained only the commercial resin, while the P1 and P2 groups contain 1wt % and 2wt % graphene-silver nanoparticles respectively.

The mixture obtained from Superacryl Plus powder and liquid was placed in a stick-shaped plaster mold, immersed in cold water, and then cured in boiling water for a total time of 45 minutes, according to the commercial product specifications concerning the fast polymerization technique. The samples were obtained by cutting the sticks (150mm/15mm) in 5x1mm disks using a precision cutting device (Isomet 1000, Precision Saw, Buehler, ITW, Illinois, USA).

3. Methods

3.1. Water sorption

For water and artificial saliva sorption, a disk-shaped mould was used to obtain specimens of 15 ± 1 mm diameter and 1 mm thickness. The discs were dried in a desiccator in the presence of calcium chloride at 37°C for 24 h till a constant weight (m_0) was obtained. The samples were then divided into two groups and then immersed into distilled water and artificial saliva, respectively. Next, the disks were introduced in an incubator for 28 days, at a constant temperature of 37°C. Every day, the samples were removed from the water and weighted after 10 min (m_1), using an electronic analytical balance. The weight changes due to water absorption (W_a) were assessed, using the following equation (1) [44].

$$W_a = (m_1 - m_0)/m_0 \times 100 \quad (1)$$

3.2. Solubility

Solubility is the characteristic of a material to dissolve in a solvent. The reduction that occurs in the mass can be used to determine the water solubility of the material, according to ISO specifications [37].

The changes in the weight values (W) referred to the initial weight were calculated (after the difference between the initial mass m_0 and the final mass m_f of the sample was determined) using the formula

$$W = (m_0 - m_f)/m_0 \times 100.$$

3.3. Residual monomer

The residual MMA was extracted from the storage liquid (water, chloroform) used for samples' immersion. MMA concentration was determined using high performance liquid chromatography (HPLC). A high-performance liquid chromatograph - HPLC (JASCO - 980) was used, equipped with: Intelligent HPLC Pump (JASCO PU-980); Ternary Gradient Unit (JASCO LG-980-02); 3-line Degasser (JASCO DG-980-50); column thermostat (JASCO CO-2060 Plus; UV-VIS detector (UV-975), and ChromPASS software. The standard monomer was Superacryl Plus liquid (cross-linked methyl methacrylate). The analytical reagent for HPLC was acetonitrile. The water used in the study was Millipore ($18.2 \text{ M}\Omega\text{mcm}^{-1}$). *Stationary phase*: LiChroSorb C18 column (25 x 0.46 cm); *Mobile phase*: Acetonitrile: water: $\text{H}_3\text{PO}_4 = 30:70:0.1$, v/v; nm elution rate: 1 mL / min; detection: UV at 220; column temperature: 40°C.

The retention time (9.2 min) was obtained after the injection of standard MMA. Next, from the standard MMA, solutions with concentrations of 31.25-250 $\mu\text{g/ml}$, were prepared in order to be used for the residual MMA determination. The peak values, obtained by UV detection (according to the solutions concentration), associated with the calibration equation, were used to assess the MMA amount.

The first group of samples was immersed in chloroform, and the second group was immersed in cell medium solution for 24 h [27], then freeze-dried using a Lyophilizator (ALPHA 1-4LDPLUS) and after that dissolved in 2ml acetonitrile. The obtained solutions were filtered and introduced in the high-performance liquid chromatograph for the MMA assessment.

3.4. Scanning electron microscopy

The scanning electron microscopy analysis of the fillers and the samples, using a FEI Inspect microscope (SEM-Inspect S, FEI Company, Hillsboro, OR, USA), S model, functional in high-vacuum and low-vacuum, tan accelerating voltage between 200V and 30kV, was performed. The microscope was equipped with CCD-IR infrared inspection camera and backscatter electron detector, with image processing up to 4096×3536 pixels. The images were obtained at a magnification of 500x and 1000x.

3.5. Statistical analysis

One-way ANOVA test (Microsoft Office, Excel) was used to analyse the statistical differences between the obtained values. Tukey test and Pearson correlation coefficient were also used to evaluate the differences between the mean values of each material and between the studied characteristics, respectively.

REFERENCES

1. F.A. Peyton; *Dent Clin North Am*, **1975**, 19, 2, 211.
2. R.Q. Fraser; R.T. Byron; P.B. Osborne; K.P. West; *J Long Term Eff Med Implants*, **2005**, 15, 6, 629.
3. M.S. Zafar; *Polimers*, **2020**, 12,10, 2299.
4. J. L. Garcia-Fierro; J. V. Aleman; *Macromolecules*, **1982**, 15, 4, 40.
5. H. Rashid; Z. Sheikh; F. Vohra; *Eur J Dent*, **2015**, 9, 4, 614.
6. L.A. Bartolini; D.F. Murchison; D.T. Wofford; N.K. Sarkar; *J Oral Rehabil*, **2000**, 27, 6, 488-93.
7. P.K. Vallittu; I.E. Ruyter; S. Buykuilmaz; *Eur J Oral Sci.*, **1998**, 106, 1, 588-93.
8. N. Celebi N; B. Yüzügüllü; S. Canay; U. Yücel; *Polym Adv Technol*, **2008**, 19, 201-6
9. T. Forati; M. Atai; A. Rashidi A; M. Imani; A. Behnamghader; *Polym Adv Technol*, **2014**, 25. 10.1002/pat.3243.
10. Z. Han; B. Zhu; R. Chen; Z. Huang; C. Zhu; X. Zhang; *Mater. Des*, **2015**, 65, 1245-1252.
11. A. Jatania; B.M. Shivalinga; *Eur J Dent*, **2014**, 8, 1, 112-7.
12. T. Kanie; K. Fujii; H. Arikawa; K. Inoue; *Dent Mater*. **2000**, 16, 2, 150-8.
13. H. Kong; J. Jang; *Langmuir*, **2008**, 24, 2051-6.
14. C. Bacali; I. Baldea; M. Moldovan et al; *Clin Oral Investig*, **2020**, 24,8, 2713-2725.
15. S.H. Tuna; F. Keyf; H.O. Gumus; C. Uzun; *Eur J Dent*, **2008**, 2, 191-197.
16. F. Ghani; R. Moosa; *J Pak Dent Assoc*, **2012**, 21, 127-135.
17. V.M. Miettinen; P.K. Valittu; *Biomaterials*, **1997**, 18, 2, 181-5.
18. A. Miettinen; P.K. Vallittu; D.T. Docent; *J Prosthet Dent*, **1997**, 77, 5, 531-4.
19. B. Zhang; P. Wei; Z. Zhou; T. Wei; *Adv Drug Deliv Review*, **2016**, 105, 145-162.
20. A. Akinci; S. Sen; U. Sen; *Composites Part B: Engineering*, **2014**, 56, 42-47.
21. S.H. Kang; T.H. Fang; Z.H. Hong; C.H. Chuang; *Diam. Relat. Mater.*, **2013**, 38, 73-78.
22. B. Lee; X. Wei; J. Kysar; J. Hone; *Science*, **2008**, 321, 385-8.
23. V. Jerolimov; S.C. Brooks; R. Huggett; J.F. Bates; *Dent Mater*, **1989**, 5, 1, 18-22.
24. D.M. Wong; L.Y. Cheng; T.W. Chow; R.K. Clark; *J Prosthet Dent.*, **1999**, 81, 3, 300-4.
25. A.M. Fletcher; S. Purnaveja; W.M. Amin; G.M. Ritchie; S. Moradians; A.W. Dodd; *J Dent Res*, **1983**, 62, 2, 118-20.
26. E. Paz; F. Forriol; J.C. del Real; N. Dunne; *Mater Sci Eng C Mater Biol Appl*, **2017**, 77, 1003-1011.
27. G. Danesh; T. Hellak; K. Reinhardt; A. Vegh; E. Schafer; C. Lippold; *Exp Toxicol Pathol*, **2012**, 64, 867-872.
28. L. Kanerva; *Acta Odontol Scand*, **2001**, 59, 320-9.
29. M. Nakamura; H. Oshima; Y. Hashimoto; *J Prosthet Dent*, **2003**, 90, 81-5.
30. M.F. Tansy; J.S. Martin; S. Benhaim; W.E. Landin; F.M. Kendall; *J Pharm Sci*, **1977**, 66, 613-9.
31. S.E. Anderson; B.J. Meade; *Environ Health Insights*, **2014**, 8, 1, 51-62.

WATER SORPTION, SOLUBILITY AND MONOMER RELEASE OF A FAST POLYMERIZED HEAT-CURING RESIN ENHANCED WITH GRAPHENE SILVER NANOPARTICLES

32. C. Bacali; S. Buduru; V. Nastase; A. Craciun; M. Constatiniuc; M. Badea; C. Sarosi; *Studia UBB Chemia*, **2019**, *2*, 471-481.
33. A. Harrison; R. Huggett; *J Dent*, **1992**, *20*, 370-4.
34. M.J. Azzarri, M.S. Cortizo; J.L. Alessandrini; *J Dent*, **2003**, *31*, 463-8.
35. T. Charasseangpaisarn; C. Wiwatwarrapan; N. Leklerssiriwong; *J Dent Scien*, **2016**, *11*, *4*, 443-448.
36. A. Doğan; B. Bek; N.N. Cevik; A. Usanmaz; *J Dent*, **1995**, *23*, 313-318.
37. ISO 1567:1999 Dentistry-Denture base Polymers.
38. L.V. Lassila; P.K. Vallittu; *J Oral Rehabil.*, **2001**, *28*, *7*, 607-13.
39. S. Sava, A Tonea, S Boboia, C Alb, C Sarosi, D Dudea; *Studia UBB Chemia*, **2015**, *60*, *2*, 71-80.
40. P. Jiman, M. Moldovan, C. Sarosi, A.muntean, A.S. Pop, V Tarmure, C. Popa, A.G. Mohan; *Studia UBB Chemia*, **2020**, *65*, 149-162.
41. D. Sucala, C. Sarosi, C. Popa, I. Cojocararu, M. Moldovan, A.G. Mohan; *Studia UBB Chemia*, **2018**, *63*, *2*, 71-80.
42. D. Olteanu; A. Filip; C. Socaci; A.R. Biris; X. Filip; M. Coros; M.C. Rosu; F. Pogacean; C. Alb; I. Baldea; P. Bolfa; S. Pruneanu; *Colloids Surf B Biointerfaces*, **2015**, *136*, 791-798.
43. X. Zhang; B. Zhu; K. Lin; J. Chang; *Dent Mater*, **2012**, *31*, 903-8.
44. W.M. Khalil; *J Bagh Coll Dentistry*, **2005**, *17*, 37-41.

PREVENTIVE AND PREDICTIVE MAINTENANCE OF AMMONIUM NITRATE GRANULATION PROCESS BASED ON PRELIMINARY HAZARD ANALYSIS TECHNIQUE

Ramona LEORDEAN^a, Alexandru OZUNU^a,
Zoltán TÖRÖK^{a,*}

ABSTRACT. A technological accident in a fertilizer production plant often results from the interaction between several hazards. Preliminary Hazard Analysis (PHA) being a general level, qualitative method, it is easily applicable for all types of operations and functions of a system. The objective of this paper is to demonstrate the importance of using PHA in the context of preventive and predictive maintenance, and to highlight the potential benefits of these strategies in mitigating the risks of potential accidents related to the granulation process of fertilizer grade AN. The results of the study show that the most dangerous scenarios identified, in terms of consequences, are potential explosions of AN due to friction and melting in case of rotative equipment failure, or auto-decomposition and explosion of AN due to contamination with organic substances. Since qualitative deterministic approaches are lacking in uncertainty and sensitivity analysis, their use should be completed by more complex quantitative analyses, in order to support efficient decision making for risk mitigation and balanced maintenance efforts.

Key words: ammonium nitrate, granulation process, preliminary hazard analysis, predictive maintenance, preventive maintenance

^a Babes-Bolyai University, Faculty of Environmental Science and Engineering, Research Institute for Sustainability and Disaster Management based on High Performance Computing (ISUMADECIP), 30 Fântânele Str., RO-40294, Cluj-Napoca, Romania

* Corresponding author: zoltan.torok@ubbcluj.ro



INTRODUCTION

While the simple periodic maintenance is still the most applied strategy in industries [1], in the recent years many chemical production companies have implemented a specific preventive maintenance (PM) strategy, such as age-based PM, respectively block PM [2], and predictive maintenance (Pr.M) strategies are also under implementation. These strategies aim to reduce, on one hand, the maintenance-related costs, estimated up to 25 % of the overall operational costs [3]. On the other hand, they can be used in order to increase the performance of a system [2], for effective risk reduction, by preventing potential accidents caused by aging or external shocks. A study investigating 183 major chemical accidents, which occurred between 2000 – 2011 in the US and Europe, reveals that 44% of these were linked to maintenance problems [4].

As a result of numerous accidents that occurred worldwide involving chemical fertilizers, especially ammonium nitrate (AN), the conditions for the production, use, handling, storage and transport of AN have become increasingly stringent, being regulated as clearly as possible both at national and international levels [5]. Besides the risks related to the AN's lifecycle, there are some other important risks that can be identified in the fertilizers production plants, such as raw and auxiliary materials, respectively the equipment carrying those materials [6]. Efficient and safe operation of the installations from the fertilizers production sites supposes their continuous operation as much as possible, in order to avoid fluctuations at start-ups and shutdowns. This practically implies a substantial reduction in the number of stops caused by various faults [7], which can be achieved by implementing PM and Pr.M strategies.

The European standard EN 13306 – Maintenance Terminology [8] defines preventive maintenance as “the maintenance carried out at predetermined intervals or according to prescribed criteria and intended to reduce the probability of failure or the degradation of the functioning of an item”. Predictive maintenance is defined as “the condition-based maintenance carried out following a forecast derived from repeated analysis or known characteristics and evaluation of the significant parameters of the degradation of the item” [8].

Although more companies are recognizing the importance of a maintenance plan, gaps in understanding remain regarding the concept of maintenance, which includes all actions and processes - scheduled or unscheduled - aimed at ensuring uninterrupted access to operational equipment in a process plant, and the potential consequences of superficial execution [9]. As Shin and Jun underline in their study, the prediction of an item's degradation relies on the premise that most anomalies do not arise suddenly, but rather progress gradually from a state of normal functioning to an abnormal one [10].

Maintaining the system is increasingly critical due to technical advancements, regulatory changes, and operational variations [11]. Inadequate planning leads to unreliable procedures and disruptions to production, as Basri et al. argue [6]. Proper planning prioritizes essential maintenance tasks and considers resources, information, and scheduling [12]. Ensuring system safety involves a formal procedure to identify and mitigate risks. Complex systems increase the likelihood of hazards, requiring effective risk analysis and management [13].

Fertilizers and other chemicals manufacturing processes rely on several key equipment to maintain efficient production rates. The ability to produce globally competitive, high-quality goods like chemical fertilizers is considerably impacted by subpar maintenance management [14].

Besides prilling, granulation is one of the most common processes used to produce solid AN, with improved handling, bulk storage and packaging qualities. Fertilizers production processes and systems are often very complex, which is why they contain a significant number of hazards, that often can lead to technological accidents in a fertilizer production site.

Preliminary Hazard Analysis (PHA) being a general level, qualitative hazard analysis method, it is easily applicable for all types of operations and functions and can be performed on a system, subsystem, unit or even on integrated set of systems [15].

The objective of this paper is to demonstrate the importance of using qualitative hazard analysis techniques, such as PHA, in the context of preventive and predictive maintenance, and to highlight the potential benefits of these strategies in mitigating the risks of potential accidents related to the granulation process of fertilizer grade AN. As Arunraj and Maiti highlight in their literature review on risk-based maintenance [16], qualitative deterministic risk analysis methods are very often used in maintenance planning.

RESULTS AND DISCUSSION

The results of the PHA are presented in table 2, in the experimental section. The analysis took into consideration only a small part of the whole AN production process, respectively the granulation step, with the main and most critical equipment involved, the rotary drum granulator and its components.

Some of the safety measures and actions proposed in the PHA analysis that are commonly used include:

- compliance with working procedures and parameters;
- periodic update of working procedures, according to legal requirements, best practices and specific guidelines;

- periodic trainings of personnel;
- laboratory check-ups, where necessary;
- emergency intervention devices and equipment are accessible and maintained in good working condition;
- employees to wear individual protective equipment in accordance with the health and safety requirements in force.

According to table 3, the results show that the majority of the hazards identified in the granulation process fall under the low and moderate risk levels. The highest risk level obtained is 12 – moderate risk, generated by potential leaks in the technological flow, due to excessive vibration of equipment.

The probability of the hazards identified ranges from *Improbable* to *Occasional*, while their consequences range between *Minor* and *Catastrophic* (in case of melted AN explosion).

As we can observe in table 2, there were also identified three of the most severe potential risks that could lead to fires and explosions, caused by leaks, contaminations or overheating due to mechanical errors or failures on specific parts of the equipment involved in the granulation process.

By the application of the PHA method several important preventive and predictive actions and measures have been identified, including visual inspections, routine realignment, tire and trunnion grinding, lubrication, and periodic operator training. For predictive measures, techniques such as vibration analysis, noise monitoring, fluid analysis, oil monitoring, tribology, and thermography were considered relevant [17].

While it is true that some of the actions and techniques suggested are already performed in fertilizer production plants as part of their routine equipment maintenance, the PHA carried out on the rotating drum granulator, as a critical piece of equipment, emphasizes the importance of visual inspection as an early and trusted method of evaluating an asset's condition. Its primary goal is to identify and address problems before they worsen. As such, it is important for operators and maintenance personnel to receive training on what to look for and when to conduct inspections.

Tires and trunnions play a crucial role in supporting the drum and ensuring its smooth rotation. Due to constant load and friction, these components are often the first to show signs of wear when problems occur, with potential causes ranging from misaligned drums to fugitive material and improper lubrication. Given their structural importance, any indication of wear should be promptly addressed and properly inspected.

Under normal conditions, rotary drum granulators produce minimal vibration signals. However, when intensive vibration signals are detected in terms of velocity, acceleration, or displacement, it is a clear sign of major issues

such as unbalance, misalignment, or worn gears or bearings, all of which require attention and repair. Special sensors and detection devices can be used for this purpose [18].

Another important predictive maintenance action is noise monitoring, which involves using acoustic sensors to detect ultrasonic and audible frequencies.

For rotating drums, oil plays a crucial role in providing lubrication, cooling, and insulation, making it essential to monitor the quality of the oil as part of the maintenance process. The oil is susceptible to contamination from various types of particles, including those caused by bearing wear and tear, partial discharges, and friction of streaming oil.

CONCLUSIONS

Effective and appropriate maintenance actions, including both predictive and preventive measures, can play a crucial role in identifying and addressing operational anomalies and equipment defects before they result in failures. Firstly, these proactive maintenance measures can help to reduce the costs associated with maintenance activities. Secondly, they can also enhance process safety by reducing the frequency of equipment breakdowns, which can be critical in some cases. Additionally, they can improve the quality of the production process and the final products.

Predictive maintenance is a type of maintenance that is triggered by the condition of a system, as opposed to preventive maintenance, which is time-driven. As a result, predictive maintenance is only performed when necessary, making it a more reliable approach compared to preventive maintenance.

The overall aim was to perform a PHA-type (Preliminary Hazard Analysis) qualitative risk assessment of hazards and associated risks found in the granulation stage of fertilizer grade AN production, emphasizing the utility and necessity of an appropriate maintenance plan comprising specific preventive and predictive measures. However, the authors acknowledge the fact that qualitative deterministic approaches are lacking in uncertainty and sensitivity analysis, therefore, their use should be completed by more complex quantitative analyses, in order to support efficient decision making for risk mitigation and balanced maintenance efforts.

The results of the study show that the most dangerous scenarios, in terms of consequences, are potential explosions of AN due to friction and melting in case of *hazard 4. Broken screw feeder shaft*, *hazard 5. Screw feeders shaft's belt overheating* or auto-decomposition and explosion of AN due to *hazard 6. Contamination with organic substances*.

A potential research objective for the future could involve examining the influence of maintenance on a fertilizer manufacturing company's profitability and product quality, utilizing data from a specific company and considering variables that offer insight into the impact of maintenance on quality. The objective is to gain a comprehensive understanding of the financial impact of maintenance measures in the long run, and how they may inform a company's strategy for reducing maintenance costs.

EXPERIMENTAL SECTION

Methods and techniques

A system is inherently susceptible to deterioration during continuous use, causing its functionality to evolve over time. Maintenance operations are conducted over a period of time, and figure 1 displays the number of failures occurring as a function of operational time [19]. Consequently, newly installed equipment is at an increased risk of malfunctioning during the first week of operation, typically due to installation issues. Thereafter, the likelihood of failures is relatively low for an extended period.

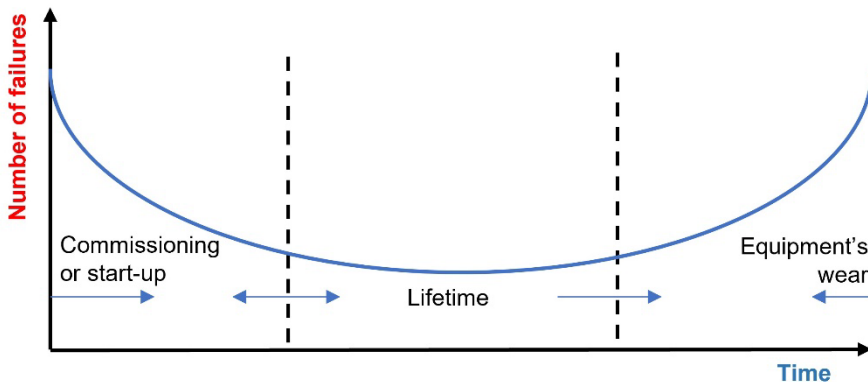


Figure 1. Representation of machine's / equipment's / system's failures during its lifecycle [19]

All fertilizers processing units, have some key equipment such as rotary drums, turbines, compressors, pumps and product transport pipes, all subject to a variety of process-driven conditions that lead to corrosion, erosion, fouling and a lot of other process-related issues, causing serious problems for the companies, the quality of the products, the environment, the health and safety of the workers [20] [21]. According to U.S. EPA AP 42, *Ammonium nitrate manufacturing industry – Technical document (1981)*, “rotary drum granulators

produce granules by spraying a concentrated ammonium nitrate melt (99.0 to 99.8 percent) onto small seed particles of ammonium nitrate in a long rotating cylindrical drum” [22].

In the PHA performed in this study, we tried to identify all potential hazards and failures that may lead to an accident during the AN granulation process, especially due to the AN’s hazardous properties [23]. The identification of the hazards has been performed considering different aspects, such as the quality of the final product, working conditions and mechanical components involved in the AN granulation process. The order of the hazards presented in table 2 is based on the appearance of ideas and discussions during the “brainstorming” process for the analysis.

The next step was to rank the identified hazards according to their probability of occurrence and their consequences’ severity, all these considering the key role of the rotary drum granulator as a critical equipment in the process [22] [24]. In the end, we have proposed some control measures and follow-up actions, based on the preventive and predictive maintenance concept, in order to mitigate the potential risk.

The risk matrix used (table 1) in the PHA aims to categorize risks, based on their level of probability (P) and consequences (C), where the risk (R) is the product of these two. The qualitative values allocated for these risk components (on a scale of 1 to 5, described in details in [25]) were chosen based on the working procedures and instructions for the AN granulation process, maintenance plan, HAZOPs, scientific literature and on the experience of the team.

Table 1. Risk matrix used in the PHA

		Consequence				
		Insignificant	Minor	Moderate	Major	Catastrophic
		1	2	3	4	5
Probability	Improbable	1	2	3	4	5
	Isolated	2	4	6	8	10
	Occasional	3	6	9	12	15
	Probable	4	8	12	16	20
	Frequent	5	10	15	20	25

Legend:

Risk level	Definition
1 – 3	Very low risk
4 – 6	Low risk
7 – 12	Moderate risk
13 – 19	High risk
20 – 25	Extrem risk

All the methodological aspects mentioned above were taken into consideration in order to underline the interdependence between maintenance, quality, productivity and safety [26].

Table 2. PHA results for the AN granulation process

Hazard	Causes	P	C	R	Expected conseq.	Existing safety measures and actions	PM actions / Pr.M actions
1. Too fine or too coarse granulation	a. Clogged, incorrectly adjusted or broken sieves	3	2	6	Affecting product quality	The concentration and pH are checked by laboratory analyses; The granulation of the recycling is checked; The opening on the mills is checked; If required, the sieving line is changed	<u>Preventive actions</u> Visual inspections;
2. High level of humidity in the granules	a. Temperature too low in granulator	3	2	6	Affecting product quality	Visual analysis Laboratory analysis for humidity and granulation; Measuring temperature in the granulator.	<u>Predictive actions</u> Thermographic testing;
3. Variations of the vacuum in the granulator	a. Clogged or uncorrelated cyclones	3	2	6	Variations in the humidity of the final product, respectively affecting the quality of the product	Unclogging the cyclones; Replacing the bags; Adjustments on the flap opening;	<u>Preventive actions</u> N.A.
	b. Broken cyclones bags	2	2	4			<u>Predictive actions</u> Pressure monitoring
4. Broken screw feeder shaft	a. Mechanical failure	2	5	10	Belt friction and ignition which can lead to possible explosion	Smoke detectors; Compliance with work parameters and manufacturing procedures; Keeping emergency intervention devices and equipment in working order	<u>Preventive actions</u> Checking the technical condition of the machines by non-destructive methods, applying up-to-date technologies;
	b. Broken screws	2	5	10			Visual inspections;
	c. Broken pallets	2	5	10			Hot-spot identification using thermal imaging cameras and warning by acoustic and optical signals;
5. Screw feeders shaft's belt overheating	a. Technical / mechanical error	2	5	10	AN melting and possible explosion	Compliance with work parameters and manufacturing procedures; Keeping emergency intervention devices and equipment in working order;	<u>Preventive actions</u> Visual inspections; <u>Predictive actions</u> Hot-spot identification using thermal imaging cameras and warning by acoustic and optical signals;
6. Contamination with organic substances	a. Crack / leaks in the granulator	1	5	5	Auto decomposition of AN and possible explosion	Compliance with work parameters and manufacturing procedures;	<u>Preventive actions</u> Visual inspections;
7. Leaks in the technological flow	a. Granulator's excessive vibrations	3	4	12	These types of leaks can lead to the occurrence of fire conditions, due to oxidizing properties of AN	Periodic check to detect any notable vibration; Periodic check to detect any notable leakage; Wearing individual protective equipment in accordance with the requirements set forth in the labor protection regulations;	<u>Preventive actions</u> Visual inspections; <u>Predictive actions</u> Vibration detection and analysis;
8. Irregularities in the technological process	a. Partial or total non-functionality of the measuring and control equipment	1	3	3	Affecting product quality Granulation process stops	Periodic check on the measuring and control equipment, according to legal requirements and internal procedures	<u>Preventive actions</u> Visual inspections; Calibration;
9. Inconstant rotation	a. Rotary drum granulator's misalignment	3	3	9	Additional stress is put on all components; Tire wear; Bearing failure; Gear damage;	Compliance with work parameters and manufacturing procedures;	<u>Preventive actions</u> Visual inspections; Routine realignment; Tire and trunnion grinding; <u>Predictive actions</u> Specific types of tribological tests; Ultrasonic tests;

**PREVENTIVE AND PREDICTIVE MAINTENANCE OF AMMONIUM NITRATE GRANULATION
PROCESS BASED ON PRELIMINARY HAZARD ANALYSIS TECHNIQUE**

Hazard	Causes	P	C	R	Expected conseq.	Existing safety measures and actions	PM actions / Pr.M actions
10. Tire and trunnion wear	a. Misaligned rotary drum granulator	3	3	9	Extensive tire / wheel wear; Damage to the tire / wheel; Major contact between the drum and thrust rollers; Additional downtime and maintenance actions;	Compliance with work parameters and manufacturing procedures;	<u>Preventive actions</u> Visual inspections; Routine realignment; Tire and trunnion grinding; <u>Predictive actions</u> Fluid analysis – oil monitoring;
	b. Improper lubrication	3	3	9	Contamination; Increased noise; Leakages that can increase the chances of seal shrinkage, resulting in the process failure; Component failures; Intensive vibration; Production losses; Added maintenance repairs and actions;	Compliance with work parameters and manufacturing procedures;	Specific types of tribological tests;
11. Intensive vibration signals	a. Granulator's unbalance	2	3	6	Premature bearing destruction; Production losses;	Compliance with work parameters and manufacturing procedures;	<u>Preventive actions</u> Visual inspections; <u>Predictive actions</u> Specific types of tribological tests;
	b. Rotary drum granulator's misalignment	2	3	6	Excessive wear or damage to tires or trunnion wheels;	Periodic lubrication; Compliance with the operating conditions and procedures;	Ultrasonic tests;
	c. Worn gears or bearings	2	3	6	Added maintenance repairs and actions;		Vibration sensors
12. Contaminated oil	a. Bearing wear and tear	2	3	6	Added maintenance repairs and actions;	Periodic change of the oil;	<u>Preventive actions</u> Visual inspections;
	b. Partial discharges or friction of streaming oil	2	4	8	Thermal degradation of the insulation;	Compliance with work parameters and manufacturing procedures;	<u>Predictive actions</u> Fluid analysis – oil monitoring; Specific types of tribological tests; Ultrasonic tests;
13. Granulation process accidentally stopped	a. Breaking of the transmission belts of the motor - reducer drive system of the granulator	2	3	6	Added maintenance repairs and actions;	Compliance with work parameters and manufacturing procedures;	<u>Preventive actions</u> Visual inspections;
	b. Blockage of the axles with pallets due to the penetration of hard, metallic bodies	1	3	3	Added maintenance repairs and actions;		
	c. Stopping of the drive motor through the overload relay (the motor takes more amperage than the maximum set value), due to material deposits (melt, crust) on the vat and on the pallets	1	3	3	Added maintenance repairs and actions;		
	d. Leaks in the melting path	2	3	6	Added maintenance repairs and actions;		

Table 3. Risk matrix completed for the AN granulation process PHA

		Consequence					
		Insignificant	Minor	Moderate	Major	Catastrophic	
		1	2	3	4	5	
Probability	Improbable	1	2	3: 8a, 13b, 13c	4	5: 6a	
	Isolated	2	4: 3b	6: 11a, 11b, 11c, 12a, 13a	8: 12b	10: 4a, 4b, 4c, 5a	
	Occasional	3	6: 1a, 2a, 3a	9: 9a, 10a, 10b	12: 7a	15	
	Probable	4	4	8	12	16	20
	Frequent	5	5	10	15	20	25

REFERENCES

1. H. E. Van Staden; L. Deprez; R. N. Boute; *Eur. J. Oper. Res.*, **2022**, 302(3), 1079-1096.
2. M. Hashemi; M. Tavangar; M. Asadi; *Comput. Ind. Eng.*, **2022**, 163, 107829.
3. A. Haroun; *J. Qual. Maint. Eng.*, **2015**, 21(3), 258-270.
4. P. Okoh; S. Haugen; *Process Saf. Environ.*, **2014**, 92(4), 346-356.
5. D. T. Anh; K. Dąbrowski; K. Skrzypek; *Found. Manag.*, **2018**, 10(1), 283 – 292.
6. E.I. Basri; I.H. Abdul Razak; H. Ab-Samat; S. Kamaruddin; *J. Qual. Maint. Eng.*, **2017**, 23(2), 114-143.
7. T. Kletz; *What Went Wrong. Case Histories of Process Plants Disasters*, 4th ed.; Gulf Publishing Company, Houston TX, USA, **1999**, pp. 370- 371.
8. EN 13306 Standard – *Maintenance – Maintenance terminology*.
9. P. Gackowiec; *Multidiscip. Asp. Prod. Eng.*, **2019**, 2(1), 126-139.
10. J.-H. Shin; H.-B. Jun; *J. Comput. Des. Eng.*, **2015**, 2(2), 119-127.
11. P Söderholm; *Reliab. Eng. Syst.*, **2007**, 92(1), 1-14.
12. O. Merkt; *Proc. Fed. Comput. Sci. Inf. Syst.*, **2019**, 693-704, doi: 10.15439/2019F101.
13. L. Swanson; *Int. J. Prod. Econ.*, **2001**, 70(3), 237-244.
14. R.S. Velmurugan; T. Dhingra; *Int. J. Oper. Prod. Manag.*, **2015**, 35(12), 1622 – 1661.
15. B. Martel; *Chemical risk analysis: a practical handbook*, Butterworth - Heinemann, United Kingdom, **2004**, pp. 29-31.
16. N. S. Arunraj; J. Maiti; *J. Hazard. Mater.*, **2007**, 142, 653-661.
17. Endevco an amphenol company, Applications, Accessed on 4 February 2023, www.endevco.com/applications/chemical-processing.
18. Wilcoxon sensing technologies, Accessed on 4 February 2023, <https://wilcoxon.com/vibration-transmitters-it-series-3/>.
19. S. O. Duffuaa; A. Raouf; J. Campbell; *Planning and Control of Maintenance Systems: Modelling and Analysis*, John Wiley & Sons Inc., New York, USA, **1999**, pp. 59-66.
20. B. Al-Najjar; *Int. J. Prod. Econ.*, **2007**, 107(1), 260–273.
21. J. C. Reynolds; R. M. Reed; *Environmental Symposium of the Fertilizer Institute*, Progress Report on Spherodizer Granulation 1975-1976, New Orleans, USA, **1976**, p. 23.
22. United States Environmental Agency; *AP 42 - Ammonium nitrate manufacturing industry – Technical document*, **1981**, pp. 7.
23. Z. Török; A. Ozunu; *Environ. Eng. Manag. J.*, **2015**, 14(11), 2671-2678.
24. D. Goyal; A. Chaudhary; R. K. Dang; B. S. Pabla; S. S. Dhami; *World Sci. News*, **2018**, 113, 98-108.
25. Z. Török, N. Ajtai, A. Ozunu, *Applications for assessing the risk of major industrial accidents involving dangerous substances (In Romanian: Aplicații de calcul pentru evaluarea riscului producerii accidentelor industriale majore ce implică substanțe periculoase)*, EFES, Cluj-Napoca, Romania, **2011**, pp. 27.
26. M. R. R. Khan; I. A. Darrab; *J. Qual. Maint. Eng.*, **2010**, 16(4), 341-353.

BULK AND BILAYER INVERTED ORGANIC SOLAR CELLS (OSCs) EXHIBITING D-A AND A-D-A DONORS WITH 2,2'-BI[3,2-*b*]THIENOTHIOPHENE UNITS AND PC₆₁BM OR C₇₀ ACCEPTORS

Levi GABRIAN^a, Gavril-Ionel GIURGI^{a,b}, Lorant SZOLGA^{a,b,*},
Andreea Petronela CRIȘAN^a, Elena BOGDAN^a, Ramona GĂLĂTUȘ^b,
Anamaria TERECA^a, Ion GROSU^{a,*}

ABSTRACT. Inverted bilayer and inverted bulk heterojunction OSCs were fabricated and investigated using D-A and A-D-A donors with bi[3,2-*b*]thienothiophene units and PC₆₁BM or C₇₀ acceptors. The cells were optimized by varying the donor/acceptor ratios, the thickness of the layers and the conditions for the spin-coating deposition of the active materials.

Keywords: organic solar cells, inverted bilayer structure, inverted bulk heterojunction, 2,2'-bi[3,2-*b*]thienothiophene donors

INTRODUCTION

2,2'-Bi[3,2-*b*]thienothiophene ([3,2-*b*]-TT) derivatives show a plethora of applications, in emerging fields as medicinal chemistry, [1-3] non-linear optic devices [4,5], materials with liquid crystal behavior [6,7] and conducting (co)polymers. [8–10]. Due to their special opto-electronic properties they were also employed for the fabrication of efficient OSCs (as building blocks in donor molecules [11–16] or non-fullerene acceptors [17–22]) or dye-sensitized solar cells (DSSCs) [23–26].

The replacing of a thiophene ring or a bithiophene unit either in acceptors (**A**) (e.g., [18]) or in donors (**D**) (e.g., [12]) with a [3,2-*b*]-TT moiety

^a Babes-Bolyai University, Faculty of Chemistry and Chemical Engineering, Department of Chemistry and SOOMCC, Cluj-Napoca, 11 Arany Janos, 400028, Cluj-Napoca, Romania

^b Optoelectronics Group, Base of Electronics Department, ETTI, Technical University of Cluj-Napoca, Str. Memorandumului, Nr.28, Cluj-Napoca, 400114, Romania

* Corresponding authors: lorant.szolga@bel.utcluj.ro; ion.grosu@ubbcluj.ro



indicated an improvement in the efficiency of the OSCs exhibiting the modified donors and/or acceptors. In order to develop our research in the field of molecules with exciting optoelectronic properties [27–31] and considering the outstanding properties of [3,2-*b*]-TT derivatives, in a recent work [32] we reported the synthesis and characterization of novel 2,2'-bi[3,2-*b*]thienothiophene derivatives as possible donors for OSCs with **D-A** or **A-D-A** systems.

The fabrication of OSCs can be carried out by vacuum deposition of bilayer planar heterojunction (PHJ) and using solution-processed bulk heterojunction solar cells (BHJ). [33-35] BHJ cells are fabricated at ambient temperature by spin-casting blend films from solutions of donor (**D**) and acceptor (**A**) materials. More stable cells could be obtained in the so called inverted structures of OSCs in which solution-processed layers of ZnO and PVD (Physical Vapor Deposition) deposited MoO₃ are inserted between the electrodes and the active materials, replacing the air and moisture sensitive PEDOT : PSS layer used in the so called direct cells. The active layer in this case can be deposited by spin-casting or PVD technique. The literature in the field underlines the higher efficiency and stability of inverted cells. [33, 35-39]

In this context we considered of interest to fabricate and investigate inverted bilayer and inverted bulk heterojunction OSCs using **D-A** (**1** and **2**, Figure 1) and **A-D-A** (**3**, Figure 1) donors with bi[3,2-*b*]thienothiophene units (unexplored in OSCs) and **PC₆₁BM** (Figure 1) or **C₇₀** (Figure 1) acceptors. Donors **1-3** are new compounds and we recently reported their synthesis and structure determinations.

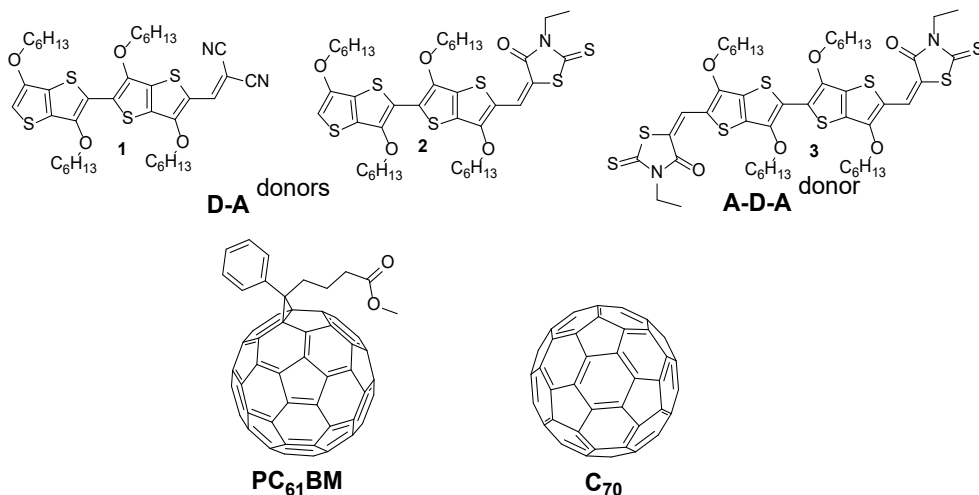


Figure 1. Chemical structures for donors (**1**, **2** and **3**) and the acceptors (C₇₀ and PC₆₁BM)

RESULTS AND DISCUSSIONS

The simplified structures of inverted-bilayer and inverted-BHJ OSCs are shown in Figure 2. For both structures (bilayer and bulk), two buffer layers were used: one of ZnO with high capability to conduct electrons to the ITO electrode and one of MoO₃ to increase hole-mobility to the Al electrode. At the same time, the MoO₃ presents very good properties for the encapsulation of the cells, protecting the active layer from the outside environment. Layers like C₇₀, MoO₃ and the Al were always deposited in the vacuum by PVD (Physical Vapor Deposition) technique. The active layer in the case of the BHJ structures was deposited by spin-coating from solution and for the bilayer structures, the donors **1** and **2** were deposited by PVD (donor **3** decomposed during the PVD deposition).

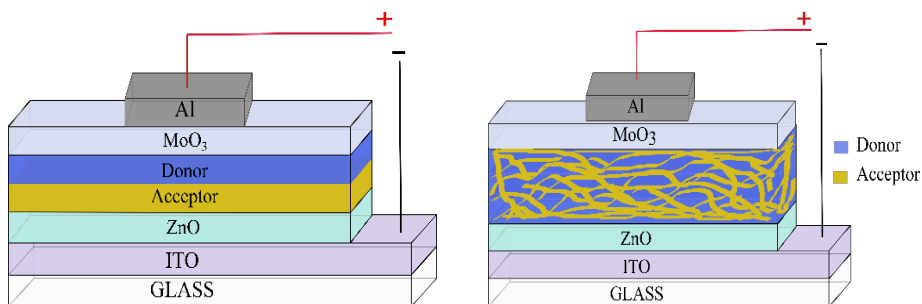


Figure 2. Simplified representations of OSC structures: inverted-bilayer (left) and inverted-BHJ (right)

Inverted-BHJ structure (ITO/ZnO/Donor:PC₆₁BM/MoO₃/Al)

We started to test out the OSC capabilities of the three compounds in inverted bulk architectures, by using a donor-acceptor (Donor: PC₆₁BM) ratio of 1:1 (w:w) and different film thicknesses.

Table 1. Inverted-bulk solar cell efficiencies using Donor-Acceptor (Donor - PC₆₁BM) ratio of 1:1 (w:w) in different active film thicknesses

Film Thickness [nm]	PCE [%]		
	Donor 1	Donor 2	Donor 3
25	0.52	0.49	1.78
35	0.62	0.59	2.28
60	0.36	0.33	1.37

The active film deposition thickness was controlled by the spin-coater speed, to obtain 60 nm, 35 nm, and 25 nm layers.

Having established the optimum film thickness we further investigated the three compounds in different donor: acceptor ratios. The efficiencies measured through these experiments are presented in Table 1, and show that the optimum thickness of the active layer should be 35 nm for all three compounds.

In the first step, we increased the ratio D:A to 1:2 (w:w). Based on the efficiency results of this experiment (Table 2), donors **1** and **2** showed a decrease in efficiency, and donor **3** an increase in efficiency in comparison to the 1:1 ratio. Thus, in the next step we evaluated the efficiency of donors **1** and **2** in a donor:acceptor ratio of 2:1 (w:w) and for compound **3** in a ratio of 1:3 (w:w). These experiments revealed (Table 2) the optimum donor:acceptor ratio of 1:1 (w:w) by the use of donors **1** and **2** with a maximum Power Conversion Efficiency (PCE) value of 0.6% and a ratio of 1:2 for donor **3** with a maximum PCE value of 2.5%.

Table 2. Inverted-bulk solar cell efficiencies using different Donor-Acceptor (Acceptor: PC₆₁BM) ratios for the 35 nm active layer thickness

Donor:Acceptor ratio (w:w)	PCE [%]		
	Donor 1	Donor 2	Donor 3
2:1	0.20	0.24	-
1:1	0.62	0.59	2.28
1:2	0.55	0.48	2.5
1:3	-	-	1.42

The electrical characteristics of the best cells and highest PCE values from Table 2, are presented in detail in Table 3 and the J_{sc}-V_{oc} (current density- open circuit voltage) and EQE (external quantum efficiency) characteristics are plotted in Figure 3, where FF stands for fill-factor.

Table 3. Electrical characteristics of the cell with the best efficiencies and the average value of the efficiencies on a batch of six cells

Comp.	V _{oc} [V]	J _{sc} [mA/cm ²]	FF [%]	PCE [%] best cells	Average PCE [%]
1	0.73	2.15	39.75	0.62	0.61
2	0.65	2.66	34.42	0.59	0.57
3	0.90	5.97	46.53	2.5	2.47

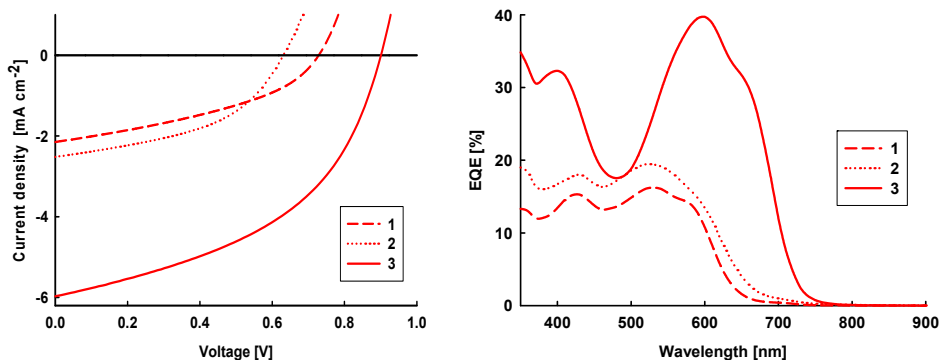


Figure 3. Current density vs voltage curves (left) and EQE curves (right) for best inverted-BHJ cells using donors **1**, **2** and **3**.

Inverted-bilayer structure (ITO/ZnO/C₇₀/Donor/MoO₃/Al)

The investigation of the OSC capabilities using the three compounds in inverted bilayer architecture was undertaken in a standard configuration of film stacking of 30 nm of the acceptor (C₇₀) and 20 nm of the donor (**1**, **2**, **3**). The deposition of the layers was fully taken in a vacuum chamber using PVD (physical vapor deposition) technique. The experiments revealed good evaporation for compounds **1** and **2** and a high degradation for compound **3**. Thus, the bilayer structure is well suited for donors **1** and **2**. The electrical characteristics of the best cells are summarized in Table 4 and the J_{sc}-V_{oc} and EQE characteristics are plotted in Figure 4.

Table 4. Electrical characteristics of the best cells in inverted-bilayer structure and the average value of the efficiencies on a batch of six cells

Comp.	V _{oc} [V]	J _{sc} [mA/cm ²]	FF [%]	PCE [%] best cells	Average PCE [%]
1	0.66	2.68	34.87	0.62	0.57
2	0.63	2.52	46.49	0.74	0.68
3	NA	NA	NA	NA	NA

*NA- does not apply

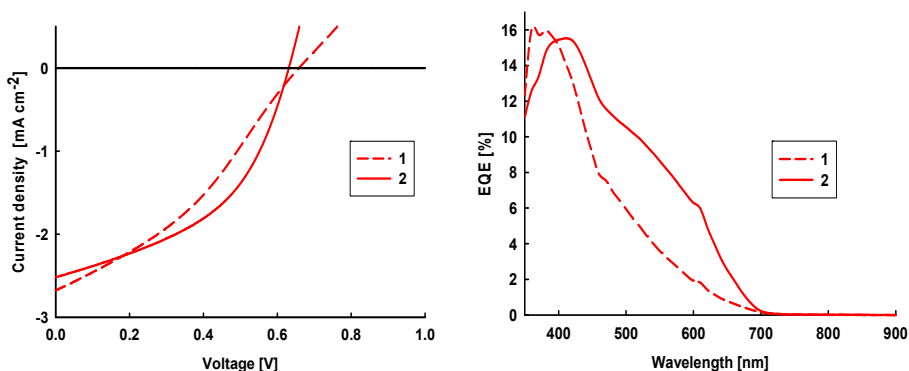


Figure 4. Current density vs voltage curves (left) and EQE curves (right) for the best inverted-bilayer cell using donors **1** and **2**.

CONCLUSIONS

D-A donors with bi[3,2-*b*]thienothiophene units **1** and **2** were successfully used in the fabrication of inverted bilayer planar heterojunction (PHJ) OSCs using C₇₀ as acceptor and PVD deposition and solution-processed bulk heterojunction solar cells (BHJ OSCs) having PC₆₁BM as acceptor. The average PCE values (Power Conversion Efficiency) obtained for these OSCs were similar for the two donors in both types of cells (BHJ **1**, PCE = 0.61 %; BHJ **2**, 0.57 %; PHJ **1**, 0.57% and PHJ **2**, 0.68 %), while the average PCE value obtained for the **A-D-A** donor in BHJ inverted cells (PC₆₁BM as acceptor) were considerably higher (2.47 %) proving that the symmetric **A-D-A** donor with bi[3,2-*b*]thienothiophene units is considerably more efficient than the **D-A** donors with the same building blocks. The high electrical parameter values (V_{oc}, J_{sc} and FF) push a superior efficiency for the inverted-BHJ cells using donor **3** compared to the other cells with the use of donors **1** and **2**. The efficiencies of these cells are comparable to those of the BHJ cells obtained with PC₆₁BM and PC₇₁BM as acceptors and classic donors with di- and triarylamine [40-42] or 2,1,3-benzothiadiazole [43] moieties.

EXPERIMENTAL SECTION

Materials and equipment

The cells were obtained using commercially available ITO-coated glass substrates of 24×25 mm. These substrates were sonicated for 10 minutes in

distilled water, ethanol (10 min), isopropanol (10 min) and finally using an UV Ozone Cleaner for 20 minutes.

PC₆₁BM, MoO₃, CHCl₃, C₆H₅Cl and Al were commercially available. The active material and ZnO were prepared accordingly to the literature data. [18] The deposition of different layers of the cells was carried out either using a classic spin-coater or a high vacuum deposition equipment (MANTIS DEPOSITION- model QUBE). The characterization of the cells was performed for the electrical parameters (current density, open circuit voltage, fill factor, power conversion efficiency) with the system formed by the small area solar simulator Newport Oriel LCS-100 (94011A-ES) and the Keithley 2400 source measure unit, for external quantum efficiency parameter the Newport IQE 200B quantum efficiency system (350-1100nm wavelength range), while the thickness of the layers was measured using the Tencor Alpha-Step D500 profilometer. The absorption spectra of the film were analyzed by UV-VIS 1900 Shimadzu spectrometer.

General procedure for the fabrication of inverted BHJs

A layer of 30 nm ZnO was deposited by spin-casting [$S = 3000$ rpm, $t = 40$ s) on clean ITO plates and then the plates were heated at 150°C for 20 min. The films of **donor** : PC₆₁BM were spun-cast ($t_1 = 40$ s, $S_1 = 4500$ rpm, $t_2 = 1$ s, $S_2 = 500$ rpm) on top of ZnO layer. The hole transporter layer (HTL) consisting in a 13 nm thick MoO₃ layer and the Al electrodes (100 nm) were deposited by thermal evaporation under high vacuum at 10⁻⁶ mbar.

ACKNOWLEDGEMENTS

This work was supported by a grant of the Romanian Ministry of Education and Research, CCCDI – UEFISCDI, project number PN-III-P2-2.1-PED-2019-2601 “REGRENPOS” within PNCDI III.

REFERENCES

- [1] H. Zhang, Y. Liang, H. Zhao, R. Qi, Z. Chen, H. Yuan, H. Liang, L. Wang, *Macromol. Biosci.* **2020**, *20*, e1900301.
- [2]. S. Kukulja, S. E. Draheim, B. J. Graves, D. C. Hunden, J. L. Pfeil, R. D. G. Cooper, J. L. Ott, F. T. Counter, *J. Med. Chem.* **1985**, *28*, 1896–1903.
- [3]. M. S. Egbertson, J. J. Cook, B. Bednar, J. D. Prugh, R. A. Bednar, S. L. Gaul, R. J. Gould, G. D. Hartman, C. F. Homnick, M. A. Holahan, *J. Med. Chem.* **1999**, *42*, 2409–2421.

- [4]. V. P. Rao, K. Y. Wong, A. K.-Y. Jen, K. J. Drost, *Chem. Mater.* **1994**, *6*, 2210–2212.
- [5]. M. M. Krayushkin, V. Z. Shirinian, L. I. Belen'kii, A. Y. Shadronov, A. Y. Martynkin, B. M. Uzhinov, *Mendeleev Commun.* **2002**, *12*, 141–143.
- [6]. X. Zhang, S. D. Hudson, D. M. DeLongchamp, D. J. Gundlach, M. Heeney, I. McCulloch, *Adv. Funct. Mater.* **2010**, *20*, 4098–4106.
- [7]. A. Liedtke, M. O'Neill, S. M. Kelly, S. P. Kitney, B. van Averbeke, P. Boudard, D. Beljonne, J. Cornil, *J. Phys. Chem. B* **2010**, *114*, 11975–11982.
- [8]. S. Saidman, R. Garay, J. Bessone, *J. Appl. Electrochem.* **2001**, *31*, 839–844.
- [9]. A. S. Diez, S. Saidman, R. O. Garay, *Molecules* **2000**, *5*, 555–556.
- [10]. K. L. Paik, N. S. Baek, H. K. Kim, Y. Lee, K. J. Lee, *Thin Solid Film.* **2002**, *417*, 132–135
- [11]. H. Wei, W. Chen, L. Han, T. Wang, X. Bao, X. Li, J. Liu, Y. Zhou, R. Yang, *Chem. Asian J.* **2015**, *10*, 1791–1798.
- [12]. Q. Zhang, Y. Wang, B. Kan, X. Wan, F. Liu, W. Ni, H. Feng, T. P. Russell, Y. Chen, *Chem. Commun.* **2015**, *51*, 15268–15271.
- [13]. M. Chang, Y. Wang, N. Qiu, Y.-Q. Yi, X. Wan, C. Li, Y. Chen, *Chin. J. Chem.* **2017**, *35*, 1687–1692.
- [14]. H.-S. Shim, C.-K. Moon, J. Kim, C.-K. Wang, B. Sim, F. Lin, K.-T. Wong, Y. Seo, J.-J. Kim, *ACS Appl. Mater. Interfaces* **2016**, *8*, 1214–1219.
- [15]. D. Patra, W. Budiawan, T.-Y. Huang, K.-H. Wei, P.-C. Wang, K.-C. Ho, Al- M. Hashimi, C.-W. Chu, *ACS Appl. Energy Mater.* **2018**, *1*, 3684–3692.
- [16]. S. S. M. Fernandes, M. C. R. Castro, A. I. Pereira, A. Mendes, C. Serpa, J. Pina, L. L. G. Justino, H. D. Burrows, M. M. M. Raposo, *ACS Omega* **2017**, *2*, 9268–9279.
- [17]. X. Li, K. Li, D. Su, F. Shen, S. Huo, H. Fu, C. Zhan, *Chin. Chem. Lett.* **2019**, *31*, 1243–1247.
- [18]. W. Wang, B. Chen, X. Jiao, J. Guo, R. Sun, J. Guo, J. Min, *Org. Electron.* **2019**, *70*, 78–85.
- [19]. M. Zhu, J. Miao, Z. Hu, Y. Chen, M.; Liu, I. Murtaza, H. Meng, *Dye. Pigment.* **2017**, *142*, 39–50.
- [20]. Y. Xu, H. Jiang, T.-K. Lau, J. Zhu, J. Wang, X. Lu, X. Zhan, Y. Lin, *J. Energy Chem.* **2018**, *37*, 58–65.
- [21]. J.-M. Su, Y.-Z. Li, Y.-H. Chang, M.-Z. Li, W.-Z. Qiu, S.-W. Liu, K.-T. Wong, *Mater. Today Energy* **2021**, *20*, 100633.
- [22]. J. Wang, P. Xue, Y. Jiang, Y. Huo, X. Zhan, *Nat. Rev. Chem.* **2022**, *6*, 614–634.
- [23]. S. Cai, G. Tian, X. Li, J. Su, H. Tian, *J. Mater. Chem. A* **2013**, *1*, 11295–11305.
- [24]. M.-W. Lee, J.-Y. Kim, D.-H. Lee, M. J. Ko, *ACS Appl. Mater. Interfaces* **2014**, *6*, 4102–4108.
- [25]. N. Cai, R. Li, Y. Wang, M. Zhang, P. Wang, *Energy Environ. Sci.* **2013**, *6*, 139–147.
- [26]. S. S. Fernandes, I. Mesquita, L. Andrade, A. Mendes, L. L. Justino, H. D. Burrows, M. M. M. Raposo, *Org. Electron.* **2017**, *49*, 194–205.
- [27]. N. Terenti, G.-I. Giurgi, A. P. Crișan, C. Anghel, A. Bogdan, A. Pop, I. Stroia, A. Terec, L. Szolga, I. Grosu, J. Roncali, *J. Mater. Chem. C* **2022**, *10*, 5716–5726.
- [28]. M. I. Nan, E. Lakatos, G.-I. Giurgi, L. Szolga, R. Po, A. Terec, S. Jungstuttwong, I. Grosu, J. Roncali, *Dye. Pigment.* **2020**, *181*, 108527.

- [29]. D. Demeter, S. Mohamed, A. Diac, I. Grosu, J. Roncali, *ChemSusChem* **2014**, *7*, 1046–1050.
- [30]. F. Piron, P. Leriche, I. Grosu, J. Roncali, *J. Mater. Chem.* **2010**, *20*, 10260–10268.
- [31]. N. Terenti, A. P. Crişan, S. Jungsuttiwong, N. D. Hădăde, A. Pop, I. Grosu, J. Roncali, *Dye. Pigment.* **2020**, *187*, 109116.
- [32]. L. Gabrian, G.-I. Giurgi, I. Stroia, E. Bogdan, A. P. Crişan, N. D. Hădăde, I. Grosu, A. Terec, *Molecules* **2022**, *27*, 8463.
- [33]. M. C. Scharber, N. S. Sariciftci, *Prog. Polym. Sci.*, **2013**, *38*, 1929-1940.
- [34]. J. Chen, Y. Chen, L.-W. Feng, C. Gu, G. Li, N. Su, G. Wang, S. M. Swick, W. Huang, X. Guo, A. Facchetti, T. Marks, *Energy Chem* **2020**, *2*, 100042.
- [35]. G.-I. Giurgi, L. Szolga, I. Kovacs, E. Bogdan, N. D. Hădăde, A. Terec, I. Grosu, J. Roncali, *Studia UBB Chemia*, **2020**, *65*, (2) 95-106.
- [36]. M. Abdallaoui, N. Sengouga, A. Chala, A. F. Meftah, A. M. Meftah, *Opt. Mater.* **2020**, *105*, 109916.
- [37]. S. Huang, B. Kang, L. Duan, D. Zhang, *Colloid.Interface Sci.*, **2020**, *583*, 178-187.
- [38]. Y. Wang, H. Cong, B. Yu, Z. Zhang, X. Zhan, *Mater.*, **2017**, *10*, 1064.
- [39]. G.-I. Giurgi, L. Szolga, A. P. Crişan, I. Grosu, J. Roncali, *Studia UBB Chemia* **2021**, *66* (3), 97-105.
- [40]. O. Vybornyi, Y. Jiang, F. Baert, D. Demeter, J. Roncali, P. Blanchard, C. Cabanetos, *Dye. Pigment.* **2015**, *115*, 17-22.
- [41]. S. Roquet, A. Cravino, P. Leriche, A. Alévêque, P. Frère, J. Roncali, *J. Am. Chem. Soc.* **2006**, *128*, 3459-3466.
- [42]. M. J. Cho, J. Seo, H. S. Oh, H. Jee, W. J. Kim, K. H. Kim, M. H. Hoang, D. H. Choi, P. N. Prasad, *Sol. Energ. Mat. Sol. C.* **2012**, *98*, 71-77.
- [43]. H. Shang, H. Fan, Y. Liu, W. Hu, Y. Li, X. Zhan, *Adv. Mater.* **2011**, *23*, 1554-1557.

COMPARATIVE CHEMICAL AND ANTIMICROBIAL CHARACTERIZATION OF NON-OZONATED AND OZONATED VEGETABLE OILS

Ana BALEA^a, Irina CIOTLĂUȘ^{a,*},
MARIA POJAR-FENEȘAN^a, Rahela CARPA^b

ABSTRACT. In this study, a comparative determination of the quality factors, chemical composition and antimicrobial activity for ozonated and non-ozonated olive, coconut and hemp oils was made. The following quality factors for non-ozonated and ozonated oils were determined: peroxide value, acidity value, iodine value and density. The composition of methyl esters of fatty acids and the final compounds resulting from the ozonation process of the studied vegetable oils was characterized by Gas-Chromatography-Mass Spectrometry (GC-MS). The oil samples showed varying degrees of antibacterial activity against selected pathogens. Ozonated oils act as a matrix capable of releasing active oxygen from ozonides, which have antimicrobial activity. Density, peroxide value and acid value increased in all ozonated oils, while iodine value decreased in all ozonated oils. The gas chromatography showed a change in the degree of unsaturation due to the ozonation process, such that: the total content of unsaturated compounds decreased by 24.58% in ozonated olive oil, by 37.88% in ozonated hemp oil and by 9.14% in ozonated coconut oil. The innovative aspect of the paper consists in the physico-chemical and chromatographic characterization of the ozonated hemp oil and the comparison of the antimicrobial activity of the studied oils.

Keywords: olive, coconut, hemp, ozonated oil, GC-MS, antimicrobial activity

^a Babeș-Bolyai University, "Raluca-Ripan" Institute for Research in Chemistry, 30 Fântânele str., RO-400294, Cluj-Napoca, Romania.

^b Babeș-Bolyai University, Faculty of Biology and Geology, Molecular Biology and Biotechnology Department, 1 M. Kogalniceanu street, 400084, Cluj-Napoca, Romania.

* Corresponding author: irina.ciotlaus@ubbcluj.ro



INTRODUCTION

The characterization of vegetable oils has been the subject of academic studies in recent years. Vegetable oils are complex mixtures of major components, such as triglycerides, partial glycerides and esters of fatty acids, unesterified free fatty acids and minor components such as sterols, hydrocarbons, pigments, phenols, flavonoids or volatile compounds. [1,2]

The ozonation of various vegetable oils has been studied, such as olive oil [3-7], sunflower oil [8-10], soybean oil [11,12] and coconut oil [13,14] under different conditions. Maritza F. Diaz *et al.* [14], studied the antimicrobial activity of coconut ozonated oil obtained by three different ozonation systems, compared to the antimicrobial activity of different antibiotics. All ozonated coconut oils showed antimicrobial activity, and those obtained by ozonating the mixture of oil with water or ethanol showed superior antibiotic activity.

Hemp seeds are a good source of oil, protein and carbohydrates. Hemp seed oil is one of the best sources of essential fatty acids with a perfect 3:1 ratio of omega-3-linolenic acid and omega-6-linoleic acid, suitable for strengthening the immune system [15-16]. It is, also a good source of gamma linoleic acid and is used to lower cholesterol in skin conditions. In Romania, hemp has been cultivated since ancient times as a textile plant as well as for oil seeds. In Romanian folk medicine, hemp seeds have been used to relieve rheumatic pain, to treat venereal diseases, pulmonary congestion, vomiting, intoxication, cough, hemorrhoids, intestinal parasites. [17] Most of this oil has been extensively investigated to determine its chemical composition [18-20] and its therapeutic properties [21], but not much is known about the physical, chemical and structural properties of the ozonated hemp oil, which offer its superior medicinal properties. [22]

Although interest in hemp oil has recently increased, it is surprising that there are few studies focusing on the antimicrobial activity of low THC essential oils, the literature presents several studies on the biological activity of compounds extracted from high THC hemp oils.

Novak *et al.* [23,24], tested the antimicrobial capacity of hemp oil on both Gram-positive and Gram-negative bacteria, with modest results.

A study evaluates the *in vitro* antimicrobial activity of essential oils extracted from the inflorescence of three legal varieties of hemp (low in THC) on Gram-positive bacteria, including *Clostridium spp.* and *Enterococcus spp.*, Gram-negative bacteria (-) including phytopathogenic bacteria: *Pseudomonas spp.* and *Pectobacterium spp.* and yeasts, related to phytopathogens or human commensals. The results showed that industrial hemp essential oils can significantly inhibit microbial growth, although the number of samples used in that study was quite limited. [25]

A recent study presents the phytochemical characterization of 17 hemp essential oils (EOs) belonging to different varieties, together with the evaluation of their antibacterial activity against some pathogenic and spoilage microorganisms isolated from food and food processing environments. [26]

Ozonated vegetable oils have many interesting applications in the food industry [27], cosmetics and pharmaceuticals [28-29], as well as in medicine. [30-33]

In a pharmacological context, the amount of ozonide is an important measure of the ability of the oil to supply active O₂ and other active species that can be exploited in the treatment of skin diseases. The judicious use of ozone (O₃) seems providential because it first eliminates pathogens and then, by releasing oxygen (O₂), it activates the proliferation of fibroblasts, hence the formation of the intercellular matrix with consecutive keratinoblast proliferation and successive healing. [31] One of the commonly used methods for ozone therapy is ozonated oils. The most commonly used type of oil is extra virgin olive oil. However, each type of unsaturated oil can be used for ozonation. [5] The ozonation process allows the properties of ozone gas to be combined with those of olive oil; the result is a compound without comparison. [34] Ozonated vegetable oils have been shown to have antibacterial and antifungal properties. [35] These properties are recommended for use in therapeutic and cosmetic purposes. [36]

The natural origin of these oils and their easy use together with their financial accessibility, place them among the best dermatological and cosmetic treatments.

Several methods are available for the characterization of ozonated vegetable oils, for example GC, GC-MS, FT-IR, NMR. [37-40] Ozonolysis is an oxidative reaction between ozone and the carbon-carbon double bond of an unsaturated compound. The reaction of ozone with these vegetable oils takes place almost exclusively at the carbon-carbon double bonds present in unsaturated fatty acids. Analysis of these reactions provide information about changes in functional groups during the ozonation process, according to the well-known Criegee mechanism for the formation of ozonides from alkenes and ozone. [41-42] The ozonolysis process involves a three-stage reaction: (1) formation of the primary ozonide, (2) breakdown of primary ozonide into aldehydes, aldo-acids and carboxylic acids, (3) recombination of carboxylic acid and aldehydes in order to form secondary ozonides. [43]

A comparative determination of the chemical composition and quality factors for ozonated and non-ozonated olive, coconut and hemp oils was made in this paper. Changes in quality factors, chemical composition and antimicrobial activity of already ozonated oils and the raw material (non-ozonated oils) were studied. The monitoring of the ozonation process was

not studied in detail. For non-ozonated and ozonated oils, the physical and chemical parameters were determined: peroxide value, acidity value, iodine value and density. The composition of methyl esters of fatty acids and the final compounds resulting from the ozonation process of the studied vegetable oils was characterized by Gas Chromatography coupled with Mass Spectrometry (GC-MS). The antimicrobial activity of non-ozonated and ozonated oils was tested “in vitro” on Gram-positive microorganisms: *Enterococcus faecalis*, *Staphylococcus aureus*, *Bacillus subtilis* and Gram-negative microorganisms: *Escherichia coli*, *Pseudomonas aeruginosa*. The relationship between the physico-chemical properties of oils and their antimicrobial activity has not been reported in the literature. Ozonated hemp oil was studied in comparison with non-ozonated hemp oil to identify physico-chemical and structural differences.

For the physico-chemical and chromatographic validation of ozonated hemp oil, we used standard procedures applied to ozonated vegetable oils.

RESULTS AND DISCUSSION

The physico-chemical characteristics of the oils before and after ozonation are shown in Table 1.

Table 1. Physico-chemical characteristics of the oils

Type of oil	Peroxide value <i>meqO₂/kg fat</i>	Acid value <i>mgKOH/g oil</i>	Iodine value <i>gl₂/100g oil</i>	Density <i>g/mL oil</i>
Olive oil	21.6	0.84	97.10	0.831
Ozonated olive oil	108.4	2.24	69.83	0.913
Hemp oil	56	5.88	132.91	0.891
Ozonated hemp oil	228.4	7.84	108.11	0.998
Coconut oil	7.6	0.28	7.02	0.901
Ozonated coconut oil	68	0.67	5.62	1.145

Table 1 shows an increase in values for three characteristics, namely: peroxide value, acid value and density. The increase in these values is due to the higher amount of peroxides due to ozonation, the higher amount of acids released by breaking the triglyceride chains under the action of ozone and oxygen saturation of the double bonds in unsaturated fatty acids. [13,40] The decrease in iodine value is due to the decrease in the degree of unsaturation after ozonation due to the oxidation of unsaturated fatty acids in the oil by the Criegee mechanism. [41] The high value of peroxide also

implies a high viscosity. [37] Bromine iodide reagent has difficult access to the double bond to react. This is a further explanation of why iodine decreases in ozonated oil samples. [22] An increase in acid and peroxide value has been observed in all oils. There is a significant increase in the value of peroxide in the study of coconut oil.

The volatile profile of vegetable oils was characterized by GC-MS. (Table 2).

Before performing GC analysis of olive oil (OO), ozonated olive oil (OOO), Hemp oil (HO), ozonated Hemp oil (OHO), coconut oil (CO) and ozonated coconut oil (OCO) a trans-esterification (derivatization) reaction was performed. For this purpose, the fatty acid components of oils are more easily converted into volatile derivatives, usually methyl esters. In their free, non-derivatized form, fatty acids from oils can be difficult to analyze because these highly polar compounds tend to form hydrogen bonds, leading to adsorption problems. By reducing their polarity by methylation, they can be analyzed much more easily. This will then allow the column chemistry to make separations by eluting the components by boiling points and also by the degree of unsaturation, the position of unsaturation and even the cis vs. trans configuration of unsaturation.

Methyl esters of saturated and unsaturated fatty acids and ozonation products were detected in the analyzed vegetable oils. GC-MS results are expressed as relative percentage compositions. (Table 2)

During the reaction between ozone and fatty acids in vegetable oils, ozonation products are formed (nonanal, nonanoic acid, methyl-9-oxo-nonanoate, monomethyl nonandioate), according to the Criegee mechanism. [41]

Non-ozonated olive oil (OO) contains mainly methyl esters of fatty acids (75.71%). The main components identified were: methyl oleate (24.75%); methyl palmitate (20.12%), methyl palmitoleate (10.14%) and squalene (10.63). Ozonated olive oil (OOO) mainly contains: ozonolysis compounds (38.84%), methyl esters of saturated fatty acids (30.74) and methyl esters of unsaturated fatty acids (23.68%). A total of 16 compounds representing 99.96% of the methyl esters of fatty acids were identified in non-ozonated hemp oil (HO). The major components identified were: methyl linoleate (28.91%); methyl palmitate (23.14%), methyl eicosanoate (7.99%); Methyl 12-hydroxy-9Z-octadecenoate (7.74%); Ozonated hemp oil (OHO) contains mainly: ozonolysis compounds (26.59%), methyl esters of saturated fatty acids (37.41%), methyl esters of unsaturated fatty acids (12.61%). Non-ozonated coconut oil (CO) contains 90.36% methylated fatty acid methyl esters and 9.32% unsaturated fatty acids. The ozonated coconut oil (OCO) contains mainly: ozonolysis compounds (14.41%), methyl esters of saturated fatty acids (82.47%) and methyl esters of unsaturated fatty acids (0.18%).

Table 2. Volatile components in vegetable oil

Oil constituent/Type	RT min	LRI	OO %	OOO %	HO %	OHO %	CO %	OCO %
1	2	3	4	5	6	7	8	9
1 Methyl hexanoate (E)	7.61	923	-	-	-	-	4.02	4.15
2 Hexanoic acid (A)	8.85	994	-	-	-	1.21	-	-
3 (E)- 3 -hexenoic acid (A)	8.97	1001	-	-	-	0.76	-	-
4 (E)-4-nonenal (ALD)	10.76	1099	-	-	-	0.93	-	-
5 Nonanal (ALD)	10.99	1112	-	8.05	-	1.58	-	4.40
6 2-Methyl octanoic acid (A)	11.09	1118	-	-	-	0.23	-	-
7 Methyl octanoate (E)	11.22	1125	-	1.86	-	3.12	13.39	12.28
8 (E)-2-Decenal (ALD)	11.95	1166	-	-	-	0.40	-	-
9 Methyl nonanoate (E)	12.97	1225	-	0.17	-	-	-	-
10 2-Octan-1-ol, acetate (E)	13.41	1251	-	-	-	0.44	-	-
11 8-Nonenoic acid (A)	14.09	1291	-	-	-	1.61	-	-
12 Nonanoic acid (A)	14.18	1296	-	9.04	-	0.86	-	3.27
13 Methyl decanoate (E)	14.70	1328	-	-	-	-	12.15	12.04
14 Methyl-10-undecanoate (E)	16.19	1422	-	-	-	1.11	-	-
15 Methyl 9-oxo-nonanoate (E)	16.52	1443	-	8.98	-	12.81	-	5.64
16 Methyl dodecanoate (E)	17.80	1529	-	0.51	-	-	26.58	21.07
17 Dimethyl nonanedioate (E)	18.13	1552	-	0.29	-	0.71	-	-
18 Monomethyl nonanedioate (E)	18.86	1603	-	7.76	-	6.16	-	2.38
19 Methyl tridecanoate (E)	19.23	1630	-	-	-	-	0.28	0.35
20 Dimethyl undecanedioate (E)	19.49	1649	-	0.50	-	-	-	-
21 13-(Z)-Tetradecenal (ALD)	20.37	1714	-	-	-	0.83	-	-
22 Methyl tetradecanoate (E)	20.63	1734	-	0.35	0.62	4.37	18.06	16.47
23 Methyl 12-oxo-dodecenoate (E)	21.59	1809	-	-	-	1.10	-	-
24 Methyl pentadecanoate (E)	21.82	1831	-	-	0.22	-	-	-
25 Methyl palmitoleate (E)	22.62	1912	10.14	3.27	-	2.78	-	-
26 Methyl palmitate (E)	22.81	1929	20.12	17.32	23.14	15.64	10.64	9.39
27 Linoleic acid (A)	23.54	2016	-	-	-	0.30	-	-
28 Methyl 10(Z)-heptadecenoate (E)	23.59	2023	1.30	2.54	-	-	-	-
29 Methyl heptadecanoate (E)	23.74	2044	-	-	-	0.84	-	0.07
30 Methyl 5-oxo-octadecanoate (E)	24.06	2088	-	-	-	-	-	0.08
31 Methyl γ -linolenate, (Z6,Z9,Z12) E)	24.09	2092	-	-	3.54	3.21	-	-
32 Methyl oleate (E)	24.18	2105	24.75	17.08	-	-	7.88	0.10
33 Methyl stearate (E)	24.75	2192	6.18	2.00	5.37	-	4.78	6.29
34 Methyl linoleate (9Z,12Z) (E)	24.91	2216	0.27	0.29	28.91	6.69	1.07	0.08
35 Methyl linolelaidate, (9E,12E) (E)	24.92	2218	-	-	3.37	-	-	-
36 Methyl-10(Z)-nonadecenoate (E)	24.97	2222	0.36	0.37	-	-	-	-
37 Methyl nonadecanoate (E)	25.16	2255	-	-	-	0.08	-	-
38 Methyl α -linolenate (E)	25.22	2263	-	-	2.11	0.28	-	-
39 α -Fenchene (Ot)	25.28	2272	-	-	-	0.44	-	-
40 1,6-Cyclodecadiene (Ot)	25.38	2278	-	-	-	1.29	-	-

COMPARATIVE CHEMICAL AND ANTIMICROBIAL CHARACTERIZATION OF NON-OZONATED
AND OZONATED VEGETABLE OILS

1	2	3	4	5	6	7	8	9
41 Methyl -cis-9,10-epoxy-stearate (E)	25.44	2296	-	1.06	-	-	-	0.42
42 (Z,Z)-9, 12-octadecadienoyl chloride (Ot)	25.51	2306	-	-	-	3.17	-	-
43 Methyl-trans-9,10-epoxy-stearate (E)	25.55	2311	-	2.32	-	-	-	-
44 Methyl-12-OH-9Z-octadecenoate (E)	25.56	2313	-	-	7.74	2.43	-	-
45 Methyl-11(Z)-eicosenoate (E)	25.60	2318	4.67	2.78	4.82	-	0.37	0.73
46 Methyl eicosanoate (E)	25.74	2338	5.21	4.09	7.99	2.53	0.73	-
47 Methyl-15-OH-9,12-octadecadienoate (E)	25.89	2358	-	-	-	0.32	-	-
48 11 -Z-Eicosenoic acid (A)	25.93	23.64	0.87	-	-	-	-	-
49 Methyl 9,10:12,13-diepoxy-stearate (E)	25.95	2367	-	0.80	-	0.70	-	-
50 Isopropyl -9,10-Epoxy-stearate (E)	26.07	2383	-	0.35	-	-	-	0.03
51 Oxiraneundecanoic acid, 3-pentyl, methyl ester, trans (E)	26.20	2401	-	0.11	-	-	-	-
52 (Z)-13-eicosenoic acid (A)	26.23	2405	-	-	-	2.13	-	-
53 Methyl heneicosanoate (E)	26.43	2430	0.36	0.32	-	-	-	-
54 α -Glyceryl-linolenate (E)	26.54	2444	-	-	-	0.36	-	-
55 Ethyl linoleate (E)	26.64	2457	0.14	0.30	-	0.94	-	-
56 Oxiraneoctanoic acid, 3-octyl, cis	26.70	2465	-	0.08	0.27	0.57	-	-
57 Z,Z-5,16-Octadecadien-1-ol, acetate (E)	26.71	2466	-	-	-	3.06	-	-
58 Glycidyl oleate (E)	26.87	2486	0.28	0.03	-	0.36	-	-
59 Methyl-Z-13-docosenoate (E)	27.09	2531	-	-	0.35	1.41	-	-
60 Methyl docosanoate (E)	27.28	2586	1.79	2.37	7.09	5.59	-	-
61 Tocopheryl acetate (E)	27.80	2682	8.70	-	-	-	-	-
62 Methyl tricosanoate (E)	28.24	2731	0.35	0.35	0.32	0.88	1.05	-
63 Heptanoic acid,docosyl ester (E)	28.52	2756	1.65	0.27	-	-	-	-
64 Glyceryl monooleate (E)	29.16	2812	1.34	-	-	-	-	-
65 Methyl tetracosanoate (E)	29.42	2832	0.78	0.83	3.54	4.00	-	-
66 Squalene (A)	30.72	3008	10.63	3.46	-	1.52	-	-
67 Methyl pentacosanoate (E)	30.81	3015	-	-	-	0.24	-	-
ESTERS (E)			88.39	79.24	99.69	83.72	99.96	99.25
ACIDS (A)			0.87	9.12	0.27	7.44	-	3.27
ALDEHYDES (ALD)			-	8.05	-	3.74	-	4.40
OTHERS (Ot)			10.63	3.46	-	4.90	-	-
Total			99.89	99.87	99.96	99.8	99.96	99.92

RT: retention time; LRI: linar retention index (on HP-5ms column); olive oil (OO), ozonated olive oil (OOO), hemp oil (HO), ozonated hemp oil (OHO), coconut oil (CO), ozonated coconut oil (OCO).

Changing the degree of unsaturation in the ozonation process

Figure 1 shows that the percentages of oleic acid in olive oil (OO) decrease from 24.75% to 17.08%, in palmitoleic acid decrease from 10.24% to 3.27%, in eicosenoic acid decrease from 5.54% to 2.78% and in squalene,

they decrease from 10.62% to 3.46%, due to the ozonation process. The total content of unsaturated compounds decreased by 24.58%. The percentages of linoleic acid, the main component of ozonated hemp oil (HO) decrease from 28.91% to 6.69% in ozonated hemp oil (OHO). In fresh hemp oil (HO), the total unsaturated fatty acid content decreased by 37.88%. The total unsaturated fatty acid content of coconut oil (CO) decreased from 9.32% to 0.18% in ozonated coconut oil (OCO).

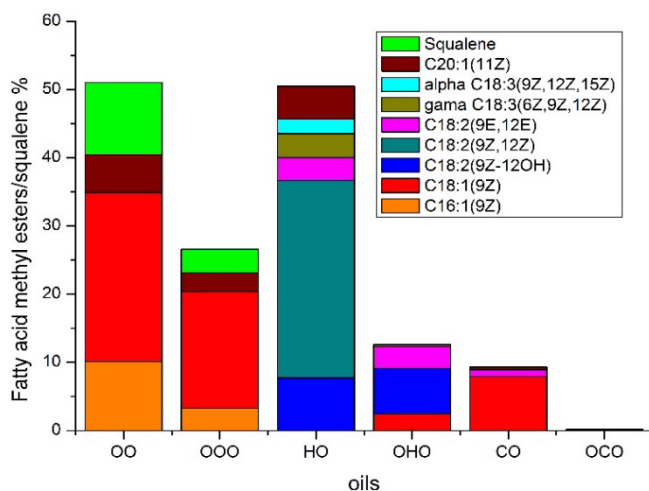



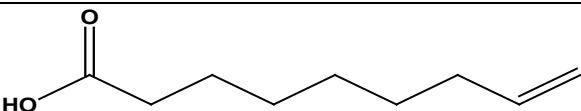
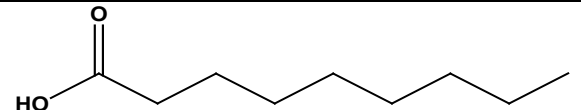
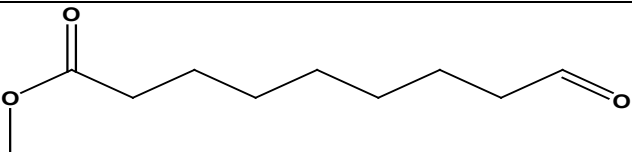
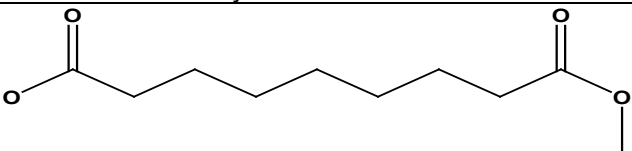
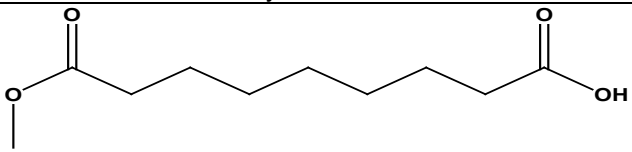
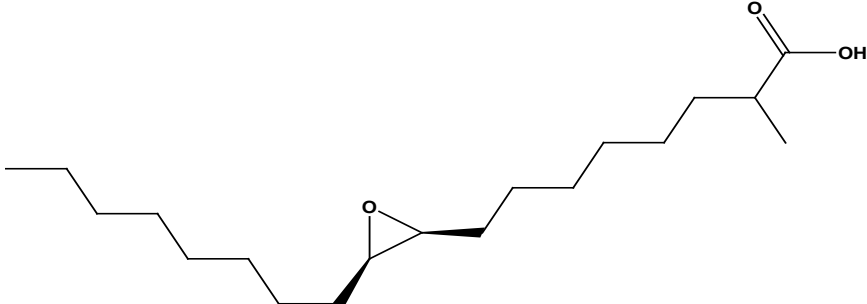
Figure 1. Percentage composition of fatty acid unsaturated methyl esters and squalene in oil samples

In the first stage, ozone reacts with the double bonds in vegetable oils to form 1,2,3-trioxolanes or molozonides. Molozonides are unstable, and those synthesized in aprotic environments tend to rearrange into more stable Criegee ozonides (secondary ozonides) through carbonyl oxide (H_2COO). In the presence of protic solvents or water, carbonyl oxides can react and form compounds with different functional groups. [41] Because secondary ozonides are composed of high molecular weight and low volatility, they cannot be analyzed by GC-MS. In this case, in our experiments, ozonolysis products resulting from the degradation of the secondary ozonide in the polar reaction environment were highlighted by GC-MS.

The volatile fraction of ozonated oils is composed of saturated aldehydes, aldo-acids, epoxides, carboxylic acids and dicarboxylic acids. Nonanal, nonanoic acid, methyl 9-oxononanoate and monomethyl nonandioate were the main components of the volatile fraction in ozonated vegetable oils. [Table 3].

COMPARATIVE CHEMICAL AND ANTIMICROBIAL CHARACTERIZATION OF NON-OZONATED AND OZONATED VEGETABLE OILS

Table 3. Final compounds resulting from the ozonation process of vegetable oils

	Compounds/Structure
1	 Nonanal
2	 8-Nonenoic acid
3	 Nonanoic acid
4	 Methyl-9-oxo-nonanoate
5	 Dimethyl nonanedioate
6	 Monomethyl nonanedioate
7	 Methyl-cis-9,10-epoxy stearate

The predominant unsaturated fatty acids in OO, HO and CO are oleic and linolenic acids, respectively, from which it is assumed that the new peaks were formed mainly by the reaction of ozone with these fatty acids. In oleic acid, the double bond is present in position C9, the linoleic acid contains two double bonds in positions C9 and C12, while the linolenic acid contains three double bonds in positions C6, C9 and C12. Thus, nonanal, nonanoic acid, 9-oxo-nonanoate were formed by the reaction between ozone and the unsaturated double bond at the C9-C10 position of these acids. [50-52]

Evaluation of antimicrobial activity

The antibacterial activity of ozonated and non-ozonated oils was evaluated by well diffusion methods. Oil samples showed varying degrees of antibacterial activity against the selected pathogens (Figure 2).

Depending on the strain tested and on the type of sample, it can be seen that the inhibition was quite variable but not very high.

The only bacterial strain in which inhibition was completely absent for both categories of oils was the Gram-positive strain *Enterococcus faecalis*.

The test results showed that the diffusion well-variant was more sensitive for ozonated oil samples. Of the 5 bacterial strains tested, only *Pseudomonas aeruginosa* showed inhibition in both types of samples (ozonated and non-ozonated) (Fig. 2).

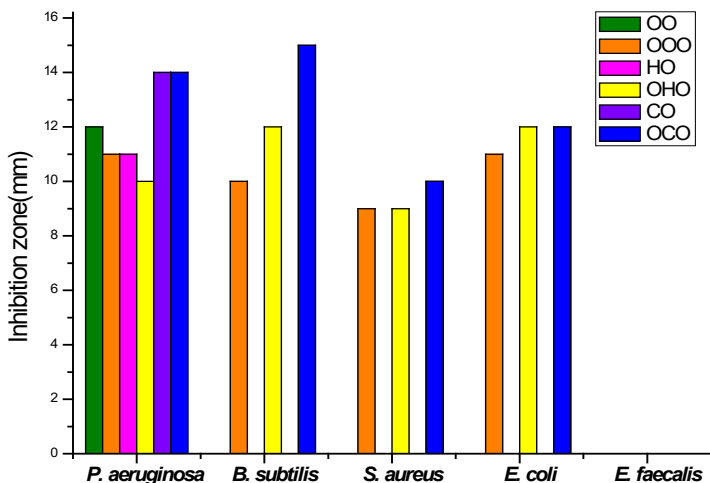


Figure 2. Antimicrobial activity of various oil samples

In the other bacterial strains, the inhibition was recorded only for ozonated oil samples. Of the 3 categories of ozonated oils, coconut oil showed the highest inhibition of all bacterial strains tested.

The antibacterial activity of coconut oil is due to both the medium chain fatty acids in its composition and the ozonides formed by ozonation [53,14]. Coconut oil is a source of beneficial medium chain fatty acids (MCFA), especially lauric acid, capric acid, caprylic acid and caproic acid [see methyl esters of these acids in Table 2]. As far as neozonated coconut oil is concerned, growth was inhibited only for the *Pseudomonas aeruginosa* strain, while ozonated coconut oil was also active for the other three strains: *S.aureus*, *E.coli* and *B.subtilis*.

The antibacterial activity of olive oil is due to both the fraction of polyphenols present in the composition⁵⁴ and the ozonides formed by ozonation. Ozonated olive oil has antimicrobial activity on the four bacterial strains that we tested, as well as other studies that suggest that ozonated olive oil has antimicrobial activity against both *S.aureus*, *E.coli*, *P.aeruginosa* and *B.subtilis*. [3,38,55]

The antibacterial activity of non-ozonated hemp oil in these organisms can be considered as modest, compared to ozonated oil. In the case of non-ozonated hemp oil, the antibacterial profile is mainly due to the cannabinoids in the composition.[23] Ozonated oil was active on the four strains: *S.aureus*, *E.coli*, *P.aeruginosa* and *B.subtilis*, with good results.

To the best of our knowledge, the tests with hemp ozonated oil on the strains studied in this paper are not mentioned in the literature. However, its use "in vivo" against *Microsporium canis* – the main zoonotic pathogenic fungus in veterinary medicine, is mentioned. [56]

CONCLUSIONS

From the physico-chemical analysis, it is observed the change of value of the quality parameters for the ozonated oils compared to the non-ozonated ones, as it follows: the peroxide value, the acid value and the density, all increase and the iodine value decreases.

The gas-chromatographic analysis shows the change in composition and the appearance of new compounds in ozonated oils compared to non-ozonated ones. The ozonation process changes the structure of the oil, so the unsaturations become ozonides, which, due to their instability, break into derivatives with oxygenated functions.

From the evaluation of the antimicrobial activity, in the case of ozonated olive and hemp oils, an efficiency is observed on new strains: *S.aureus*, *E.coli* and *B.subtilis*, where the non-ozonated oils did not show any type of activity.

This research indicates that at higher levels of peroxide, acidity and density, the antimicrobial activity of olive and hemp oils is higher for *S.aureus*, *E.coli* and *B.subtilis* and less for *P.aeruginosa*. Coconut oil showed the highest inhibition compared to the other oils studied in the 4 bacterial strains tested.

The innovative aspect consists in the physico-chemical, gas-chromatographic characterization and the antibacterial profile of the ozonated hemp oil. Ozonated hemp oil has been studied in comparison with non-ozonated hemp oil to identify the physical, chemical and structural differences that give its superior properties, which can be exploited in the treatment of skin diseases.

No published results were found for ozonated hemp oil on the correlation between chemical composition and biological activity. This study shows that ozonated hemp oil was active on the four strains with good results: *S.aureus*, *E.coli*, *B.subtilis* and *P.aeruginosa*.

The natural origin of these oils and their easy way of use, place them among the best treatments.

EXPERIMENTAL SECTION

Materials

Reagents: Hexane, chloroform, ethanol, ethyl ether, glacial acetic acid, potassium iodine, potassium hydroxide, thiosulfate, starch, phenolphthalein. Reagents/solvents were purchased from Merk, Hohenbrunn-Germany by a local supply company. The oils used for studies in this article were supplied to us by a Romanian manufacturer of ozonated oils. The instrument used for ozonation process was ozone generator (model OzoneFix Business 3) with ozone flow of 3 g O₃/h. All samples was ozonated at a temperature of 25°C for 6 hours. For this study we used three types of oils: olives, coconut and hemp, non-ozonated and ozonated types, so 6 samples in total. The oils studied originate from organic crops and were obtained from the seeds of Hemp (*Cannabis sativa*), Olives (*Olea europaea*) and Coconut (*Cocos nucifera*) by cold pressing.

Physico-Chemical Parameters

a. Peroxide value (PV)

The peroxide value was determined according to SR EN ISO 3960: 2005 - *Animal and vegetable oils and fats. Determination of the peroxide value*. [45]

The peroxide value for all determinations is calculated by the equation:

$$PV = \frac{1000 (V1 - V0) c}{m} \quad (1)$$

where V1 is the volume in mL of thiosulphate solution used for titration, V0 is the volume in mL of thiosulphate solution used for titration of a control, c is the mol L⁻¹ thiosulphate concentration and m the amount of sample (grams).

The peroxide value, confirms the process of ozonation of oils.

b. Acid value (AV) - represents the amount of potassium hydroxide needed to neutralize the free acids present in the 1g oil sample. It indicates the degree to which the triglycerides in the oil have decomposed to release free fatty acids. The acid value was calculated by the equation:

$$AV = \frac{M \times C \times V}{m} \quad (2)$$

where AV - the acid value expressed as a mass fraction, M is the molar mass, in grams per mole, for KOH, C is the L⁻¹ mole concentration of the standard volumetric solution of potassium hydroxide KOH used, V is the volume, in milliliters, of KOH and m is the mass, in grams, of the oil sample.

The Acid value was determined according to SR EN ISO 660:2009-*Animal and vegetable fats and oils. Determination of acid value and acidity*. [46]

c. Iodine value (IV) - Represents the amount of iodine that will react with the double bonds, number of grams of iodine consumed per 100g of fat. A higher iodine value indicates a higher degree of unsaturation. IV is calculated according to the monographs of Pharmacopoeia.

$$IV = \frac{1,256 (V1 - V2)}{m} \quad (3)$$

where V1 is the volume in mL of thiosulphate solution (0,1 M) used for a blank test, V2 is the volume in mL of thiosulphate solution (0,1 M) used for titration and m the amount, in grams, of the substance. The value of acid iodine was determined according to SR EN ISO 3961: 2018 - *Animal and vegetable fats and oils. Determination of iodine value*. [47]

d. Determination of density

The oil density was determined at 20⁰ C by weighing an exact volume (2 ml) of oil; the determination was carried out three times for each oil sample.

Determination of Fatty Acid Profile

The Gas-Chromatographic analysis was performed on a Gas-chromatography Mass Spectrometer (GC-MS), purchased from Agilent Technologies, Santa Clara California, USA, by Agilrom Scientific SRL Romania.

a. Sample preparation

The methylation reaction occurs in a cooled methanolic solution of potassium hydroxide, according to the standard procedure. In a test tube with a 5 ml cap, 0.10 g of oil sample was added to a mixed solution of 3 mL of hexane and 500 μL of 2 N mol L^{-1} methanolic KOH. The sample was stirred vigorously for 15 s, allowing the layers to separate until the top solution became clear. The upper layer containing the methyl esters was decanted and dried over MgSO_4 .

b. Chromatographic conditions

Determinations of methylated fatty acids were performed on an Agilent 7890 & 5975 Series MSD Gas Chromatography Mass Spectrometer (GC-MS) equipped with a HP-5MS chromatographic column (5% phenyl)-methyl polysiloxane, (30 m x 0.25 mm x 0.25 μm) Agilent model, helium carrier gas, injection volume 1 microliter. GC parameters were obtained under the following conditions: helium carrier gas (He 6.0), flow rate 1 ml / min, injector temperature was 260 °C, splitless mode. The column temperature was initially set at 50 °C, then increased at a rate of 8 °C / min to 220 °C / min, then from 220 °C to 280 °C, increased by 20 °C / min, where kept at 280 °C for 5 minutes. MS detector parameters: electron impact mode (EI +), 70 eV, ion source temperature, 230 °C. Mass spectra were recorded in the range of 50-500 a.m.u, in scan mode. All tests were performed in duplicate. Data acquisition and processing were performed using a MSD ChemStation software. An alkane standard (Alkanes Standard Solution C8-C20, C 21 - C40 alkanes Sigma Aldrich) was used to calculate the linear retention index (LRI), and the experimental values were compared to those in the literature, under similar chromatographic conditions. The identification of fatty acid methyl esters was performed by comparing the retention times (RT) in the samples with those of a known standard (Supelco® 37 Component FAME Mix) and by comparing the mass spectra with those in the NIST 14 L database. The composition of methyl esters in vegetable oils was expressed as a percentage of each component in relation to the total area of the chromatogram.

Antibacterial testing

The microorganisms tested in this study were Gram positive: *Enterococcus faecalis* ATCC-29212, *Staphylococcus aureus* ATCC-25923 and *Bacillus subtilis* ATCC-6633 and Gram negative: *Escherichia coli* ATCC-25922 and *Pseudomonas aeruginosa* ATCC-27853 from the Microbiology Laboratory, Faculty of Biology and Geology, UBB, Cluj.[48]

The antimicrobial test method was the diffusimetric one, of the 5 mm diameter, wells cut aseptically in the culture medium (agar well diffusion method) [48]. The wells were then filled with sterile cotton granules. Each granule was loaded with 20 μ L of each oil sample. Bacterial suspensions were made from fresh bacterial strains in saline and adjusted to a McFarland turbidity of 0.5 which were inoculated over the entire surface of the agar plates using a sterile cotton swab. The culture medium used to inoculate the bacterial suspensions was Mueller Hinton [49]. After inoculation, the samples were incubated at 37 °C for 24 hours. The diameter of the inhibition zone was then measured for each sample and for each microorganism. At the end of the incubation period, the diameters of the inhibition zones for each oil sample were measured with a ruler.

REFERENCES

1. F.D. Gunstone; *Vegetable oils in food technology: Composition, Properties and Uses*, Blackwell Publishing Ltd, Oxford, UK, **2011**, pp1-352
2. D. Bozdogan-Konuskan; A. Canbas; *Rev. Chim. (Bucharest)*. **2014**, *65*, pp. 788-791
3. M.F. Díaz; R. Hernández; G. Martínez; G. Vidal; M. Gómez; H. Fernández; R. Garcés; *J. Braz. Chem. Soc.* **2006**, *1*, 403-416.
4. R. Seda Tigli Aydin; F. Kazanci; *J Am Oil Chem Soc.* **2018**, *95*, pp.1385-1398
5. B. Uysal; *Intercult Ethnopharmacol.* **2014**, *3*, 49-50.
6. M.F.Díaz; J. A. Gavin -Sazatornil; O. Ledea; F. Hernandez; M. Alaiz; R. Garces; *Sci. Eng.* **2005**, *27*, 247- 253.
7. V. Georgiev; M. Anachkov; T. Batakliiev; S. Rakovsky; *Bulgarian Chem. Commun.* **2013**, *45*, 203-207.
8. O.E. Ledea-Lozano; L.A. Fernández-García; D. Gil-Ibarra; N. Tenab; R. Garcés; E. Martínez-Force; J.J. Salas; *Grasas Aceites* **2019**, *70*, 1 –12.
9. N.U. Soriano; V.P. Migo; M. Matsumura; *Phys. Lipids.* **2003**, *126*, 133-140.
10. S. Moureu; F. Violleau; D. Ali Haimoud-Lekhal; A. Calmon; *Chem. Phys. Lipids* **2015**, *186*, 79-85.
11. P. Tran; D. Graiver; R. Narayan; *J. Am. Oil Chem. Soc.* **2005**, *82*, 653-659.
12. H.R. Liu; P.J. White; *J. Am. Oil Chem. Soc.* **1992**, *69*, 528-532.
13. H.S. Enjarlis; Y. Anwar; *Int. J. Eng. Technol.* **2018**, *7*, 146-149.

14. M.F. Díaz; N. Núñez; D. Quincose; W. Díaz; F.Hernández; *Ozone: Sci. Eng.* **2005**, *27*, 153-157.
15. S. Shobha-Borhade; *Archives of Applied Science Research.* **2013**, *5*, 5-8.
16. S. Montserrat-De La Paz; F. Marín-Aguilar; M. D. García-Giménez; M. A. Fernández-Arche; *J. Agric. Food Chem.* **2014**, *62*, 1105-1110.
17. S. Manea; *Rev. Hofigal.* **2014**, *41*, 40-41.
18. F. Anwara; S. Latifa; M. Ashraf; *J. Am. Oil Chem. Soc.*, **2006**, *83*, 323-329.
19. S. Sapino; M. E. Carlotti; E. Peira,; Gallarate, M.; *J. Cosmest. Sci.* **2005**, *56*, 227-251.
20. İ. Orhan; Ş. Küsmenoğlu; B. Şener; *J. Fac. Pharm. Gazi.* **2000**, *17*, 79-81.
21. R. Iseppi; V. Brighenti; M. Licata; A. Lambertini; C. Sabia; P. Messi; F. Pellati Benvenuti; *Molecules.* **2019**, *24*, 2302.
22. N. Rodrigues De Almeida; A. Beatriz; E. José De Arruda; D. Pires De Lima; L.C. Silva De Oliveira; A.C. Michelett; *Ozonized Vegetable Oils: Production, Chemical Characterization and Therapeutic Potential in Vegetable Oil Properties, Uses and Benefits*; Brittany Holt- Nova Editor Science Publishers, **2016**, *Chapter 5*, pp. 129-149.
23. G. Appendino; S. Gibbons; A. Giana; A. Pagani; G. Grassi; M. Stavri; E. Smith; M. M. Rahmanm; *J Nat Prod.* **2008**, *71*, 1427-1430.
24. J. Novak; S. Karin Zitterl-Eglseer; G. Deans; C.M. Franz; *Flavou Fragr. J.* **2001**, *16*, 259-262.
25. G. Zengin; L. Menghini; A. Di Sotto; R. Mancinelli; F. Sisto; S. Carradori; S. Cesa; C. Frascetti; A. Filippi; L. Angiolella; M. Locatelli; L. Mannina; C. Ingallina, V. Puca; M. D'Antonio; R. Grande; *Molecules*, **2018**, *23*, 3266.
26. R. Iseppi; V. Brighenti; M. Licata; A. Lambertini; C. Sabia; M. Patrizia; F. Pellati; S. Benvenuti; *Molecules*, **2019**, *24*, 2302.
27. Z. B. Guzel-Seydim; A.K. Greene; A.C. Seydim; *Lebensm. Wiss. Technol.* **2004**, *37*, 453-460.
28. M. Cirlini; A. Caligiani; G. Palla; A. De Ascentiis; P. Tortini; *Ozone: Sci. Eng.* **2012**, *34*, 293-299.
29. N. Bordei-Ionescu; M. Popescu; A. Bratu; D. Istrati; C. Ott; A. Meghea; *Rev. Chim. (Bucharest)*, **2015**, *66*, 1267-1272.
30. H. Kataoka; M. Semma; H. Sakazaki; K. Nakamuro; T. Yamamoto; S. Hirota; K. Tazuya-Murayama; A. Ichikawa; *Ozone Sci. Eng.* **2009**, *31*, 238-246.
31. V. Travagli; I. Zanardi; G. Valacchi; V. Bocci; *Mediators Inflamm.* **2010**, *2010*, 1-9.
32. E. Ugazio; V. Tullio; A. Binello; S. Tagliapietra; F. Dosio; *Molecules*, **2020**, *25*, 334
33. N.S.I Geweely; *Int.J. Agric. Biol.* **2006**, *8*, 670-675.
34. E. Carata; B. A. Tenuzzo; L. Dini; *Powerful Properties of Ozonated Extra Virgin Olive Oil*, in *Herbal Medicine* Edited by Philip F. Builders, IntechOpen, **2018**.
35. M. Montevecchi; A. Dorigo; M. Cricca; L. Checchi; *The New Microbiologica: official journal of the Italian Society for Medical Virology (SIVIM).* **2013**, *36*, 28 - 302.

COMPARATIVE CHEMICAL AND ANTIMICROBIAL CHARACTERIZATION OF NON-OZONATED
AND OZONATED VEGETABLE OILS

36. J. Lu; M. Chen; L.Gao; Q. Cheng; Y. Xiang; J. Huang; K. Wu; *J. Dermatol. Treatment.* **2018**, *29*, 676-681.
37. J. Sadowska; B. Johansson; E. Johannessen; R. Friman; L. Broniarz-Press; J. B. Rosenholm; *Chem. Phys. Lipids.* **2008**, *151*, 85-91.
38. R. Seda Tigh Aydin; F. Kazanci; *J Am Oil Chem Soc.* **2018**, *95*, 1385-1398.
39. P. Guerra-Blanco; T. Poznyak; I. Chairez; M. Brito-Arias; *Eur. J. Lipid Sci. Technol.* **2015**, *117*, 988-998.
40. I. Zanardi; V. Travagli; A. Gabbrielli; L. Chiasserini; V. Bocci; *Lipids.* **2008**, *43*, 877-886.
41. R. Criegee; *Angew. Chem. Internat.* **1975**, *14*, 745-752.
42. O. Ledea; T. Correa; M. Escobar; A. Rosado; J. Mario; C. Hernandez; D. Jardines; *Ozone Sci. Eng.*, **2001**, *23*, 121-126.
43. J. Zahardis; G. A. Petrucci; *Atm. Chem.Phys.*, **2007**, *7*, 1237-1274.
44. G. Martinez Tellez; O. Ledea Lozano; M. D'iaz Gomez; *Ozone: Sci. Eng.*, **2006**, *28*, 181-185.
45. SR EN ISO 3960: **2005** - *Animal and vegetable oils and fats. Determination of the peroxide index*
46. SR EN ISO 660:**2009**- *Animal and vegetable fats and oils. Determination of acid value and acidity*
47. SR EN ISO 3961: **2018** - *Animal and vegetable fats and oils. Determination of iodine value.*
48. R. Carpa; M. Drăgan-Bularda; V. Muntean; *Microbiologie Generală Lucrări Practice*, Ed. Presa Univ. Clujeană, 2014.
49. R. M. Atlas; *Handbook of Microbiological Media*, 4th edition, CRC Press, New York, 2010.
50. C. M. Paraguassú Cecchi; D. Cesarín-Sobrinho; A. B. Buarque-Ferreira; J. C. Netto-Ferreira; *Catalysts*, **2018**, *8*, 6,1-21
51. A. Soutelo-Maria; J. L. Dubois; J. L. Couturier; G.Cravotto; *Catalysts*, **2018**,*8*, 1-17
52. K. Y. L. Alex; K. C. Chak; *J. Phys. Chem. A.* **2007**, *111*, 6285-6295.
53. F. C. Peedikayi; V. Remy; S. John; T. P Chandru; P. Sreenivasan; G. A. Bijapur; *J. Int Soc Prevent Communit Dent* **2016**, *6*, 447-452.
54. F. Nazzaro; F. Fratianni; R. Cozzolino; A. Martignetti; L. Malorni; G. V. De Feo; A. Cruz; A. Acierno; *Microorganisms*, **2019**, *7*, 321.
55. M. Montevecchi; A. Dorigo; M. Cricca & L. Cecchi; *New Microbiologica*, **2013**, *36*, 289-302.
56. G. Appendino; S. Gibbons; A. Giana; A. Pagani; G. Grassi; M. Stavri; E. Smith; M. Mukhlesur Rahman; *J. Nat. Prod.* **2008**, *71*, 1427-1430.